MEASURING THE DIELECTRIC PROPERTIES OF CRUSHED COPPER ORE

by

Nico Albert Groenewald

Thesis submitted in partial fulfilment
of the requirements for the Degree

of

MASTER OF SCIENCE IN ENGINEERING (MINERAL PROCESSING)

in the Department of Process Engineering
at the University of Stellenbosch

Supervised by

Prof. Steven Bradshaw

STELLENBOSCH
December 2010

Declaration

I, the undersigned, hereby declare that the work contained in this thesis is my own original work and that I have not previously in its entirety or in part submitted it at any University for a degree.

Signature

18 November 2010

Date

Abstract

Previous work has shown that microwave heating of mineral ores induces micro cracks within the ore structure, which can be attributed to the difference in the adsorption of microwaves amongst the different mineral phases. This reduces the energy required during subsequent grinding and enhances the liberation of valuable minerals. In order to design microwave applicators for this purpose, knowledge of the effective dielectric properties of the crushed ore is required. Of particular interest is the effective complex permittivity of the bulk crushed ore. The measurement of the effective permittivity of a large volume of crushed ore is most readily accomplished using the waveguide measurement technique. In this method a representative sample of the material is placed in a defined and fixed volume in a standard size rectangular section metallic waveguide. The magnitude and phase angle of the transmitted and reflected low power microwaves through and from the sample are measured. The complex permittivity can be extracted from these so-called scattering, or S_{ij} parameters.

In this study the effective complex permittivities for two porphyry copper ores and a copper carbonatite ore were determined as a function of particle size distribution (-26.5+2mm) using two sizes of waveguide (WR284 and WR340). The sample holders incorporate dielectric windows for the location of the material under test. The extraction of dielectric properties from S_{ij} parameter measurements is problematic using standard algorithms in such cases. Accordingly a new Database Extraction (DBE) Algorithm has been developed. In this method, a database of scattering parameters is established through electromagnetic modelling of the measurement system. A search algorithm is used to determine the effective complex permittivity of the modelled load whose scattering parameters provide the best fit to the experimental data. The goodness of the experimental fit of the simulated to the measured S_{ij} parameters is determined by a root mean squared deviation minimisation metric.

Results show that the method can be used successfully to determine an effective complex permittivity for a bulk volume of the crushed material. It is concluded that the dielectric property extraction over the full operational frequency interval (2.3-3 GHz) is preferred as it has a larger degree of extraction confidence and hence reliability.

Results show that with increasing particle size, the experimental fit between the simulated and measured S_{ij} parameters becomes increasingly poor, as wall effect become more prominent. The effect is most prominent for the smaller WR284 waveguide size. It is shown that for a waveguide size of similar size to the particle size, the S_{ij} parameter fitting is poorer compared to when a larger waveguide size is used. The extracted complex permittivity reproducibility between repeated dielectric property measurements is improved for the WR340 waveguide size, as the extractions in the WR284 waveguide is dominated by the combined particle size and wall-effects of the sample holder.

Ore mineralogy is identified as a key parameter that influences the dielectric properties of the crushed ore. For ores with a dominant microwave absorbent mineral phase, the dielectric constant and loss factor is found to be larger, compared with ores with a more dominant microwave transparent gangue mineral phase.

Opsomming

Navorsing toon dat die verhitting van mineraal erts, met mikrogolwe, mikroskaal frakture in die mineraalstruktuur teweeg bring weens die verskil in die adsorpsie van mikrogolwe in die verskillende mineraalfases. Gevolglik verminder die energievereiste vir die vergruising van die erts en verbeter die vrystelling van waardevolle minerale wat vasgevang is in die mineraalmatriks. Vir die ontwerp van mikrogolfapplikators vir dié doel, word die effektiewe diëlektriese eienskappe van die vergruisde erts benodig. Van spesifieke belang is die effektiewe komplekse permittiwiteit van die erts. Die effektiewe permittiwiteit van `n vergruisde materiaal monster word met behulp van die golfgeleier tegniek gemeet. Vir dié tegniek word `n verteenwoordigende monster van die materiaal in `n rigiede volume in `n standaard grootte reghoekige golfgeleier geplaas. Die grootte en fasehoek komponente van die deurgelate en weerkaatste mikrogolwe deur en van die oppervlak van die materiaal word gemeet. Die komplekse permittiwiteit van die vergruisde materiaal kan geëkstrakteer word vanaf hierdie sogenaamde verspreide, of S_{ij} parameters.

In hierdie studie word die effektiewe permitiwiteit van twee porforie koper ertse en `n koper karbonatiet erts bepaal as funksie van partikel grootte (-26.5+2 mm) deur gebruik te maak van twee standaard grootte golfgeleiers. Die monster houers inkorporeer diëlektriese vensters om die vergruisde materiaal monster in posisie te hou. In so `n geval is die ekstraksie van die diëlektriese eienskappe vanuit die S_{ij} parameter metings problematies. Gevolglik is 'n nuwe Databasis Ekstraksie Algoritme ontwikkel wat `n databasis van verspreide parameters opstel deur die elektromagnetiese simulasie van die metingsisteem. `n Soek-algoritme word gebruik om die effektiewe komplekse permitiwiteit van die gesimuleerde monster te bepaal wat die beste ooreenstem met dié van die gemete eksperimentele S_{ij} parameter data. Die mate van ooreenstemming tussen die parameters, word bepaal aan die hand van die minimaliserings prosedure.

Resultate toon dat dié metode geskik is vir die bepaling van die effektiewe komplekse permitiwiteit van die vergruisde monster. Dit word vasgestel dat die betroubaarheid van die geëkstraeerde S_{ij} parameters, en gevolglik die diëlektriese eienskappe van die erts, toeneem indien die algoritme oor `n groter frekwensie band uitgevoer word.

Resultate toon verder dat met toenemende partikel grootte, die mate waartoe die absolute grootte en fasehoek komponente van die gesimuleerde en gemete S_{ij} parameters ooreenstem, versleg. Dit word toegeskryf aan wand-effekte. Hierdie verskynsel is veral opmerklik vir die kleiner grootte golfgeleier. Dit word getoon dat vir metings waar die golfgeleier dieselfde orde grootte geometriese afmetings het as die vergruisde erts self, die passing tussen die gesimuleerde en gemete S_{ij} parameters swakker is, wanneer dit vergelyk word met metings waar dit nie die geval is nie. Die reproduseerbaarheid van die geëkstraeerde diëlektriese eienskap waardes verbeter vir lesings wat uitgevoer word in `n groter grootte golfgeleier. Laasgenoemde word toegeskryf aan die meer dominante wand-effekte wat kenmerklik is vir `n kleiner golfgeleier.

Erts mineralogie word geïdentifiseer as `n sleutel parameter wat die diëlektriese eienskappe van die vergruisde materiaal beïnvloed. Beide die diëlektriese konstante en verliesfaktor is groter vir ertse met `n oorheersende mikrogolf absorberende mineraalfase.

Acknowledgements

I would like to thank the following individuals whom without this report would not have been possible:

***Prof. Steven Bradshaw**, for your guidance and support that you gave me throughout the course of the project. Thank you for believing in me, and giving me the financial support. Without it, this project would not have been possible. Your academic knowledge and enthusiasm has been inspirational.*

***Renier Marchand**, for the assistance with the Database Extraction Algorithm. Without your inputs, this thesis would not have been possible.*

***Jannie Barnard** and **Anton Cordier**, for the construction of the waveguide sample holders. Without your technical guidance and inputs, the thesis would not have been possible.*

***Martin Siebers**, who supervised all waveguide measurements conducted at the Department of Electrical Engineering (University of Stellenbosch).*

***Vincent Lotter**, for the support and encouragement that you have always given me and without whom this thesis would not have been possible.*

*To my **parents, George and Martha**, thank you for all the sacrifices you made for me. You truly inspire me.*

Table of Contents

List of Figures

List of Tables

Nomenclature

2/3D	Two and three dimensional
ANA	Automatic Network Analyser
BJ	Baker Jarvis
DB	Database (Algorithm)
DBE	Database Extraction (Algorithm)
FDTD	Finite Difference Time-Domain
GHz	Gigahertz
HP	Hewlett Packard
M1/2	Measurement 1 or 2
MHz	Megahertz
MLA	Mineral Liberation Analyzer
MOC	Material of Construction
MUT	Material Under Test
MW	Microwave
NRW	Nicholson Ross Weir (algorithm)
PET	Polytethyleneterathalyte
QEMSEM	Quantative Electron Microscope Scanning Electron Microscope
QW	QuickWave®
SC	Split cycle
SEM	Scanning Electron Microscope
SMA	Standard Military Adapter
SSA	Successive Split Adding
USA	United States of America
VST	Vibratory Sieve Test
Wt%	Weight percentage

Roman Alphabet

a	Waveguide dimension in x-dimension	mm
b	Waveguide dimension in y-dimension	mm
c	Waveguide dimension in z-dimension	mm
$\bar{d}_p$	(Arithmetic) mean particle size	mm
$f_{c_{mn}}$	Cut-off frequency (m=1, 2, 3… and n=1, 2, 3…)	GHz
f_{end}	Ending operational frequency	GHz
f_{start}	Starting operational frequency	GHz
$\Delta f_{interval}$	Frequency interval size	MHz
m_i	Ore mass used per individual ore test	g
$\bar{m}_n$	Mean mass of ore used in n tests	g
$\bar{m}_i$	Mean ore mass used per individual ore test	g
m	Number of variations in the x-direction	
n	Number of algorithm simulations	
N	Number of frequency points	
n	Number of variations in the y-direction	
p	Weighing factor used in the calculation of the metric	
S_{ij}	Scatter parameter (i=1,2 and j=1,2)	
$\lvert S_{ij} \rvert$	Magnitude component of S_{ij} parameter	
$S_{ij_{measured}}$	Measured S_{ij} parameter	
$\angle S_{ij}$	Phase angle component of S_{ij} parameter	
$S_{ij_{simulation}}$	Simulated S_{ij} parameter	
$\bar{V}_{particle}$	Mean particle volume	mm^3
$\bar{V}_i$	Mean volume of water displaced across i tests	ml
$\bar{V}_n$	Mean volume of water displaced across n tests	ml
$V_{sample\ cell}$	Volume of empty ore cavity	mm^3
V_i	Volume of water displaced per individual ore density test	ml
x	Directional axis in x dimension	
y	Directional axis in y dimension	
z	Directional axis in z dimension	
Z_0	Characteristic impedance of free space	Ω

Greek Alphabet

ε^*	Effective complex permittivity	
ε'	Dielectric constant	
ε''	Dielectric loss factor	
ε_r	Relative permittivity	
ε_r^*	Relative complex permittivity	
ε_r'	Relative dielectric constant	
ε_r''	Relative dielectric loss factor	
ε_0	Permittivity of free space (8.85×10^{-12} F/m)	F/m
$\varepsilon^*_{\text{simulated}}$	Simulated effective permittivity	
$\varepsilon^*_{\text{measured}}$	Measured effective permittivity	
$\varepsilon'_{\text{var}}$	Variable dielectric constant	
$\varepsilon''_{\text{var}}$	Variable dielectric loss factor	
λ_g	Guide wavelength	mm
λ_0	Free-space wavelength	mm
λ_c	Cut-off frequency wavelength	mm
θ_{min}	Minimum ore volume packing fraction	%
θ_{max}	Maximum ore volume packing fraction	%
$\theta_{average}$	Average ore volume packing fraction	%
μ^*	(Effective) complex permeability	
μ'	Real part of the complex permeability	
μ''	Imaginary part of the complex permeability	
μ_r	Relative permeability	
μ_r^*	Relative complex permeability	
μ_r'	Real part of the relative complex permeability	
μ_r''	Imaginary part of the relative complex permeability	
μ_o	Permeability of free space	H/m
ρ_{ore}	Experimental ore density	kg/m^3
σ	Electrical Conductivity	S/m

Other

$\|\bullet\|_{min}$	Minimum metric
$\|\bullet\|_{max}$	Maximum metric
$\|\bullet\|_{Port\,1}$	Metric value at port 1 of the experimental waveguide sample holder
$\|\bullet\|_{Port\,2}$	Metric value at port 2 of the experimental waveguide sample holder

Chapter 1

Introduction

1.1 Material Dielectric Property Measurement Review

Previous studies showed that microwave treatment of ore material would result in a significant ore strength reduction as a pre-treatment step prior to comminution that will result in major running-cost reductions (Kingman et al., 2004; Sayhoun et al., 2005). This requires the design of microwave applicators that can successfully treat ore capacities of thousands of tons of ore per hour in operational commercial treatment facilities.

In order to design these applicator units, the dielectric properties of the mineral ore to be treated needs to be determined as they strongly influence the applicators' power density, electric field strength, residence time of the ore within the applicator and most importantly the geometrical design specifications (Kingman et al., 2004; Bradshaw et al., 2007). Recently Ali and Bradshaw, 2010, modelled the heating rate and fracture patterns of ore material, which consisted of different mineralogies, ore textures and microwave power density. However, no large-scale commercial application of microwave-assisted comminution has been implemented to date.

The electromagnetic design of the applicator unit uses the dielectric properties in mathematical models to determine its dimensions. Accurate measurement of the dielectric properties, and more specifically the complex permittivity, is a key design consideration.

The permittivity of an ore particle is expressed as a complex quantity consisting of indicates to the ability of the ore to store electric energy and generate an electric flux, ultimately determining the microwave wavelength in the ore particle itself.

The imaginary part is known as the dielectric loss factor and indicates the amount of microwave energy that is converted into heat energy when the ore particle is exposed to an electromagnetic environment.

Various dielectric property measurement techniques exist of which the coaxial probe and waveguide procedures are particularly useful as they measure over a wide frequency range. The measurement of the effective permittivity of a large volume of crushed ore is best accomplished using the waveguide measurement technique as it allows for clear determination of the characteristic behaviour of the crushed load within an electromagnetic environment. Various sample holder configurations have been proposed and used by previous authors. However, a design proposed by Pauli et al., 2005, gives additional flexibility as it allows for the measurement of both solids and liquids and ensures a fixed sample cavity with known volume.

It is particularly important to measure the dielectric properties of the crushed material, in such a way that allow for the design of the applicator through electromagnetic simulation, as the particulate load is presented to the microwave applicator itself.

The aim of this thesis therefore is to measure the complex permittivity, the dielectric property of interest, of crushed mineral ores and investigate the influence of particle size, ore mineralogy, packing density and the size of the sample holder that are commonly available to experimentalists. This will aid in the design of plant-compatible microwave applicators in future.

As the material under test is exposed to an electromagnetic environment, the material absorbs and reflects a fraction of the microwave that it receives. The relative absorption and reflection through and from the material under test known as scattering parameters.

Previous authors (Nicholson et al., 1970, and Baker-Jarvis, 1990) have presented a number of analytical extraction algorithms to invert the scattering parameters into a set, consisting of one dielectric constant and loss factor value. However both these algorithms exhibit a disadvantage for use in the experimental setup presented as part of this thesis.

The Baker-Jarvis algorithm cannot be used when dielectric property windows form part of the experimental set-up. The Nicholson Weir Ross algorithm suffers from loss of measurement information when the sample length is a multiple of a half guide wavelength in the material.

A Database Extraction Algorithm has been developed to extract the effect complex permittivity of a heterogeneous particulate load when it is considered as a homogeneous block. In this method, a database of scattering parameters is established through electromagnetic modelling of the measurement system. A search algorithm is used to determine the effective complex permittivity of the modelled load whose scattering parameters provide the best fit to the experimental data. The goodness of the experimental fit of the simulated to the measured Sij parameters is determined by a root mean squared deviation minimalisation metric.

1.2 Thesis Overview

Chapter 2 introduces the electromagnetic spectrum and discusses the fundamentals of the microwave frequency interval. The dielectric properties used for the design of microwave applicators through simulation are discussed with specific focus on the complex permittivity. The complex permittivity of a material under test provides insight into the sizing of the applicator. Chapter 2 furthermore presents a literature survey of recent work that focussed on dielectric property measurements with specific focus on determining key factors that affect the dielectric properties of a material under test.

In Chapter 3, the coaxial probe and waveguide measurement techniques are discussed. The focus however, will be on the waveguide technique, which is used throughout the remainder of the thesis. Basic waveguide theory is provided. The experimental setup used for all dielectric property measurements is presented.

Chapter 4 describes the porphyry copper, copper carbonatite and quartz monzonite porphyry copper ores as the materials of interest for which dielectric properties are measured. All three of these ores are multi-phase inhomogeneous and anisotropic copper bearing ores. The chosen particle size distribution of interest is -26.5+2 mm. The riffle splitting procedure is chosen as the representative sampling method.

Chapter 5 focuses on the crushed ore packing density. The packing density is a measure used to indicate the void space fraction between individual particles per size class of the particulate load. The combined effect of particle size and sample holder size is investigated.

In Chapter 6, the experimental setup used for all dielectric property measurements throughout the thesis is discussed. The calibration standards used and calibration procedure followed to calibrate the measurement setup (ANA) are provided. The Database Extraction Algorithm used to extract the dielectric properties of crushed ore is presented and discussed. Detail is provided on the theoretical background of the algorithm, the electromagnetic modelling of the sample holders in two waveguide sizes, the generation of the simulated scattering parameters and the search algorithm used to scan the database for simulated scatter parameters, that provide the best fit to the measured parameters. The effect of the cut-off frequency is investigated for two standard waveguide sizes. The Database Extraction Algorithm is used to extract the dielectric properties of crushed Porphyry Copper ore in the -26.5+2 mm particle size distribution. Extraction results over piecewise 100 MHz and 250 MHz frequency intervals are compared to an extraction over a 700 MHz frequency interval. The results are visually compared.

To facilitate the interpretation of the results, the magnitude and phase angle of the measured and simulated scatter parameters for Porphyry Copper ore, in the -16+11.2 mm particle size class, are compared followed by quantitative and qualitative analysis of the difference in the extracted dielectric properties for extractions executed over narrow and broader frequency intervals.

In Chapter 7, the effect of particle and sample holder size is investigated for each of the ores of interest. Particulate loads of copper carbonatite and porphyry copper ore are used to establish how the dielectric properties vary with ore mineralogy. The effect of sample holder size and successive ore packings are investigated for each of the copper ores of interest.

In Chapter 8 the main conclusions and recommendations of the thesis are presented.

1.3 Thesis Objectives

The two main objectives of the thesis are as follows:

Objective 1

Design a measurement system and develop a property extraction methodology to establish effective permittivity for crushed mineral ores

The experimental waveguide dielectric measurement system proposed in this thesis incorporates dielectric windows within the waveguide to keep the crushed particulate load in position (Figure 4). The windows allow for a fixed and rigid sample cavity with a known volume. The waveguide technique facilitates a clear understanding of how the particulate load behaves when placed within an electromagnetic environment. The relative degree of absorption and reflection is reported as S_{ij} scattering parameters.

Available analytical measurement techniques cannot be used to extract the dielectric properties of the material if the sample holder setup incorporates dielectric windows within the sample cavity.

This has led to the development of a new extraction procedure presented as part of this thesis and is labelled as the *Database Extraction Algorithm*. This procedure uses electromagnetic simulation to simulate the sample holders in QuickWave3D® (Section 6.4). The coarse particulate load is modelled as a solid homogeneous load with effective dielectric properties. The reason for this is twofold:

- It is currently not possible to make a geometrical tractable representation of inhomogeneous, multiphase, irregular particles where phase-specific properties are unknown. This would result in a model with too many degrees of freedom.
- The mesh-size that would be required to resolve the mineral phases on the sub-millimeter scale is computationally incompatible with typical applicator dimensions (several meters).

Accordingly, database of S_{ij} scattering parameters is generated for different values of the dielectric constant and dielectric loss factor. A search algorithm searches the database. The simulated parameters closest to the experimental S_{ij} parameter set is selected to effectively represent the complex permittivity of the crushed ore load under test.

Objective 2

Determine the limits for reliable property measurement and extraction as a function of particle size distribution in a measurement system

Microwave measurement syste4ms are available only in standard waveguide sizes, effectively constraining the size of the sample holders used for the material under test. As the particle size approaches the size of the sample holder it is expected that wall effects will severely compromise the measurement. Determining the upper particle size limit (for a narrowly distributed particulate material) for each of the sample holders is crucial for reliable dielectric property measurement.

Chapter 2

Literature Survey

2.1 Introduction

The use of microwaves, both industrially and commercially, dates back to the early 1940's when radar systems were developed and used during World War II. This resulted in the first commercially available microwave oven manufactured by the Raytheon Corporation in 1947. Osepchuk, 1984, gives a detailed description of the history of microwave technology and how it has developed through the years. Despite the widespread domesticl use of microwaves, their application in industrial operations has shown only steady development over the last three decades.

The utilization of microwaves has shown to be potentially advantageous in the mineral processing industry where microwave pre-treatment can possibly play a pivotal role in the reduction of the energy consumption during milling and comminution operations at economically viable energy inputs (Jones et al., 2006). As a result, microwave pre-treament may potentially result in operational cost savings and reduce the global energy/electricity demand. In turn this will result in less CO_2 emissions from coal based energy generation processes.

Taking into account that comminution is a highly energy inefficient industrial process (Jones et al., 2006), which accounts for the bulk of the electricity demand of a typical mineral processing plant, processing alternatives need to be investigated.

Microwave processing of mined ore has been identified as a suitable technology not only to reduce energy demand, but also to improve the liberation of valuable minerals.

Despite the considerable effort that was made during the past decade, no commercial application of microwave treatment of ore has been recorded to date. The technology is still in its developmental stages and the industrial application thereof needs further development. A key element to the microwave treatment of ore is the determination of the dielectric properties of the ore to be treated. The dielectric properties, especially the complex permittivity, are of particular importance as they is used in simulation to design the microwave applicators.

The real part of the complex permittivity, also known as the dielectric constant, is of particular importance when designing microwave applicators as it determines not only the wavelength of the microwave within the material subjected to an electromagnetic field, but also partly determines the penetration behaviour of microwave as it passes through the sample. The dielectric constant also gives an indication of the materials' ability to store electric energy and hence to generate an electric flux. The complex part, known as the dielectric loss factor, determines the amount of microwave energy dissipated into heat energy and the penetration depth of the microwaves into the material of interest. Both these quantities are used in design simulations to determine the applicator dimensions. The correct sizing of the applicator is of critical importance as to provide for the most effective thermal heating of the ore to be treated.

2.2 Electromagnetic Spectrum

The electromagnetic spectrum is categorised into various bands. Each frequency section has a specific range of wavelengths, each corresponding to a specific frequency interval. Gamma rays, X rays, UV (ultraviolet), IR (infra-red), MW (microwave), Radio Wave (FM and AM) and Long Radio Waves account for the whole electromagnetic spectrum.

The use of microwaves dates back to the 1940's when radar communication systems were developed during World War II (Meredith, 1998). The development of the early microwave technology resulted in the first commercially available microwave oven in 1951 (Osepchuk, 1984).

Despite the commercial use of microwaves, the household microwave oven being the most obvious example, their potential use to thermally induce micro fractures/cracks in mineral ores,

specifically along different grain boundaries, is a more recent development (Fitzgibbon and Veasey, 1990). This could be done prior to final grinding which will aid the liberation of valuable minerals trapped within the gangue material and reduce the required energy demand during the comminution process. Microwave assisted micro crack formation within the ore structure has been shown to be economically viable (Kingman et al., 2004).

The induced micro cracks reduce the energy required during subsequent grinding and enhance the liberation of valuable minerals. Potentially the addition of microwave processes on plants can result in enhanced liberation of valuable minerals at close to native grain size, reducing the required fineness of grind and slimes losses.

It is also noted by Sahyoun et al., 2005, that microwave assisted comminution has a major cost benefit, as 5% of global electricity demand annually is consumed by comminution alone (Rhodes, 1998). In the USA alone, comminution accounts for 29.3% of the total mining energy requirement (Tromans, 2008).

2.3 Dielectric Material Properties

In the proposed process, microwave applicators are used to rapidly heat crushed ore prior to comminution and milling processes when subjected to an electromagnetic field. The heating process is a function of applicator size and design which is determined by the dielectric properties of the material. These properties therefore determine how well a material will heat in the presence of microwaves in an electromagnetic field. Other microwave heating parameters, such as the electromagnetic power density, are also proportional to a material's dielectric properties.

The dielectric property of particular concern in this thesis is the complex permittivity, denoted by the symbol ε^*. Section 2.3.1 will discuss this property further.

2.3.1 Complex Permittivity

The complex permittivity of a material comprises two parts. The first is termed the dielectric constant, denoted by ε′. The dielectric constant is of particular importance when designing microwave applicators as it determines not only the wavelength of the microwave within the material subjected to an electromagnetic field, but also describes the penetration behaviour of microwaves as they passes through the sample. The dielectric constant gives an indication of the materials' ability to store electric energy and hence generate an electric flux. The dielectric constant is used to determine the physical dimensions of the microwave applicator by means of a mathematical simulation.

The second part is known as the dielectric loss factor, denoted by ε″. The dielectric loss factor is related to the amount of microwave energy that is dissipated as heat. The complex permittivity is defined by Metaxas and Meredith, 1983, as follows:

Equation 1: Complex Permittivity

$$\varepsilon^* = \varepsilon' - j\left(\varepsilon'' + \frac{\sigma}{\omega\varepsilon_0}\right)$$

For dielectric materials, the electrical conductivity component, denoted by σ in Equation 1, is negligible; the expression for the determination of the complex permittivity subsequently reduces to:

Equation 2: Complex Permittivity with Zero Electrical Conductivity

$$\varepsilon^*_{\sigma=0} = \varepsilon = \varepsilon' - j\varepsilon''$$

The permittivity could also be expressed in terms of a relative permittivity parameter. In such cases, the relative permittivity is defined as:

Equation 3: Relative Permittivity

$$\varepsilon_r = \frac{\varepsilon}{\varepsilon_0}$$

In Equation 3, the relative permittivity of free space is by ε_0 (=8.85x10^{-12} F/m).

Substituting Equation 3 into Equation 2 the complex permittivity, assuming the electrical conductivity is zero, can be expressed in terms of relative permittivity as follows:

Equation 4: Relative Complex Permittivity with Zero Electrical Conductivity

$$\varepsilon_r^* = \varepsilon_r' - j\varepsilon_r''$$

The loss tangent, which is the ratio of the dielectric loss factor to the dielectric constant is given by Equation 5:

Equation 5: Loss Tangent

$$\tan(\delta) = \frac{\varepsilon''}{\varepsilon'}$$

Dielectric losses are due mainly to dipolar polarisation. This in turn is due to the polarisation of dipoles in a material that tend to re-orientate when exposed to a time harmonic electromagnetic field. Dipolar polarisation is prominent, but not only restricted to, the microwave frequency band. Other losses include Maxwell-Wagner polarisation effects and polar dielectric contributions. For a more detailed discussion on the dielectric loss mechanism, refer to Metaxas and Meredith, 1982.

For the rest of this thesis the notation given in Equation 2 will be used throughout, where ε′ denotes the dielectric constant and ε″ denotes the dielectric loss factor.

2.4 Literature Overview

The use of microwave technology in the mineral processing industry in recent years has become a significant research field. Kingman et al., 2003, reported on recent developments in microwave-assisted comminution. Kingman et al., 2003, showed that over short exposure times, typically 0.1s, and high microwave power densities in a single mode microwave cavity a significant reduction in ore strength is possible due to thermal heating/expansion along mineral phase boundaries.

To design microwave applicators for this purpose, knowledge of the dielectric properties of the material to be treated is required.

Many different dielectric property measurement techniques exist, which vary in cost, accuracy and complexity. Nyfos and Vainikainen, 1989, categorised these measurement techniques into four groups namely lumped circuit, free-space, resonator and transmission line methods. Of these, only the last three are predominantly used today as most materials used for industrial heating processes are low loss and operational frequency levels are reasonably high. Venkatesh and Raghavan, 2005, argue that lumped circuits are therefore no longer preferred measuring techniques and that only measuring instruments and techniques that provide reliable scattering parameters, denoted as S_{ij} parameters, for the determination of dielectric properties within the frequency band of particular interest must be employed (Nelson, 1998).

The coaxial probe and transmission line (waveguide) techniques are particularly attractive methods due to their high degree of accuracy in the measured S_{ij} parameter data and ease of use (Venkatesh and Raghavan, 2005).

For the coaxial probe technique, a polished and even surface material is placed onto a coaxial probe, which is connected to an Automatic Network Analyzer (ANA). The ANA generates low power microwaves, which are then passed through the coaxial cable to the sample via the probe interface.

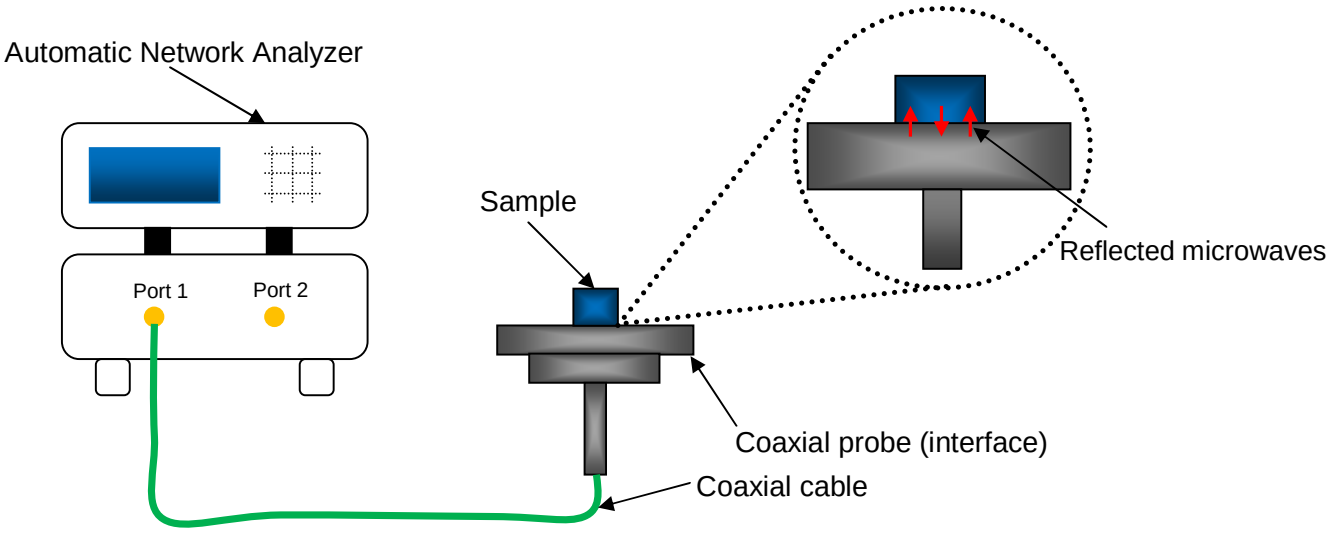

Figure 1: Coaxial measurement technique

The S_{ij} parameter data are measured at the material/probe interface, recorded by the ANA, and converted into a magnitude and phase angle component. The dielectric constant and loss factor values are exatrcted with the aid of a mathematical inversion procedure. Perfect electromagnetic contact between the material and probe is essential for reliable S_{ij} parameter measurement.

For coarse and uneven material surfaces, the coaxial probe technique is not applicable for dielectric property measurement. In such cases waveguide systems are preferred where the material is of irregular shape and form. Venkatesh and Raghavan, 2005, note that for frequencies above 1 GHz transmission-line techniques are usually preferred.

In this method, a representative sample of the material is placed in a defined and fixed volume in a standard size rectangular section metallic waveguide. The waveguide is connected to an ANA where low power microwaves are passed through the material under test.

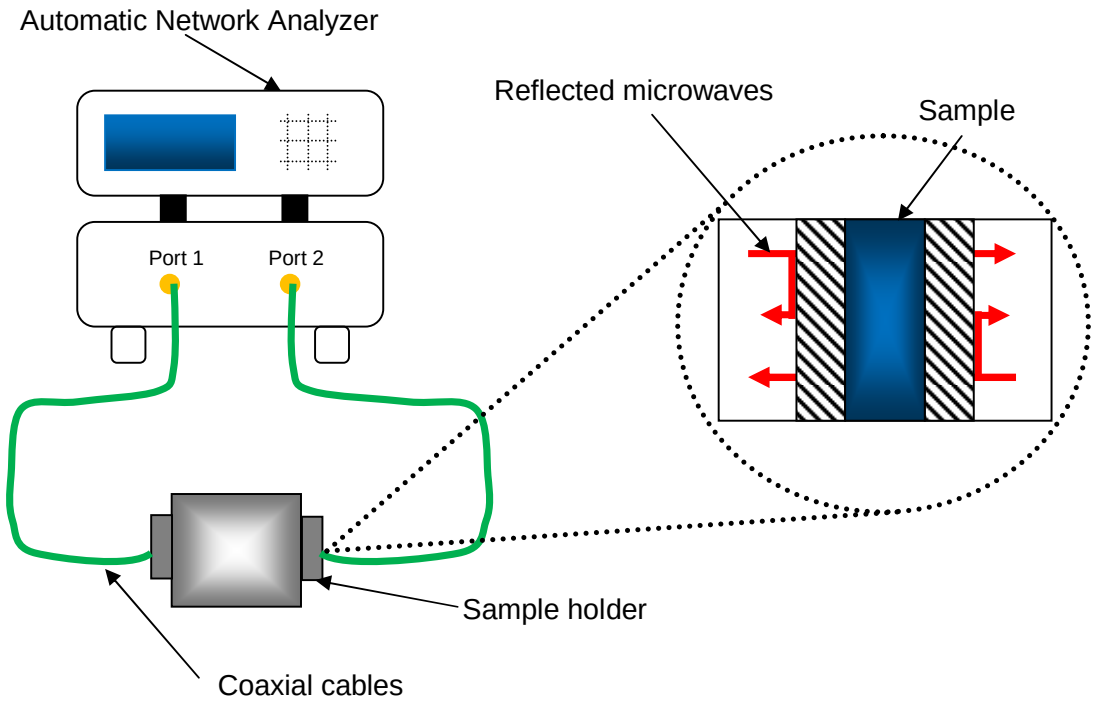

Figure 2: Waveguide measurement technique

The magnitude and phase of the transmitted and reflected low power microwaves from and through the sample are measured with the aid of the ANA. The complex permittivity is extracted from the measured S_{ij} parameters with mathematical algorithms.

Talbot et al., 2002, investigated the electromagnetic characterization of a fine-scale particulate composite material. Two powdered materials are used, namely ZnO and γ -Fe_2O_3. Experimental results showed that the electromagnetic properties of these materials were strongly dependent on the particle size of the powered particulate sample as well as the air volume fraction between the particles in the sample cavity. The use of nanotechnology, to improve the reliability of powder circuits in the metallurgical industry, has necessitated the characterization of the dielectric properties of nano-scale mineral phases and crushed particulate loads. The degree to which the particulate load is polarized or magnetised is dependent of the electromagnetic properties of the material, which is in turn a function of particle size. The study concluded that the particle size

and ore mineralogy are two key factors that determine the dielectric properties of a material under test. The bulk density of the crushed ore sample, influenced by the particle size, and void air space between the individual particles of a particulate load can influence the dielectric properties significantly (Nelson, 1988).

Louw, 2005, investigated the heating of multiphase inhomogeneous materials both in crushed and solid states, using both the coaxial probe and waveguide techniques. The dieletric properties of crushed copper carbonatite ore were measured. The dielectric properties of a solid slab of calcite were measured and found to differ from its particulate counterpart. This highligthed that the form of the material under test strongly influences the measured dielectric property. Louw, 2005, used a WR284 waveguide. The size of the waveguide sample holder limits the amount of crushed material of increased size that can physically fit into the sample holder. For smaller standard sized waveguide sizes, the wall effects of the sample holder should become noticeable as the particles becomes increasingly larger. For larger particle size classes this will lead to a decrease in the reproducibility in the measured dielectric properties of material between measurements with increasing particle size.

Louw, 2005, used a waveguide sample holder cavity that is bolted between two coaxial-waveguide transitions, which in turn are connected to the ANA. The crushed Copper Carbonatite ore was kept in position using two sheets of transparent film on either side of the sample holder cavity. This raised some concern as the volume of the sample cavity was not fixed, as the films were non-rigid. For reliable, repeatable, dielectric property measurements the geometry of the sample holder cavity needs to be rigid.

To ensure a fixed sample cavity Pauli et al., 2005, used a sample holder with fixed dielectric sheets, referred to as windows, to keep a granular soil sample in position for dielectric property measurement. The windows were precisely dimensioned to the waveguide dimensions, which ensures that there are no air gaps between the windows and waveguide walls. This ensures perfect electromagnetic contact between the sample holder walls and the dielectric windows (Pauli et al., 2005).

Nelson 2008, presented work on the use of dielectric properties to determine the moisture content of agricultural products. The dielectric properties are used in the microwave heating of grain and seed materials. The measurement of the dielectric properties of particulate grain and seed material, gives some indication as to how the effective complex permittivity and permeability of the material change as function of particle size. Nelson, 2008, showed that the dielectric constant and loss factor of ground hard red winter wheat exhibits a dependency on temperature and frequency. Both properties increase with temperature and decrease with increasing frequency.

A study by Fouché, 2003 investigated the effect of porosity on the extracted dielectric constant and loss factor of a particulate load. It was concluded that both the dielectric constant and loss factor varied for different crushed particle configurations at a fixed porosity of 50%. This highlights particle configuration as a key parameter, which has an effect on the extracted dielectric constant and loss factor values.

Various mathematical methods exist to convert the measured ANA S_{ij} parameters to the dielectric property values. Contelles-Cervena, 2005, presented a method based on the modal analysis of a partially filled waveguide by comparing the measured and theoretically calculated scatter parameters. However, this method is not applicable when dielectric windows are used as part of the sample holder to keep the particulate load in place.

Louw, 2005, used an analytical approach incorporating the Nicholson, Ross and Weir (NRW) inversion algorithm to model and measure the microwave heating of multiphase materials. Originally developed by Nicholson and Ross, 1970, and Weir, 1974, this algorithm explicitly gives a solution for the dielectric properties of the material as a function of the measured S_{ij} parameters in the time and frequency domain (Baker-Jarvis, 1990). Despite its apparent well-structured mathematical appearance, the NRW-algorithm demonstrates very divergent behaviour with increasing frequency (Weil, 1992) due to the half-guide wavelength anomaly.

Weil, 1992, recommended that samples be used that are shorter than a half-guide wavelength to solve this problem. However Baker-Jarvis, 1990, warns that this may drastically increase dielectric property measurement uncertainty.

Other works on the measurement of dielectric properties include that of Stuchly and Matuszewski, 1978, who found explicit equations for the determination of permittivity, however also suffering a lack of accuracy at frequency multiples of one-wavelength (Baker-Jarvis, 1990).

In an effort to increase the accuracy of the NRW-algorithm at higher frequencies Cloete, 1990, added a delay technique that resolves the mathematical phase uncertainty when the material under test is longer than the guide wavelength within the material being tested (Cloete, 1990, and Louw, 2005). Nontheless, even after the refinement, the NRW-algorithm still exhibited unstable behavior at frequencies corresponding to multiples of a half-wavelength in the material under test (Weil, 1992). At these frequencies the dielectric properties exhibit spikes as a function of frequency which is attributed to the phase uncertainties at these frequancies (Weil, 1992).

In 1990, in an effort to improve the accuracy of extraction algorithms, the National Institute of Standards and Technology (NIST) based in the USA started work on developing improved algorithms for calculating dielectric properties from S_{ij}-parameter data collected from ANA measurements.

Baker-Jarvis, 1990, presented an iterative algorithm which is stable over the whole frequency spectrum (Baker-Jarvis, 1990 and Weil, 1992). The permeability is set to one which reduces the uncertainties in the calculation of the complex permittivity. However, this method is not suited for waveguide measurements using windows as part of the experimental setup.

This led to the necessity of developing a simple yet accurate extraction algorithm for use in this thesis. The algorithm compares the measured S_{ij} parameters, expressed as a magnitude and phase angle component, to a database of simulated S_{ij} parameters. Each S_{11}, S_{12}, S_{21} and S_{22} parameter pair represents a complex permittivity value, consisting of a dielectric constant and loss factor component. The best fit to the experimental data, is used as the effective complex permittivity of

the material under test. Based on a minimisation procedure the effective dielectric properties are extracted accurately and precisely.

The Database Extraction Algorithm should deliver highly accurate and stable results over a range of frequencies, which would make it the preferred extraction method over that of the Nicholson Ross Weir algorithm.

2.5 Conclusions

Chapter 2 presented basic microwave fundamentals and introduced the reader to the electromagnetic spectrum. A short historical account is given for the use of microwaves which dates back to the 1940's when radar communication systems was developed during World War II (Meredith, 1998). This led to the first commercially available microwave oven in 1951 (Osepchuk, 1984).

The use of microwaves, as an adjunct to comminution had been identified as a possible means to reduce the energy demand on a typical mineral processing plant.

The dielectric property of concern, namely the complex permittivity, is introduced. The permittivity of a material comprises the real (dielectric constant) and imaginary parts (dielectric loss factor), both of which are important parameters used in the design of microwave applicators. The magnitude of these parameters describes the behaviour of the material in an electromagnetic field.

The literature survey focussed on some specific studies that measured the dielectric properties of a material under test. The works of Talbot et al., 2002, Louw, 2005 and Nelson 2008 identified particle size, void space between individual material particles, material composition and temperature as key parameters that influence the measured dielectric properties of a material under test.

Various mathematical extraction algorithms are used to convert the magnitude and phase angle components of the transmitted and reflected low power microwaves (S_{ij} parameters) from and through the sample, to the complex permittivity of the material under test.

Commonly available algorithms such as the NRW and BJ algorithms are known to be inadequate for a dielectric window-sample-window sample holder configuration. This has led to the development of a DBE Algorithm.

Chapter 3

Dielectric Property Measurement Techniques

3.1 Introduction

In Chapter 3, the coaxial probe and waveguide dielectric property measurement techniques are discussed. The waveguide technique is used for all dielectric property measurements included in this thesis (Section 3.2). Fundamental waveguide theory is presented in Section 3.2.1.1 which focuses on waveguide sizing, waveguide cut-off frequency and electromagnetic modes within a waveguide. The experimental setup, comprising a newly design waveguide sample holder and ANA, is presented in Section 3.2.1.2. The newly designed sample holder exhibits distinct advantages over its predecessor used in a study by Louw, 2005.

The four S_{ij} parameters, S_{11}, S_{12}, S_{21} and S_{22}, used in this thesis for dielectric property extraction of the material under test are discussed in Section 3.2.1.3.

The chapter presents a conclusion of the main findings in Section 3.3.

3.2 Dielectric Property Measurement Systems

A number of different techniques exist to measure the complex permittivity and permeability of a material. These techniques can be categorised into two distinct groupings:

- Resonant techniques and
- Reflection-transmission techniques

Resonant techniques suffer from two main disadvantages. Firstly, resonant techniques can only measure the permittivity or permeability of a material during one dielectric property measurement. In order to measure the other dielectric property, another separate dielectric

property measurement needs to be conducted. Secondly, each of these measurements is for a single frequency and is therefore not suitable for broadband frequency measurements.

However, reflection transmission line techniques measure the complex permittivity and permeability of a material over a large frequency range from 1-3 GHz (Venkatesh, Raghavan, 2005)

Two transmission line techniques commonly used to measure the dielectric properties of materials are:

- The coaxial probe technique
- The waveguide transmission line technique

A discussion on both these dielectric measurement techniques will follow. The emphasis however, will be on the waveguide measurement technique as all measurements included in this thesis are conducted using a newly designed waveguide measurement for use in this thesis.

3.2.1 Waveguide Transmission Measurement System

3.2.1.1 Waveguide Theory

A waveguide is a metal duct structure that allows for the propagation of electromagnetic waves at and above a certain frequency. This frequency is known as the critical cut-off frequency, which is a function of the particular waveguide system being used. Pozar, 1998, gives the specific cut-off frequency for a particular mode as follows:

Equation 6: Mode cut-off frequency for rectangular waveguide

$$f_{c\,mn} = \frac{1}{2\pi\sqrt{\mu^*\varepsilon^*}}\sqrt{\left(\frac{m\pi}{a}\right)^2 + \left(\frac{n\pi}{b}\right)^2}$$

In Figure 3 a metallic sectioned waveguide structure is presented. Dimension c is referred to as the thickness of the ore sample cavity.

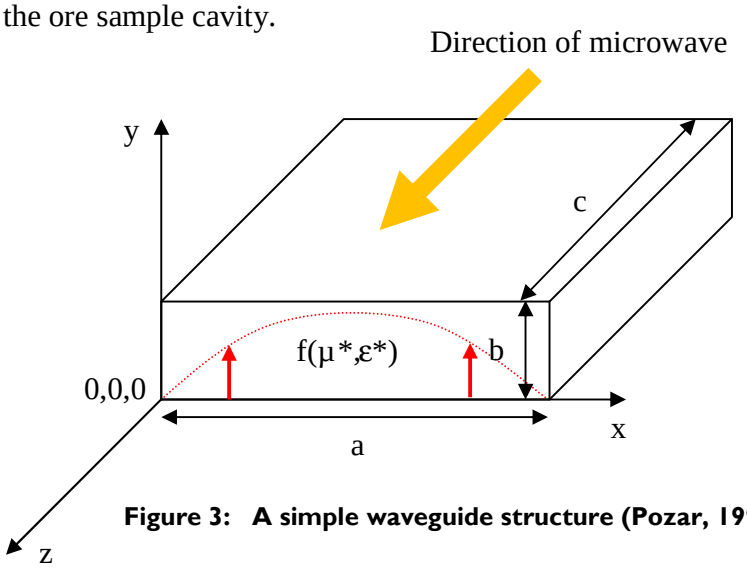

Figure 3: A simple waveguide structure (Pozar, 1998)

The TE_{10} mode, where the electromagnetic field is transverse to the direction microwave propagation in the waveguide, is the dominant mode for all rectangular waveguide systems having. The "1" and "0" refer to the single half sinusoidal variation in the x and y planes. For a full graphical representation of the magnitude of the magnetic and electric field distributions in $TE_{10,}$ refer to Pozar, 1998.

When substituting m=1 and n=0 Equation 6 it is observed that for a rectangular waveguide the cut-off frequency is a function of only the specific permittivity and permeability of the material as well as the width of the waveguide (dimension a in Figure 3) as shown in Equation 7:

Equation 7: TE_{10} mode cut-off frequency

$$f_{c\,10} = \frac{1}{2a\sqrt{\mu^{*}\varepsilon^{*}}}$$

In Equation 7, ε* and μ* are the complex permittivity and complex permeability respectively.

The wavelength of the TE_{10} mode changes as it enter the waveguide and is termed the guide wavelength (Kraus, 1999). The guide wavelength is calculated by means of Equation 8:

Equation 8: Guide Wavelength

$$\lambda_g = \frac{\lambda_0}{\sqrt{\varepsilon_r^* \mu_r^* - \left(\frac{\lambda_0}{\lambda_c}\right)^2}}$$

For ores with a dielectric constant of the order of 3, the guide wavelength of the ore would be approximately 75 mm at 2.6 GHz. The dielectric window thickness is set at 35 mm, which is smaller than half the guide wavelength (37.5 mm). This restricts the presence of the haf guide wavelength anomaly.

The waveguide technique will induce measurement error if the sample thickness of the material is an odd multiple of half a guide wavelength long. This is referred to as the half guide wavelength anomaly. The anomaly causes a large degree of S_{ij} parameter measurement uncertainty. It is therefore important that a parameter extraction algorithm be used that will not only test for the presence of this anomaly but also corrects the S_{ij} parameter.

Waveguides are classified according to their physical geometrical dimensions. Two systems are of importance for this thesis, namely WR284 and WR340 of which the latter is the larger of the two. Both these standard waveguide sizes permit the evaluation of the dielectric properties of the material under test at 2.45 GHz.

Table 1: Standard waveguide dimensions and cut-off frequency (Pozar, 1998)

Waveguide System	Sample Holder Dimensions (mm)			Sample Holder Volume (mm^3)	Recommended Frequency Range (GHz)	TE_{10} Cut-off Frequency (GHz)
	a	b	c			
WR 284	72.14	34.03	35	85.92	2.60 – 3.95	2.078
WR 340	86.36	43.18	35	130.52	2.20 – 3.30	1.736

3.2.1.2 Experimental Dielectric Property Measurement Setup and Design

Louw, 2005, modelled and measured the microwave heating and properties of multiphase materials using a standard WR284 waveguide size. Crushed particulate ore material was placed within a defined sample volume within the rectangular waveguide duct, which made up the sample holder.

The sample holder design suffered from three distinct shortcomings:

1. The sample holder thickness of 20 mm and 25 mm limited the amount of crushed ore that could be loaded into the sample cavity. If the average particle size is of the order of 20 mm, the effect of the sample holder size becomes more apparent due to the wall effects of the cavity. This affects not just the extracted dielectric are determined.
2. The limited cavity thickness limits the particle size of the material that could physically fit into the sample cavity. The latter placed an upper bound on the size of the particles that could be loaded and subsequently measured during the investigation.
3. The crushed ore particles were kept inside the ore cavity using two thin sheets of transparency. This caused bulging to occur at the extremities of the sample cavity, which introduced measurement error due to the variable thicknesses of the sample cavity amongst different dielectric property measurements.

This led to the need for an improved waveguide sample holder system to be designed and constructed from mild steel for use in this thesis. This will specifically address the shortcomings experienced with the previous sample holder. Refer to Appendix I for the design drawings for both the WR284 and WR340 sample holders.

Figure 4 illustrates the newly designed experimental setup used for both the WR284 and WR340 dielectric property measurements of crushed mineral ore.

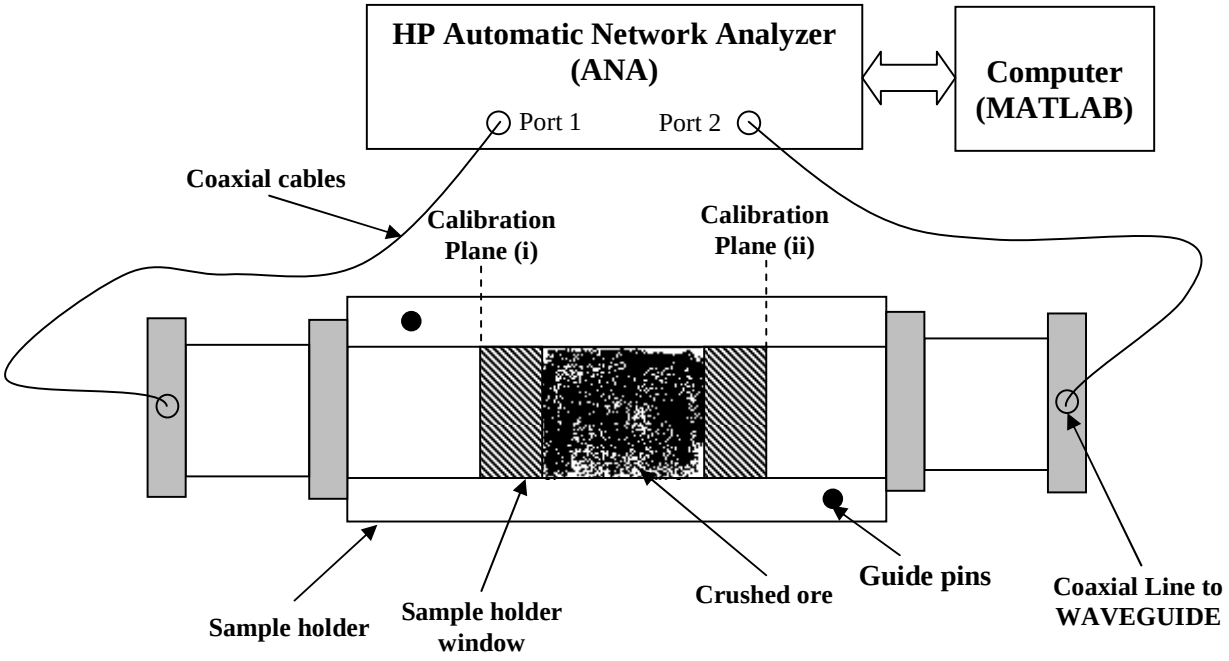

Figure 4: Designed experimental measurement setup

The main components of the experimental setup used are:

Trough shaped sample holder design

The base of the sample holder is rectangular in shape, which ensures that the holder stays stable at all times. The holder is fitted with a detachable lid, providing easy loading/unloading of the sample cavity between individual dielectric property measurements. Guide pins ensure that the lid is securely fitted onto the base of the sample holder. The different ores are placed in the ore sample cavity via the lid that is bolted onto the trough-shaped base, collectively forming the waveguide structure. The material of construction for both the sample holders was chosen to be mild steel as it provides a high degree of mechanical machinability with a high resistance to wear.

Automatic Network Analyzer (ANA: HP 8510)

An ANA generates the microwaves, which are then transmitted from Port 1 through a coaxial cable into the sample holder via the coaxial/waveguide transition port. The microwave will then propagate through the waveguide from left to right through the window-sample-window configuration and exits the system again at the coaxial/waveguide transition port and back into the ANA at Port 2.

Coaxial Line /Waveguide Transition Ports

The sample holder is fitted with two Coaxial/Waveguide Transition Ports on either side of the holder. The ports introduce the generated microwaves into the waveguide structure. These transitions are located in the middle of the waveguide geometry.

PET Sample Holder Windows

The crushed ore particles are kept in position by two firm and rigid blocks, called sample holder windows, made from isotropic PET (polyethyleneterathylate) that collectively form the sample cavity. PET offers excellent machinability and exhibits a high resistance to wear.

The rigid PET windows fit tightly into the waveguide and ensure that the sample holder volume is fixed and rigid. To ensure that minimal S_{ij} parameter measurement error occurs, a window thickness of 20 mm was chosen. The tight fit of the windows ensures perfect electromagnetic contact between the windows and mild steel waveguide structure. The particle size distribution of interest in this thesis is -26.5+2 mm. To minimise the wall effects of the sample holder (Section 3.2.1.2), the PET windows are placed 35 mm apart in an effort to minimise the wall effects of the waveguide structure on the extracted dielectric constant and loss factor.

For larger sample holder sizes it is believed that the effect of the sample holder walls is reduced and that the measured S_{ij} parameters will be more representative of the actual dielectric properties, in comparison to the S_{ij} parameters when using smaller sample holders. The larger sample holder size will eliminate the half guide wavelength anomaly.

Desktop Computer

The computer unit serves as interface between the ANA and the person conducting the experiments. All the necessary data files is transferred from the ANA to the computer.

3.2.1.3 Waveguide Scattering Parameters (S_{ij}-parameters)

After a full 2-port calibration (Section 6.3) of the ANA, the dielectric properties of the material under test can be determined by means of the measured scattering parameters. These parameters, better known as S_{ij} parameters, can mathematically inverted, using an extraction algorithm, to the desired dielectric properties.

The scattering parameters originate from the reflection and transmission of microwaves within the waveguide as they travel through the window-sample-window configuration. From Figure 5 it is observed that the four S_{ij} parameters of concern are S_{11}, S_{12}, S_{21} and S_{22}. Each parameter is an indication of the degree of adsorption and or reflection the incident microwaves experience as they enter the waveguide at the coaxial/waveguide transition ports and passes through the material under test.

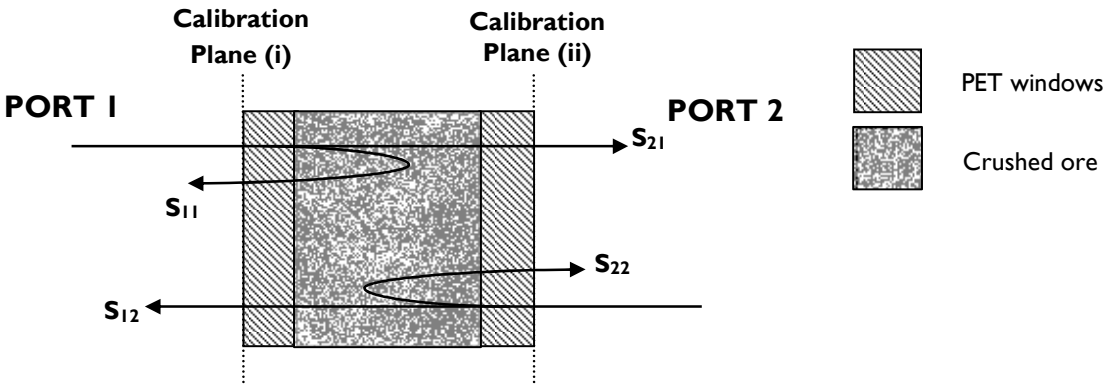

Figure 5: S_{ij} scattering parameters at Port 1 and Port 2 of the ANA

The S_{ij} parameters are defined as follows:

S_{11}: The S_{ij} parameter represents the fraction of incident microwaves, entering the waveguide at Port 1, which are reflected by the material under test/dielectric windows to the ANA via the coaxial line to waveguide transition port and coaxial cable lines at Port 1

S_{12}: The S_{ij} parameter represents the fraction of incident microwaves, entering the waveguide at Port 2, which pass through the material under test/dielectric windows and which are returned to the ANA via the coaxial line to waveguide transition port and coaxial cable lines at Port 1.

S_{21}: The S_{ij} parameter represents the fraction of incident microwaves, entering the waveguide at Port 1, which passes through the material under test/dielectric windows and which are returned to the ANA via the coaxial line to the waveguide transition port and coaxial cable lines at Port 2.

S_{22}: The S_{ij} parameter represents the fraction of incident microwaves, entering the waveguide at Port 2, which are reflected back by the material under test/dielectric windows via the coaxial line to waveguide transition port and coaxial cable lines at Port 2.

Each of the S_{ij} parameters is a voltage ratio, consisting of a magnitude and phase angle component. Both the components are a function of frequency. Section 6.12 discusses the variation of the magnitude and phase angle components for different crushed particle size classes.

The orientation of the material under test, within the sample cavity, is a key consideration (Louw, 2005). For isotropic materials the (S_{11}; S_{22}) and ($S_{12;}$ S_{21}) parameter pairs will be equal as the dielectric properties of the material under test are not influenced by its orientation in the electromagnetic field. For an anisotropic material the (S_{11}; S_{22}) and ($S_{12;}$ S_{21}) parameter pairs will not be equal.

3.3 Conclusions

Chapter 3 discussed the available measurement techniques for the measurement of the complex permittivity of a material under test. A short overview of the coaxial probe measurement technique was provided. The waveguide measurement technique was discussed and was chosen as the technique for all dielectric property measurements included in this thesis. Fundamental waveguide theory was presented alongside the experimental measurement setup and sample holders used. The dielectric property windows in each of the sample holders provide for a defined and fixed volume in which the material under test is located. The waveguide cut-off frequency, guide wavelength and the half a wavelength anomaly were discussed.

Two standard sized waveguide sample holders, measuring 72.14 x 34.03 x 35 mm and 86.36 x 43.18 x 35 mm respectively, are used for all dielectric property extractions included in this thesis. The size of the waveguide sample holder configuration is believed to be a key parameter in the measurement of the dielectric properties of the material under test as it determines the amount of crushed material that can fit into a sample cavity.

The four S_{ij} parameters, which are expressed as a magnitude and phase angle component of the transmitted and reflected low power microwaves through and from the sample, are presented. The complex dielectric properties are extracted from the measured S_{11}, S_{12}, S_{21} and S_{22} scatter parameters via a suitable mathematical algorithm.

Chapter 4

Crushed Ore Properties

4.1 Introduction

In Chapter 4, the ores of interest are described. The mineral phase analysis for each of the ores is discussed (Section 4.2). The Copper Carbonatite, Porphyry Copper and Quartz Monzonite Porphyry Copper ores, are all copper bearing ores that contain both microwave transparent gangue and microwave absorbent mineral phases (Table 2). The particle size distribution (Section 4.3) and bulk ore sample preparation procedure (Section 4.4) are presented and discussed. A standard vibratory sieve test is used to classify the crushed material into each of the particle size classes of interest. The representative ore sampling procedure is discussed (Section 4.5).

The chapter presents a conclusion of the main findings in Section 4.6.

4.2 Ore Mineralogy

The ores investigated in this thesis are a copper carbonatite, porphyry copper and a quartz monzonite porphyry copper ore, all of which are copper bearing.

The mineralogy for each of the three copper ores was reported in confidential reports, which formed part of previous joint experimental investigation conducted by The University of Nottingham and Stellenbosch University and e2v technologies. The ore mineralogy for copper carbonatite was determined using QEMSEM analysis, whilst for mineralogy for porphyry copper and quartz monzonite porphyry copper ore was determined using Mineral Liberation Analysis.

The ore mineralogy for each of the three copper ores is given in Table 2. Only the most dominant contributing mineral phases in the microwave absorbent and transparent groups are given.

Table 2: Ore Mineralogy

Mineral Ore	Microwave Adsorbent/ Transparent	Mineral Name	Chemical Composition	Weight %
Copper Carbonatite	Absorbent	Magnetite	Fe_3O_4	43
		Spinel	$MgAl_2O_4$	1.1
		Chalcocite	Cu_2S	0.3
	Transparent	Calcite	$CaCO_3$	29.4
		Olivine	$(Mg,Fe)_2[SiO_4]$	10.2
		Apatite	$Ca_5(PO_4)_3(OH,F,Cl)$	7.5
Porphyry Copper	Absorbent	Pyrite	FeS_2	23.1
	Transparent	Quartz	SiO_2	34.2
		Pyrophyllite	$Al_2Si_4O_{10}(OH)_2$	17.6
		Illite	$(K,H_3O)(Al,Mg,Fe)_2(Si,Al)_4O_{10}[(OH)_2,(H_2O)]$	11.2
Quartz Monzonite Porphyry Copper	Absorbent	Hematite	Fe_2O_3	17.2
		Chalcopyrite	$CuFeS_2$	2.9
		Pyrite	FeS_2	0.6
	Transparent	Plagioclase feldspar	$(Na,Ca)(Al,Si)_4O_8$	42.7
		Quartz	SiO_2	18.7

Copper carbonatite ore contains 43% microwave absorbent magnetite, porphyry copper ore 34% microwave transparent quartz and quartz monzonite porphyry copper 43 wt% microwave transparent plagioclase feldspar mineral phase. The ore density for each of the ores was experimentally determined by a water displacement technique (Appendix B). The densities for

porphyry copper, copper carbonatite and quartz monzonite porphyry copper ore were experimentally determined as 2428 kg/m^3, 2891 kg/m^3 and 2447 kg/m^3 respectively.

4.3 Particle Size Distribution of Interest

The particle size distribution of interest is chosen to be -26.5+2 mm for each of the copper ores. For particle sizes below 2 mm, it becomes increasingly difficult to establish a large enough electromagnetic field in the applicator, at economical energy inputs, to induce micro cracks within the ore matrix, as substantial damage to the ore is not obtainable.

The particle size distribution was divided into eight size classes using a $\sqrt{2}$ sieve series, *viz.* -26.5+16 mm, -16+11.2 mm, -11.2+8 mm, -8+6.7 mm, -6.7+5.6 mm, -5.6+4.75 mm, -4.75+3.35 mm and -3.35+2 mm. The sieving was done using a standard vibratory sieve shaker with a sieve duration of 15 minutes. The largest and smallest aperture sized sieves were 26.5 mm and 2 mm respectively. The combined mass in each particle size class formed a cumulative particle size distribution. Appendix A gives the vibratory sieve test results for each of the ores.

The -26.5+16 mm size class was chosen as the largest size class based for three reasons:

1. Both the WR284 and WR340 waveguide sizes are small. This limits the size and amount of ore particles than can physically fit into the waveguide sample holder. The wall effects of the sample cavity will also become more prominent with increasingly larger particle sizes.

2. Current microwave applicators, at The University of Nottingham, limit the particle size of ore material to $d_p \approx 30$ mm.

3. For the ores of interest the bulk of the received material had a particle size, d_p, smaller than 30 mm. After crushing (Section 4.4), enough material is collected in each of the particle size classes of interest. The arithmetic mean of the upper and lower limits for each particle size class is used to each of the particle size classes.

4.4 Crushed Ore Sample Preparation

The ores used in this thesis were provided by The University of Nottingham and could be classified into three categories:

- Material that was crushed into particle size classes of interest for use in this thesis.
- Material that was crushed previously into size classes of which the particle sizes are not of interest for use in this thesis.
- Material that was crushed previously and for which the particle size distribution was unknown.

For the ore material in the latter two categories, the ore samples were crushed again to generate enough material in each of the particle size classes of interest (Section 4.3).

Particle size classes were generated with the aid of a jaw and cone crusher at the Department of Process Engineering, University of Stellenbosch.

4.4.1 Jaw Crusher

During the primary crushing phase a jaw crusher was used to reduce the particle size of the largest particles first. The crusher consists of a moveable crushing jaw pivoted at the top. As the material is fed to the crusher the jaw crushes the material against a fixed plate discharging the product into a collection pan.

Figure 6: Cone and jaw crusher (University of Stellenbosch)

The closed side setting, the smallest distance between the fixed crushing plate and moving jaw, wa adjusted to produce a range of different crushing particle sizes. It was found by experiment that a large amount of crushed material was produced in each of the size classes over the entire -26.5+2 mm particle size distribution when the aperture size was set at approximately 8 mm.

4.4.2 Cone Crusher

Following the primary crushing phase, a portion of the primary crusher product was used as feed material to the cone crusher (refer to Figure 6) The material was crushed to generate enough ore in each of the lower particle size classes.

Crushing is facilitated when the feed material is trapped between the rotating cone and the outer metal cone of the cone crusher. The crushed material is collected in a collection pan. It was found by experiment that a large amount of secondary crushed material was produced in the particle size classes for $\bar{d}_p$ < 8 mm when the cone aperture size was set to approximately 5 mm.

4.4.3 The Vibratory Sieve Test

Following the primary and secondary crushing steps, it is essential to establish the particle size distribution of the crushed material to ensure that enough material were generated in each of the particle size classes to *completely* fill a WR284 and WR340 sample cavity. This was achieved with the aid of a Vibratory Sieve Test (VST) using a number of sieves stacked on top of each other. The largest aperture sized sieve (26.5 mm) is placed at the top of the stack with the smallest aperture sized sieve (2 mm) at the bottom. Figure 7 illustrates a standard vibratory sieve setup.

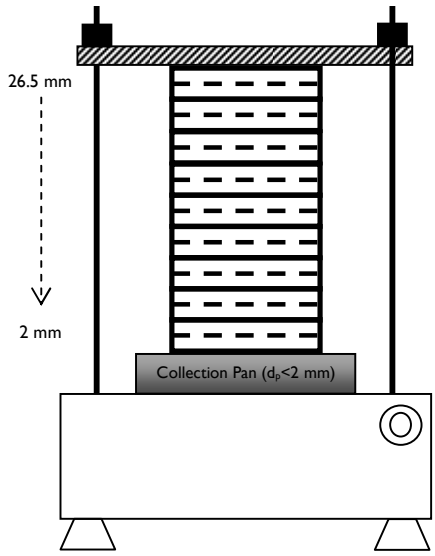

Figure 7: Apparatus used during the vibratory sieve test

The material was loaded onto the mesh of the top sieve. The sieves were secured with a circular metal disc at the top of the sieve stack. The sieves were sandwiched together between the metal disc and surface of the sieve shaker.

The vibration of the sieve shaker causes the crushed ore particles to fall through the mesh of each of the sieves in a step-wise fashion retaining only the fraction crushed material with a $\bar{d}_p$ larger than the aperture size of the sieve. Crushed particles with $\bar{d}_p$ < 2 mm were collected in the collection pan. After 15 minutes the shaker was stopped and the crushed material collected on each sieves are bagged. The combined mass in each particle size class forms a cumulative particle size distribution.

4.5 Representative Sampling

In order to obtain enough representative crushed material in each of the particle size classes for both the WR284 and WR340 sample cavities, riffle splitters were used.

In this thesis two riffle splitters were used to representatively split the crushed material load with an average passing-size of 6 mm (marked A) and 24 mm (marked B) respectively (Refer to Figure 8).

(a) (b)

Figure 8: Riffle splitters – (a) passing-size 6 mm and (b) passing-size 24 mm

Riffle splitter A wa used to sample particles with $\bar{d}_p \leq 6$ mm and splitter B wa used to sample particles with $\bar{d}_p \leq 24$ mm.

Riffle splitting has the following distinct advantages:

- Only a small quantity of material is lost during the sampling process. It is essential to preserve as much of the original crushed ore as possible for future experimental investigations.
- Riffle splitters serve as an excellent mass reduction tool and provides for fast and effective splitting of the material.

The representative sampling procedure is illustrated in Figure 9:

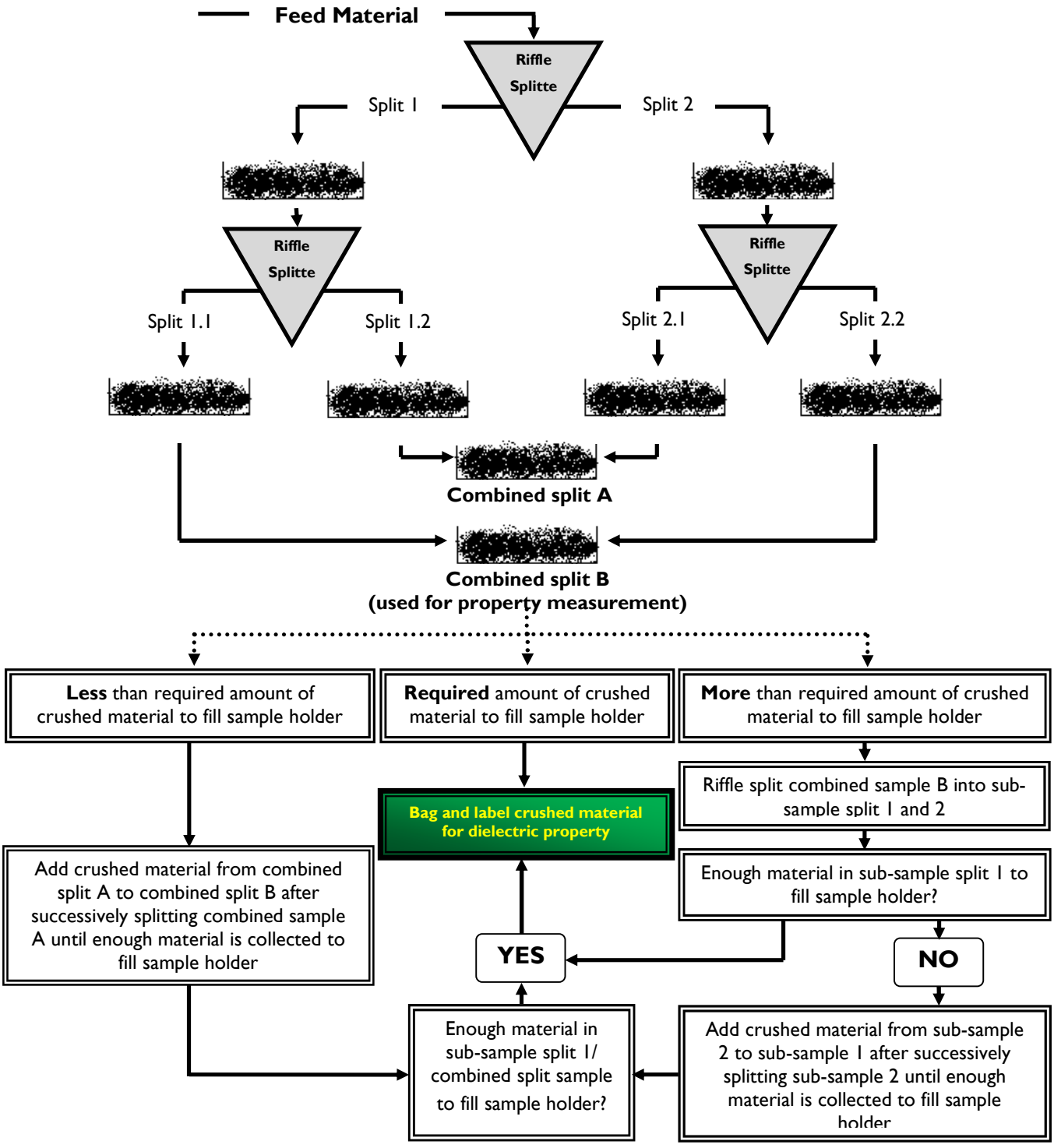

Figure 9: Riffle splitting representative sampling procedure

In a standard riffle splitting procedure the mass of the ore material that is fed to the splitter is halved. Theoretically, two representative samples are available after one splitting cycle, and four representative samples if these two halves are again individually split during splitting cycle 2.

The amount of crushed material that can be loaded into a sample cavity is ultimately a function of $\overline{d}_p$:

- The *larger* the average d_p, the *smaller* the amount of material that can fit into each of the sample cavities due to wall effects.
- The *smaller* the average d_p, the *larger* the amount of material that can fit into each of the sample cavities. Wall effects are less prominent.

The riffle splitting procedure is divided into four sections:

1. Crushed ore sample splitting section.
2. Sub-sample combination section.
3. Mass evaluation section.
4. Mass sub-sample modification section.

Each of the splitting components will be discussed in Sections 4.5.1 – 4.5.4.

4.5.1 Crushed Ore Sample Splitting

A mass of crushed material, with a known size distribution,is fed to a riffle splitter. The material is introduced to the chutes with the aid of laboratory pan to ensure that all the chutes receive the same amount of feed material.

Split cycle 1, SC 1, produces two sub-samples, Split 1 and Split 2. During SC 2, Split 1 is again fed to the riffle splitter, in the same fashion as in SC1, to generate two smaller sub-samples, Split 1.1 and Split 1.2. Split 2.1 and Split 2.2 are generated in the same manner.

4.5.2 Sub-Sample Combination

Up till this point in the sampling procedure four smaller sub-samples were generated to be used as individual representatives samples, however not one of these samples alone is enough to fill the WR284 and WR340 sample cavities. This implies that more than one sub-sample needs to be taken as a combined representative sample to fill the holders to its designed capacity.

It was decided to enhance the statistical reliability, due to a greater degree of particle randomness, of the riffle splitting procedure by combining all odd and even numbered splits and therefore:

- Splits 1.2 and 2.1 are combined to form Combined Split A
- Splits 1.1 and 2.2 are combined to form Combined Split B

Two combined splits are therefore available to be used as representative sub-samples, which were randomly generated with a high degree of particle mixing induced by the chutes of the riffle splitter. For the rest of this thesis Combined Split B will be used as the primary crushed ore material source.

4.5.3 Mass Evaluation

The amount of crushed material in Combined Split B needs to be evaluated to ensure that enough material has been generated in the Sub-Sample Combination step of the riffle splitting procedure to completely fill a WR 284 and WR 340 sample cavity. The mass evaluation step establishes if crushed material needs to be added or removed from Combined Split B in order to completely fill a sample cavity for either two of the WR 284 and WR 340 sample holders.

4.5.4 Combined Split Mass Modification

Following the Mass Evaluation step, Combined Split B can either have too much or too little crushed ore to fill WR 284 and WR 340 sample cavity. To ensure that only the required amount of material is available two possible scenarios arise:

1. Removing crushed material from Combined Split B if there is more than the required amount of crushed material with the combination of Splits 1.1 and 2.2. The additional material is then added to Combined Spit A.

   This procedure starts off by splitting Combined Split B again with the aid of the riffle splitter into two smaller sub-sample splits. If there is enough crushed material in Split 1 to fill the sample holder, then the procedure is stopped and the material is bagged and labelled for future use. If there is not enough material in Split 1 then additional material is required from Split 2. The procedure followed will be called Successive Split Adding (SSA) due to the fact that before any material is added to Split 1 material from Split 2 is again split into two subsections of which only one is added to Split 1. In turn the particle randomness is increased. The whole procedure is repeated until enough crushed material is collected to fill both the WR 284 and WR 340 sample cavities.

2. Adding crushed material to Combined Split B if not enough crushed material is formed with the combination of Splits 1.1 and 2.2. The additional material is obtained from Combined Split A.

   SSA will again be employed as in the case when removing crushed material, the only difference being that instead of taking material from one of the sub-samples obtained from riffle splitting Combined Split B, Combined Split A is used to fill the sample holder.

Appendix C presents a brief overview of the different representative sampling methods that are commonly used.

4.6 Conclusions

For each of the ores under investigation, the mineral composition consists of different wt% microwave absorbent and transparent gangue mineral phases. The ore mineralogy is believed to affect the dielectric properties of the ore. A standard vibratory sieve test was used to generate each of the particle size classes. Riffle splitters were used to generate representative samples in each of the particle size classes of interest.

Chapter 5

Crushed Ore Packing Density

5.1 Introduction

In Chapter 5, the focus is shifted to the determination of the fractional packing density (Section 5.2) of the crushed ore samples in each of the particle size classes for both standard WR284 and WR340 waveguide sizes. The fractional packing density serves as a measure to establish the fraction void space between the individual crushed ore particles in each of the particle size classes and sample holders. The effects of ore cavity thickness and waveguide size are investigated in Section 5.3.1 and Section 5.3.2 respectively.

The chapter presents a conclusion of the main findings in Section 5.4.

5.2 Fractional Packing Density

The minimum and maximum fractional packing density, $\theta_{max/min}$, serves as indication of the amount of particulate material that can fit into the sample cavities. The packing density is affected by two factors:

1. The size of the waveguide sample holder (WR284 and WR340)
2. Particle size of the material of interest

For a larger particle size, less material will be able to fit into the sample cavity, which will decrease the fractional packing density due to wall effects for the constrained sample holders used in this thesis. Smaller sized particles reduce the wall effect, hence increasing the fractional packing density.

The fractional packing density is determined by establishing the amount of crushed material, for a specific particle size class, that is required to fill the sample holder. The average mass of three loadings is obtained and denoted as $\bar{m}_i$.

The average particle volume is determined by Equation 9.

Equation 9: Average particle volume

$$\bar{V}_{particle} = \frac{\bar{m}_i}{\rho_{ore}}$$

The average volume packing fraction is determined as the fraction of the available sample cavity volume that is occupied by crushed particulate material.

Equation 10: Average Volume Packing Fraction

$$\theta_{average} = \frac{\bar{V}_{particle}}{V_{sample\ cell}}$$

The maximum and minimum particle volume fractions, denoted as $\theta_{\max}$ and $\theta_{\min}$ respectively, are determined by replacing $\bar{m}_i$ in Equation 9 by either the maximum or minimum mass loadings. The fractional packing densities for crushed Porphyry Copper, Copper Carbonatite and Quartz Monzonite Porphyry Copper ore are included in Appendix D for both the WR284 and WR340 sample holders (35 mm sample cavity thickness).

5.3 Effect of Ore Cavity and Sample Holder Size on Particle Packing Density

Studies conducted by Fouché, 2003, and Louw, 2005, used a sample cavity thickness of 20 and 25 mm for a standard WR284 waveguide size (Figure 3, dimension c).

The sample holder size raised three concerns:

1. Not all of the available larger sized particles fits into the sample holder cavities. This gives rise to large voidage in the sample holder.

2. It is expected that the dielectric property measurement error will increase with increasing particle size due to the wall effects of the constrained sample cavity becoming increasingly larger.

3. How does a larger sample holder affect the particle fractional packing density of crushed ore and the subsequent dielectric property measurement?

In Section 5.3.1 the effect of the sample cavity thickness is investigated for a WR284 sample holder using a sample cavity thickness of 20 mm and 25 mm respectively. This was done by determining the fractional packing density of a representative sample of crushed Porphyry Copper ore for three different particle size classes namely -31.5+26.5 mm, -12.5+9.5 mm and -4.75+0 mm (Appendix D). The distinctly individual particle size classes will aid in determining which particle size class has the largest effect on the particle fractional packing density.

In Section 5.3.2 the effect of a larger sample holder is investigated by comparing the fractional packing density of a representative amount of crushed Porphyry Copper Ore in the -31.5+26.5 mm, -12.5+9.5 mm and -4.75+0 mm particle size classes using a WR284 and WR340 sample holder, both with a sample cavity thickness of 35 mm.

5.3.1 Effect of Waveguide Sample Holder Thickness

To determine the effect of the sample cavity thickness the fractional packing density of crushed porphyry copper ore was determined for a WR284 sample holder with a cavity thickness of 20 mm and 25 mm respectively for each of the particle size classes presented in Section 4.3.

The average fractional packing density of 3 samples has been used.

The results are illustrated in Figure 10 and Figure 11.

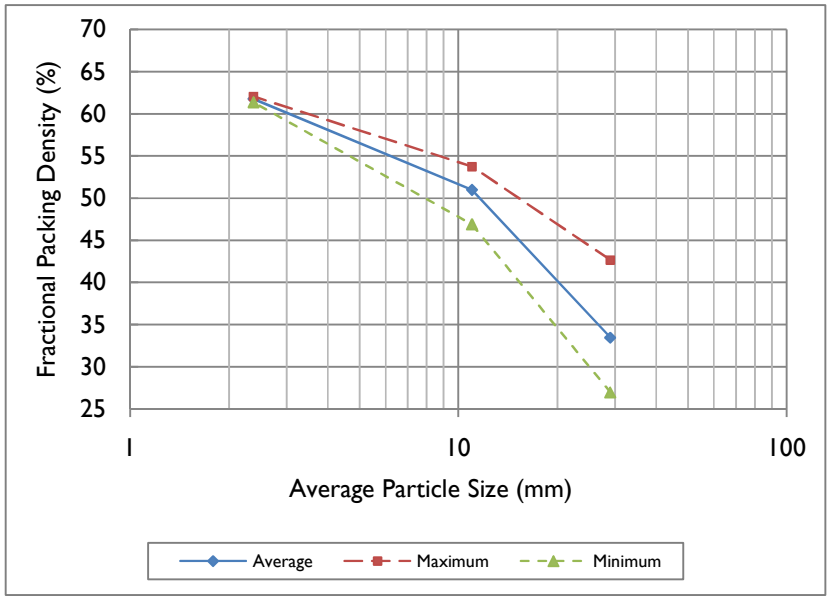

Figure 10: Fractional packing density as function of d_p (WR284, holder thickness 20 mm)

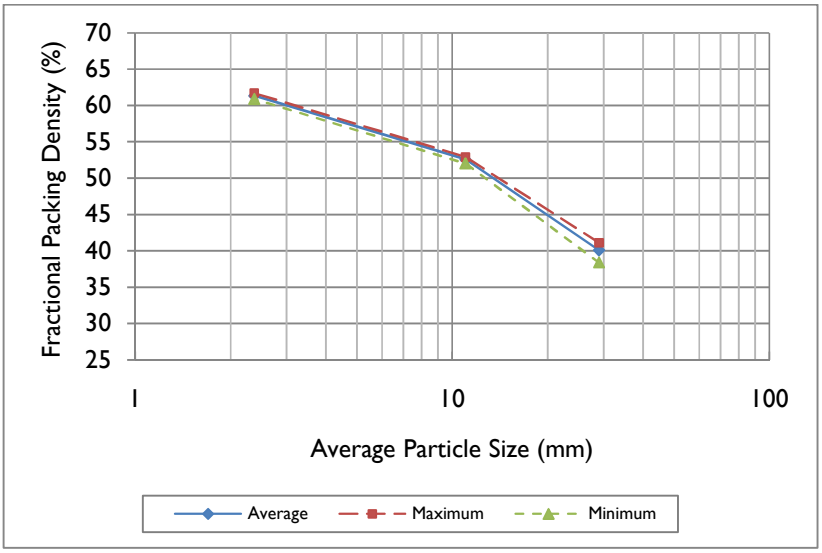

Figure 11: Fractional packing density as function of d_p (WR284, holder thickness 25 mm)

From Figure 10 and Figure 11 the following were concluded:

- The crushed ore fractional packing density decreases with increasing particle size irrespective of the sample cavity thickness. The wall effect of the sample holders is smaller for the 25 mm thick sample holder, which is evident in the decrease in the minimum and maximum variation from the average volume fractional pacing density compared with the 20 mm thick sample holder.

- With increasing particle size, reproducibility in the fractional packing density decreases. This will also be the case for the ore dielectric properties. With increasing particle size, the dielectric constant and loss factor for the same particle size class will deviate between successive dielectric property measurements. This is attributed to the spatial variation between individual particles of increased size. For smaller sized particles, the particulate load is spatially more homogeneous when compared with larger sized particle sizes.

- For sample holders, of which the dimensions are of the same order of magnitude as the particle size, packing reproducibility of the crushed particulate load becomes poor, which will require more dielectric property measurements to be conducted in order to obtain a average complex permittivity value for the material under test.

This suggests the use of a sample holder with a sample cavity thickness larger than 20 mm and 25 mm used by Louw, 2005.

A 35 mm thick sample cavity wa chosen to be used throughout this thesis for both WR 284 and WR 340 sample holder sizes.

The advantage is twofold:

- A larger sample holder size will lessen the wall effects of the sample holder, which will in turn increase the reproducibility between individual dielectric property measurements.
- More crushed ore material will be able physically fit into each sample cavity, which will in turn better represent industrial mass loadings versus the constrained ore cavity size used by Louw, 2005.

Appendix D presents the fractional packing densities obtained for a sample cavity thickness of 20 mm and 25 mm in WR284 for crushed Porphyry Copper ore.

The effect of the larger 35 mm thick sample holder is illustrated in Figure 12:

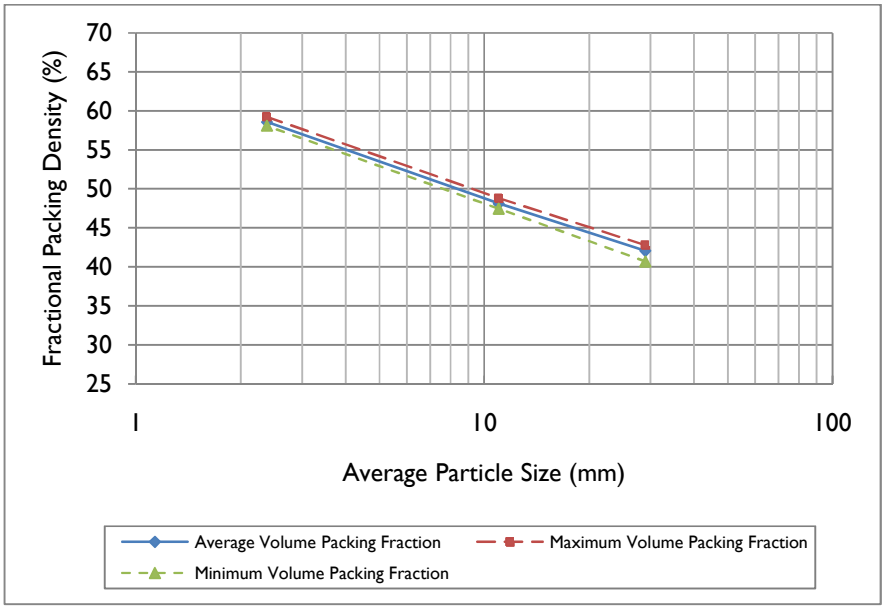

Figure 12: Fractional packing density as function of d_p (WR284, holder thickness 35 mm)

From Figure 11 and Figure 12 the following is concluded:

- When the sample cavity is of the same magnitude as the particle size, the wall effect is still significant. This is observed in the divergent behaviour for both sample cavity thicknesses at larger particle sizes.

- A trade-off exits between the fractional packing densities obtained for smaller and larger particle sizes. The obtained fractional packing density for a *35 mm* cavity thickness is less than for a 25 mm thickness for $\overline{d}_p$ < 20 mm. At $\overline{d}_p$ ≥ 20 mm for a *35 mm* sample cavity thickness, however the packing density *increases* compared with a *25 mm* sample cavity thickness. This observation clearly indicates that as particle size *increases*, so should the size of the waveguide sample cavity.

Appendix D presents the fractional packing density obtained for a sample cavity thickness of 25 mm and 35 mm in WR284 for crushed Porphyry Copper ore.

5.3.2 Effect of Waveguide Sample Holder Size

The effect of the sample holder size is investigated by comparing the fractional packing densities obtained for a WR284 and WR340 waveguide system using a sample cavity thickness of 35 mm. A representative crushed sample of Porphyry Copper for the -31.5+26.5 mm, -12.5+9.5 mm and -4.75+0 mm particle size classes. The results are graphically illustrated in Figure 13 and Figure 14.

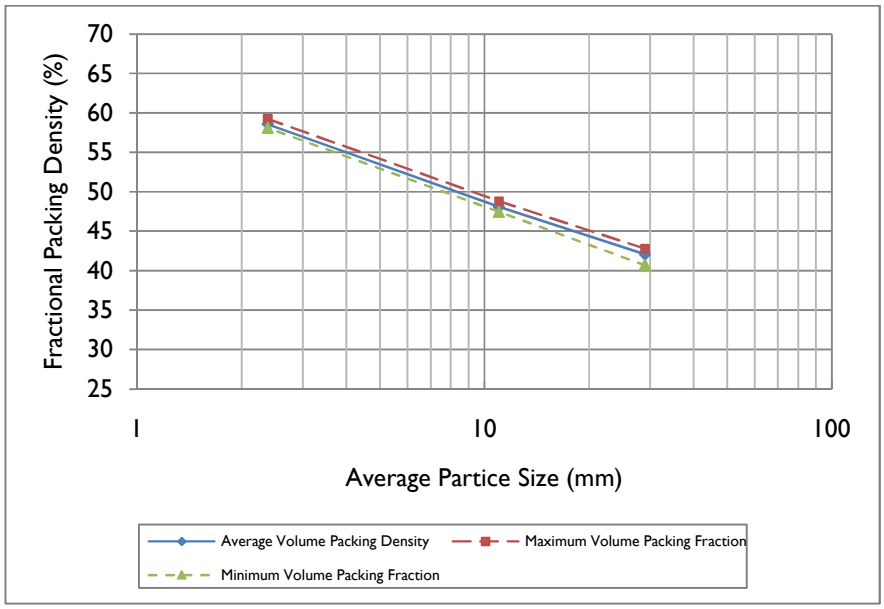

Figure 13: Fractional packing density as function of d_p (WR284, holder thickness 35 mm)

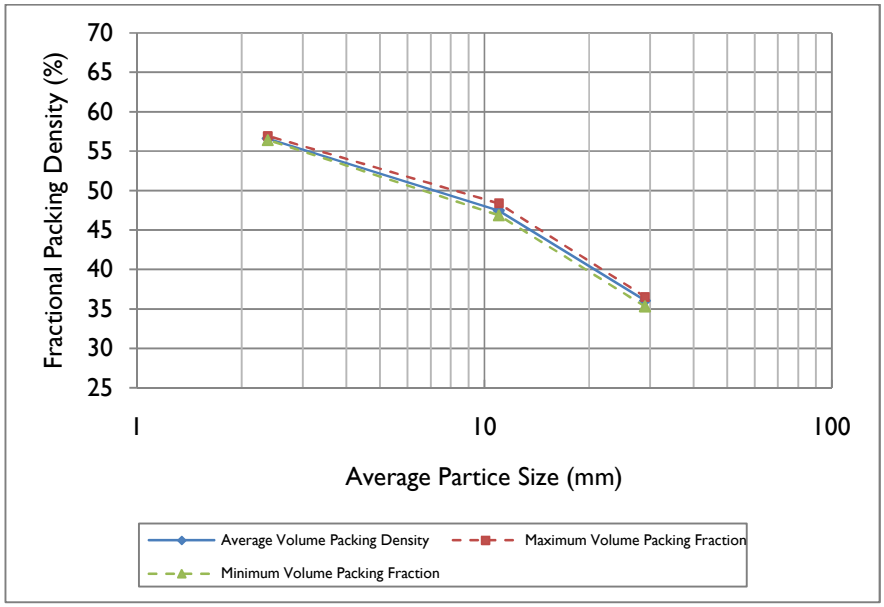

Figure 14: Fractional packing density as function of d_p (WR340, holder thickness 35 mm)

From Figure 13 and Figure 14 it can be seen that two regions are clearly distinguishable:

- The first region is marked by the similarity between the fractional packing density obtained using a WR 284 and WR 340 standard waveguide size. This tendency is observed in the -12.5+0 mm particle size interval.

- The second region is marked by a difference in the obtained fractional packing density between the two standard waveguide sizes for the -31.5+26.5 mm particle size interval. Especially for the WR 340 waveguide size a decrease in the fractional packing density is observed with increasing particle size compared with that of the WR284 waveguide size.

This observation suggests that a trade-off exists between the particle size of the crushed material to be loaded into a sample cavity and the size of the waveguide used. Although the WR340 waveguide is larger than its WR284 counterpart, it does not necessarily allow for the addition of larger sized particles in the sample holder cavity. This results in a smaller amount of larger sized particles that can be loaded into the WR340 sample cavity, with a subsequent decrease in the fractional packing density. This effect is not only due to the particle size of the crushed particulate load, but more so the combined particle-wall-effect of the sample cavity.

5.4 Conclusions

In Chapter 5, the effect of particle and sample holder size is investigated and quantified by means of the fractional packing density.

It is concluded that the fractional packing density of crushed Porphyry Copper ore varies significantly for a sample cavity thickness of 20 mm and 25 mm respectively. The latter is evident especially for larger particle size classes that exhibited a decrease in the fractional packing density for both waveguide WR284 and WR340 sample holder sizes. For a larger sample cavity thickness, the wall effect decreases and fractional packing density increases. Based on the findings a sample cavity thickness of 35 mm is chosen for WR284 and WR340 sample holder.

For the larger WR340 sample holder the wall effect of the sample cavity is reduced. The observed fractional packing density obtained for both sample holders suggested that a trade-off exists between the particle size of the crushed particulate load and the sample cavity and size of the waveguide used for dielectric property measurement.

Chapter 6

Analysis of Dielectric Property Measurement and Extraction

6.1 Introduction

Chapter 6 will focus on the measurement of the S_{ij} parameters which are used to determine the dielectric constant and loss factor for each of the particle size classes, for each of the ores of interest in both the WR284 and WR340 sample holders. In Section 6.2 the measurement settings for the ANA are provided. The calibration standards, which include a sliding matched load, fixed matched load, offset short circuits and a "thru" standard, for dielectric property measurement are discussed in Section 6.3, followed by the calibration procedure. The isolation, reflection and transmission calibration sequences are provided as part of the ANA calibration.

A Database Extraction (DBE) Algorithm is used to extract the dielectric constant and loss factor from the measured S_{ij} parameters (Section 6.4). The DBE Algorithm fits the measured S_{ij} parameters to a set of simulated S_{ij} parameters. The goodness of the experimental fit is evaluated based on a metric value. The DBE Algorithm, the electromagnetic modelling of the sample holders, search algorithm and metric are discussed Section 6.4. The selection of the frequency interval size over which the DBE Algorithm fits the measured S_{ij} parameters is discussed in Section 6.5 and Section 6.6.

The effect of cut-off frequency in the WR284 and WR340 sample holders is discussed in Section 6.7.1 and Section 6.7.2 respectively. The dielectric property measurement of polypropylene as reference material and polytethyleneterathalyte as window material is presented in Section 6.8 and Section 6.9 respectively. The importance of ANA port selection is discussed in Section 6.10.

The extracted dielectric constant and loss factor over 100 MHz, 250 MHz and 700 MHz frequency intervals for the -26.5+2 mm particle size distribution for Porphyry Copper ore is presented and discussed in Section 6.11.1, Section 6.11.2 and Section 6.11.3 respectively.

In Section 6.12.1 and Section 6.12.2, the magnitude and phase angle of the measured S_{22} parameter are compared to the simulated S_{22} parameter over 100 MHz, 250 MHz and 700 MHz frequency intervals for the -16+11.2 mm particle size class for crushed porphyry copper ore for two successive ANA dielectric property measurements. In Section 6.12.3 a summary of the comparison of the magnitude and phase angle of the S_{ij} parameters are provided.

The chapter provides a conclusion of the main findings in Section 6.13.

6.2 ANA Setup for Material Properties

Prior to dielectric property measurements the following settings were selected on the ANA:

- The ANA was left running for 15 minutes prior to calibration and dielectric property measurement. This was to ensure that thermal stability was reached which will in turn increase the repeatability of all the measurements.
- Step mode was selected for the frequency sweep.
- The averaging factor was set at 128. A average factor of 128 allows for a trade-off between the accuracy of the dielectric property extraction and the speed by which the measurements is executed.
- The starting frequency, f_{start}, was chosen to be 2.1 GHz, which falls within the frequency band of interest.
- The ending frequency, f_{end}, was chosen to be 3 GHz, which falls within the frequency band of interest.
- 201 frequency points, N, were measured within the desired frequency range. The ANA sectioned the operational frequency band into smaller 4.5 MHz frequency intervals. For each of these bands the ANA reports four S_{ij} parameters, expressed as a magnitude, $|S_{ij}|$, and phase angle, $\angle S_{ij}$, component.

- The characteristic impedance, Z_0, within the offset length was set to 1Ω.

Connectors were cleaned using liquid n-butyl acetate. A torque wrench was used to tighten the standard military adapter (SMA) to ensure that the connectors make the same contact with the coaxial/waveguide transition ports and to prevent a over-tightening that might damage the connectors. During the connection of the coaxial cables to the ANA and sample holder, a static wristband was worn. This ensured that no static interference was present.

The same phase stable SUCCOFLEX 104 coaxial cables were used for every measurement. This ensures physical consistency between measurements and limits equipment error. Bending and movement of the cables were kept to a minimum to prevent phase swift and thermal drifting of the equipment. All the experiments were carried out at room temperature. The room temperature was not controlled.

6.3 Full 2-Port ANA Calibration

The 2-Port Waveguide Error Model accounts for twelve possible measurement errors. In each of the measurement directions six errors are recorded (Fouché, 2004). These errors are compensated for by means of a full 2-Port ANA calibration prior to any dielectric property measurements. The aim of the calibration is to increase the accuracy of the measured magnitude and phase of the S_{11}, S_{22}, S_{12} and S_{21} scatter parameters (HP Product Note 8510-5A, 1985).

To compensate for possible errors in the equipment (e.g. systematic, random and drift), the calibration procedure uses known electrical standards, located at different places on the Smith Chart, in the calibration procedure. The ANA identifies and determines the magnitude of the measurement error and subsequently eliminates it from subsequent dielectric property measurement.

The calibration standards comprise a sliding load, short, open and THRU connections. The calibration standards used in this thesis are discussed in Sections 6.3.1 and 6.3.2.

6.3.1 Calibration Standards

6.3.1.1 Sliding Matched Load

The sliding matched load consists of a metallic waveguide fitted with a carbon foam wedge flanged to the coaxial/waveguide transitions. At S-band frequencies the sliding load provides an accurate impedance standard at frequencies exceeding 2 GHz. This multi-position load enables the determination of the directivity vector by eliminating the terminal impedance. Figure 15 graphically represents the sliding load:

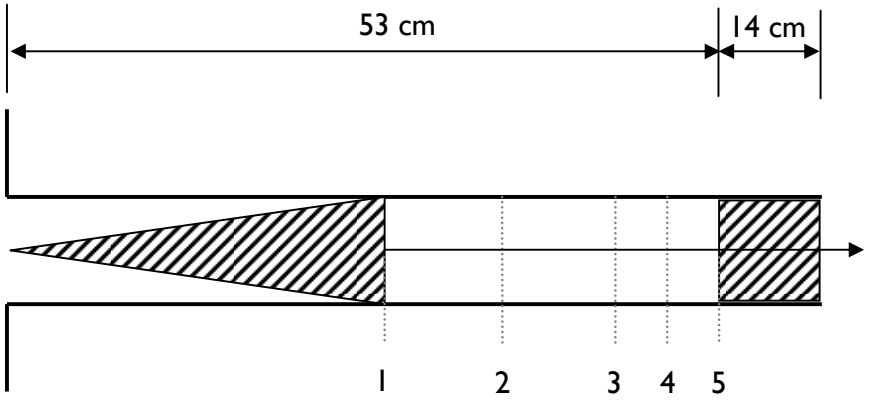

Figure 15: Sliding matched load – positioning of carbon wedged foam (Louw, 2005)

The sliding load is fitted with a second piece of carbon foam, which terminates the microwave energy at the end of the sliding matched load. This is due to the waves not being reflected at the end of the carbon foam wedge at position 1 (Figure 15). This results in a measurement error, called the sliding load offset error, which will affect all the dielectric property measurements to be conducted (Louw, 2005).

Louw, 2005, gives a detailed account as to how to compensate for this sliding load offset error by means of a polyfit function in Matlab® which "smoothes" the measured S_{ij} parameter data.

6.3.1.2 Fixed Matched Loads and Offset Short Circuits

Both the fixed matched loads and offset short circuits are metallic waveguide metallic standards, with known length, used during the calibration procedure of the ANA.

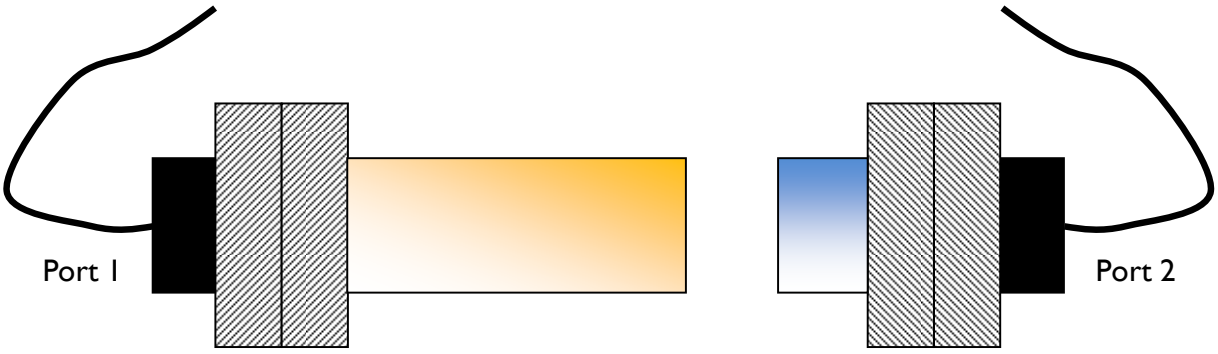

Figure 16: ANA calibration standards - fixed matched load and offset short circuits

The ANA uses the standards to identify errors in the equipment, and compensate for them. Both the loads and circuits have a known location of the Smith Chart. During the calibration procedure, the ANA determines the position of the loads and circuits on the Smith Chart. As both these standards have a fixed known position on the Smith Chart, the difference is compensated for through a mathematical matrix correction calculation.

6.3.1.3 THRU standard

The THRU calibration standard is formed by connecting the coaxial to waveguide transition ports to one another. This creates a standard with no length as shown in Figure 17.

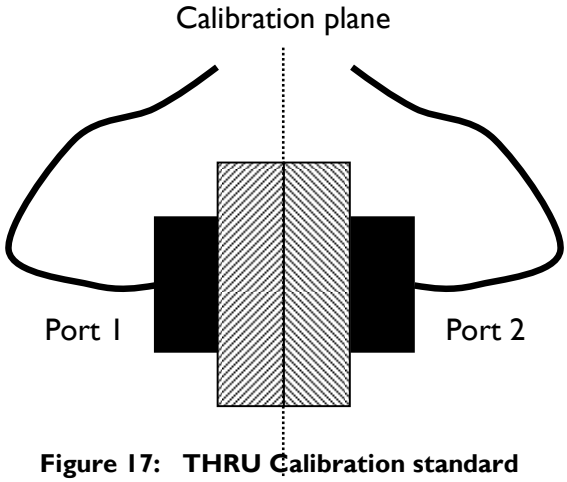

Figure 17: THRU Calibration standard

As the reference plane is located at the coaxial/waveguide transition interface, the THRU standard should have a zero electromagnetic delay, capacitance and inductance. Should any of the parameters be measured during the calibration procedure, it is compensated for and eliminated from the dielectric property measurement.

6.3.2 Calibration Procedure

6.3.2.1 Isolation

During the isolation step of the calibration procedure the sliding load is connected to Port 1 of the ANA and the fixed matched load to Port 2. A forward and reverse isolation step is performed.

6.3.2.2 Reflection

After isolation, still with the loads connected as before, a reflection step is implemented consisting of a number of sub-steps.

Firstly, the sliding load is calibrated at Port 2 for each of the five carbon foam wedge positions illustrated in Figure 15. When the port calibration with the sliding load is completed, the loads are switched and the sliding load is connected to Port 1 of the ANA. Hence, the fixed matched load is connected to Port 2 and calibrated. Port 1 is calibrated with the sliding load, for each of the five (5) carbon foam wedge positions. The reflection step is concluded when Port 1 is calibrated with the fixed matched.

Following the reflection step, both offset short circuits are connected in turn to Ports 1 and 2, calibrated individually, in any preferred order.

6.3.2.3 Transmission

During the transmission calibration, the systematic load match error is determined (HP Product Note 8510-5A, 1985). The shorts are disconnected from the coaxial/waveguide transitions and

are flanged together with no calibration standard between them. A forward (Port 1 to 2) and reverse (Port 2 to 1) transmission match is carried out in any preferred order. The transmission step allows for the load match and frequency response of S_{21} and S_{12} to be measured (HP Product Note 8510-5A, 1985). After the 2-port calibration procedure is completed, the sample holders are connected to the coaxial/waveguide transitions.

6.4 The Database Extraction (DBE) Algorithm

6.4.1 Background

The measured S_{ij} parameters provide an indication of the amount of absorption and reflection that microwaves undergo when passing through a crushed load of particulate ore contained within a waveguide structure. The S_{ij} parameters are expressed in terms of the magnitude $|S_{ij}|$ and phase angle, $\angle S_{ij}$, components. Both ε' and ε'' values for the material can be extracted from the measured S_{ij} parameter data using well established algorithms such as the Baker Jarvis Extraction Algorithm (Baker-Jarvis, 1990).

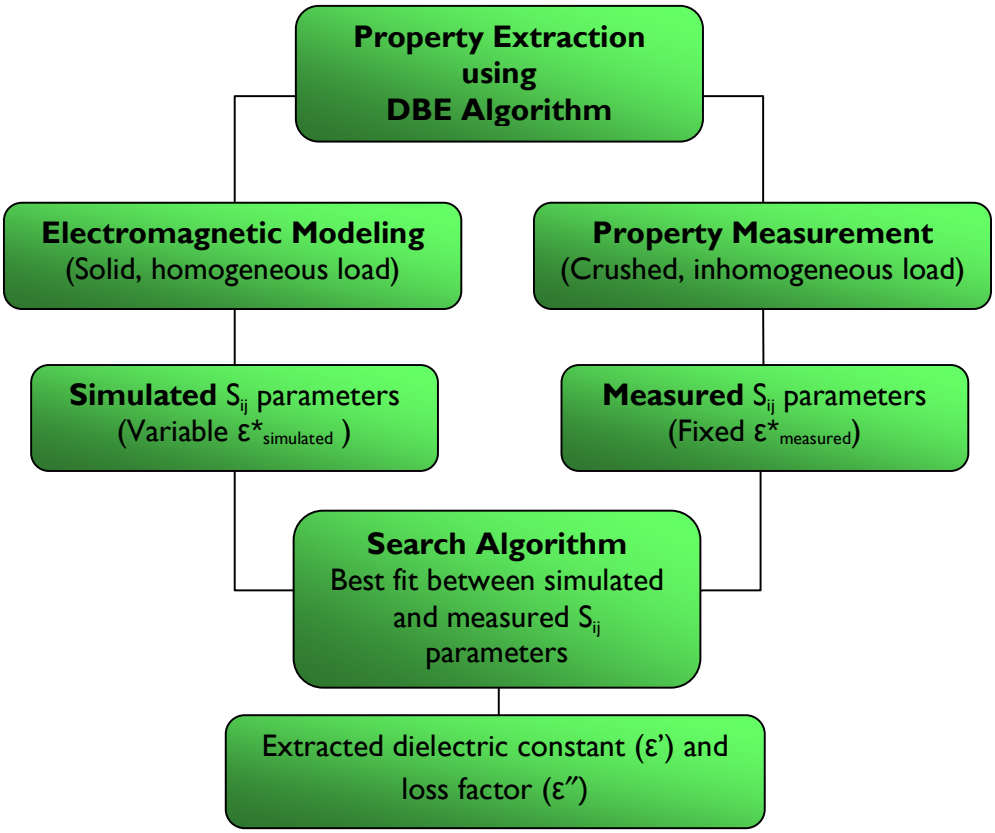

Figure 18: Flow diagram for the DBE Algorithm

The sample holders, shown in Figure 5, incorporate dielectric windows for the location of the material under test. The extraction of dielectric properties from S_{ij} parameter measurements is problematic using standard algorithms (e.g. Nicholson Ross Weir, 1970, Baker-Jarvis, 1990) in such cases. Accordingly a new Database Extraction (DBE) Algorithm was developed. Figure 18 provides a flow diagram for the major components of the DBE Algorithm.

In the DBE Algorithm, a database of scattering parameters is established through electromagnetic simulation of the measurement system. A *search algorithm* is used to determine the effective complex permittivity of the modelled load whose scattering parameters provide the best fit to the experimental data. In electromagnetic modelling the simulation of the sample cavity (filled with crushed ore) is done using a solid, homogeneous load to represent the particulate load.

To design microwave applicators through simulation, the complex permittivity of the material under test is required. A typical microwave applicator is 3 m in length, and it is therefore computationally impractical to use a mesh-size that could resolve each individual mineral phase within the ore particles. Furthermore it is not known how to make a geometrically tractable representation of the inhomogeneous, multiphase, irregular particles where the phase-specific properties of the ore are unknown. This results in a model with too many degrees of freedom.

Although methods do exist for representing complex structures such as 2D sections of ore particles, at least as binary particles, this can be done only with a grid resolution of the order of 0.1 mm which is incompatible with the scale of the applicator structure. Hence, a model is used that represent the properties of a particulate load using effective bulk properties.

6.4.2 Electromagnetic Modelling

Both sample holders (WR284 and WR340) were modelled in QuickWave3D®, a Finite Difference Time-Domain (FDTD) simulation. Figure 19 represents a 3-D model of the simulated sample holders.

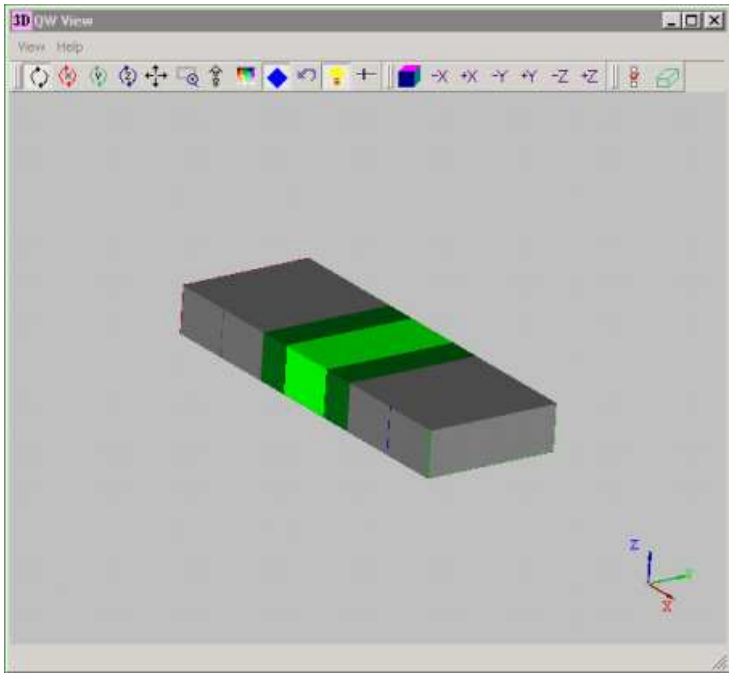

Figure 19: QuickWave® electromagnetic simulation of waveguides

The x, y and z-dimensions used for the 3D modelling of the WR284 and WR340 sample holders are provided in Table 1. The grey sections (between the dashed blue lines and the dark green sections, x=35 mm) represent the coaxial/waveguide transitions connected to the ANA ports. The dark green sections (x=25 mm) represent the PET sample holders windows that enclose the sample cavity (light green area, x=35 mm) in Figure 5. The electromagnetic simulation uses a solid, homogeneous load (light green section), with the complex permeability set to unity, to represent the crushed ore load in the sample cavity for both the WR284 and WR340 sample holders. The z-dimension for WR284 is 34.04 mm. For the WR340 sample holder the z-dimension is 43.18 mm.

The QuickWave3D® model in Figure 20 indicates the electromagnetic configuration of the simulated sample holder ports. The red port (left-hand side, QW Port 1) generates the electromagnetic energy for simulation. The green port (right-hand side, QW Port 2) absorbs the electromagnetic energy generated by QW Port 1.

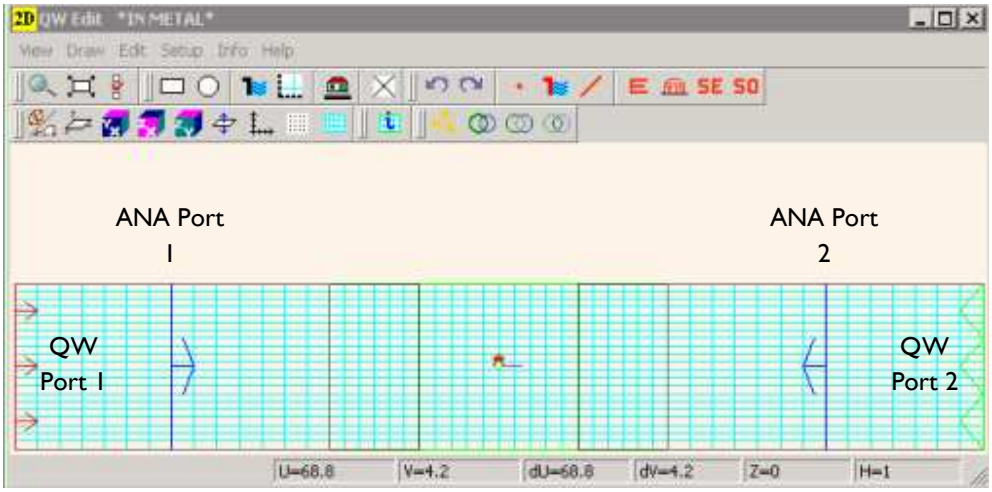

Figure 20: QuickWave3D® Electromagnetic modelled sample holder (WR284 and WR340)

QuickWave3D® governs the placement of the simulated and actual waveguide ports. The actual ANA ports correspond to the positioning of the blue markings in Figure 20. QW Port 1 and QW Port 2 is located at a distance from the actual ANA ports equal to the distance between the ANA port and PET sample holder window (35 mm). The latter ensures sufficient electromagnetic energy generation at QW Port 1. The S_{ij} parameters are measured from the actual ANA ports and is corrected by QuickWave3D® .

6.4.3 Simulated S_{ij} parameters: Database Generation

The sample cavity (filled with crushed ore) of the modelled sample holder(s) is represented by a solid homogenous block (Figure 19). Electromagnetic modelling of the sample holder provides the block with variable dielectric properties (ε'_{var} and ε''_{var}). Simulation of the measurement

system with ε'_{var} and ε''_{var} result in four QuickWave3D® simulated S_{ij}-parameters $\left(S_{11_{simulated}}, S_{12_{simulated}}, S_{21_{simulated}}, S_{22_{simulated}}\right)$.

For each simulated run (1, 2, …n) and different set of chosen $\varepsilon'_{var(1,2,\ldots n)}$ and $\varepsilon''_{var(1,2,\ldots n)}$ values, the simulation produces a set of 4 simulated $S_{ij\ simulated}$ values expressed as magnitudes and phase angle components for each of the S_{ij} parameters (Figure 21).

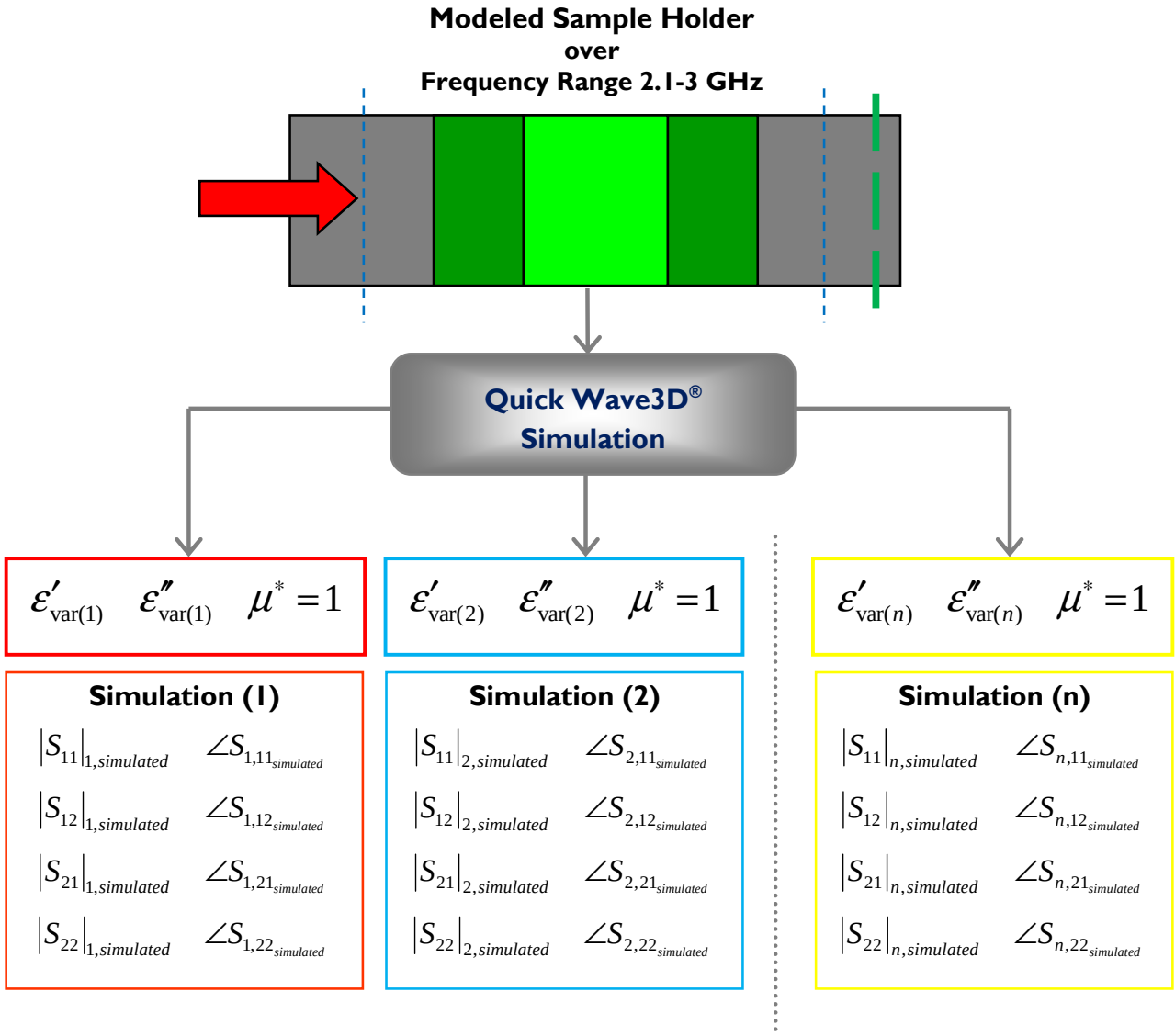

Figure 21: QuickWave3D® simulation process

For *n* simulations, 4*n* S_{ij} parameters are generated. Each of the simulated parameters is expressed in terms of a magnitude and phase angle component. Each of the four $S_{ij(simulated)}$ parameter sets represents 1 point in the complex permittivity plane (Figure 22).

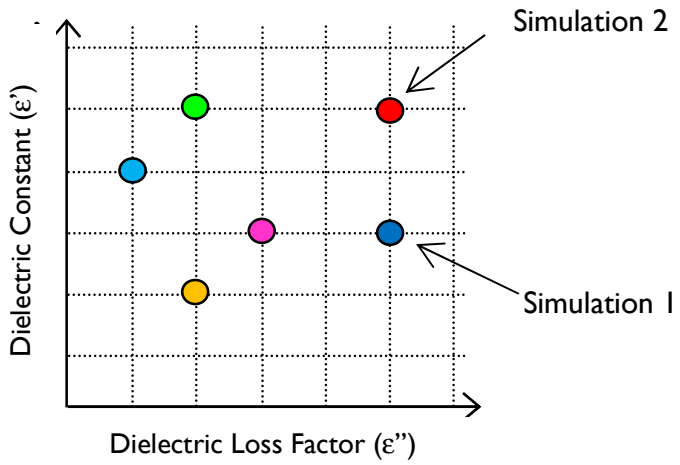

Figure 22: Simulated dielectric constant and loss factor

Each point in Figure 22 is generated in a structured approach. Using fixed intervals between values, a mesh (matrix) of simulated ε'_{var} and ε''_{var} -values is obtained in the complex permittivity plane. Table 3 summarises the parameters used for the generation of the DBE database for both WR284 and WR340 sample holders.

Table 3: Database Extraction Algorithm Parameters

Database Name	Database Size (files)	Intervals		Limits			
		$\varepsilon'_{simulation}$	$\varepsilon''_{simulation}$	$\varepsilon'_{simulation}$		$\varepsilon''_{simulation}$	
				Min	Max	Min	Max
DB 284_air_rem	230000	0.01	0.001	1.0	4.99	0	0.999
DB 340_air_rem	40000	0.01	0.01	1.0	4.99	0	0.99

It was assumed that for all three the copper bearing ores included in this thesis the complex permeability, $\mu^*=\mu'+j\mu''$, was constant and equal to unity cross the frequency spectrum.

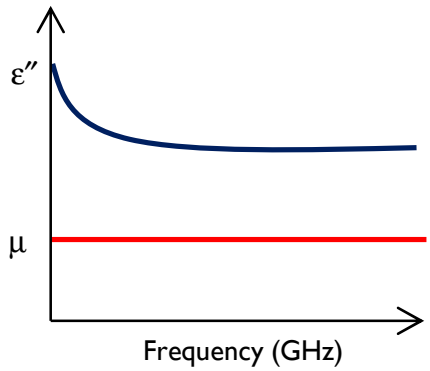

Figure 23: Correlation between dielectric loss factor (ε″) and dielectric permeability(μ*)

If it is possible to reproduce the observed behaviour well with such a model, it can be assumed that this model is adequate, and that the loads have been represented the behaviour well enough for the required purpose. Throughout the thesis the experimental data were well-fitted by the DBE Algorithm, and hence the model, assuming $\mu^*=1$.

This is applying the principle of Occam's Razor, whereby the simplest model that produces the desired results should be used. Provided that it is possible to obtain adequate fits for the required purpose, there is little benefit to be gained by increasing the model complexity. This would have made the database search space much larger, hence more computationally intensive, which could have been justified only if the fitting had been inadequate between the experimental and simulated S_{ij} parameters.

Taking into account that the DBE Algorithm models a crushed heterogeneous particulate load as a homogeneous block with effective dielectric properties, it is fair to assume that simulation of the sample holders with $\mu^*=1$, is not unreasonable.

A trade-off exists between the time spent to generate each database and the accuracy of the extracted ε' and ε''-values. For the **DB 284_air_rem** database the imaginary interval was chosen

to be 0.001 compared with 0.01 for the **DB 340_air_rem** database and hence a large difference in file size for each of the databases.

With the generation of the **DB 284_air_rem** database, a small dielectric loss factor interval was chosen to improve the experimental fit between the measured and simulated DB S_{ij} parameter in magnitude and phase angle component. However, after investigative property extractions it was concluded that the smaller mesh size did not significantly improve the goodness of fit and that the extraction itself was computationally expensive. The finer incremental size resulted in one extraction taking more than double the time to be completed compared with the extractions with the larger incremental frequency size.

Hence, for the generation of the **DB 340_air_rem** database, a larger mesh of 0.01 for the dielectric loss factor was chosen. The additional time spent generating the **DB 284_air_rem** database, with smaller mesh intervals, does not justify the apparent increase in the accuracy of the extracted values.

Due to the larger **DB 284_air_rem** database, the extraction process is more computationally intensive with a longer extraction time needed compared with the **DB 340_air_rem** database. This is attributed to the larger amount of simulated datapoints that the DBE Algorithm needs to search through in order to identify the best experimental fit to the measured S_{ij} parameter set.

6.4.4 Search Algorithm

A *search algorithm* was used by the DBE Algorithm to determine the effective complex permittivity of the modelled load whose scattering parameters provide the best fit to the measured data. The goodness of the fit is represented by the metric, $\|\bullet\|_{Port\ 1,2}$, depending on the port that is used for the extraction of the dielectric properties. The *search algorithm* comprises the following steps:

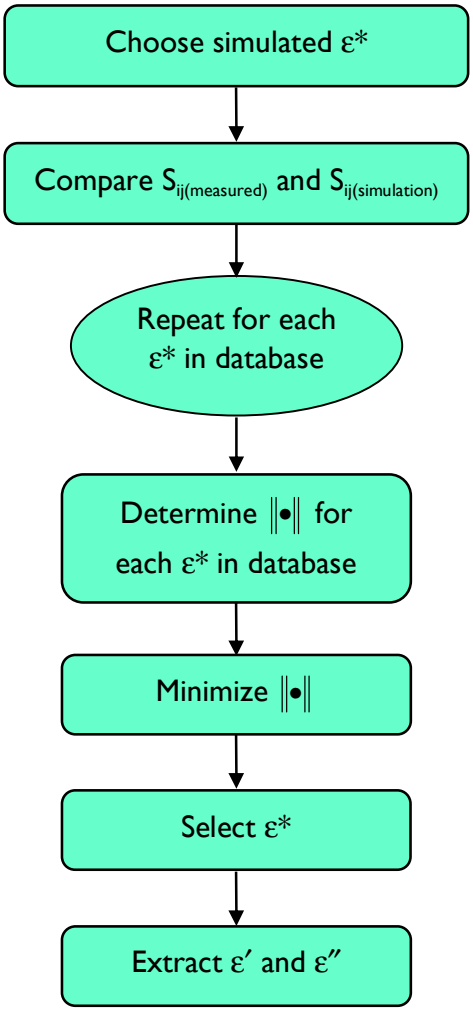

Figure 24: Flow diagram for the DBE search algorithm

The *search algorithm* compares $S_{ij(measured)}$ and $S_{ij(simulation)}$ (Section 6.4.3) in the database of S_{ij} parameter data points (Figure 22). Requena-Perez et al., 2005, used a fitness function (labelled in this thesis as a *metric*) to compare the measured and simulated scattering parameters. The variation in the magnitude and phase angle of the S_{ij} parameter was used to determine the quality of fit between the simulated and measured datasets.

After execution of the search algorithm the **`extract.py`** program (Appendix E) reports the metric as a minimum, $\|\bullet\|_{min}$, and maximum, $\|\bullet\|_{max}$, for the frequency interval of interest. The

metric limits represent a range of metric values obtained during property extraction for a specific defined frequency interval over which the DBE Algorithm is executed. Each frequency interval consists of a number of frequency points, which collectively represents a piece of the operational frequency band. The ANA sections the operational frequency band (2.1-3 GHz) into 201 frequency points. Only $\|\bullet\|_{min}$ is used to ascertain the quality of the experimental fit.

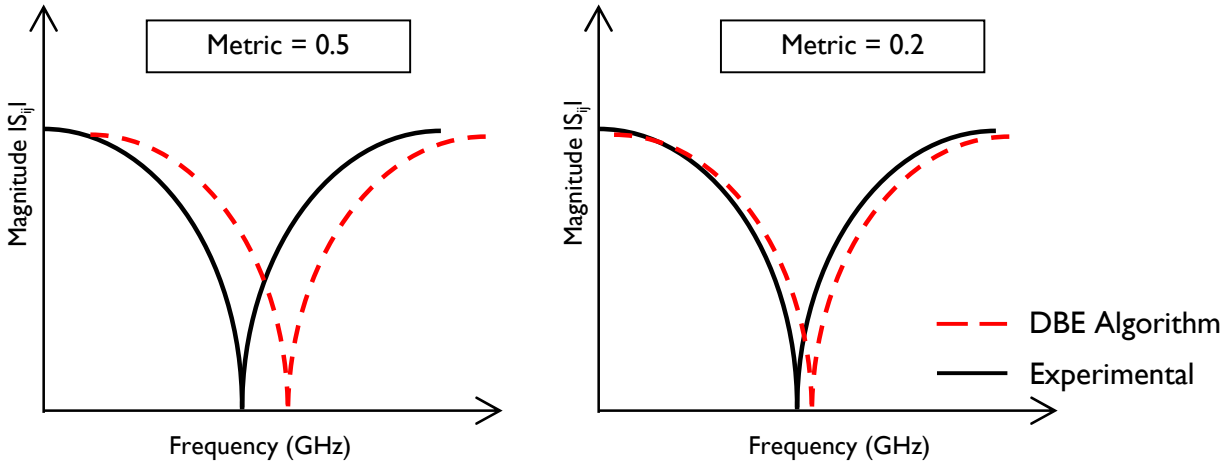

Figure 25: Experimental S_{ij} parameter fitting

The DBE Algorithm uses the database of simulated S_{ij} parameters to fit to the experimental measured S_{ij} parameter set. For each of the simulated data sets, the extent to which it corresponds to the measured S_{ij} parameter is ascertained by the magnitude of $\|\bullet\|_{min}$.

The smaller the value of $\|\bullet\|_{min}$, the better the goodness of the fit to the experimental dataset (Figure 25). The simulated data set that minimises the metric, is selected by the *search algorithm* and the effective ε* is extracted.

The metric, shown in Equation 11, is a weighted root mean squared variation function that is to be minimised by the DBE Algorithm (*search algorithm*) based on the best fit to the measured set of 4 S_{ij} parameters. The variation in the phase angle is normalised by 2π.

Equation 11: Metric

$$\|\bullet\| = \sum_{i=1}^{2}\sum_{j=1}^{2}\sqrt{\frac{1}{N}\left(p\sum_{k=1}^{N}\underbrace{\left(\left|S_{ij}(k)\right|_{measured} - \left|S_{ij}(k)\right|_{simulation}\right)^2}_{\text{Magnitude Contribution}} + (1-p)\underbrace{\frac{\sum_{k=1}^{N}\left(\theta_{ij}(k)_{measured} - \theta_{ij}(k)_{simulation}\right)^2}{2\pi}}_{\text{Phase Angle Contribution}} \right)}$$

The metric sums the variation in the magnitude and phase angle components between the measured and simulated S_{ij} parameter. In Equation 11, the weighing factor, $p \in [0,1]$, is set at 0.50, giving equal contribution to the magnitude and (normalised) phase angle for each S_{ij} parameter in the determination of the metric. Requena-Perez et al., 2005, concluded that the inclusion of the phase angle contribution in the evaluation of the metric, ambiguous permittivity extraction is avoided. This is especially true for multilayered experimental configurations as used in this thesis. In Equation 11, N represents the number of frequency points in the frequency interval of interest over which the property extraction is performed.

6.4.5 Extracted Dielectric Properties

The DBE Algorithm requires the frequency band over which the dielectric property extraction to be specified (Section 6.5.3). The dielectric property extraction is executed over either narrower piecewise frequency intervals or over the entire operational frequency interval. As the characteristic trend of the S_{ij} parameter varies with frequency, the selection of the frequency interval over which the DBE Algorithm is performed is a key aspect.

For piecewise extractions the operational frequency band was segmented into smaller frequency intervals and the DBE Algorithm fitted the simulated S_{ij} parameter (coloured bands), in magnitude and phase angle, to the measured parameter (solid blue) in each of the frequency bands. For each of the frequency bands the goodness of fit between the parameters was quantified by the metric (Figure 26, (a)).

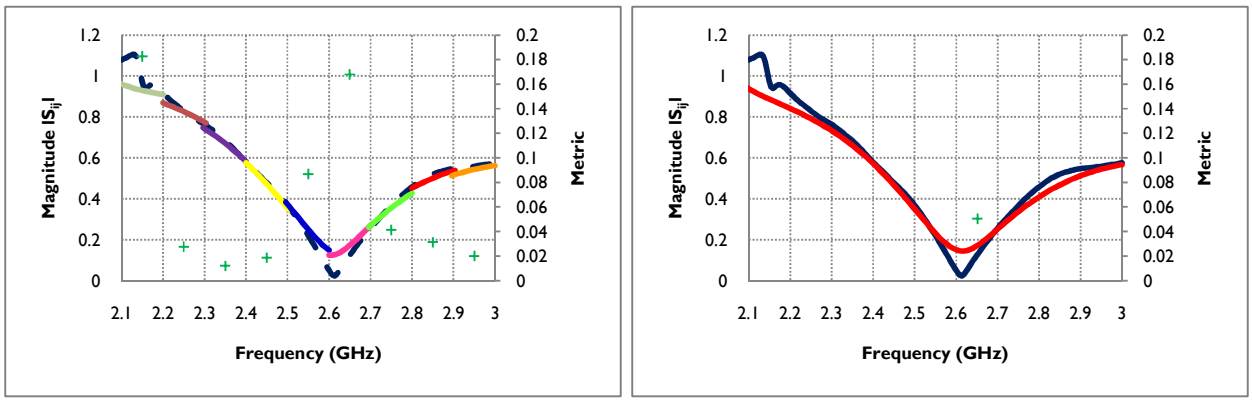

(a) **(b)**

Figure 26: Comparison of piecewise (a) and full band (b) dielectric property extraction

For a full frequency band extraction, the experimental S_{ij} parameter fitting was executed over the entire frequency band of interest. As only one fit to the magnitude and phase angle component of the measured S_{ij} parameter was performed, only one metric value is presented for the extraction. In Figure 26 (b) a full band extraction (2.3-3 GHz) is presented for the same particle size and ore type as in (a). The effect of frequency band size is observed in Figure 26. For the dielectric property extraction over narrower 100 MHz frequency intervals, the DBE Algorithm (coloured

lines) misaligns the magnitude component of the S_{ij} parameter. This is especially true in the 2.5-2.6 GHz and 2.6-2.7 GHz frequency intervals where the resonance is misaligned. For the full band extraction, the improvement in the alignment of the S_{ij} parameter is clearly observed in the smaller reported metric value.

Throughout the thesis, the 2.1-2.3 GHz frequency band has been omitted for all full band extractions due to the cut-off frequency effect (Section 6.7). Refer to Section 6.5.3 for a discussion on frequency band sizes and its effect on the extracted dielectric properties.

6.5 Pre-Extraction Input Specification

Four `extract.py` program variables need to be specified. These variables are:

- DBE database size
- Frequency boundary
- Frequency intervals
- ANA port selection

Each variable affects the value of the extracted dielectric properties and is discussed below.

6.5.1 DBE Database Size

The size of the databases differ considerably (Table 3). The DBE Algorithm enables the user to specify the size of the simulated S_{ij} database. However, for all the dielectric property extractions included in this thesis, the whole database for both WR284 and WR340 sample holders was used. Using the entire DBE database comes at computational expense and will result in a longer extraction run time. However, the extracted property results will be more reliable in comparison to using only a portion of the available database of simulated S_{ij} parameters.

6.5.2 Frequency Boundary

The inclusion of the cut-off frequency effect (Section 6.7) at lower frequency intervals during dielectric property extraction results in a poorer fit between the simulated and measured S_{ij} parameters. For all experimental measurements, f_{start} was set at 2.1 GHz and f_{end} as 3 GHz. After investigation (Section 6.7.1), all full band extractions included in this thesis excluded the 2.1 – 2.3 GHz frequency interval due to its large associated $\|\bullet\|$-values. Full band extractions started at f_{start} = 2.3 GHz. For all full band extractions, the DBE Algorithm provides a single extracted ε′ and ε″ value for the 2.3 – 3 GHz frequency interval.

6.5.3 Frequency Interval

A full band extraction uses the 700 MHz frequency band between 2.3 GHz and 3 GHz as one frequency interval. The DBE program enables the partitioning of the frequency band into smaller frequency intervals, $\Delta f_{interval}$. The partitioning of the frequency band enables the dielectric property extraction of the material under test over smaller frequency intervals. Each interval has an ε′, ε″ and $\|\bullet\|$-value. The extracted properties may vary considerably between frequency intervals. Prominent (in depth and width) resonances in the behaviour of $|S_{ij}|$ give rise to a featured frequency interval, providing sufficient characteristic information of the behaviour of the reflected low power microwaves. A better-featured space provide for lower $\|\bullet\|$-values. Small $\Delta f_{interval}$ (e.g. 100 MHz) may give rise to featureless frequency intervals with large associated $\|\bullet\|$-values. Larger $\Delta f_{interval}$ (e.g. 250 MHz) may tend to generate featured partitioned frequency intervals with smaller associated $\|\bullet\|$-values.

6.5.4 ANA Port Selection

The DBE program permits the selection of port 1, 2 or both ports of the ANA. If port 1 is selected, S_{21} and S_{11} are used in the dielectric property extraction. When port 2 is selected, S_{12} and S_{22} are used in the dielectric property extraction. All four the S_{ij} parameters are used when both ports are selected. ANA port selection influences the reported $\|\bullet\|$-values for each dielectric property extraction.

For all extractions included in this thesis, either port 1 or 2 was used in the DBE Algorithm, based on the minimum reported metric for an air measurement, prior to the dielectric property measurement of the crushed ore samples. The extraction of the air properties (by definition ε*=1-0j) was done for a full band extraction over the 2.1 GHz-3 GHz frequency interval. The alignment of the waveguide coaxial/transition ports flanged to the sample holders, in particular influences the goodness of the dielectric property measurements (Figure 4). The ANA setup (coaxial cables and coaxial/waveguide transition ports) was kept bolted to the sample holders and not (re)moved during the remaining crushed ore dielectric property measurements.

6.6 Frequency Band Selection

The DBE Algorithm was used to extract the dielectric loss factor and dielectric constant of a particulate load of crushed ore. Each dielectric property extraction was repeated twice for each of the particle size classes. Repeated loadings of the crushed ore sample were used to investigate the packing effect (on the extracted dielectric property) as a function of particle size for successive loadings of the sample into the sample cavity.

The dielectric property extraction was categorised as either a piecewise or full band extraction. The use of piecewise frequency intervals compared to using full band extractions was investigated. The size of the frequency band over which the DBE Algorithm extracts the dielectric properties of the crushed mineral ore, was selected in the **`extract.py`** program. Each of these extraction types is discussed below.

6.6.1 Piecewise Extractions

In this thesis, frequency intervals of 100 MHz and 250 MHz, were selected for the extraction of the dielectric loss factor and dielectric constant.

Table 4: Piecewise Frequency Interval Selection

Frequency Interval	Frequency Bands (GHz)	Number of Frequency Bands	Number of Frequency Points (N) in Band
100 MHz	2.1-2.2, 2.2-2.3, 2.3-2.4, 2.5-2.6, 2.6-2.7, 2.7-2.8, 2.8-2.9, 2.9-3	9	22
250 MHz	2.1-2.35, 2.35-2.6, 2.6-2.85, 2.85-3	4	50

Using 100 MHz frequency intervals generates nine frequency bands across the 2.1-2.3 GHz frequency range. If the effect of the cut-off frequency is excluded, the 2.1-2.2 GHz and 2.2-2.3 GHz frequency bands were eliminated from the frequency range of interest resulting in seven frequency bands.

Using 250 MHz frequency intervals generates four frequency bands across the 2.1-2.3 GHz frequency range. If the effect of the cut-off frequency is excluded, the 2.1-2.35 GHz frequency band was eliminated from the frequency range of interest resulting in three frequency bands.

Upon completion of the DBE Algorithm, each frequency band reports a dielectric loss factor, dielectric constant and metric, based on the fit between the measured and simulated S_{ij} parameters in the DBE Algorithm.

6.6.2 Full Band Extractions

Table 5: Full Band Extractions

Frequency Interval	Operational Frequency Band	Number of Frequency Bands	Generated Frequency Band	Number of Frequency Points (N) in Band
Full band extraction	2.1-3	1	900 MHz	201
	2.3-3	1	700 MHz	156

Full band extractions utilise the full operational frequency band as one frequency interval. With a starting frequency of 2.1 GHz, the frequency interval generated is 900 MHz. If the starting frequency is at 2.3 GHz, the frequency interval generated is 700 MHz.

Upon completion of the DBE Algorithm, only one dielectric loss factor, dielectric constant and metric is reported for the entire operational frequency band based on the fit between the measured and simulated S_{ij} parameters in the DBE Algorithm.

6.7 Effect of Cut-off Frequency

6.7.1 Effect of Cut-Off Frequency: WR284

The effect of the cut-off frequency in the WR284 sample holder was investigated. The extent to which the cut-off frequency influences the DB extracted dielectric constant, loss factor and metric is determined by the specified starting frequency of the DBE Algorithm.

For WR284 the cut-off frequency is at 2.078 GHz and although this value is below the set ANA minimum frequency of 2.1 GHz, the effect thereof is still evident in the extracted properties at frequencies approximately 2.1 GHz and 2.2 GHz.

The effect of the cut-off frequency leads itself to dubious extracted data in the lower frequency band with associated large metric values.

The extent to which the cut-off frequency affects the DBE Algorithm's ability to fit the measured and simulated S_{ij} parameters is determined by the starting frequency the DBE Algorithm uses to extract the dielectric properties. The lower frequency bands, which are affected worst by the cut-off frequency effect, can be excluded from the DBE Algorithm. The effect of the starting frequency was determined for the W284 sample holder using a full band extraction with starting frequencies selected as 2.1, 2.2, 2.3, 2.4, 2.5 and 2.6 GHz respectively. For each of the runs the maximum frequency was set at 3 GHz. Crushed porphyry copper ore with a particle size of -6.7+5.6 mm was used. The -6.7+5.6 mm particle size class was chosen to be generally representative of the -26.5+2 mm particle size distribution of interest.

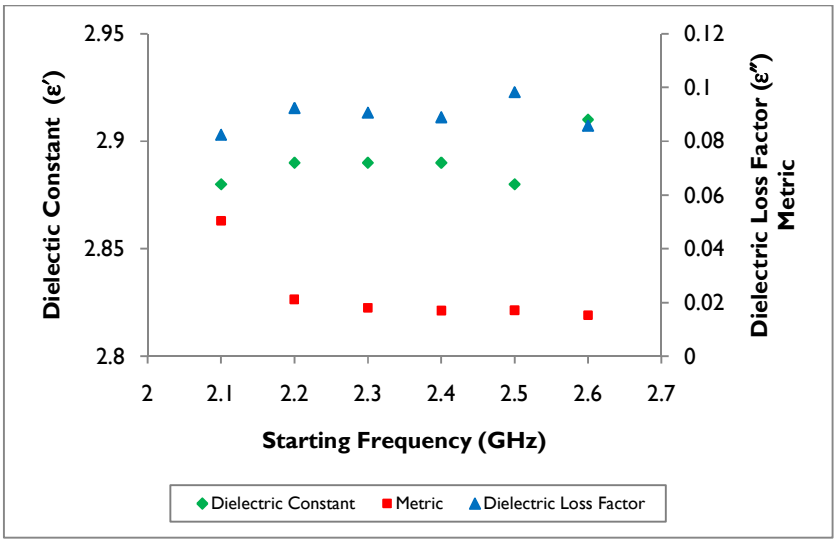

Figure 27: Porphyry copper ore - effect of DBE algorithm starting frequency (WR284)

From Figure 27 the effect of the cut-off frequency is clearly visible in the 2.1-2.2 GHz frequency band. At a starting frequency close to the WR284 cut-off frequency (2.078 GHz) a larger metric value was observed which is attenuated with increasing starting frequency.

At starting frequencies of 2.2 GHz, 2.3 GHz or 2.4 GHz, little change in the extracted dielectric loss factor and dielectric constant was observed. However, with a starting frequency of 2.5 GHz and above, the dielectric loss factor and dielectric constant deviates from the general trend. This is attributed to too much of the operational frequency band being excluded from the DBE

Algorithm which leads to unreliable extracted dielectric constants and loss factors. Choosing too narrow a frequency band for inclusion in the DBE Algorithm excludes a large frequency band in which characteristic S_{ij} parameter features are unaccounted for, resulting in unreliable extracted dielectric properties.

It is important to note that the effect of ore type is not considered in the discussion. The effect of the starting frequency was assumed to be the same for roughly equiaxed particles irrespective of ore type. For the WR284 sample holder the cut-off frequency is fixed at 2.078 GHz. The effect would therefore be visible in the 2.1-2.3 GHz for all ore types.

Based on these results, it was decided to extract the dielectric properties in the 2.3-3 GHz frequency interval for the WR284 sample holder.

6.7.2 Effect of Cut-Off Frequency: WR340

Similarly to the WR284 sample holder, the effect of the cut-off frequency for the WR340 sample holder was investigated. The same procedure as for the WR284 sample holder was used. Again, crushed porphyry copper ore from the -6.7+5.6 mm particle size class was used in the analysis.

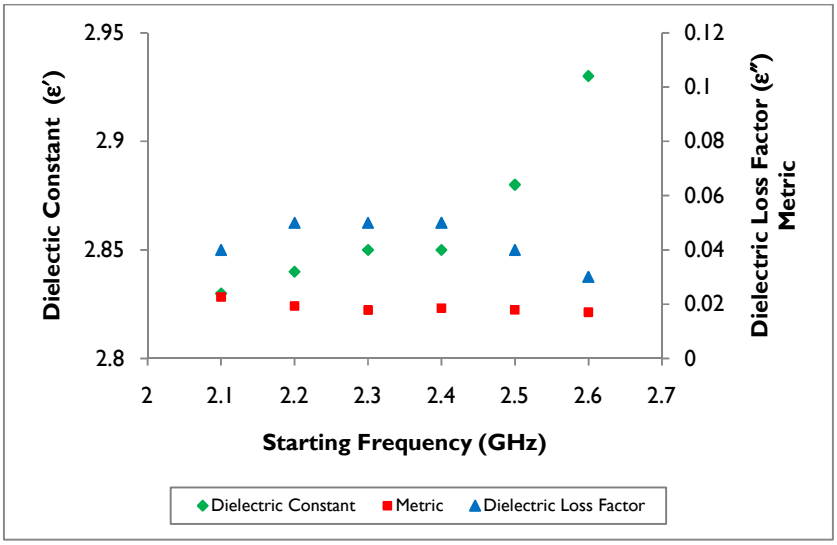

Figure 28: Porphyry copper ore - effect of DBE algorithm starting frequency (WR340)

The effect of the starting frequency is less noticeable for the WR340 sample holder, due to the lower cut-off frequency at 1.736 GHz. For a starting frequency of 2.3 and 2.4 GHz the dielectric loss factor, dielectric constant and metric have stabilised. A starting frequency of 2.5 GHz excludes a large part of the operational frequency band resulting in a large variation in the dielectric constant and dielectric loss factor (Figure 28). The same trend is observed for the WR284 sample holder. The variation in these properties is more significant for the WR340 sample holder, compared with the values obtained for the WR284 sample holder (Figure 27). The dielectric constant exhibits divergent, dubious, behaviour due to the narrow frequency band over which the dielectric property extraction is executed. In part, this is due to the smaller number of frequency points in the WR340 database (Table 3). It was concluded that for all full band extractions in the WR340 sample holder, a starting frequency of 2.3 GHz is suitable.

6.8 Dielectric Property Measurement: Reference Material

Polypropylene, which has known dielectric properties, was chosen as a reference material to establish the accuracy to which of the DBE Algorithm extracts the properties of the material under test. The complex permittivity of a solid block of polypropylene was measured in a WR284 sample holder. The DB extracted ε′ and ε″ over the 2.1-3 GHz frequency interval was compared to reported literature values. The results are summarised in Figure 29.

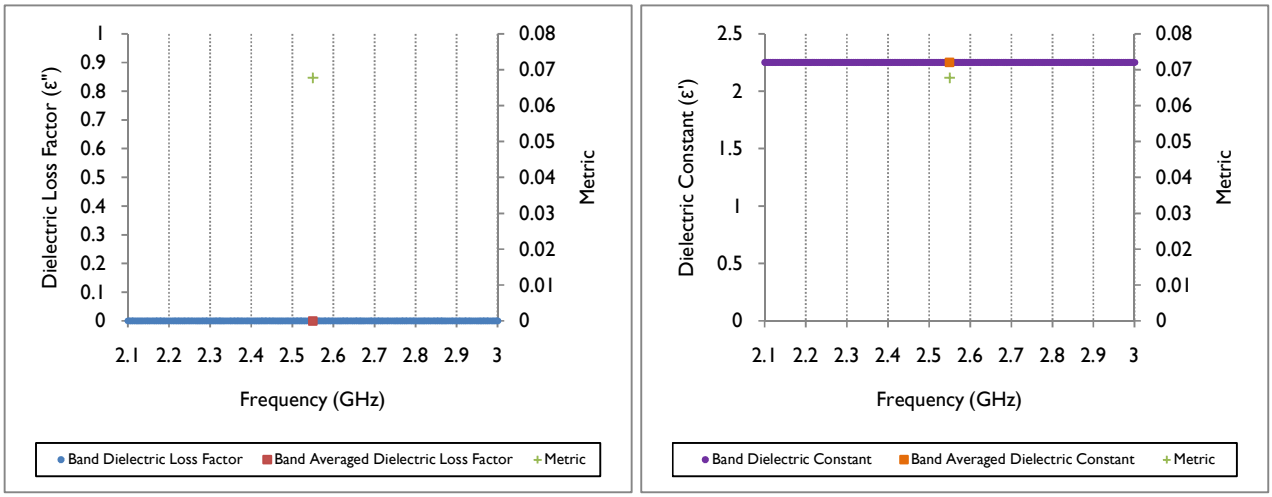

Material	ε'	ε''	ε' (Lit)	ε'' (Lit)
Polypropylene	2.54	0	2.54	7.01×10^{-4}

Figure 29: Polypropylene - extracted ε′ and ε″ values

The literature values are quoted from Von Hippel (1954) under atmospheric conditions (25°C and 1 atm).

The extracted dielectric constant corresponds to the reported literature value. The similarity in the values is indicative of a high level of accuracy associated with the extraction of the dielectric constant using the method included in this thesis.

However, a small variation was observed in the value for the dielectric loss factor between the measured and experimental values. Von Hippel (1954) used the coaxial probe technique for measurement of the dielectric loss factor for polypropylene. This technique is known to be more precise than its waveguide counterpart. The variation ($7.01 \times 10^{-4} \approx 0$) between the extracted and literature values was concluded to be negligible. This established that the DBE Algorithm method works for a well-characterised, homogeneous, isotropic low-loss material.

6.9 Dielectric Property Measurement: Window Material

Polytethyleneterathalyte, PET, was chosen as the window material for each of the sample holders. PET has a high degree of machinability, is a non-laminate material, and has a high abrasion resistance, which is an important characteristic as the PET surfaces are exposed to the crushed ore material. PET has ε′and ε″ values similar to the ore properties to be measured. The complex permittivity of a solid block of PET was measured in a WR 284 sample holder. The dielectric properties were extracted using the Baker Jarvis (BJ) Extraction Algorithm and presented in Figure 30.

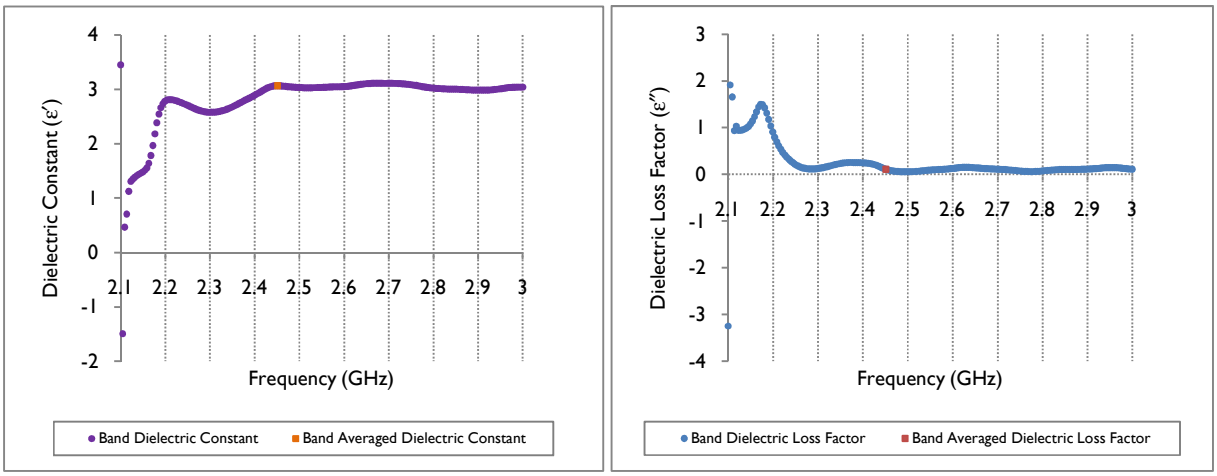

Material	ε'	ε''	ε' (Lit)	ε'' (Lit)
PET	3.07	0.113	3.04	0.134

Figure 30: Polyethyleneterathylate - extracted ε′ and ε″ values

The literature values for PET are quoted from personal correspondence with Prof. Howard Reader (Department of Electrical Engineering, University of Stellenbosch). The experimental and literature values show good agreement.

The BJ Algorithm extracts the dielectric loss factor and dielectric constant for the full operational frequency band. In contrast to the DBE Algorithm, no metric is reported, as the BJ Algorithm does not fit the measured and simulated S_{ij} parameters, but iteratively solves a set of simultaneous mathematical equations. The complex permittivity for PET was computed as $\varepsilon^*=3.07-0.113j$ (at 2.45 GHz).

The dielectric window properties were incorporated in the electromagnetic simulation of the sample holders to generate the database of simulated S_{ij} parameters.

6.10 Dielectric Property Measurement: Port Selection

Prior to dielectric property measurement of the crushed ore samples, the complex permittivity of air is measured in the empty sample holder. Before the dielectric property extraction of the crushed ore samples, the DBE Algorithm was used to extract the dielectric loss factor and dielectric constant for the air sample. The extraction was carried out with only port 1, only port 2 and both port 1 and 2 selected in the **`extract.py`** program for a full band (2.1-2.3 GHz) extraction. By definition the complex permittivity of air is $\varepsilon^*=1-0j$. For all the air-extractions, irrespective of the port selection, the dielectric constant was determined to be 1 and the dielectric loss factor as zero.

Table 6: Dielectric Constant and Loss Factor for Air

Extraction #	Port Selection	ε'	ε''	Metric Range	
				Minimum	Maximum
1	Port 1	1	0	0.078035785	0.45371156
2	Port 2	1	0	0.07624808	0.451815031
3	Port 1 and Port 2	1	0	0.154283862	0.905526591

*Note: The property extraction of air is carried out for each measurement day on which several ore dielectric property measurements is conducted. The air extraction in Table 7 is for 09/03/2010.

The ANA port with the smallest minimum metric is used in the DBE Algorithm for all measurements done on a specific day. Refer to Appendix G for a full list of the selected ANA ports for all dielectric property measurements.

6.11 Dielectric Property Measurement: Crushed Particulate Ore Loads

An outline of the discussion of the dielectric property extractions is summarised in Table 7:

Table 7: Extracted dielectric constant and loss factor - discussion outline

<table>
<tr><th rowspan="2">Ore of Interest</th><th colspan="2">WR 284</th><th colspan="2">WR 340</th></tr>
<tr><th>Measurement 1</th><th>Measurement 2</th><th>Measurement 1</th><th>Measurement 2</th></tr>
<tr><td>Porphyry Copper Ore</td><td colspan="2">Section 6.11.1
Section 6.11.2
Section 6.11.3</td><td colspan="2" rowspan="3">Appendix H</td></tr>
<tr><td>Copper Carbonatite</td><td colspan="2" rowspan="2">Appendix H</td></tr>
<tr><td>Quartz Monzonite Porphyry Copper Ore</td></tr>
</table>

A comparison between the extracted dielectric constant and loss factor was done for extractions over a narrow (100 MHz and 250 MHz frequency intervals) and broad frequency interval (a full band extraction *viz* 700 MHz frequency interval).

The merits of both extraction methods are discussed in Section 6.11.1 through Section 6.11.3. The discussion is limited to both measurements (denoted as M1 and M2) for crushed Porphyry Copper ore in the WR 284 sample cavity.

In some cases the metric-value in the 2.1-2.2 GHz frequency interval is omitted in the graphical representation for the dielectric constant and loss factor, as its inclusion would dominate the characteristic trend of the band metrics due to their relative size compared with the other metrics.

Interpretation of the results will be sufficient to judge if a full band frequency extraction is preferred over a piecewise frequency extraction. In each section the DB extracted dielectric loss factor and dielectric constant is graphically presented followed by a summary of the extracted values obtained for each frequency band.

6.11.1 Piecewise Frequency Extraction: 100 MHz

6.11.1.1 Particle Size: -26.5+16 mm

The DBE Algorithm extracted the following dielectric loss factor and dielectric constant for crushed Porphyry Copper ore (-26.5+16 mm).

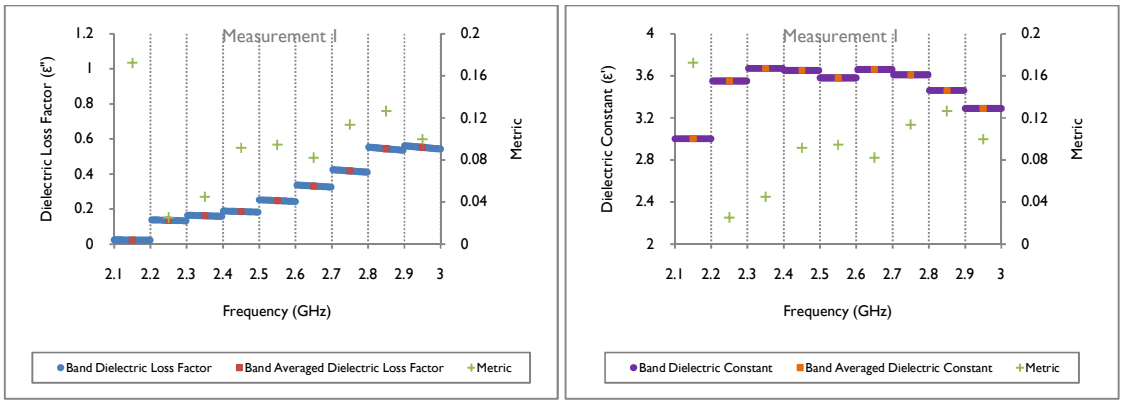

Figure 31: Extracted ε′ and ε″ for Porphyry Copper ore (-26.5+16 mm, Measurement 1, WR284)

For Measurement 1, denoted from now on as M1, the extracted ε″ vary significantly between the individual frequency bands. The effect of the cut-off frequency in the 2.1-2.2 GHz frequency interval is clearly noticeable in the small reported ε″ compared with the remaining factors, which are all a factor of 10 larger. This frequency interval is characterised by a large metric value compared with those in the remaining frequency intervals. The extracted ε″ suffers from a metric insensitivity across the 2.4-3 GHz frequency interval where a relatively similar metric value was obtained for very different extracted ε″ values. Ignoring the cut-off frequency effect, the extracted ε″ value varies over a large range, ranging from 0.13 in the 2.2-2.3 GHz frequency interval to 0.55 in the 2.9-3 GHz frequency interval.

The extracted ε′ varies between the individual frequency bands however, not as severely as is the case with the extracted ε″ value. The cut-off frequency effect is observed for ε′ in the 2.1-2.2 GHz frequency interval.

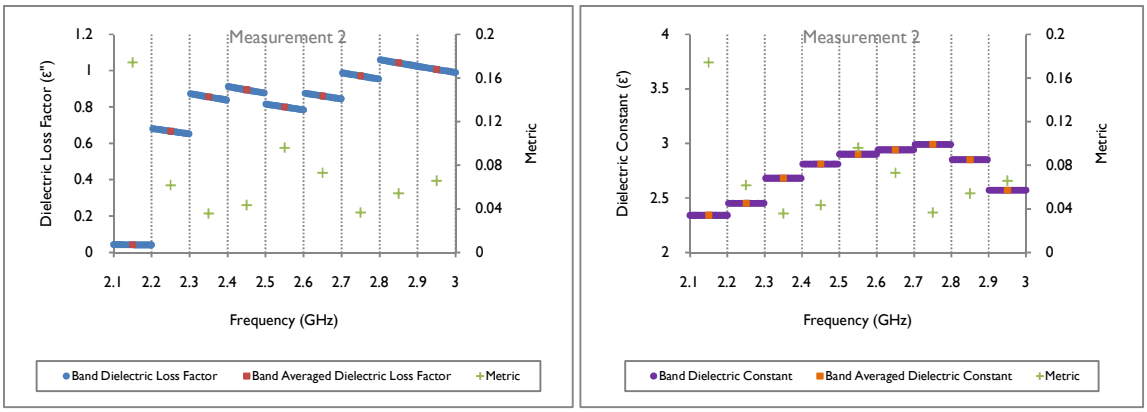

Figure 32: Extracted ε′ and ε″ for Porphyry Copper ore (-26.5+16 mm, Measurement 2, WR284)

For Measurement 2, denoted as M2 from now on, the same variation in the extracted ε″ values was observed, as was the case for M1. However, the metrics seem to represent the change in the extracted values, as observed in the change variation in values between the individual frequency intervals.

The variation in the extracted ε′ and ε″ values between M1 and M2 is due to the difference in the measured S_{ij} parameter (Figure 131). The -26.5+16 mm particle size class is of the same magnitude as the dimensions of the WR284 sample holder. This implies that the wall effects of the sample holder are significant and that this affects the extracted ε′ and ε″ values. With a larger particle size, a larger fraction of void space is present between the individual particles (Appendix D).

The combined effect of the sample holder size and the particle size, results in a difference in the S_{22} parameter resonance feature. For the -26.5+16 mm particle size class the resonance feature varies in width and depth between M1 and M2 as is observed in the 2.5-2.7 GHz frequency interval.

On average, the metric values tend to be large in comparison to the metric for the smaller sized particles classes (-8+6.7 mm and smaller). For smaller sized particles, the particulate load is more spatially homogeneous and wall effects smaller and hence the DB model better represents the measured S_{ij} parameter data.

The dielectric constant exhibits, on average, a 29% difference between M1 and M2 across the particle size distribution. The ε'' exhibits, on average, a 223% variation between M1 and M2 across the particle size distribution. The significant variation in ε'' is attributed to the large degree of misalignment of the S_{22} parameter between M1 and M2 (Figure 131).

The ε'' is less sensitive to the DB fitting of the S_{ij} parameters compared with ε', as observed in the relative variation of the extracted values.

6.11.1.2 Particle Size: -16+11.2 mm

The extracted ε′ and ε″ for the -16+11.2 mm particle size class are presented in Figure 33 and Figure 34.

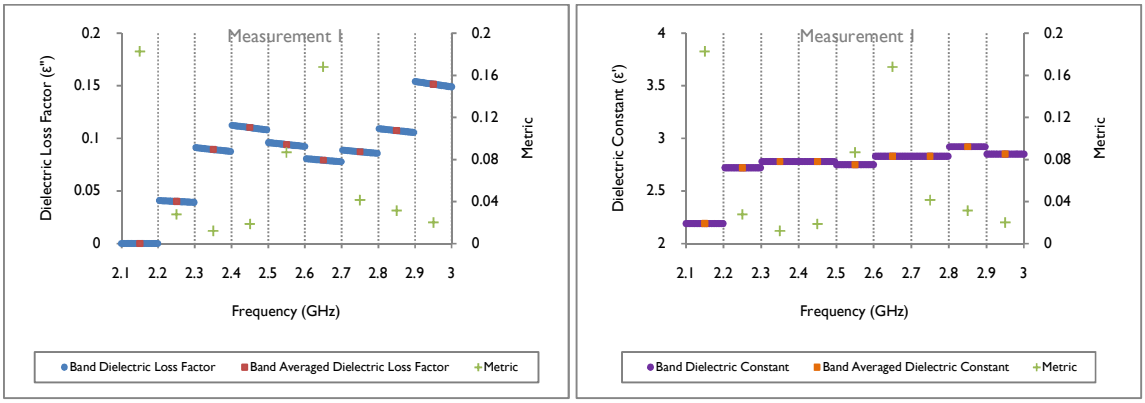

Figure 33: Extracted ε′ and ε″ for Porphyry Copper ore (-16+11.2 mm, Measurement 1, WR284)

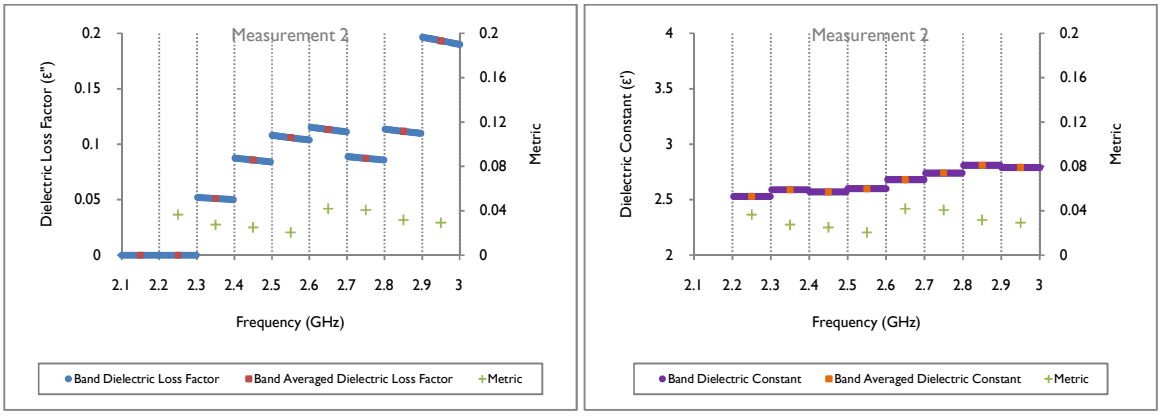

Figure 34: Extracted ε′ and ε″ for Porphyry Copper ore (-16+11.2 mm, Measurement 2, WR284)

For M1 and M2 the cut-off frequency effect is clearly visible in the 2.1-2.2 GHz frequency interval seen by the large metric values and dubious extracted ε′ and ε″ values. For M1, the metric increases as the resonance feature is developed (Figure 132) over the operational frequency interval. For M1 the resonance feature is fully developed in the 2.5-2.7 GHz frequency interval, which corresponds to the same frequency interval over which a larger metric is

observed (Figure 33). This indicates that the DBE Algorithm extracts the ε″ property, but with a large degree of extraction uncertainty. As the DBE Algorithm requires featured frequency space to confidently extract dielectric property data, high levels of uncertainty results in unreliable extracted dielectric properties. If large metrics, especially in the resonance frequency inter, are reported, experimental fitting to the measured S_{ij} parameter is poor and leads to unreliable extracted values for ε′ and ε″. As in the case for the 26.5+16 mm particle size class, ε″ varies significantly between the individual frequency intervals. It seems that the metric is relatively insensitive to ε″.

When comparing Figure 131 and Figure 132, it is observed that the S_{ij} parameters for individual ANA measurements have a larger degree of alignment for the smaller -16+11.2 mm particle size class. Approximating the particulate load by a homogeneous, solid body with an effective ε* property, is better for smaller particle sizes, as the wall effects of the sample holder is less prominent. This tendency is observed when comparing Figure 31, Figure 32, Figure 33 and Figure 34 where the extracted ε′ and ε″ values have a higher degree of correspondence between different measurements for the -16+11.2 mm particle size class. By visually comparing the obtained metrics for the -26.5+16 mm and -16+11.2 mm particle size classes it is clear that the -16+11.2 mm particle size class has, on average, a smaller reported metric value across the entire frequency interval.

The ε′ exhibits, on average, a 6% variation between M1 and M2 across the particle size distribution. The ε″ exhibits, on average, a 187% variation between M1 and M2 across the particle size distribution. The latter is attributed to the large degree of misalignment of the S_{22} parameter between M1 and M2 (Figure 132). The decrease in the average variation between the -26.5+16 mm and -16+11.2 mm particle size classes is due to the improved alignment of the S_{22} parameter between individual measurements for the smaller particle size. As is the case with the -26.5+16 mm particle size class, the extracted ε″ value is less sensitive to the fitting of the S_{ij} parameters, compared with ε′.

6.11.1.3 Particle Size: -11.2+8 mm

The extracted ε′ and ε″ values for the -11.2+8 mm particle size class are presented in Figure 35 and Figure 36.

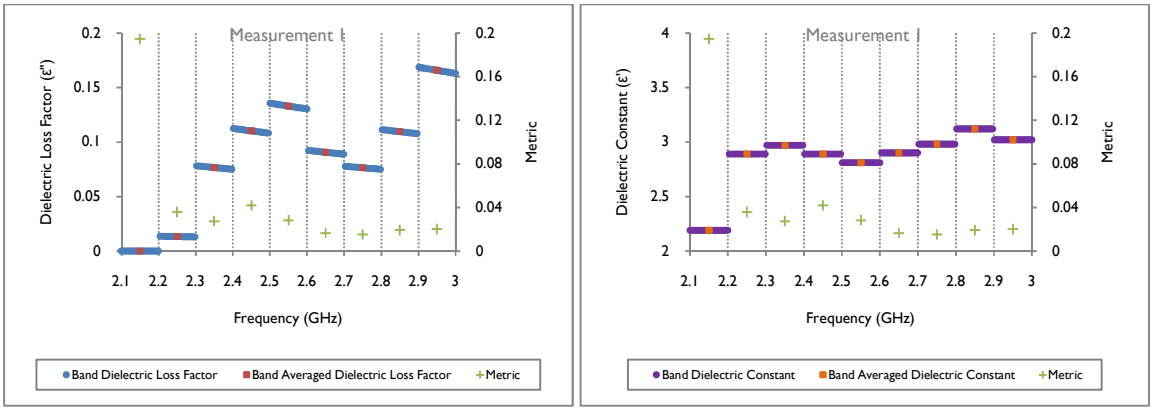

Figure 35: Extracted ε′ and ε″ for Porphyry Copper ore (-11.2+8 mm, Measurement 1, WR284)

For M1 and M2 the insensitivity of the extracted ε′ and ε″ values to the associated metrics it is clearly observed in Figure 35 and Figure 36. This is especially evident for M1. The ε″ values exhibit variation between the individual frequency intervals, despite similar metric values in the 2.5-3 GHz frequency interval.

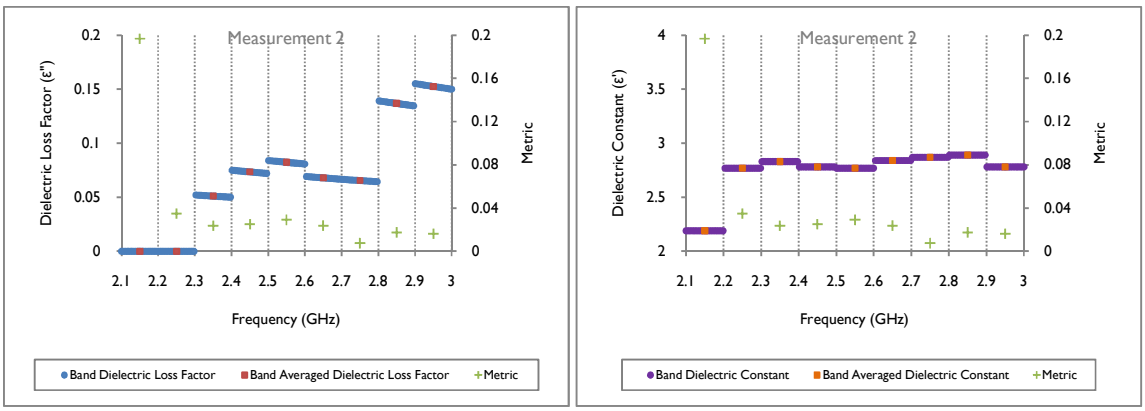

Figure 36: Extracted ε′ and ε″ for Porphyry Copper ore (-11.2+8 mm, Measurement 2, WR284)

The same general trend in the ε″ values is observed for M1 and M2, which is attributed to the improved similarity between the measured S_{ij} parameters (Figure 134). With decreasing particle size, wall effects decrease. For both M1 and M2, no excessively large metric is observed at the

resonanct frequency, as was the case for the -16+11.2 mm particle size class. For M1 and M2, ε′ exhibits some variation between the individual frequency intervals although limited and not as severe as in the case for ε″.

The dielectric constant exhibits, on average, a 4% variation between M1 and M2 across the particle size distribution. The dielectric loss factor exhibits, on average, a 38% variation between M1 and M2 across the particle size distribution. The significant variation in the dielectric loss factor is attributed to the misalignment of the S_{11} parameter between M1 and M2 (Figure 133).

6.11.1.4 Particle Size: -8+6.7 mm

The extracted ε′ and ε″ values for the -8+6.7 mm particle size class are presented in Figure 38.

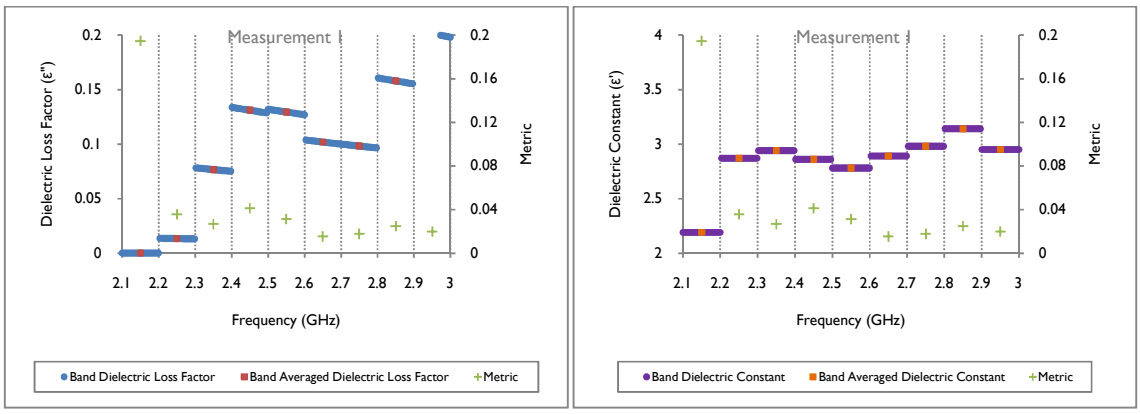

Figure 37: Extracted ε′ for Porphyry Copper ore (-8+6.7 mm, Measurement 1, WR284)

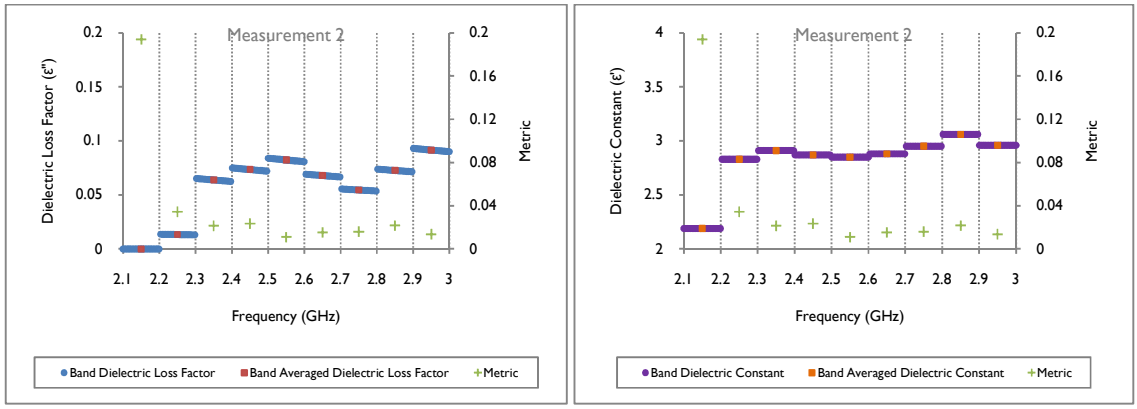

Figure 38: Extracted ε″ for Porphyry Copper ore (-8+6.7 mm, Measurement 2, WR284)

M1 and M2 exhibit, as before, variation in the extracted ε″ value between the individual frequency intervals. Due to the near perfect alignment of the S_{11} parameter (Figure 135) for M1 and M2, the extracted ε′ and ε″ in the corresponding frequency intervals exhibited similarity across the operational frequency interval. The measured S_{11} parameter only exhibits partial misalignment between M1 and M2 in 2.5-2.6 GHz and 2.9-3 GHz frequency intervals resulting in a larger variation in the extracted ε′ and ε″ values (Figure 38) in the corresponding frequency intervals.

The extracted ε′ value also exhibits some variation between the individual frequency intervals. This is noted for M1 in the 2.2-2.5 GHz and 2.6-3 GHz frequency intervals. For M2 the variation is less in the corresponding frequency intervals. As with the -26.5+16 mm, -16+11.2 mm and -11.2+8 mm particle size classes the variation in ε″ is significantly more noticeable between the individual frequency intervals than for the extracted ε′ value.

The dielectric constant exhibits, on average, a 1% variation between M1 and M2 across the particle size distribution. The dielectric loss factor exhibits, on average, an 82% variation between M1 and M2 across the particle size distribution.

6.11.1.5 Particle Size: -6.7+5.6 mm

Little difference between the measured S_{11} parameter between M1 and M2 is observed in Figure 135.

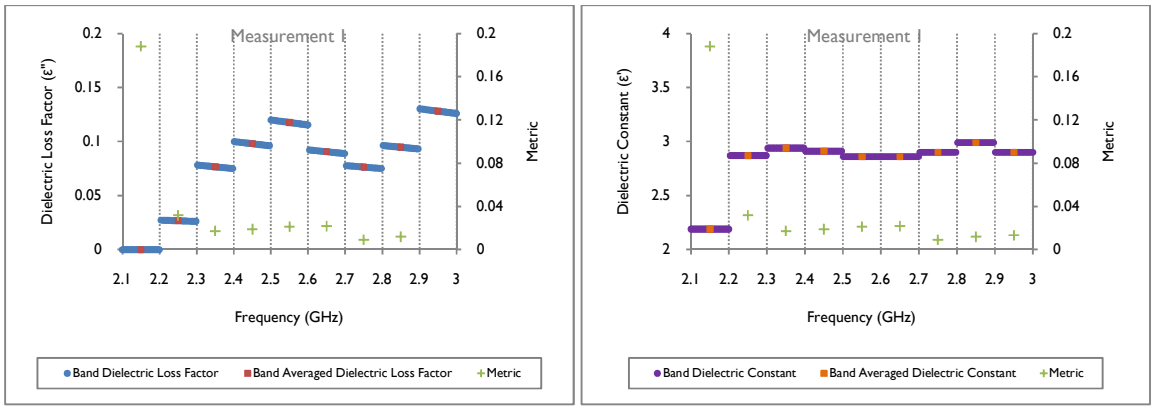

Figure 39: Extracted ε′ and ε″ for Porphyry Copper ore (-6.7+5.6 mm, Measurement 1, WR284)

The similarity in the S_{11} parameter results in comparable extracted ε′ and ε″ values for M1 and M2. From Figure 39 and Figure 40 this tendency is seen across the entire frequency interval between the individual frequency bands except for the 2.5-2.6 GHz frequency interval. In this frequency band, the extracted ε″ value differs by 100% between M1 and M2. The latter corresponds to the same frequency interval in which the magnitude component of the S_{11} parameter differs (Figure 135) noticeably between M1 and M2.

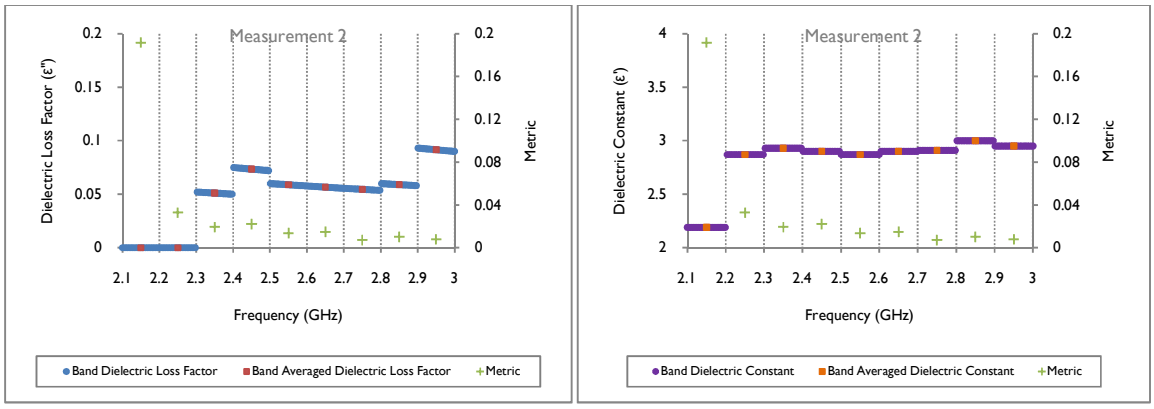

Figure 40: Extracted ε′ and ε″ for Porphyry Copper ore (-6.7+5.6 mm, Measurement 2, WR284)

However, despite similarity between the S_{11} parameter for M1 and M2, the extracted ε″ value varies to a greater extent compared with the ε′ value.

Referring to Figure 135 it is observed that the S_{11} parameter resonance is developed over the 2.5-2.7 GHz frequency band. Despite the more highly featured data, the DBE Algorithm produces metrics, which are larger in magnitude, compared with the frequency space on either side of the resonance frequency interval. This is attributed to the poorer fit to the measured S_{11} parameter over a narrower frequency interval despite the frequency interval's position in a theoretically highly featured frequency space.

The dielectric constant exhibits, on average, <1 % variation between M1 and M2 across the particle size distribution. The dielectric loss factor exhibits, on average, a 58% variation between M1 and M2 across the particle size distribution. The significant variation in the dielectric loss factor is attributed to the large degree of misalignment of the S_{11} parameter between M1 and M2 (Figure 135).

6.11.1.6 Particle Size: -5.6+4.75 mm

The extracted ε′ and ε″ values for the -5.6+4.75 mm particle size class are presented in Figure 41 and Figure 42.

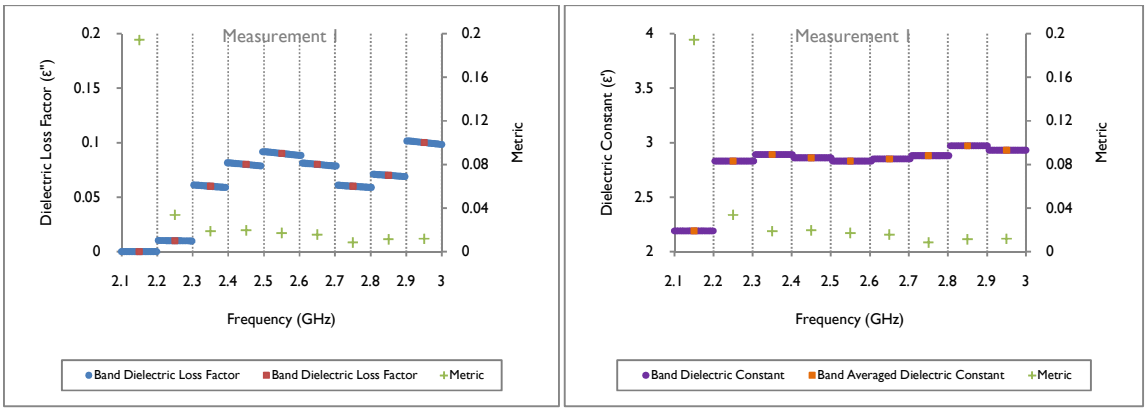

Figure 41: Extracted ε′ and ε″ for Porphyry Copper ore (-5.6+4.75 mm, Measurement 1, WR284)

As expected with decreasing particle size, the measured S_{11} parameter for M1 and M2 is similar in size across the 2.1-3 GHz frequency interval (Figure 136).

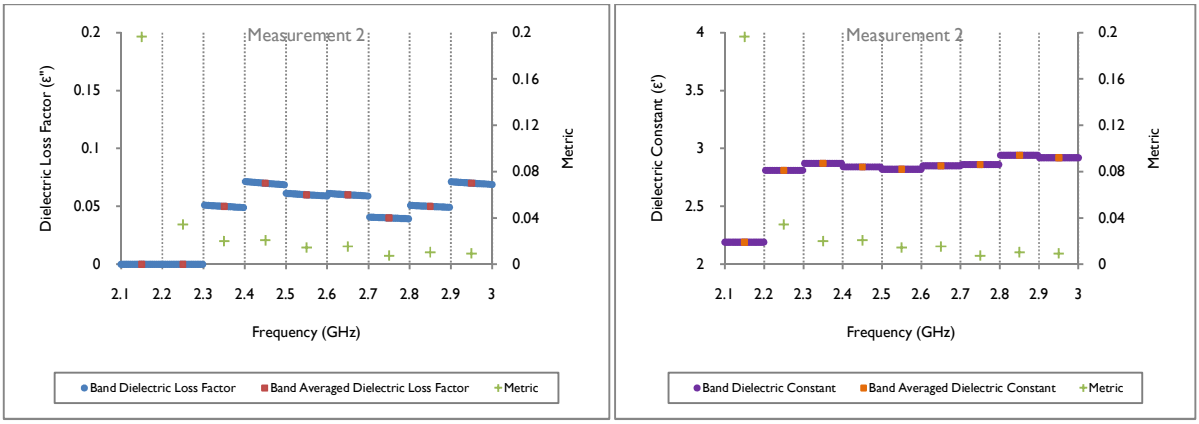

Figure 42: Extracted ε′ and ε″ for Porphyry Copper Ore (-5.6+4.75 mm, Measurement 2, WR284)

Despite the large degree of similarity in the measured S_{11} parameter for M1 and M2, the extracted ε″ varies between each of the frequency intervals. The same trend is observed for ε′, although to a much lesser extent.

On average the extracted ε′ exhibits a negligible difference (<1%) between M1 and M2 across the operational frequency band. The extracted ε″ exhibits a significant difference (37.5%) between M1 and M2 across the operational frequency band.

6.11.1.7 Particle Size: -4.75+3.35 mm

As in the case for the -6.7+5.6 mm particle size class, the extracted ε″ for M1 and M2 exhibit the same general trend across the operational frequency interval except in the 2.4-2.5 GHz frequency interval. From Figure 137 it is seen that for the same frequency interval, the S_{11} parameter differs slightly between M1 and M2, which gives rise to the difference in the extracted ε″ value.

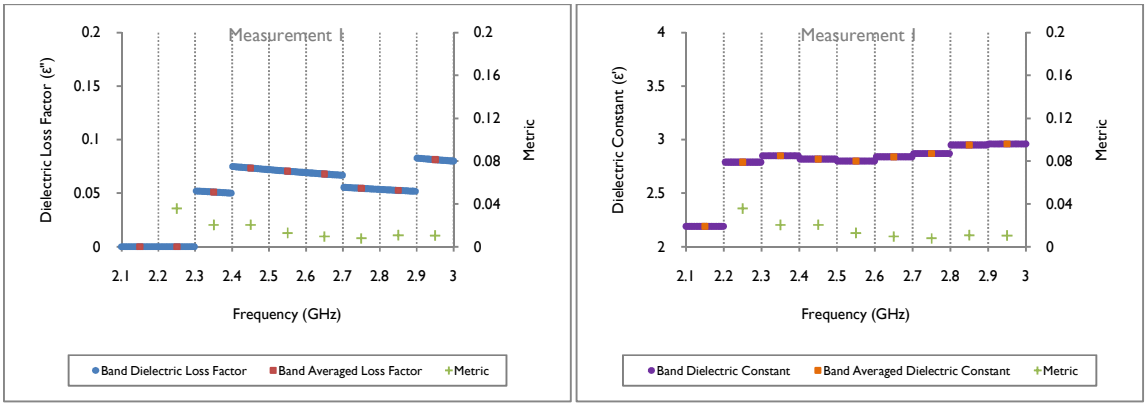

Figure 43: Extracted ε′ and ε″ for Porphyry Copper ore (-4.75+3.35 mm, Measurement 1, WR284)

The average metric value for the -4.75+3.35 mm particle size class is a factor 8 smaller when compared with the larger particle size classes (-26.5+16 mm and -16+11.2 mm). The smaller metric suggests that the measured S_{ij} data are better fitted by the DBE Algorithm due to the increase in the spatial homogeneity between the individual particles close to the wall in the smaller particle size classes. It is observed that with smaller particle size classes, the variation in the extracted ε′ and ε″ values decrease for successive measurements for corresponding particle size classes. This emphasises the importance of particle size relative to the sample holder and how it affects the effective dielectric properties of the material under test.

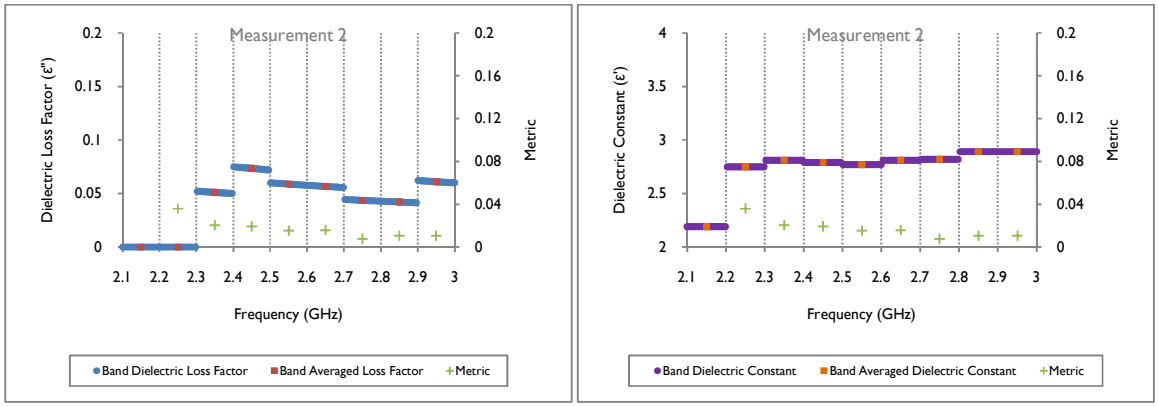

Figure 44: Extracted ε′ and ε″ for Porphyry Copper ore (-4.75+3.35 mm, Measurement 2, WR284)

M1 and M2 exhibit a decrease in the reported metric values in the 2.5-2.8 GHz frequency interval, which corresponds to the same interval over which the S_{11} resonance feature develops in width and depth (Figure 137). The DBE Algorithm extracts the dielectric properties with more confidence due to the higher degree of reflected microwave characteristics and smaller particle size, which in turn increases the spatial homogeneity throughout the sample holder, relative to the wavelength.

The dielectric constant exhibits, on average, 1 % variation between M1 and M2 across the particle size distribution. The dielectric loss factor exhibits, on average, a 13% variation between M1 and M2 across the particle size distribution. The significant variation in the dielectric loss factor is attributed to the large degree of misalignment of the S_{11} parameter between for M1 and M2 (Figure 137).

6.11.1.8 Particle Size: -3.35+2 mm

As the smallest particle size, the -3.35+2 mm particle size class exhibits variation between the extracted ε″ values across the operational frequency interval. This is observed for both M1 (Figure 45) and M2 (Figure 46).

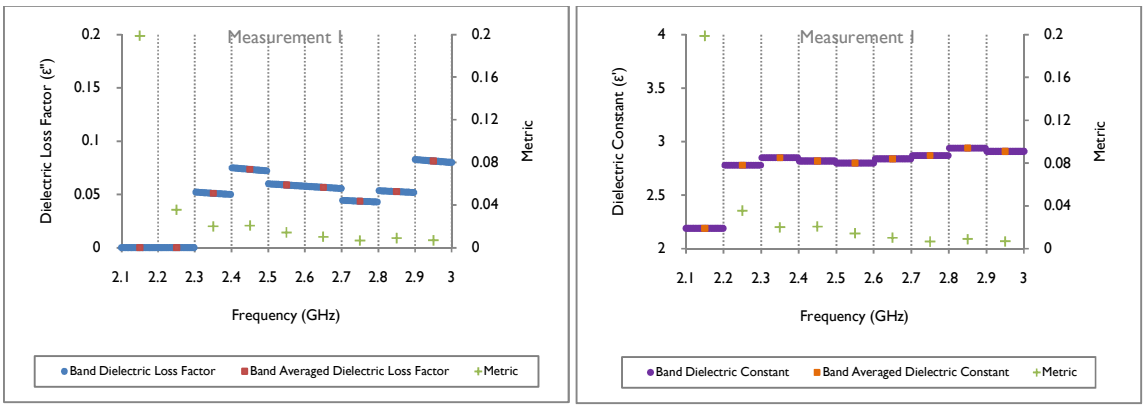

Figure 45: Extracted ε′ and ε″ for Porphyry Copper ore (-3.35+2 mm, Measurement 1, WR284)

The finely crushed -3.35+2 mm particle size class exhibits a large degree of spatial homogeneity throughout the entire sample holder volume resulting in a negligible average difference (~2%) between the extracted dielectric constant between M1 and M2. This is attributed to the same equivalent spatial distribution for successive dielectric property measurements at the wavelength scale and the high degree of similarity in the measured S_{11} parameters (Appendix H, Figure 138) for M1 and M2.

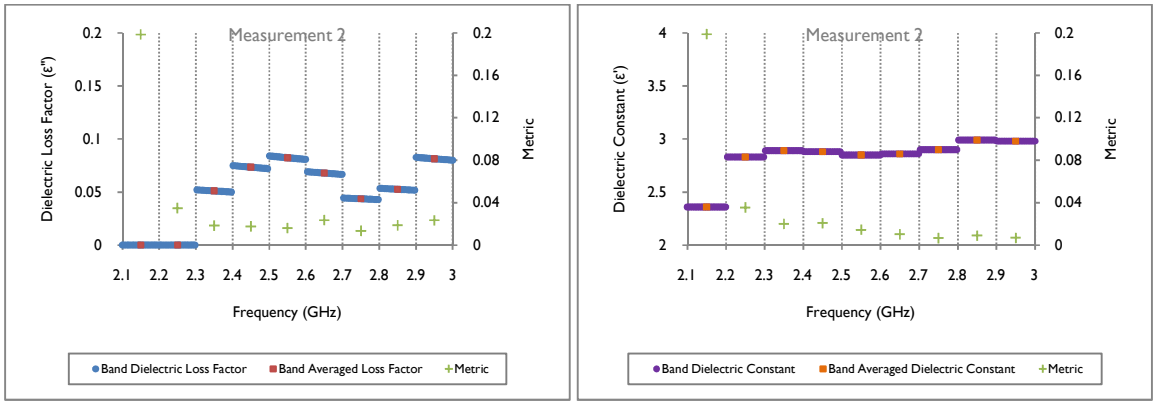

Figure 46: Extracted ε′ and ε″ for Porphyry Copper ore (-3.35+2 mm, Measurement 2, WR284)

However, the dielectric loss factor exhibits a large degree of variation in the 2.5-2.6 GHz and 2.6-2.7 GHz frequency interval. Both these frequency intervals are within the resonance frequency band. In the 2.5-2.6 GHz frequency interval, the extracted dielectric loss factor differs by more than 33% between M1 and M2. In the 2.6-2.7 GHz frequency interval, the extracted dielectric loss factor differs with 17% between M1 and M2.

Despite the improved spatial homogeneity, the DBE Algorithm extracts dielectric loss factor values with little reproducibility between individual ANA measurements in the resonance feature, which should be an interval characterised by a high degree data feature. The dielectric constant exhibits, on average, 2% variation between M1 and M2 across the particle size distribution. The dielectric loss factor exhibits, on average, a 6% variation between M1 and M2 across the particle size distribution.

6.11.2 Piecewise Frequency Extraction: 250 MHz

6.11.2.1 Particle Size: -26.5+16 mm

The extracted ε′ and ε″ properties vary considerably between the different frequency intervals across the operational frequency interval for M1 (Figure 47).

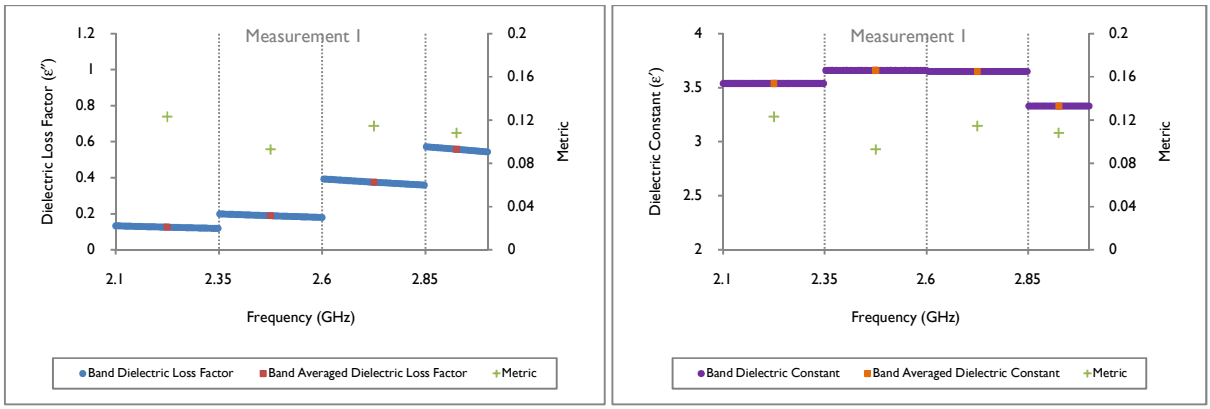

Figure 47: Extracted ε′ and ε″ for Porphyry Copper Ore (-26.5+16 mm, Measurement 1, WR284)

For M1 and M2, variation in the extracted ε′ and ε″ is observed across the frequency band. The effect of particle size is evident in the large magnitude of the metrics in each of the frequency bands, when compared with the reported metrics for the 100 MHz piecewise extractions in the smaller particle size classes.

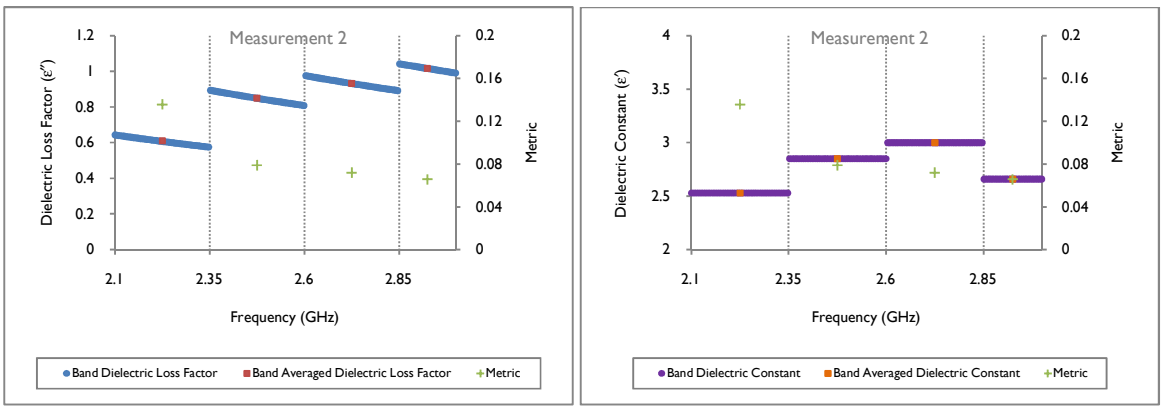

Figure 48: Extracted ε′ and ε″ for Porphyry Copper ore (-26.5+16 mm, Measurement 2, WR284)

For M1 and M2 the extracted dielectric properties exhibit insensitivity to the metric. This is evident in the variation in ε′ and ε″ in the 2.35-3 GHz frequency interval with approximately unchanged metric values.

For M1 the S_{22} resonance feature is developed in depth and width over the 2.35-2.6 GHz frequency interval (Figure 131). This results in a more featured frequency interval, which provides more information to the DBE Algorithm for dielectric property extraction, resulting in a better experimental fit to the measured S_{ij} parameter data *viz*. a smaller metric value.

The ε′ exhibits, on average, a 29% variation between M1 and M2 across the particle size distribution. The ε″ exhibits, on average, a 236% variation between M1 and M2 across the particle size distribution. The significant variation in both these properties is attributed to the large degree of misalignment of the S_{22} parameter between for M1 and M2 (Figure 131). The metrics for M2 are smaller when compared with that of M1. Although the magnitude component of M2 (Figure 131) is broader and flatter compared with M1, on average the metrics are larger. The latter is attributed to the phase angle component of the S_{22} parameter that contributes to a larger reported metric (Equation 11).

6.11.2.2 Particle Size: -16+11.2 mm

For M1, a large metric of 0.1129 in the 2.6-2.85 GHz frequency interval is indicative of a poor fit to the measured S_{22} parameter, as explained in Section 0. From Figure 71 and Figure 72 it is observed that the DBE Algorithm fails to fit the phase angle component of the DB S_{22} parameter to that of the measured S_{22} parameter. This results in a large variation in the phase angle contribution of the metric (Equation 11).

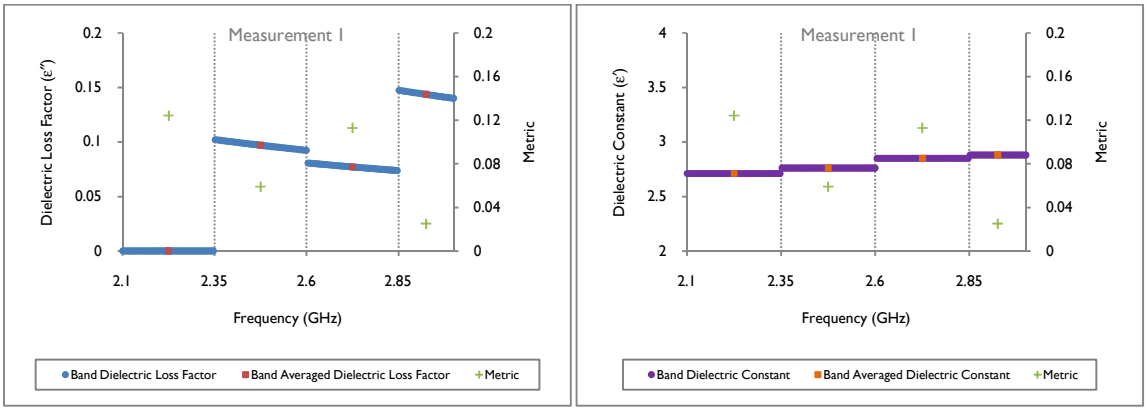

Figure 49: Extracted ε′ and ε″ for Porphyry Copper ore (-16+11.2 mm, Measurement 1, WR284)

Due to the smaller particle size, the difference in the measured S_{22} parameter for M1 and M2 has decreased as seen in Figure 132, compared with the difference observed for the -26.5+16 mm particle size class (Figure 131).

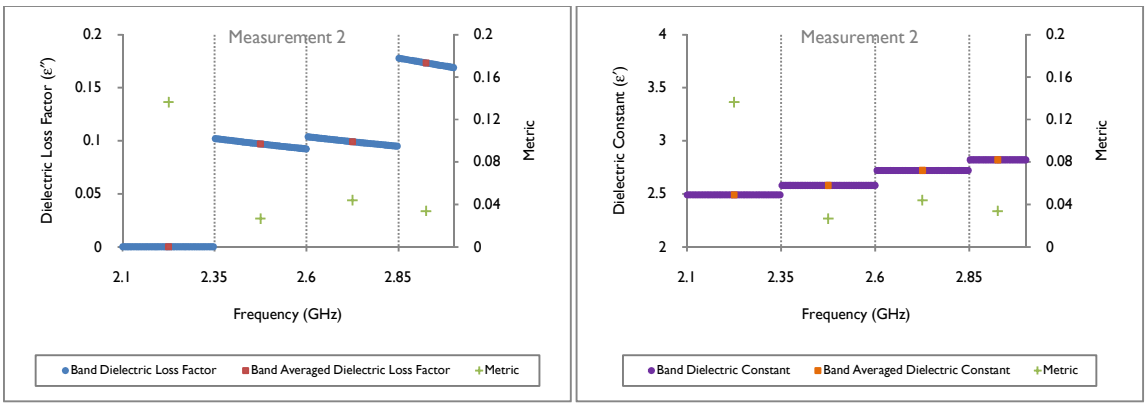

Figure 50: Extracted ε′ and ε″ for Porphyry Copper ore (-16+11.2 mm, Measurement 2, WR284)

For M2, the metric in the 2.6-2.85 GHz frequency interval has decreased compared with M1 in the same frequency interval (Figure 49). As with M1, the DBE Algorithm fails account for the S_{22} resonance feature (Figure 83) for M2. However, the variation between the measured and simulated phase angle of the S_{22} parameter is less for M1 (Figure 84) resulting in a smaller metric.

The dielectric constant exhibits, on average, a 6% variation between M1 and M2 across the particle size distribution. The dielectric loss factor exhibits, on average, a 12% variation between M1 and M2 across the particle size distribution. The significant variation in the dielectric loss factor is attributed to the large degree of misalignment of the S_{22} parameter between M1 and M2 (Figure 132).

6.11.2.3 Particle Size: -11.2+8 mm

From Figure 51, the extracted ε″ values exhibit insensitivity to the metric in the 2.35-3 GHz frequency interval. Both properties vary between the individual frequency bands, despite similar sized metrics.

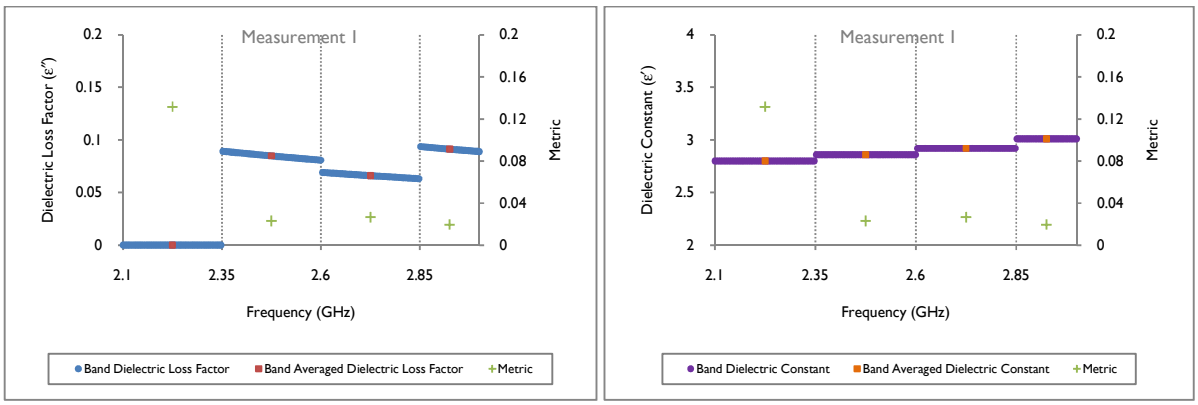

Figure 51: Extracted ε′ and ε″ for Porphyry Copper ore (-11.2+8 mm, Measurement 1, WR284)

Although the difference between the measured S_{11} parameter is smaller for the -11.2+8 mm particle size compared with the -26.5+16 mm and -16+11.2 mm particle size classes, the difference in the extracted ε′ and ε″ is noticeable for M1 and M2 (Figure 51 and Figure 52).

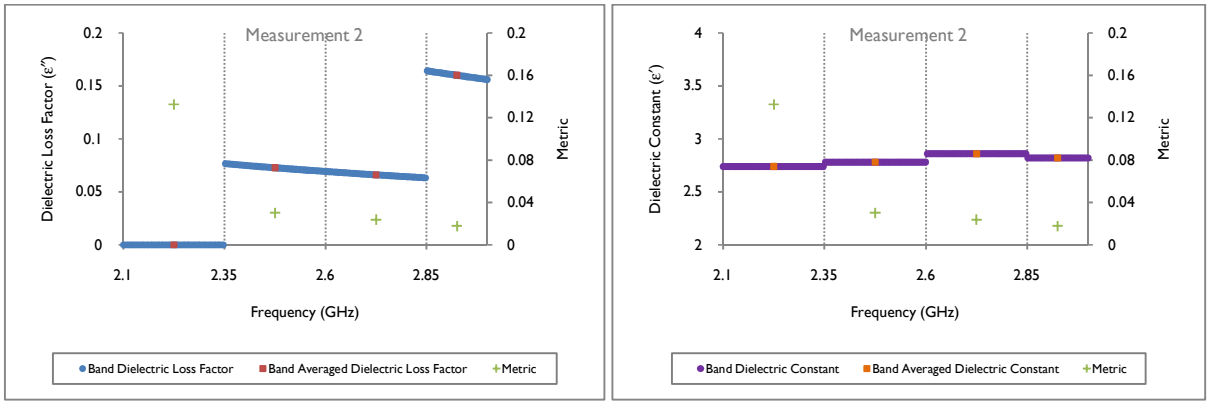

Figure 52: Extracted ε′ and ε″ for Porphyry Copper ore (-11.2+8 mm, Measurement 2, WR284)

For M2 the extracted ε″ in the 2.85-3 GHz frequency interval is suspicious when compared with the rest of the values in the 2.35-2.6 GHz and 2.6-2.85 GHz frequency intervals. The magnitude of the ε″ value in this band appears to be excessively large when compared with the 0.07 in the 2.35-2.6 GHz and 2.6-2.85 GHz frequency intervals. However, the metric is smaller in the 2.85-3 GHz frequency band compared with that of the remaining frequency intervals, which does indicate that the DBE Algorithm extracted the dielectric properties in this band with a higher confidence. For M1 the extracted ε″ in the 2.6-2.85 GHz and 2.85-3 GHz frequency intervals is significantly different, despite approximately similar metric values. This underlines the inconsistency amongst extracted ε′ and ε″ over narrow frequency intervals and the relative inconsistency of the reported metric to ε″ values.

The dielectric constant exhibits, on average, a 5% variation between M1 and M2 across the particle size distribution. The dielectric loss factor exhibits, on average, a 30% variation between M1 and M2 across the particle size distribution. The significant variation in the dielectric loss factor is attributed to the large degree of misalignment of the S_{11} parameter between M1 and M2 (Figure 133).

6.11.2.4 Particle Size: -8+6.7 mm

From Figure 53 and Figure 54 it is noticed that the extracted ε′ values for M1 and M2 only differ noticeably in the 2.1-2.35 GHz and 2.35-2.6 GHz frequency intervals. For the 2.35-2.6 GHz frequency interval the difference is attributed to the cut-off frequency effect. For the 2.35-2.6 GHz frequency the difference in the extracted ε′ is attributed to the variation in the measured S_{11} parameter between M1 and M2 in the 2.5-2.6 GHz frequency interval (Figure 134).

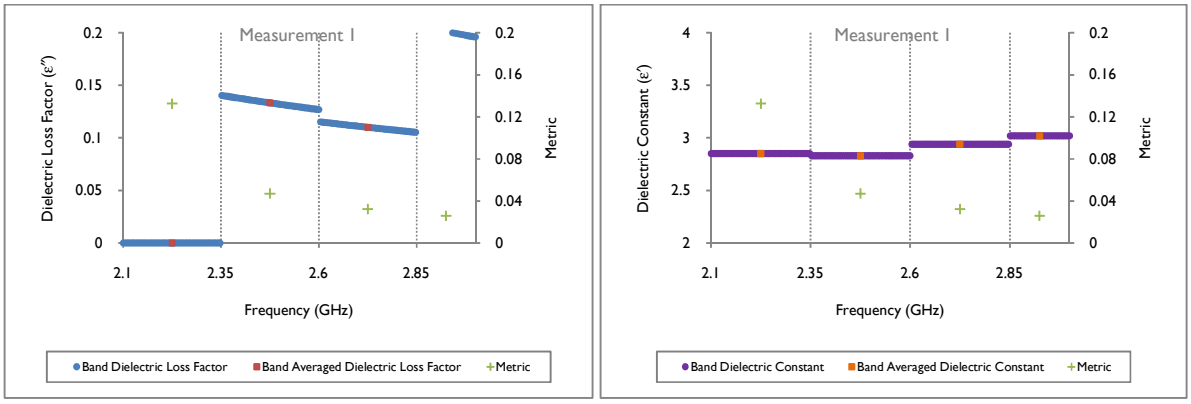

Figure 53: Extracted ε′ and ε″ for Porphyry Copper Ore (-8+6.7 mm, Measurement 1, WR284)

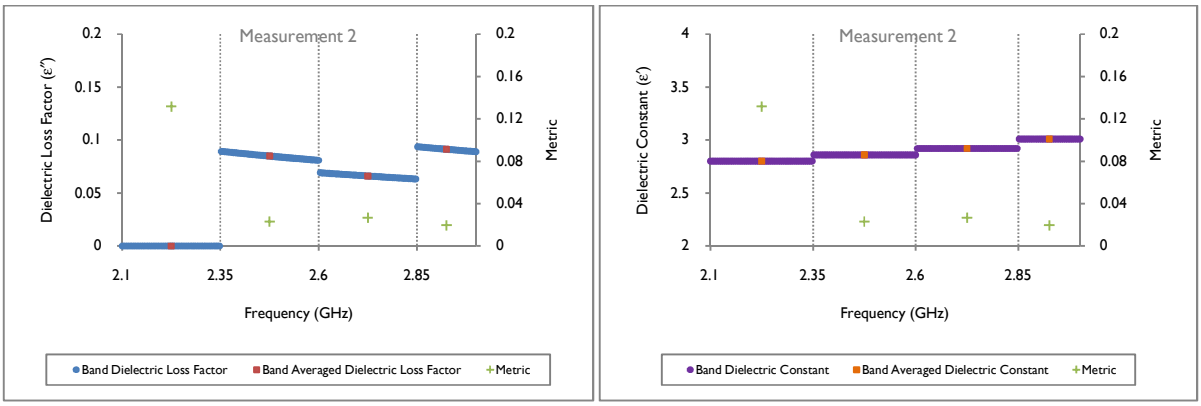

Figure 54: Extracted ε′ and ε″ for Porphyry Copper ore (-8+6.7 mm, Measurement 2, WR284)

The extracted ε″ values for M1 and M2 in each of the frequency intervals differ significantly. On average, the extracted ε″ value per frequency interval, differs 81% from the extracted value in the corresponding frequency interval for the other measurement. The two largest differences,

63% and 122%, are observed in the 2.35-2.6 GHz and 2.85-3 GHz frequency interval respectively. These frequency intervals are also the frequency intervals in which the magnitude of the measured S_{11} parameter, for M1 and M2, exhibits a noticeable difference (Figure 134).

The dielectric constant exhibits, on average, a <1% variation between M1 and M2 across the particle size distribution. The dielectric loss factor exhibits, on average, a 60% variation between M1 and M2 across the particle size distribution.

6.11.2.5 Particle Size: -6.7+5.6 mm

The effect of a reduced particle size becomes apparent when comparing the magnitude component of the measured S_{11} parameters (Figure 135). A large degree of similarity exists between the measured S_{11} parameter across the operational frequency interval for M1 and M2.

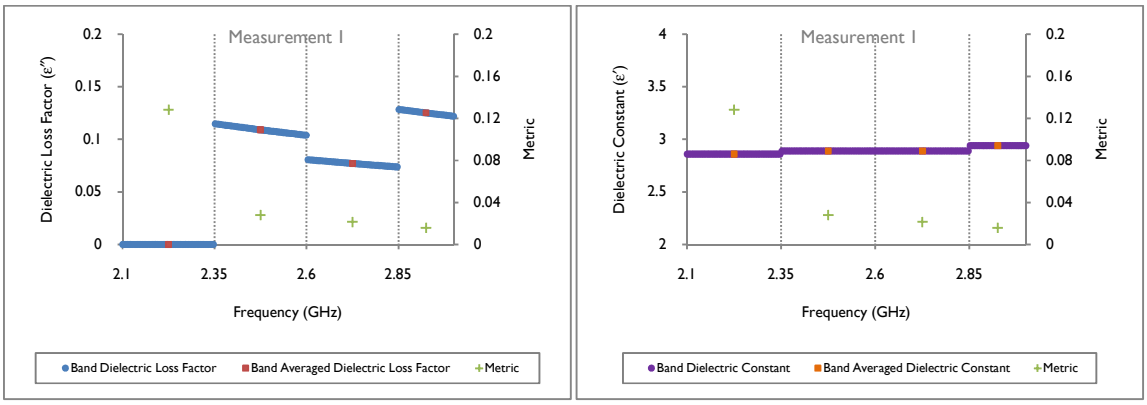

Figure 55: Extracted ε′ and ε″ for Porphyry Copper ore (-6.7+5.6 mm, Measurement 1, WR284)

The only noticeable difference in the measured S_{11} parameter for M1 and M2 is in the 2.85-3 GHz frequency interval. For M1 the extracted ε′ value stays constant in the 2.35-2.6 GHz and 2.6-2.85 GHz frequency intervals except for the 2.85-3 GHz frequency interval where ε′ increases from 2.89 to 2.94.

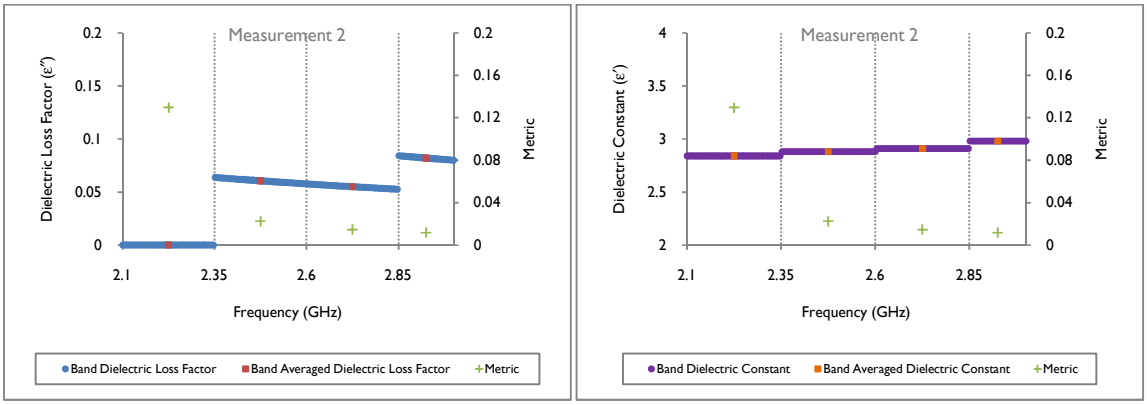

Figure 56: Extracted ε′ and ε″ for Porphyry Copper ore (-6.7+5.6 mm, Measurement 2, WR284)

The extracted ε″ value across the operational frequency interval exhibits a significant variation (60%) between the individual frequency intervals. The smaller particle size has reduced the variation by 20%. This is attributed to the smaller spatial variation in the particle orientation in the sample holder between dielectric property measurements.

Metric insensitivity is observed for M1 (2.35-2.6 GHz, 2.6-2.85 GHz) and M2 (2.6-2.85 GHz, 2.85-3 GHz) where similar metrics are insensitive to dissimilar values extracted for ε′ and ε″ (Figure 55 and Figure 56).

6.11.2.6 Particle Size: -5.6+4.75 mm

The extracted ε′ and ε″ values for the -5.6+4.75 mm particle size class are presented in Figure 57 and Figure 58.

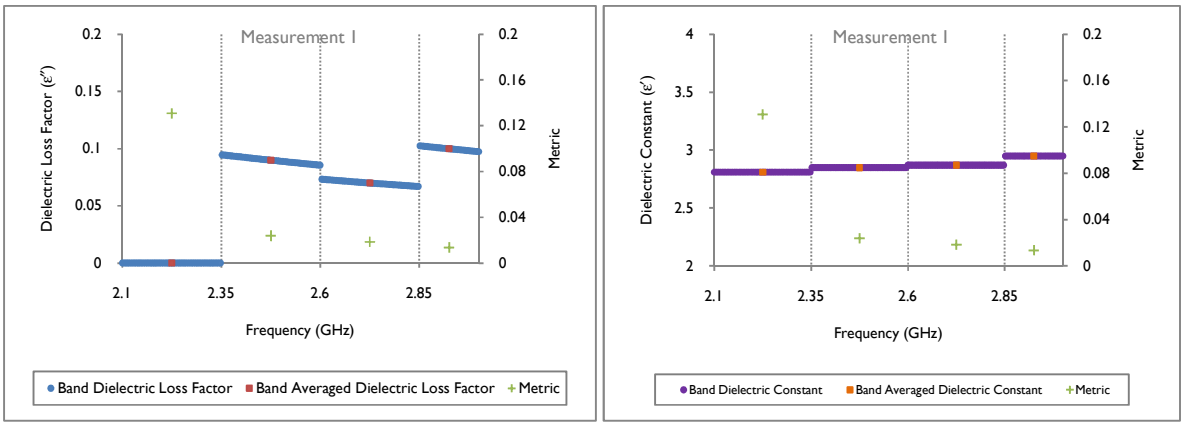

Figure 57: Extracted ε′ and ε″ for Porphyry Copper ore (-5.6+4.75 mm, Measurement 1, WR284)

M1 and M2 exhibit a similar general trend in the extracted ε″ across the operational frequency interval. The smaller particle sizes limit the wall effect of the sample holder. This results in a smaller variation in the extracted dielectric properties. The smaller particle size introduces spatial homogeneity for the crushed particulate load resulting in a smaller variation in the extracted dielectric properties between individual dielectric property measurements.

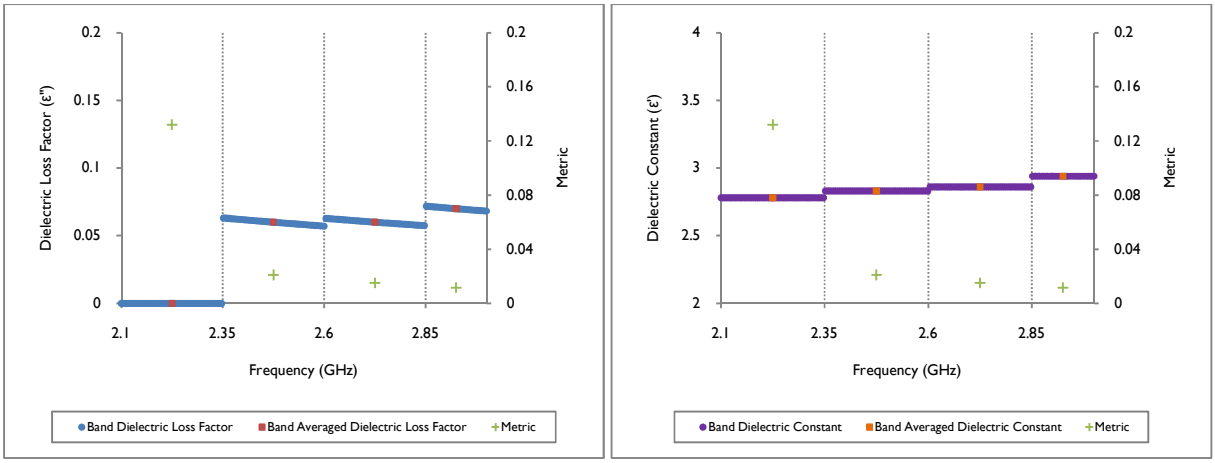

Figure 58: Extracted ε′ and ε″ for Porphyry Copper ore (-5.6+4.75 mm, Measurement 2, WR284)

The dielectric constant exhibits, on average, a <1% variation between M1 and M2 across the particle size distribution. The dielectric loss factor exhibits, on average, a 30% variation between M1 and M2 across the particle size distribution. The significant variation in the dielectric loss factor is attributed to the large degree of misalignment of the S_{11} parameter between M1 and M2 (Figure 133).

6.11.2.7 Particle Size: -4.75+3.35 mm

As for the -6.7+5.6 mm and -5.6+4.75 mm particle size classes, the measured S_{11} parameter for the -4.75+3.35 mm particle size class, exhibits a high degree of similarity between M1 and M2 (Figure 137). This results in the same general trend for both ε′ and ε″ values (Figure 59 and Figure 60).

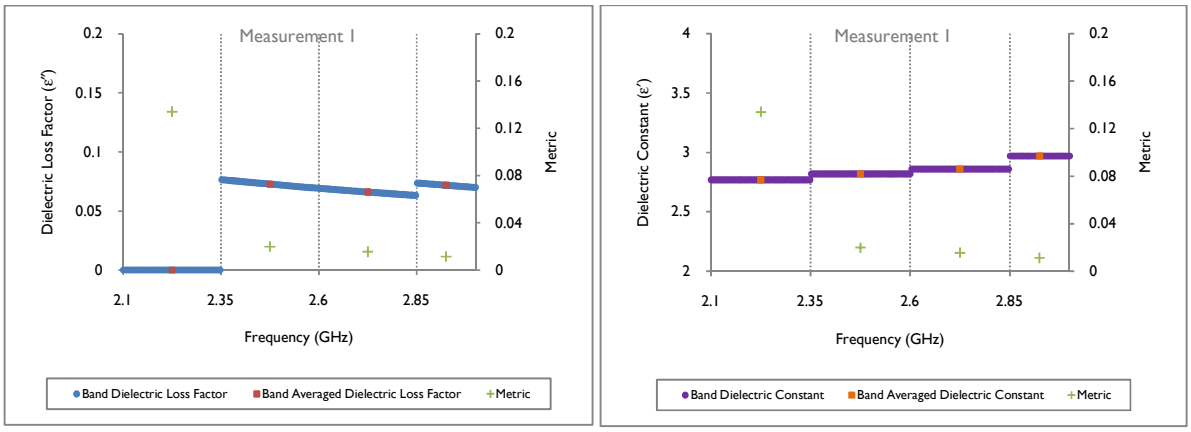

Figure 59: Extracted ε′ and ε″ for Porphyry Copper ore (-4.75+3.35 mm, Measurement 1, WR284)

The average difference in the extracted ε′ value between the individual frequency intervals for M1 and M2 is 2%.

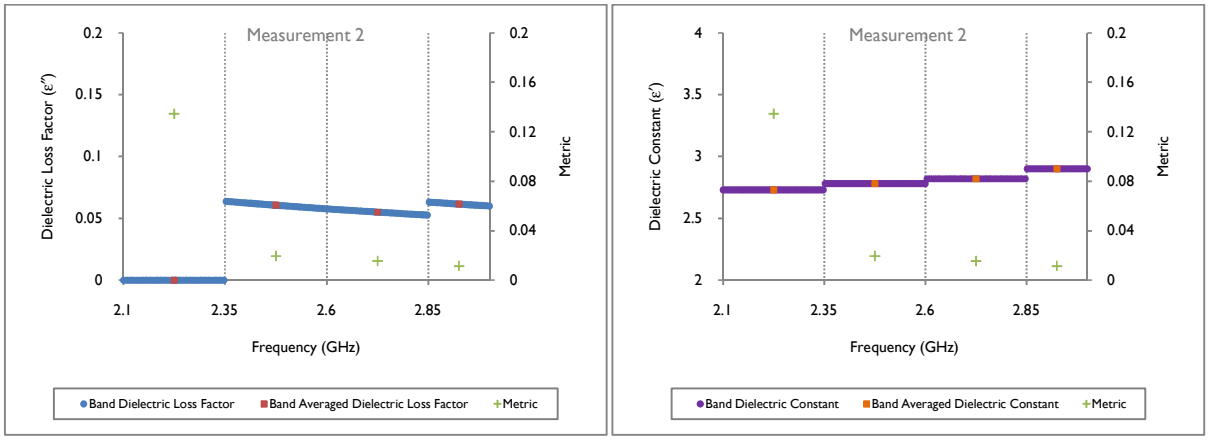

Figure 60: Extracted ε′ and ε″ for Porphyry Copper ore (-4.75+3.35 mm, Measurement 2, WR284)

For the extracted ε″ values, the average variation between the individual frequency intervals for M1 and M2 is reduced to 17%. This clearly indicates that with decreasing particle size, the magnitude of the variation between individual ε″ is significantly reduced, increasing the extracted property reproducibility which is a key aspect when designing microwave applicators.

6.11.2.8 Particle Size: -3.35+2 mm

For the smallest particle size class, the average variation in the extracted ε″ values between the individual frequency intervals is reduced to 6%, observed in Figure 61 and Figure 62.

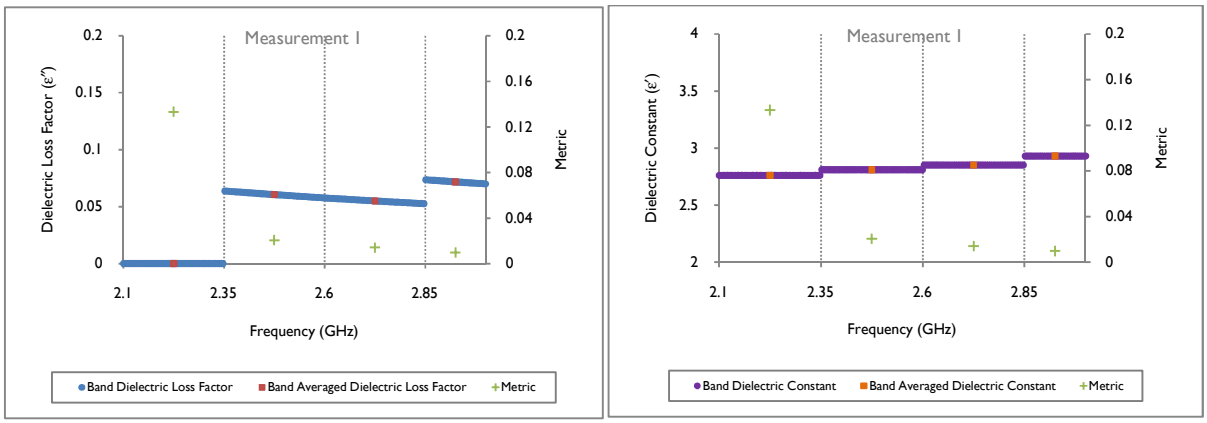

Figure 61: Extracted ε′ and ε″ for Porphyry Copper Ore (-3.35+2 mm, Measurement 1, WR284)

An average variation of 2% in the extracted ε′ values was determined between the frequency intervals for M1 and M2. The measured S_{11} parameter for M1 and M2 exhibits a large degree of similarity across the 2.1-3 GHz frequency interval (Figure 138).

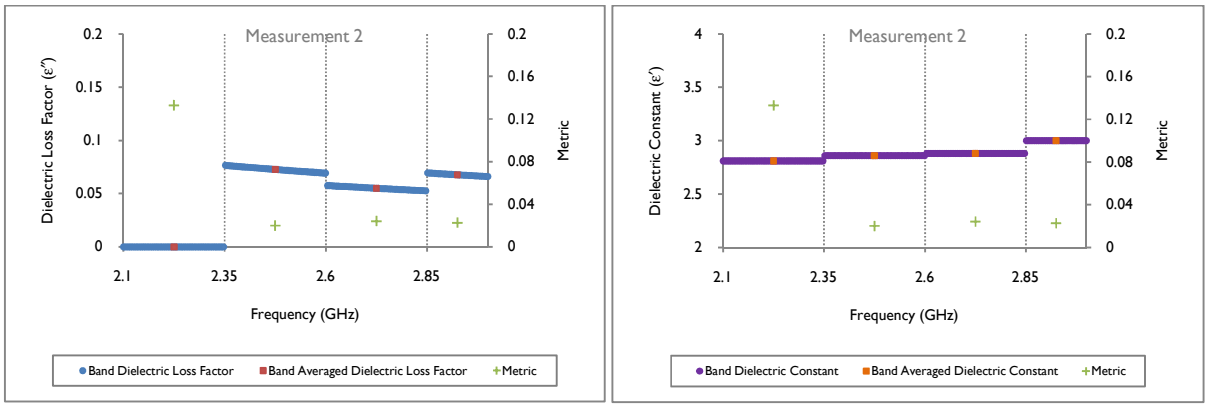

Figure 62: Extracted ε′ and ε″ for Porphyry Copper Ore (-3.35+2 mm, Measurement 2, WR284)

For M1 and M2, the metric is of the same order of magnitude. Ignoring the cut-off frequency effect in the 2.1-2.35 GHz frequency interval, the reported average metric is significantly smaller when compared with that of a larger particle size class. When compared with the -26.5+16 mm particle size class, the average metric for the -4.75+3.35 mm particle size class is 52% smaller.

6.11.3 Full Band Extraction: 700 MHz (2.3-3 GHz)

For the 100 MHz and 250 MHz piecewise frequency interval extractions, the DBE Algorithm experimentally fits the measured S_{ij} parameter in each of the narrow frequency intervals producing 9 and 4 extracted ε′ and ε″ values respectively for each extraction. The full band extraction provides a single ε′ and ε″ value over the entire 700 MHz frequency interval for each dielectric property extraction.

The extracted dielectric constant and loss factor for the -26.5+16 mm particle size class (Measurement 1 and 2) are shown in Figure 63 and Figure 64:

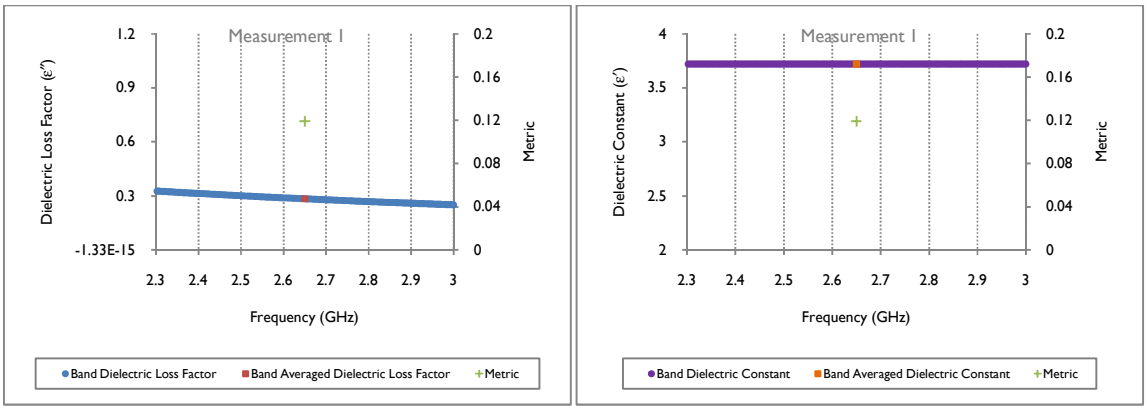

Figure 63: Extracted ε′ and ε″ for Porphyry Copper ore (-26.5+16 mm, Measurement 1, WR284)

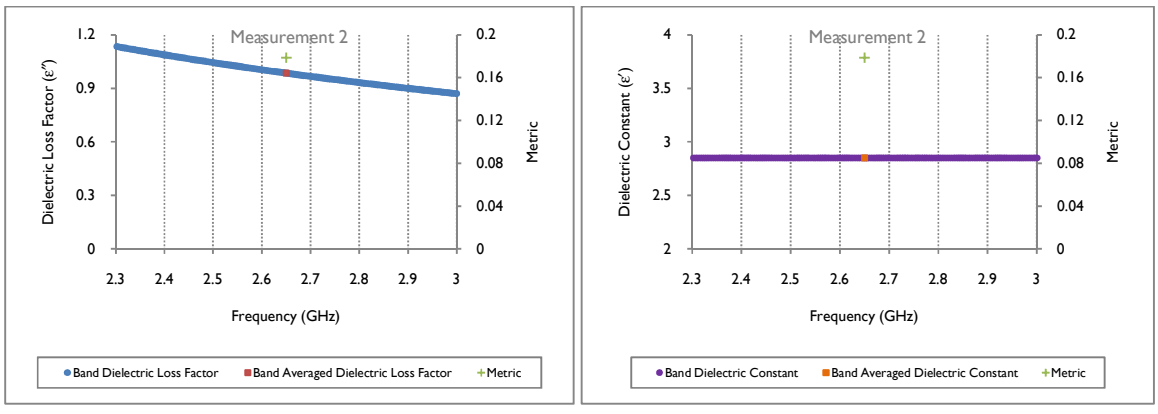

Figure 64: Extracted ε′ and ε″ for Porphyry Copper ore (-26.5+16 mm, Measurement 2, WR284)

The extracted dielectric constant and loss factor for the remaining particle size classes exhibit the same general trend as illustrated in Figure 63 and Figure 64. The results for the remaining particle size classes are included in Appendix H1.

A summary of the extracted dielectric properties is provided in Table 8:

Table 8: Porphyry copper ore - extracted ε′ and ε″ (WR284, full band extraction)

Particle Size (mm)	Measurement 1			Measurement 2		
	ε'	$\varepsilon''_{corr,interval}$	$\|\bullet\|_{min}$	ε'	$\varepsilon''_{corr,interval}$	$\|\bullet\|_{min}$
-26.5+16	3.72	0.28	0.1191	2.85	0.99	0.1786
-16+11.2	2.79	0.11	0.0505	2.64	0.10	0.0945
-11.2+8	2.90	0.13	0.0437	2.81	0.10	0.0431
-8+6.7	2.88	0.15	0.0390	2.89	0.10	0.0334
-6.7+5.6	2.89	0.11	0.0298	2.90	0.08	0.0258
-5.6+4.75	2.87	0.08	0.0250	2.89	0.06	0.0250
-4.75+3.35	2.84	0.07	0.0235	2.80	0.06	0.0228
-3.35+2	2.84	0.07	0.0229	2.88	0.07	0.0265

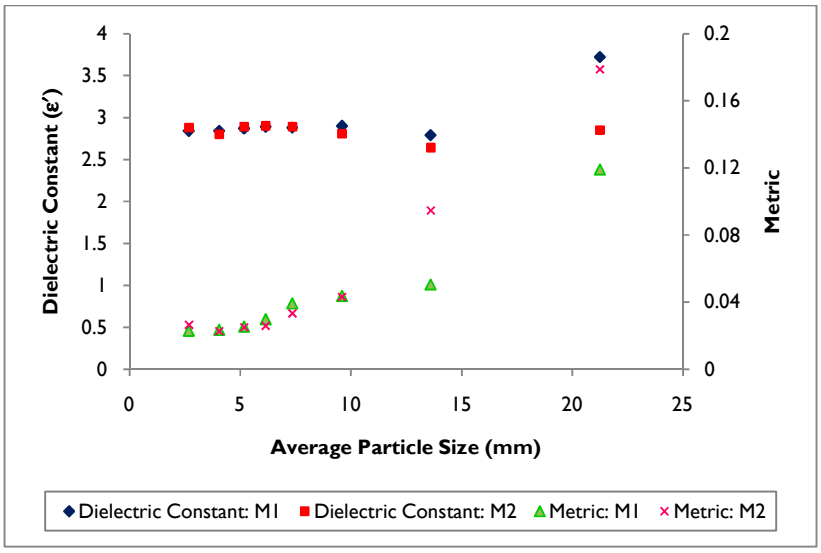

Figure 65: Porphyry copper ore – extracted ε′ (WR284)

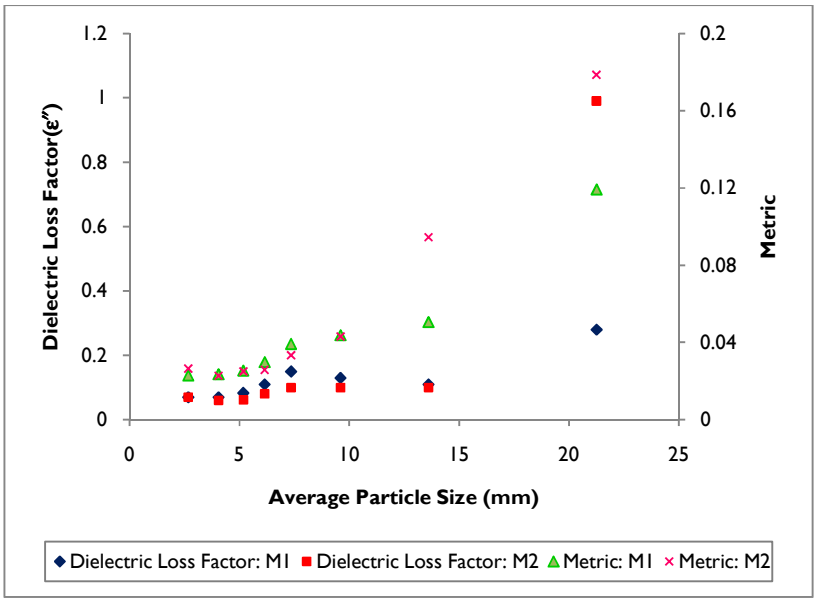

Figure 66: Porphyry copper ore - extracted ε″ (WR284)

From Figure 65 and Figure 66 the effect of particle size is observed for both the extracted ε′ and ε″ values across the particle size distribution.

The extracted ε′ and ε″ values exhibit a large degree of similarity in the -3.35+2 mm, -4.75+3.35 mm, -5.6+4.75 mm, -6.7+5.6 mm and -8+6.7 mm particle size classes.

With increasing particle size (-11.2+8 mm, -16+11.2 mm and -26.5+16 mm), the difference between the extracted ε′ values for M1 and M2 becomes increasingly larger, which is attributed to the wall effects of the sample holder.

A significant difference in the extracted ε′ values between M1 and M2 are observed in the -26.5+16 mm (30.5%) particle size class. For the -16+11.2 mm particle size class the variation is reduced to 6% with the remaining particle size classes the variation is less or equal to 1%. On average across all particle size classes the variation in ε′ is 5%.

A significant difference in the extracted ε″ value between M1 and M2 is observed in the -26.5+16 mm (254%), -16+11.2 mm (10%), -11.2+8 mm (30%), -8+6.7 mm (50%) and -6.7+5.6 mm (38%) particle size classes. The wall effects become significant if the particle size is of the same magnitude of the sample holder dimension used for dielectric property measurement.

With increasing particle size, the particulate load becomes spatially less homogeneous and hence the S_{ij} parameter data is fitted more poorly with the homogeneous load. The poorer fit of the simulated S_{ij} parameter to the measured S_{ij} parameter is observed in the increase in magnitude of the metrics in the three largest particle size classes (Table 8).

For the -26.5+16 mm and -16+11.2 mm particle size classes, the extracted ε′ and ε″ vary considerably between M1 and M2. However, for the WR284 sample holder, and for particle sizes greater than 11.2 mm the homogeneous load less reliably represents the ore.

6.12 Comparison of S_{ij} – Experimental and DBE Algorithm

In Section 6.11, the dielectric loss factor and dielectric constant for crushed Porphyry Copper ore (Measurement 1 and 2) were determined for a piecewise and full band frequency extraction for each particle size class. Interpretation of the results led to the following conclusions:

100 MHz Piecewise Frequency Extraction

- The 100 MHz piecewise frequency extraction suffered from fitting insensitivity. For approximately the same goodness of fit (metric value), largely differing values for ε″ were extracted in the different frequency bands with the aid of the DBE Algorithm. From Figure 31 through Figure 46 the same tendency is observed for Measurement 1 and 2 in predominantly the 2.7-3 GHz frequency band.
- Dielectric property extractions over narrower 100 MHz frequency bands resulted in a significantly different extracted ε″ values between the individual frequency intervals. It is believed that the narrower frequency interval contains insufficient information to allow good fitting.

250 MHz Piecewise Frequency Extraction

- As was the case with the 100 MHz piecewise extractions, the 250 MHz piecewise frequency extractions exhibited variation in ε″ between the individual frequency intervals.
- The metric followed the same trend, with considerable variation between the individual frequency intervals.
- The larger 250 MHz tended to decrease the variation in the dielectric properties between individual ANA measurements due to the inclusion of a larger frequency interval over which the experimental S_{ij} parameter fitting was done.

700 MHz Full Band Frequency Extraction

- The DBE Algorithm used the entire 700 MHz frequency interval to extract only one ε′ and one ε″ value. The larger frequency interval provided more data with a greater range of features; this resulted in the inclusion of the full resonance feature in contrast to the piecewise extractions. The latter breaks up the frequency interval over which the resonance feature is developed and hence results in a loss of featured frequency space.
- The larger frequency interval over which the DBE Algorithm extracted the dielectric properties resulted in an increase in the confidence of the extracted ε′ and ε″ values. This is seen in the smaller metrics reported throughout the -26.5+2 mm particle size distribution compared with the piecewise 100 MHz and 250 MHz frequency interval extractions.
- Only one metric over the entire 2.3-3 GHz frequency interval was determined. This single metric value represents goodness of fit between the simulated DB and measured S_{ij} parameter over the full frequency interval and gives some generalised feel of the degree of confidence to which the DBE Algorithm extracts the ε′ and ε″ values.

Based on these conclusions, full band extractions are preferred over piecewise extractions and will be used throughout the remainder of this thesis for the extraction of ε′ and ε″. In Section 6.12.1, the attention is focussed on the comparison of the S_{22} parameter between the experimental (measured) S-parameter and that obtained by the DBE Algorithm for crushed Porphyry Copper Ore, Measurement 1. In Section 6.12.2 the same is done for Measurement 2.

The DBE Algorithm produces the magnitude and phase angle of the S_{ij} parameter as a complex number (a+bj) at each frequency point in the operational frequency band. The magnitude (or modulus) of S_{ij} is calculated by Equation 12.

Equation 12: Simulated S_{ij} parameter magnitude

$$\left|S_{ij}\right| = \sqrt{a^2 + b^2}$$

The phase angle component is calculated using Equation 13.

Equation 13: Simulated S_{ij} parameter phase angle

$$\phi = \arctan\left(\frac{b}{a}\right)$$

The discussion is restricted to only Porphyry Copper ore, as the same logic can be applied to any ore of interest. Only the -16+11.2 mm particle size class will be discussed for the piecewise 100 MHz (Section 6.12.1.1), 250 MHz (Section 0) and full band extraction (Section 6.12.1.3) using the DBE Algorithm. All measurements were conducted in the WR284 sample holder.

The -16+11.2 mm particle size class was chosen as it exhibits a large metric in the resonance frequency band 2-6-2.7 GHz compared with the rest of the reported metrics (Figure 33). Despite the large resonance metric, the -16+11.2 mm particle size class exhibited large variation in the extracted loss factor for the different 100 MHz frequency bands (Section 6.11.1.2).

The interpretation of the results serves as a case study to compare piecewise frequency extractions to full band frequency extraction for a single particle size class. The conclusions drawn from the discussion will aid in selecting either piecewise property extraction or full band extractions for use in the remainder of the thesis.

Only the S_{22} scattering parameter is referred to in the discussion as only ANA Port 2 was used for the dielectric property extraction.

6.12.1 Porphyry Copper Ore (-16+11.2 mm, Measurement 1)

6.12.1.1 Piecewise Frequency Extraction (Frequency Interval: 100 MHz)

In Section 6.11.1 variation in the extracted dielectric loss factor and dielectric constant was identified between the different frequency bands. The 100 MHz piecewise frequency extraction suffered from extraction insensitivity (negligible change in metric, large variation in loss factor), and large metric values in the featured resonance frequency space (usually between 2.6 and 2.7 GHz). To understand this phenomenon, the S_{22} scattering parameters for the measured and DB extraction are compared in Figure 67.

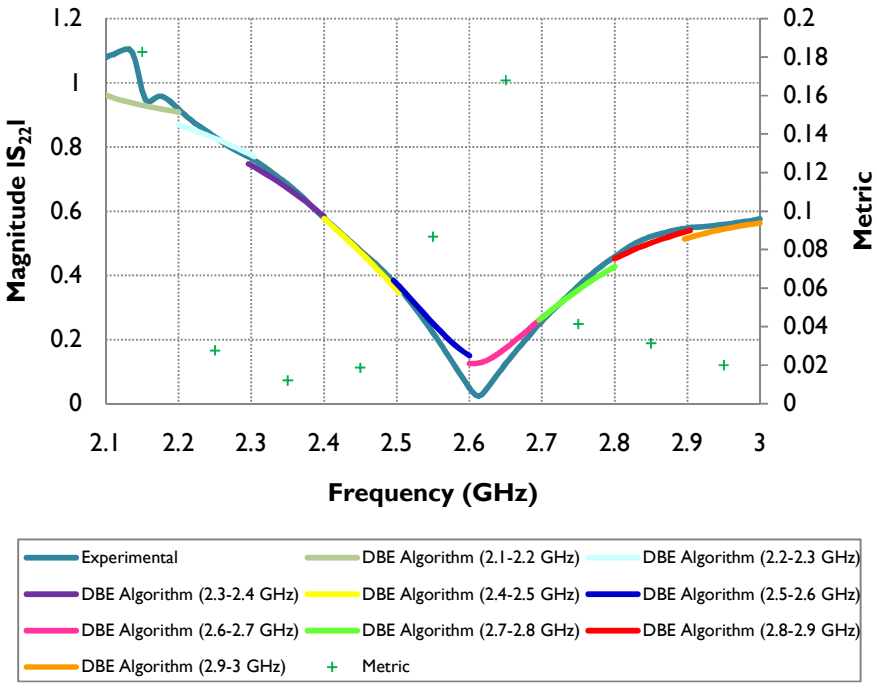

Figure 67: Porphyry copper ore – experimental and DBE algorithm $|S_{22}|$ comparison (100 MHz)

In Figure 67 the effect of the cut-off frequency is noticeable as seen in the oscillatory behaviour of the experimental S_{22} parameter in the 2.1-2.2 GHz frequency interval. The large metric reported for the 2.1-2.2 GHz frequency interval is attributed to the large difference between the simulated and measured S_{22} parameters. The effect is still observed in the 2.2-2.3 GHz frequency interval due to the smaller, but still prominent, difference in measured and DB S-parameter despite similarity in phase angle (Figure 68).

For the 2.3-2.4 GHz frequency interval, the goodness of fit has improved as the effect of the cut-off frequency has become smaller. The same trend, although to a lesser extent, is observed for the 2.4-2.5 GHz frequency band.

In the 2.5-2.6 GHz and 2.6-2.7 GHz frequency bands, large metrics are observed when compared with the remaining metrics across the frequency range. A larger degree of extraction uncertainty is reflected by the increase in the reported metric. The extracted ε″ and ε′ values reflect the poor fit between the simulated and measured S_{22} parameter reference (Figure 33).

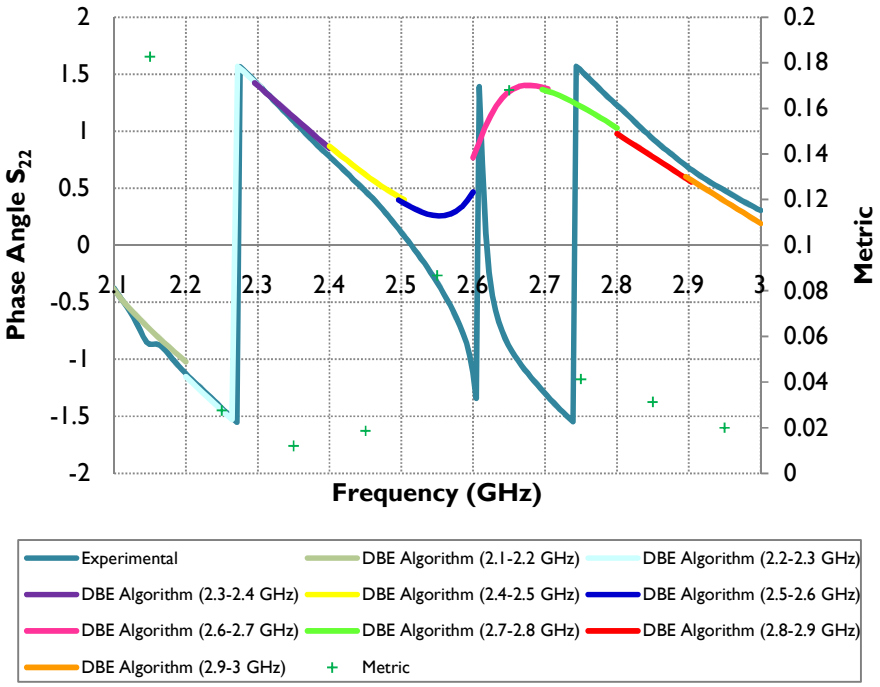

Figure 68: Porphyry copper ore - experimental and DBE algorithm $\angle S_{22}$ comparison (100 MHz)

In the 2.6-2.7 GHz frequency band, the measured and simulated S_{22} parameters differ significantly from one another. The metric reflects this.

The metric is determined by the joint contribution of the magnitude and phase angle of the difference between the S_{ij} parameter(s), with equal weight given to both quantities (Equation 11). The gradual increase in the reported metric values is attributed to the increasingly larger variation in phase angle contribution. From Figure 68 the phase angle deviates substantially from the phase angle (trend) of the measured S_{ij}-parameter; hence, a larger metric is reported. This is especially true for the 2.6-2.7 GHz frequency interval where the difference in S_{22} in both magnitude and phase angle between the measured and DB S_{ij} parameter reaches a maximum. The phase angle behaviour in the 2.6-2.7 GHz frequency interval is poorly modelled, and the metric in this band is correspondingly large.

For the 2.7-2.8 GHz and 2.8-2.9 GHz frequency bands the experimental fit gradually improves, despite misaligned phase angles, with near constant reported metrics and dielectric loss factors.

However, for the 2.9-3 GHz frequency band, despite an improved experimental fit, the dielectric loss factor deviates from the general trend observed in the 2.7-2.8 GHz and 2.8-2.9 GHz frequency bands (Figure 33). The behaviour in the extracted dielectric loss factor is not reflected by the variation in magnitude or phase angle in the 2.9-3 GHz frequency band and is explained by the flat, featureless data space. The DBE Algorithm requires a featured frequency interval in which adequate changes in the measured S-parameter across the frequency band of interest to provide a good fit.

For the 100 MHz piecewise frequency extraction the DBE Algorithm misplaces the DB resonance feature (Figure 132).

The minimum measured resonance magnitude, 0.023 at 2.613 GHz, is located 5 MHz from the DB minimum resonance, 0.124 at 2.608 GHz. Hence, the difference in magnitudes is 0.101. Misalignment of the simulated and measured S_{22} parameter directly affects the extracted ε' and ε'' values. The extent to which the measured and simulated resonance feature differs in depth and width from each other can be related to the magnitude of dielectric constant and dielectric loss

factor. In general, the width of the resonance is related to the dielectric loss factor and the location of the resonance to the dielectric constant.

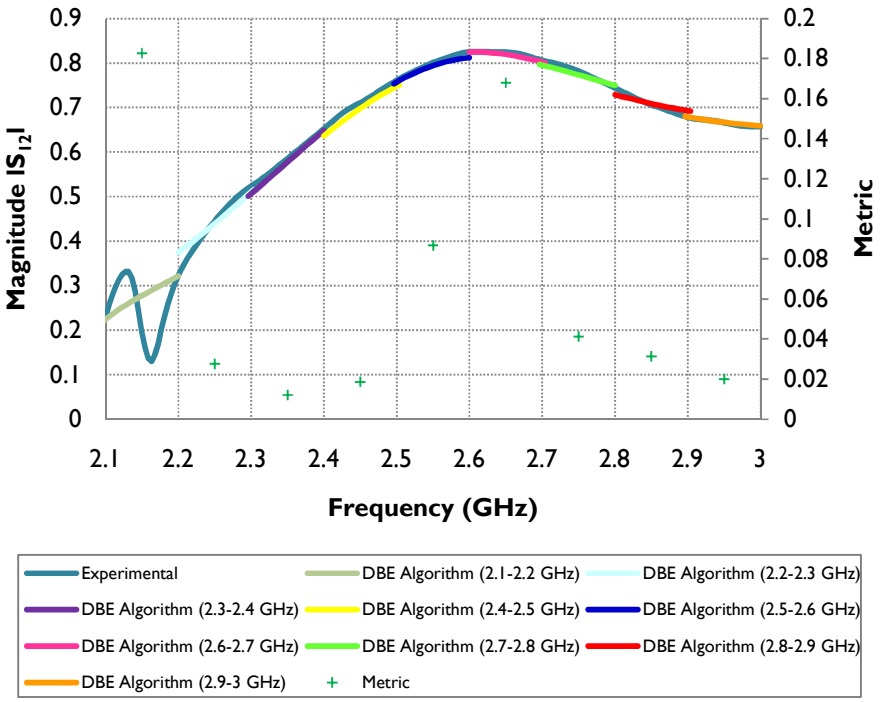

Figure 69: Porphyry copper ore - experimental and DBE algorithm $|S_{12}|$ comparison (100 MHz)

For the S_{12} parameter, the DBE Algorithm fits the experimental S_{12} parameter set well across the 2.3-3 GHz frequency interval. For the 2.1-2.3 GHz frequency interval, the effect of the cut-off frequency is clearly observed in the large metric.

The larger metrics seen in the 2.5-2.6 GHz and 2.6-2.7 GHz were attributed to the contribution of $\angle S_{22}$ where a significant difference in the phase angle component is observed between the measured and simulated S_{22} parameter (Figure 68).

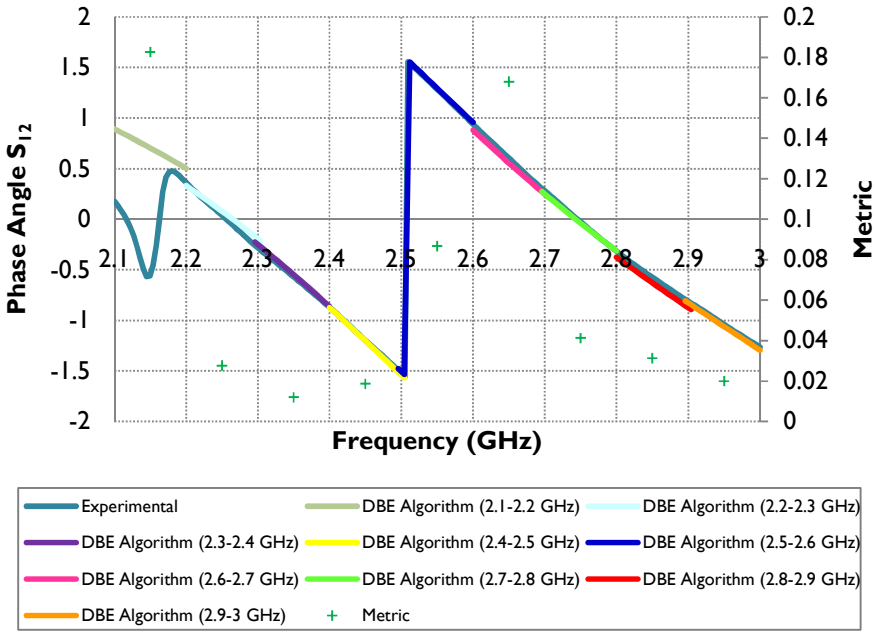

Figure 70: Porphyry copper ore - experimental and DBE algorithm $\angle S_{12}$ comparison (100 MHz)

The DBE Algorithm produced a good fit between the phase angle components of the measured and simulated S_{ij} parameter set across the 2.3-3 GHz band (Figure 70). The DBE Algorithm correctly locates the point where the S_{12} phase angle unwraps through 180°. This is observed in the 2.5-2.6 GHz frequency interval (blue curve) where the DBE Algorithm correctly accounts of the 180° phase change ($\angle S_{12}$= ±1.5).

6.12.1.2 Piecewise Frequency Extraction (Frequency Interval: 250 MHz)

In Section 6.12.1.1 variation between the extracted dielectric loss factor and dielectric constant was identified between the different frequency bands. A comparison between the measured and simulated S_{22} parameter is presented in Figure 71.

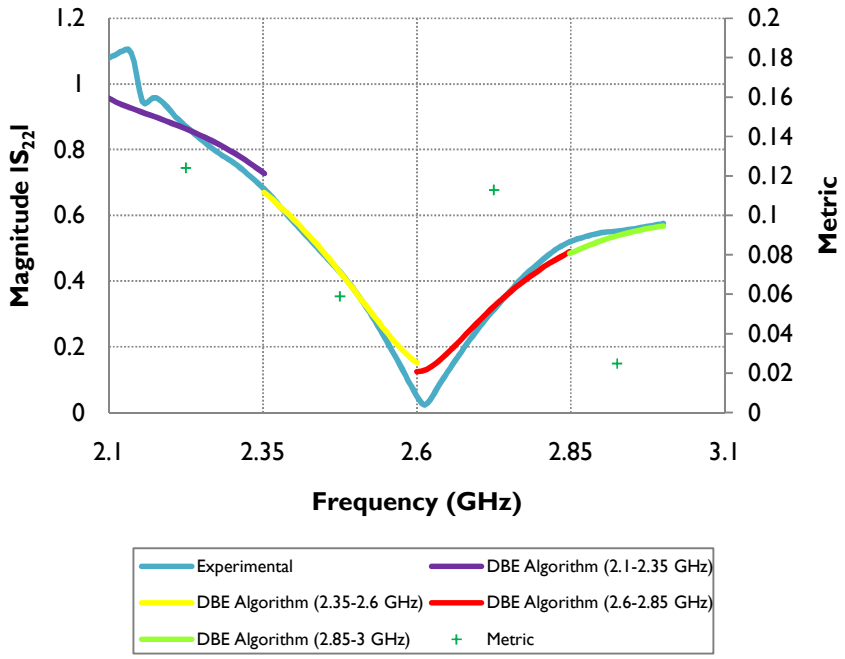

Figure 71: Porphyry copper ore - experimental and DBE algorithm $|S_{22}|$ comparison (250 MHz)

The effect of the cut-off frequency on the reported metric value for the 2.1-2.35 GHz frequency interval has become smaller due to the larger frequency band over which the DBE Algorithm performs the dielectric property extraction. In the 2.35-2.6 GHz frequency band the metric decreases due to the better alignment of the measured and simulated S_{22} parameter seen in Figure 71. In this frequency band, the phase angle contributes the most to the reported metric value as a substantial variation from the measured S_{22} phase angle trend is observed.

In the 2.6-2.85 GHz frequency band the goodness of fit decreases to a minimum and is attributed to the joint effect of both the magnitude and phase angle deviating from the measured S_{22} parameter.

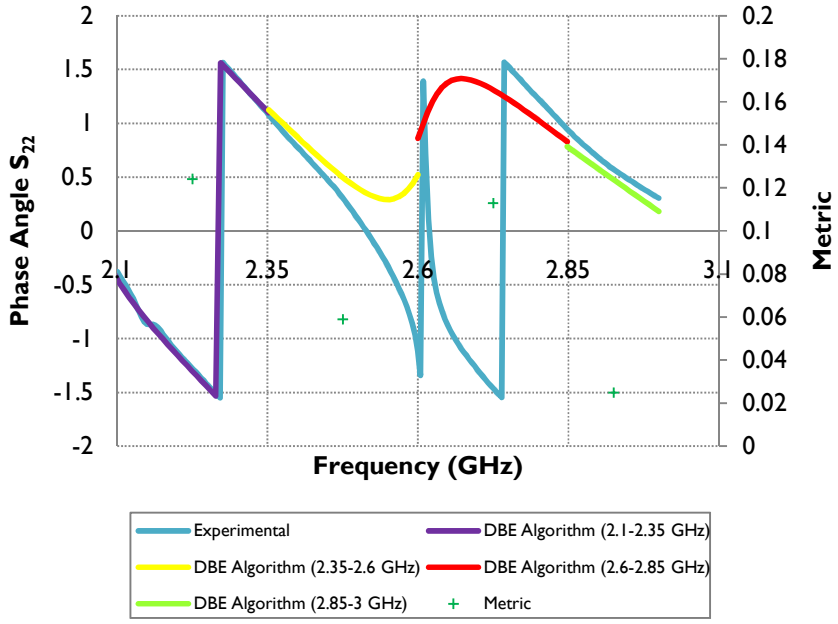

Figure 72: Porphyry copper ore - experimental and DBE algorithm $\angle S_{22}$ comparison (250 MHz)

In the 2.85-3 GHz frequency band the metric decreases as the difference between the magnitude and phase angle of the measured and simulated S_{22} parameter decreases. The poor fit in phase angle fit seen in the 2.6-2.85 GHz (resonance) frequency band is no longer noted at higher frequencies.

Similarly to the 100 MHz piecewise frequency extraction, the DBE Algorithm misplaced the measured resonance by 13 MHz. However, the magnitude of the difference between the minimum measured and DB resonance magnitudes was reduced to 0.101 compared with 0.128 for the 100 MHz piecewise frequency extraction. This clearly shows that the larger 250 MHz piecewise extraction better aligns the resonance feature as it minimised the magnitude difference between the measured and simulated S_{22} parameter.

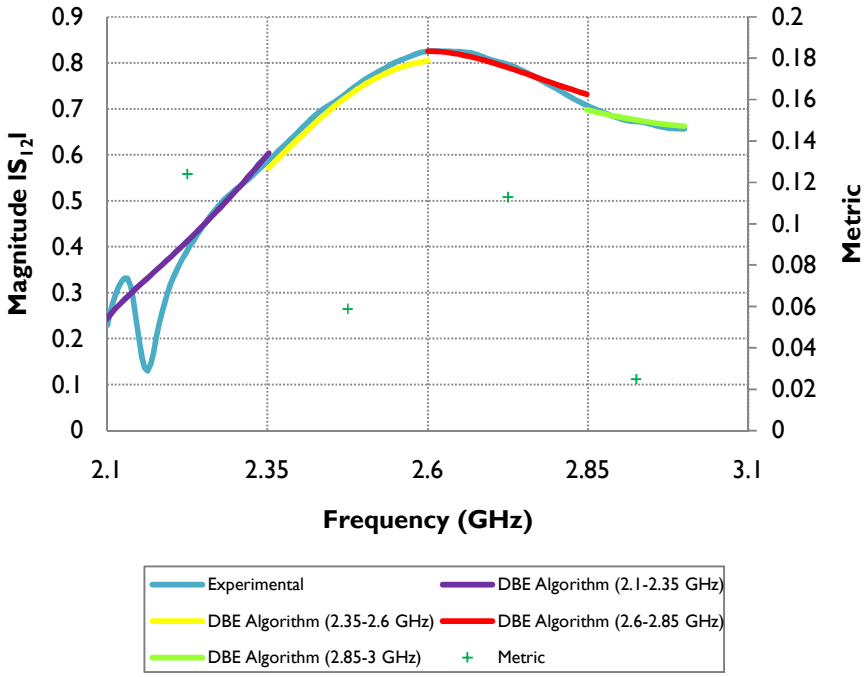

Figure 73: Porphyry copper ore - experimental and DBE algorithm $|S_{12}|$ comparison (250 MHz)

The magnitudes of the simulated and measured S_{12} parameter corresponds well in Figure 73. This is evident in the smaller reported metrics in the resonance frequency interval compared with those of the 100 MHz piecewise extraction (Figure 67).

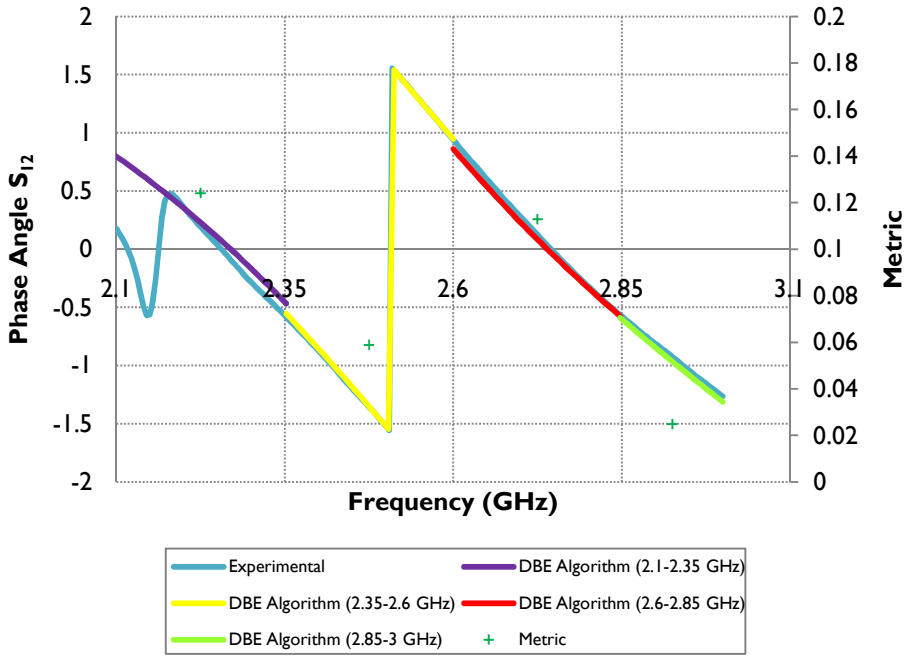

Figure 74: Porphyry copper ore - experimental and DBE algorithm $\angle S_{12}$ comparison (250 MHz)

As is the case for the 100 MHz piecewise extraction (Figure 70) the DBE Algorithm closely aligns the simulated and measured S_{12} parameter across the 2.3-3 GHz frequency band. The DBE Algorithm also correctly models the phase unwrapping observed in the 2.35-2.6 GHz frequency interval (yellow curve) where the DBE Algorithm correctly accounts of the 180° phase change ($\angle S_{12}= \pm 1.5$).

The relatively larger metric in the 2.6-2.85 GHz frequency interval is attributed to the contribution of the variation in the magnitude (Figure 71) and phase angle (Figure 72) between the DB and measured S_{22} parameter.

6.12.1.3 Full Band Frequency Extraction (Frequency Interval: 700 MHz)

The full band frequency extraction comparison between measured and DB S_{22} parameter is shown in Figure 75.

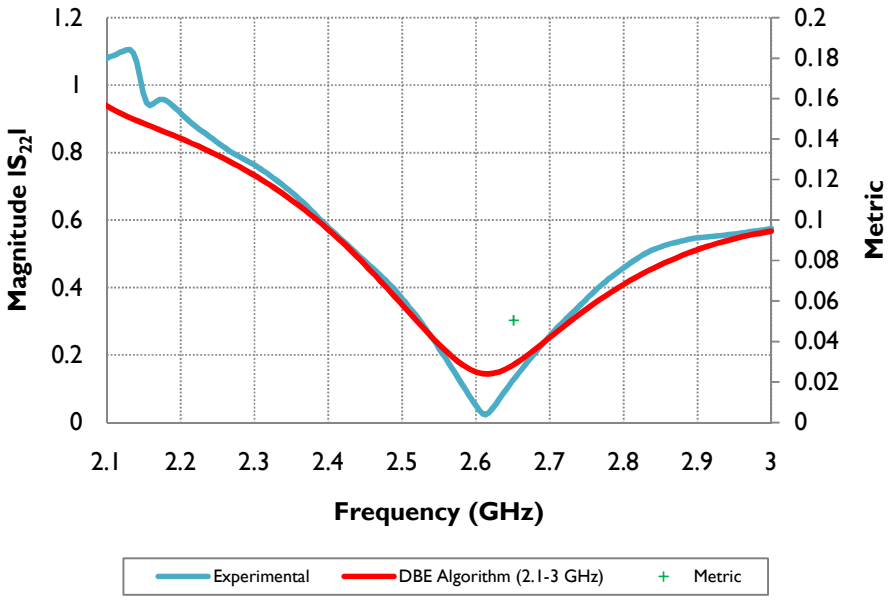

Figure 75: Porphyry copper ore - experimental and DBE algorithm $|S_{22}|$ comparison (700 MHz)

Across the entire 2.3-3 GHz frequency interval the magnitude of the simulated S_{22}-parameter compares well to that of the measured data. The goodness of fit is significantly better than is the case with the piecewise 100 MHz and 250 MHz frequency extractions. The minimum measured resonance magnitude, 0.023, is located at 2.613 GHz whilst the DBE Algorithm produces a value of 0.144 at 2.616 GHz. The offset is only 3 MHz, compared with the 5 MHz and 13 MHz obtained for the 100 MHz and 250 MHz piecewise frequency extractions respectively. The full band extraction provides for a better alignment of the resonance feature compared with smaller piecewise extractions.

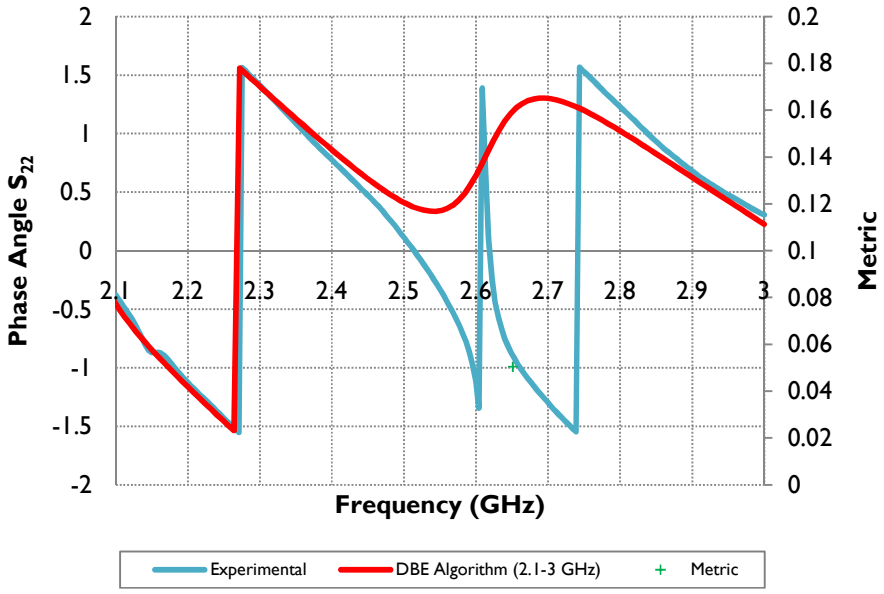

Figure 76: Porphyry copper ore – experimental and DBE algorithm $\angle S_{22}$ comparison (700 MHz)

However, the full band extraction provide for a poorer fit of the phase angle component compared with the magnitude of the S_{22} parameter. This leads to a metric value dominated by the phase angle contribution. This is seen in Figure 76, where the simulated behaviour at resonance fails to follow the experimental data.

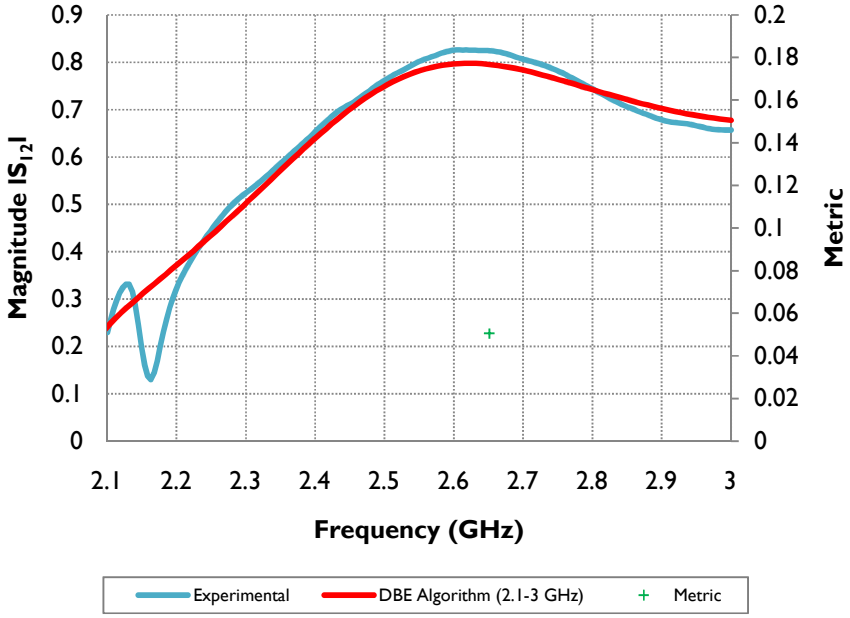

Figure 77: Porphyry copper ore – experimental and DBE algorithm $|S_{12}|$ comparison (700 MHz)

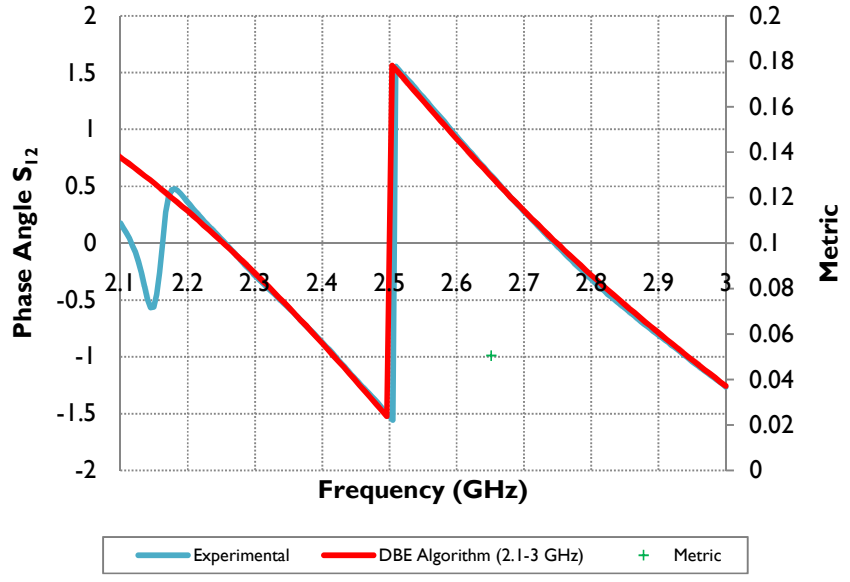

Figure 78: Porphyry copper ore – experimental and DBE algorithm $\angle S_{12}$ comparison (700 MHz)

The DBE Algorithm aligned the phase angle component of the S_{12} parameter (Figure 78). The DBE Algorithm located the phase unwrapping correctly. This is observed in the 2.5-2.6 GHz frequency interval (red curve) where the DBE Algorithm correctly accounts of the 180° phase change ($\angle S_{12}= \pm 1.5$).

In Figure 78, the sudden jump in the phase angle component of the measured S_{12} parameter is due to crossing -180° degrees on the Smith Chart at a frequency of 2.5 GHz. The phase angle component of the S_{22} parameter (Figure 76) only moves closer to the axis origin on the chart, however never crossing it. The parameter only only moves closer to the origin and then away. This is accounted for by the simulated parameter. Hence, the simulated S_{22} phase angle smoothly decreases and then increases as the phase angle component of the measured S_{22} parameter moves away from the axis-origin on the Smith Chart.

A slight variation is observed in the magnitude fitting of the S_{12} parameter (Figure 77). However, as the DB fitting of the S_{ij} parameter was executed over the entire 2.3-3 GHz frequency band, the overall goodness of fit for the full band extraction is better. Although the DB S_{12} parameter deviates from the measured set in the resonance frequency interval, the DBE Algorithm aligns the S_{22} parameter in width to the experimental value (Figure 75). Alignment in the resonance frequency interval tends to decrease the overall metric. This is seen in the comparison between the resonance metrics for the 100 MHz and 250 MHz piecewise extractions with that of the full band extraction. For the 100 MHz extraction, a metric of 0.1680 (Figure 33) is obtained versus a metric of 0.1129 (Figure 49) for the 250 MHz piecewise extraction. For the full band extraction (Table 8) the metric is the lowest in the resonance frequency *viz.* 0.0505.

It is concluded that with increasing frequency band size over which the DBE Algorithm is executed, the associated confidence in the extracted ε' and ε'' is increased.

6.12.2 Porphyry Copper Ore (-16+11.2 mm, Measurement 2)

6.12.2.1 Piecewise Frequency Extraction (Frequency Interval: 100 MHz)

The effect of the cut-off frequency is noticed in the 2.1-2.2 GHz and 2.2-2.3 GHz frequency bands. The DB S-parameter deviates substantially from the measured data set particularly in the 2.1-2.2 GHz frequency band (Figure 79), with a large band metric of 0.139 compared with the rest of the reported metric values. The DBE Algorithm fails to accurately fit the simulated S_{22} parameter to the experimental data. This is substantiated by the variation in the phase angle in Figure 80. The same trend is observed in the extractions included in Section 6.12.1.1 through 6.12.1.3.

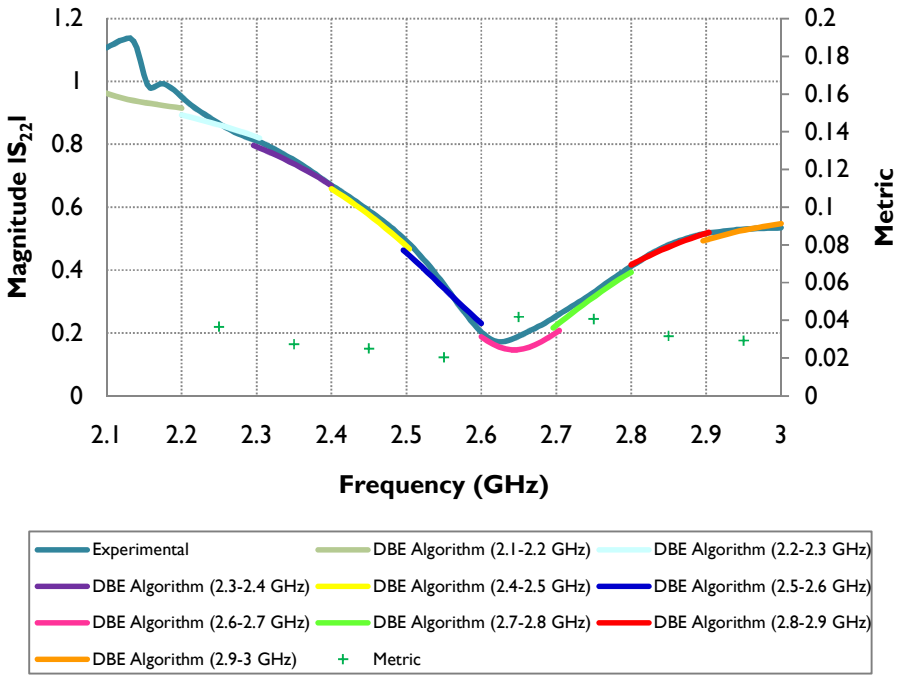

Figure 79: Porphyry copper ore - experimental and DBE algorithm $|S_{22}|$ comparison (100 MHz) Metric = 0.203 (2.1-2.2 GHz)

The DBE Algorithm provides a good fit to the measured S_{22} parameter in the 2.3-2.4 GHz and 2.4-2.5 GHz frequency intervals. The same observation was made for Measurement 1, Figure 67, despite dissimilar measured S_{ij} parameter characteristics (Appendix F, Figure 132). The goodness of fit is especially observed in Figure 79 where the simulated data correspond well in magnitude to the experimental data in the 2.3-2.5 GHz frequency band. The misplacement of the phase angle (Figure 80) in the corresponding frequency bands contributes largely to the reported metric.

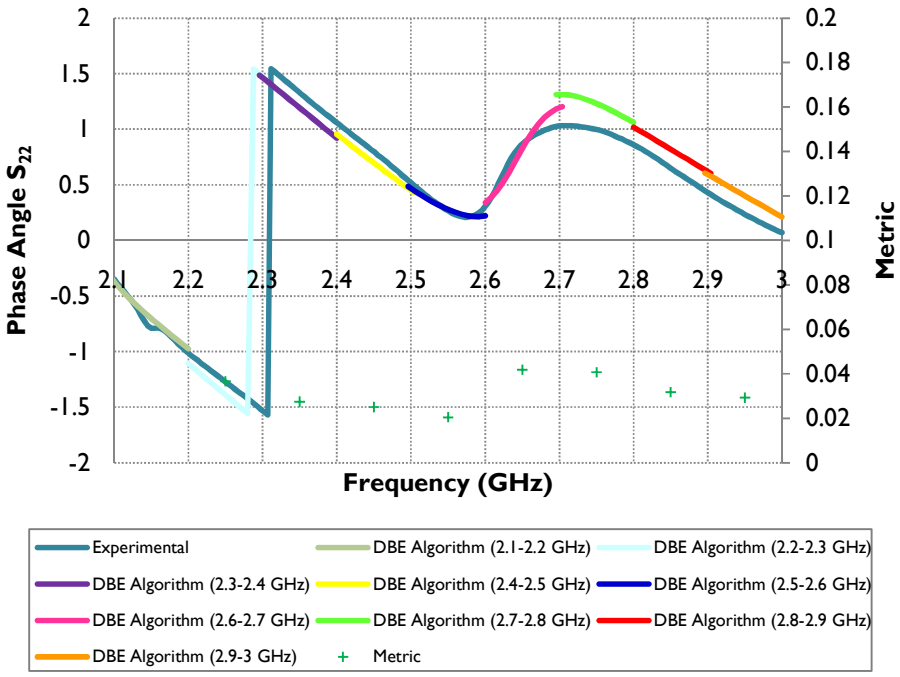

Figure 80: Porphyry copper ore - experimental and DBE algorithm $\angle S_{22}$ comparison (100 MHz) Metric = 0.203 (2.1-2.2 GHz)

For the 2.5-2.6 GHz and 2.6-2.7 GHz frequency bands, the DBE Algorithm fails to fit the magnitude and phase angle components of the S_{22} parameter respectively. The same behaviour is observed for Measurement 1, Figure 71 and Figure 72, although to a much larger extent than is the case for Measurement 2.

It would seem that the DBE Algorithm struggles to fit the simulated S_{ij} parameter to the measured values in *narrow* frequency bands, theoretically characterised by sufficient wave information, to confidently extract the dielectric loss factor and dielectric constant.

The DBE algorithm misplaces the simulated magnitude resonance (Figure 79) and fails to align the S_{22} phase angles. The 2.6-2.8 GHz frequency band contains the measured S_{22} resonance feature. Failure to fit to the measured value results in a poorer fit and hence a large metric value compared with the rest of the frequency intervals. Measurement 1 exhibits similar trends with a total breakdown in fit for the S_{22} phase angle component.

The minimum measured resonance magnitude, 0.172 at 2.626 GHz, is located 21.5 MHz from the simulated minimum resonance, 0.146 at 2.648 GHz. Hence, the difference between in magnitudes is 0.026 compared with 0.128 for Measurement 1 at a 13 MHz offset. In essence, this indicates that measurement reproducibility is poor, which is attributed to the combined effect of the relatively large particle size, the restricted size of the sample holder and the narrow frequency interval over which the dielectric property extraction is performed.

For the 2.7-3 GHz frequency band the experimental fit between the simulated and measured S_{22} parameter becomes increasingly better further away from the resonance feature. This is seen in the decrease in the reported metric values.

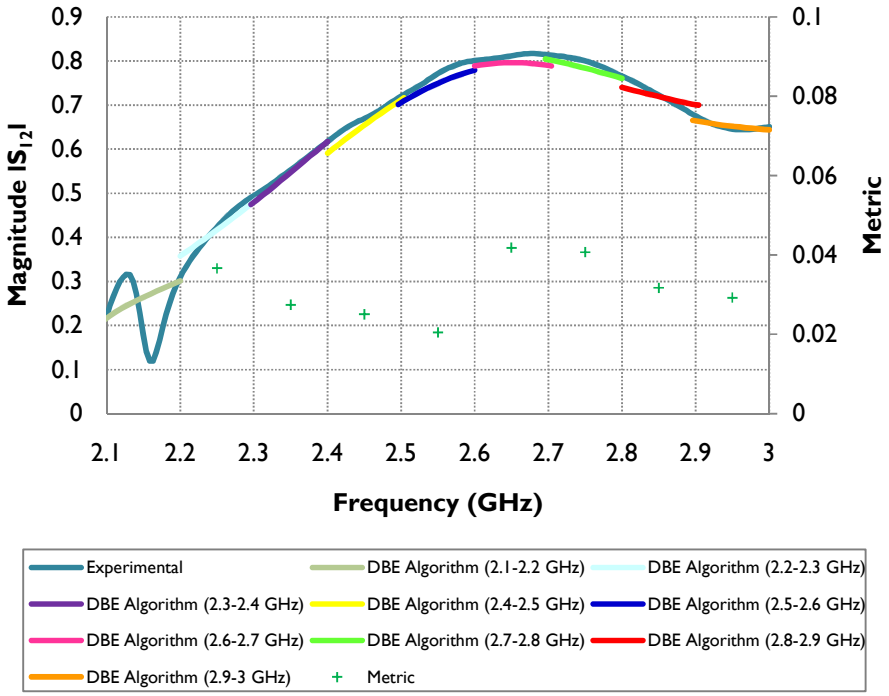

Figure 81: Porphyry copper ore - experimental and DBE algorithm $|S_{12}|$ comparison (100 MHz) Metric = 0.203 (2.1-2.2 GHz)

The magnitude component of the simulated S_{12} parameter is fitted fairly well. However, for Measurement 1, the DBE Algorithm did fit the S_{12} parameter better as is seen by visual inspection of Figure 69. The smaller metrics obtained for Measurement 2 are attributed to the smaller variation between the simulated and DB S_{ij} parameter dataset. For Measurement 1 (Figure 68), the simulated $\angle S_{22}$ parameter differs significantly from the measured trend.

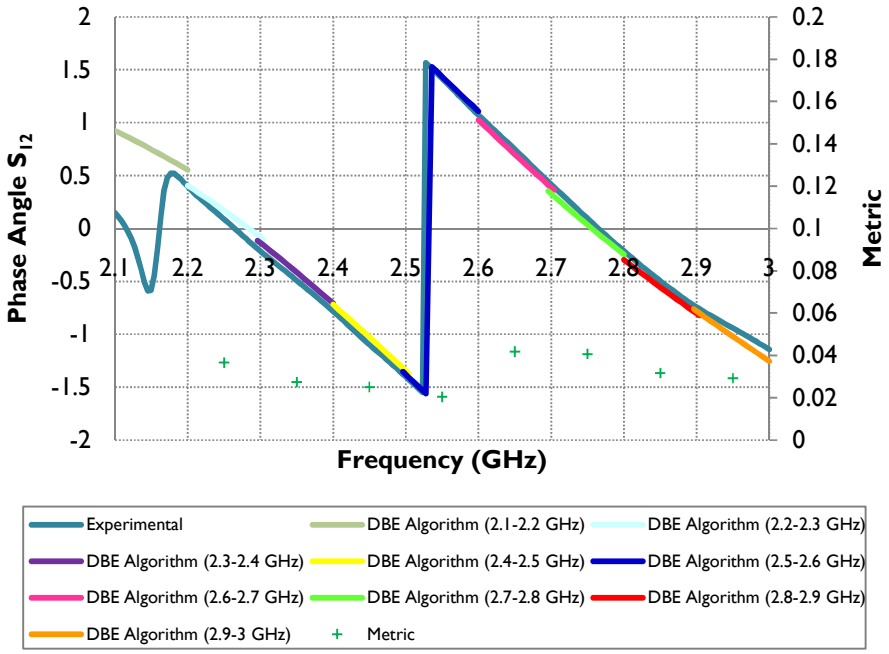

Figure 82: Porphyry copper ore - experimental and DBE algorithm $\angle S_{12}$ comparison (100 MHz) Metric = 0.203 (2.1-2.2 GHz)

As in the case for Measurement 1 (Figure 68), the DBE Algorithm aligns the magnitude component of the simulated and measured S_{12} parameter. This is seen in Figure 82, where little difference between the S_{ij} parameters is observed across the 2.3-3 GHz frequency band.

6.12.2.2 Piecewise Frequency Extraction (Frequency Interval: 250 MHz)

The comparison between the measured and DB S_{22} parameter is presented in Figure 83.

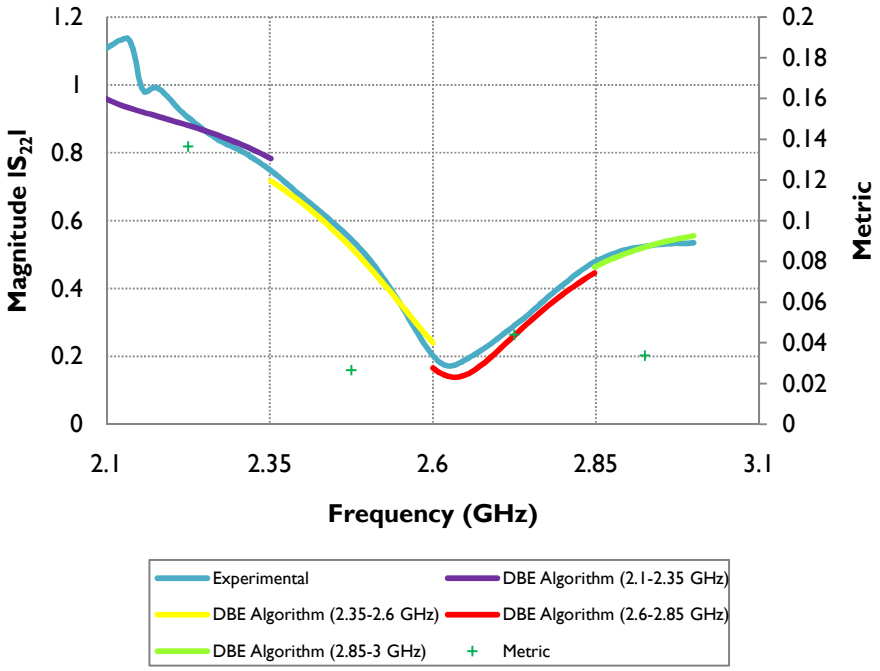

Figure 83: Porphyry copper ore - experimental and DBE algorithm $|S_{22}|$ comparison (250 MHz)

In the 2.35-2.6 GHz frequency interval the DBE Algorithm closely fits the simulated and measured S_{22} parameter. This is seen for both magnitude (Figure 83) and phase angle (Figure 84) components. A deviation does occur at 2.55 GHz where both simulated components tend to diverge from the measured S_{22} parameter. A similar, but larger, deviation for Measurement 1 is observed judging from the reported metric values (Measurement 1: Metric = 0.0589, Measurement 2: Metric = 0.0265).

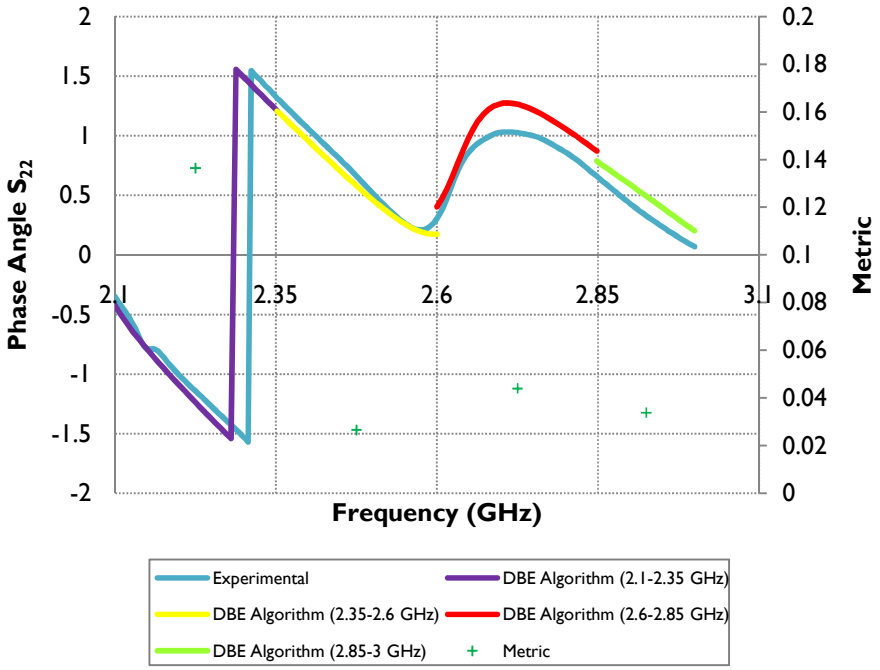

Figure 84: Porphyry copper ore - experimental and DBE algorithm $\angle S_{22}$ comparison (250 MHz)

In the 2.6-2.85 GHz frequency band, around the resonance, deviation between the simulated and measured S_{22} parameter can be seen for both the magnitude (Figure 83) and phase angle components (Figure 84), resulting in a poorer S_{22} parameter fit by the DBE Algorithm. This is observed in the larger metric value for both measurements (M1: Figure 71 and Figure 72) compared with the metrics in the 2.35-2.6 and 2.85-3 GHz frequency intervals.

Similarly to the 250 MHz piecewise frequency extraction for Measurement 1, the DBE Algorithm misplaces the measured resonance, however reducing the offset to 10 MHz. The difference between the minimum measured and DB resonance magnitudes is reduced to 0.033 compared with the 0.101 for Measurement 1.

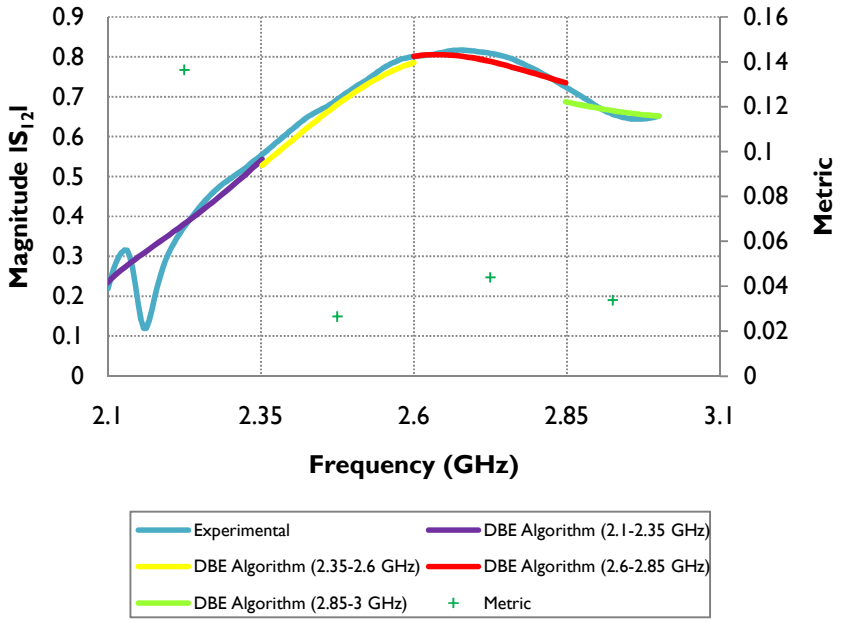

Figure 85: Porphyry copper ore - experimental and DBE algorithm $|S_{12}|$ comparison (250 MHz)

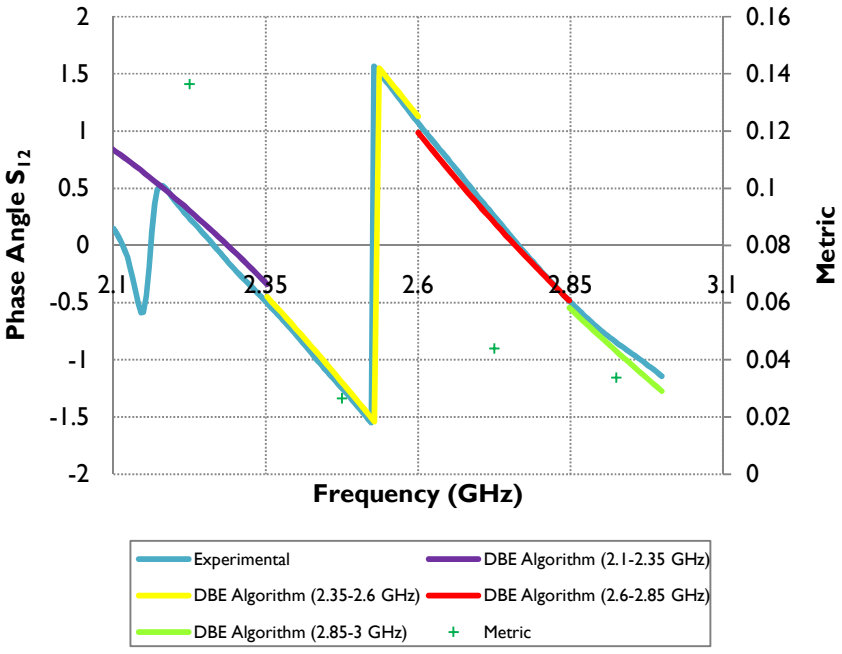

Figure 86: Porphyry copper ore - experimental and DBE algorithm $\angle S_{22}$ comparison (250 MHz)

For the S_{12} parameter, the DBE Algorithm fits the simulated dataset reasonably well to the measured S_{ij} parameter. This is observed for both the magnitude (Figure 85) and phase angle (Figure 86) components of the reflected wave. The smaller metrics, especially in the 2.6-2.85 GHz frequency interval for Measurement 2, are due to the improved goodness of fit between the simulated and measured S_{12} and S_{22} parameters, in both magnitude and phase angle component.

6.12.2.3 Full Band Frequency Extraction (Frequency Interval: 700 MHz)

The full band extraction for Measurement 2 performs worse than for Measurement 1 (Figure 75) across the entire 2.3-3 GHz frequency band. For Measurement 2, both the magnitude and phase angle components differ from the measured S_{ij} scattering data. For the latter, only the variation in phase angle contributed substantially to the reported metric.

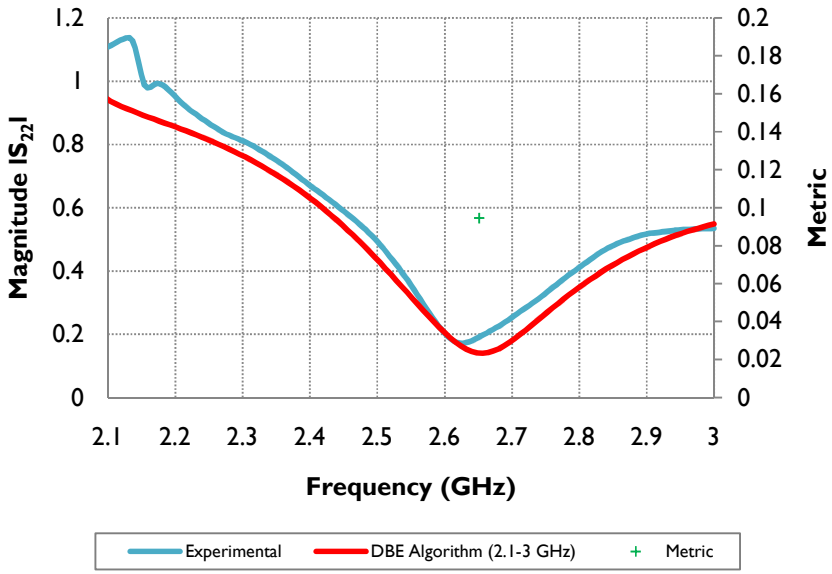

Figure 87: Porphyry copper ore - experimental and DBE algorithm $|S_{22}|$ comparison (700 MHz)

The full band extraction does prove however, to reduce the difference in simulated and measured magnitude minima to 0.1164, with an offset of 43 MHz.

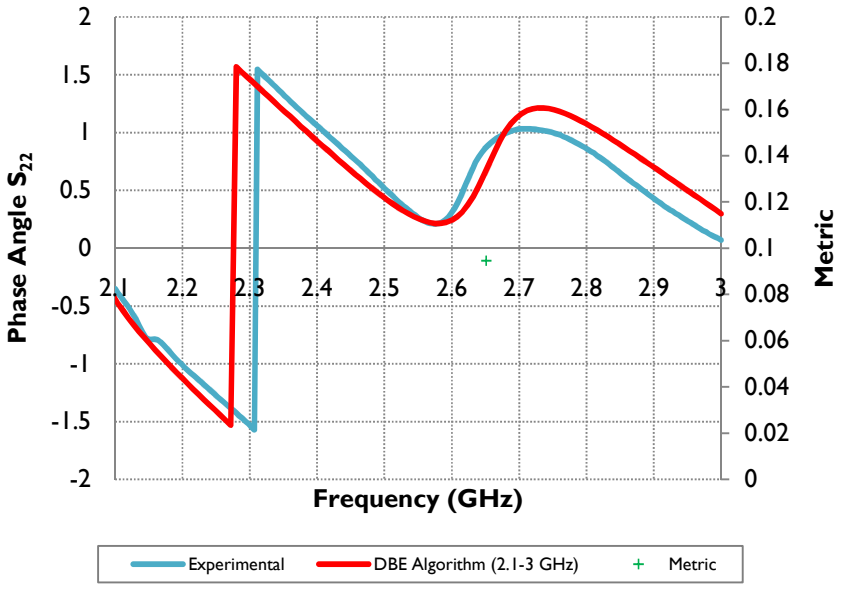

Figure 88: Porphyry copper ore - experimental and DBE algorithm S_{22} comparison (700 MHz)

A variation in the phase angle component between the simulated and measured S_{22} parameter is observed in Figure 88, although not as severe as in the case with Measurement 1. For Measurement 2 the phase angle in the resonance frequency, 2.6-27 GHz, is better fitted than is the case for Measurement 1.

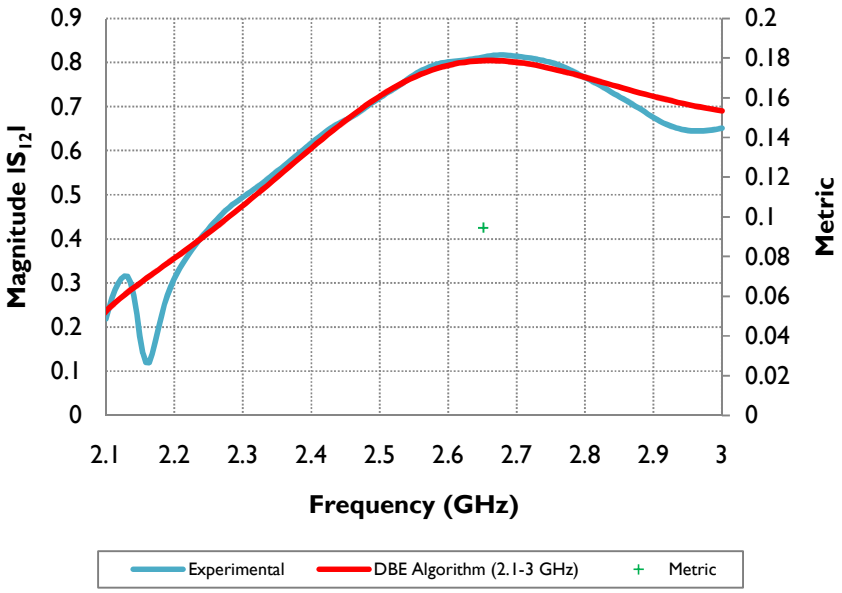

Figure 89: Porphyry copper ore - experimental and DBE algorithm $|S_{12}|$ comparison (700 MHz)

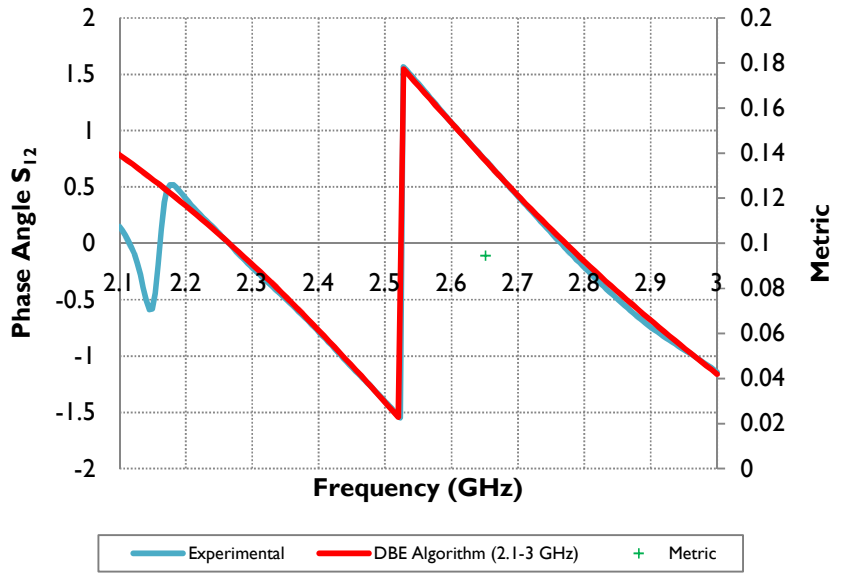

Figure 90: Porphyry copper ore - experimental and DBE algorithm S_{12} comparison (700 MHz)

The phase angle component of the simulated S_{12} parameter fits the measured S_{ij} parameter across the 2.3-3 GHz frequency interval. The magnitude component (Figure 89) exhibits some variation in the 2.6-3 GHz frequency interval.

6.12.3 Piecewise Frequency Extraction: Frequency Band Selection and Validation

Sections 6.12.1 and 6.12.2 presented a visual comparison between the measured S_{22} parameter and the simulated S-parameter generated with the aid of electromagnetic modelling of the sample holder. The comparison was done for crushed -16+11.2 mm Porphyry Copper ore, in a WR 284 sample holder. Two measurements were conducted for the same particle size. The dielectric loss factor and dielectric constant for the crushed load were extracted with the aid of the DBE Algorithm. The extraction for each measurement was conducted using 100 MHz, 250 MHz or full band extractions (700 MHz). For Measurement 1 the results were presented in Section 6.12.1.1 through 6.12.1.3. For Measurement 2 the results were presented in Section 6.12.2.1 through 6.12.2.3. Sections 6.12.3.1 through 6.12.3.3 will critically validate the use of piecewise and full band frequency extractions based on the conclusions drawn from Sections 6.11, 6.12.1 and 6.12.2.

6.12.3.1 Piecewise Frequency Extraction: 100 MHz

The 100 MHz piecewise frequency extraction exhibits distinct frequency intervals where the DB S_{22}-parameter deviates significantly in both magnitude and phase angle from the measured data. The tendency is particularly observed in the resonance frequency interval (2.6-2.7 GHz) where a dubious dielectric loss factor value is reported with above average metrics. For Measurement 1, this is seen in Figure 67 through Figure 70. For Measurement 2 this is seen in Figure 79 through Figure 82). The narrow 100 MHz piecewise frequency extraction suffers from extraction insensitivity. In many cases, the metric value stays reasonably constant across the individual frequency bands, despite variation in the extracted properties. Table 10 summarises the extraction insensitivity observed for crushed Porphyry Copper ore samples across the -26.5+2 mm particle size distribution. The measurements were conducted in the WR284 sample holder.

Table 9: Porphyry copper ore - Piecewise frequency extraction insensitivity

Particle Size Class (mm)	Measurement		Property Affected		Frequency Band(s) (GHz)	Reference
	1	2	Dielectric Loss Factor (ε″)	Dielectric Constant (ε′)		
-26.5+16	×					
		×				
-16+11.2	✓		✓	×	2.7-3	Figure 33
		✓	✓	×	2.3-2.6 2.7-3	Figure 34
-11.2+8	✓		✓	×	2.7-3	Figure 35
		✓	✓	×	2.4-3	Figure 36
-8+6.7	✓		✓	×	2.6-3	Figure 38
		✓	✓	×	2.4-3	Figure 38
-6.7+5.6	✓		✓	×	2.5-3	Figure 39
		✓	✓	×	2.6-3	Figure 40
-5.6+4.75	✓		✓	×	2.4-3	Figure 41
		✓	✓	✓	2.4-2.6 2.8-3	Figure 42
-4.75+3.35	✓		✓	✓	2.5-3	Figure 43
		✓	✓	✓	2.6-2.8 2.7-2.9	Figure 44
-3.35+2	✓		✓	×	2.5-3	Figure 45
		✓	✓	✓	2.4-2.9 2.6-3	Figure 46

Note: ✓ = DBE Algorithm insensitivity is exhibited; × = DBE Algorithm insensitivity is not exhibited.

From Table 9 it is concluded that the extraction insensitivity is observed for the bulk of the measurements conducted in the WR 284 sample holder with only the -26.5+16 mm particle size class not being affected. It appears that the dielectric loss factor suffers the most extraction insensitivity across the whole particle size distribution. The dielectric constant stays relatively constant and does not vary as significantly as is the case with the dielectric loss factor between the individual frequency bands. However, extraction insensitivity is observed for smaller particle size classes. The extraction insensitivity is measurement independent as the same trend in the extracted dielectric loss factor and dielectric constant is observed for Measurement 1 and 2.

By visual observation of (Figure 132) the DBE Algorithm misaligns the simulated S_{22} parameter in the magnitude resonance regime with the measured scattering data in depth and width. For confident, and hence more accurate, property extraction, the DBE Algorithm requires a frequency space, with sufficient features in the scattering parameter for the extraction of the dielectric loss factor and dielectric constant. The resonance feature is the most featured frequency space in the operational S-band frequency regime and misalignment therefore by the DBE Algorithm will result in large uncertainty in the extracted dielectric loss factor and dielectric constant.

Despite the misalignment of the magnitude component, the DBE Algorithm also fails to align the simulated phase angle to the measured S_{ij} parameter phase angle. As in the case with the magnitude contribution, failing to align the resonance will lead to large variations in the extracted properties.

The 100 MHz piecewise frequency extraction performs poorly in the alignment of the simulated S-parameter in both magnitude (Figure 67, Figure 79) and phase angle (Figure 68, Figure 80). The large variation in the metric in the resonance frequency band, 2.6-2.7 GHz, for both Measurements 1 and 2 can be seen in Figure 67 and Figure 79 respectively. For Measurement 1 the resonance metric is reported as 0.168, compared with the average of approximately 0.054 when ignoring the effect of the cut-off frequency below 2.3 GHz. For Measurement 2 the resonance metric is reported as 0.042, compared with the average of approximately 0.031 when ignoring the effect of the cut-off frequency.

6.12.3.2 Piecewise Frequency Extraction: 250 MHz

The larger sized frequency band improves the confidence in the extracted dielectric loss factor and dielectric constant. As the featured frequency space over which the dielectric property extraction is executed is 150 MHz larger, compared with the 100 MHz frequency intervals, more data points are included in the extraction. The increase in the extraction confidence is observed in the smaller average metric across the individual frequency bands for both Measurement 1 (Figure 71 through Figure 74) and Measurement 2 (Figure 83 through Figure 86).

As in the case with the 100 MHz piecewise frequency extraction, the misalignment of the simulated and measured S_{ij} parameters at the resonance frequency leads to large metric values that differ substantially from those in the other frequency bands.

For Measurement 1, a metric of 0.1129 is reported in the 2.6-2.7 GHz frequency interval, compared with the average of approximately 0.066 when ignoring the effect of the cut-off frequency below 2.35 GHz. For Measurement 2, a metric of 0.044 is reported in the 2.6-2.7 GHz frequency interval, compared with the average of approximately 0.035 when ignoring the effect of the cut-off frequency.

Table 10: Piecewise extraction misalignment of S_{ij} magnitude resonance

Frequency Interval Size	Measurement 1		Measurement 2		Reference
	Difference in Resonance Minima	Offset	Difference in Resonance Minima	Offset	
100 MHz	0.128	5 MHz	0.026	21.50 MHz	*Figure 67* *Figure 79*
250 MHz	0.101	13 MHz	0.033	10 MHz	*Figure 71* *Figure 83*

From Table 10 it is observed that the broader 250 MHz frequency band slightly decreases the difference between the measured and simulated S_{ij} parameter for Measurement 1. For Measurement 2 the offset between the S_{ij} parameter sets is reduced to 10 MHz although the difference in resonance minima has increased. Taking into account the effect of repetitive packing and the relatively large -16+11.2 mm particle size, the larger frequency band in general improves the experimental fit between the measured and simulated S_{ij} parameters.

Judging from Sections 6.11.1 and 6.11.2, the narrower 100 MHz frequency band exhibits a large variation in metric values between the different frequency bands resulting in a large difference in confidence in the extracted ε' and ε'' values.

Hence, the broader 250 MHz frequency bands are preferred to the narrower 100 MHz frequency bands.

6.12.3.3 Piecewise Frequency Extraction: Full Band Extraction (700 MHz)

Ignoring the effect of the cut-off frequency, this band covers 700 MHz, between the 2.3 and 3 GHz frequency limits.

When selecting broad frequency bands for which the dielectric loss factor and dielectric constant are extracted, the resonance feature is better aligned between the measured and the simulated S_{ij} parameters than is the case for the narrower partitioned 100 MHz and 250 MHz frequency intervals.

Table 11: Full band extraction misalignment of S_{ij} magnitude resonance

Piecewise Frequency Interval	Measurement 1		Measurement 2		Reference
	Difference in Resonance Minima	Offset	Difference in Resonance Minima	Offset	
Full Band Extraction (700 MHz)	0.121	3 MHz	0.117	43 MHz	*Figure 75* *Figure 87*

From Table 11 it is clear that the simulated S_{ij} parameters are better fitted to the measured S_{ij} parameters when compared with the fit obtained using 100 MHz and 250 MHz frequency bands. For Measurement 1, the DBE Algorithm aligns the simulated S_{ij} parameter with only a 3 MHz offset variation between the minimum measured and simulated parameter. The DBE Algorithm predicts the resonance feature in the measured S_{ij} parameter and fits the simulated parameter accordingly. The inclusion of the featured resonance feature is crucial for dielectric property extraction as to provide sufficient information to the algorithm for confident dielectric property extraction. Narrower sized frequency bands tend to exclude the resonance feature leading to large extraction uncertainty. This is evident in the reported metrics in the 2.6-2.7 GHz and 2.6-2.85 GHz frequency bands for the 100 MHz and 250 MHz piecewise frequency extractions.

For Measurement 1, the full band extraction seems best, compared with the 250 MHz piecewise frequency extraction, Table 10. Although no improvement in the difference between the measured and simulated S_{ij}-parameters was observed, the full band extraction does reduce the offset to 3 MHz. The DBE Algorithm accounts for the S_{22} resonance in depth and width, Figure 75, whereas the 100 MHz and 250 MHz extractions fail to do so.

From Table 11, the difference in the resonance minima was reduced for Measurement 2 using a full band extraction compared with using a 250 MHz piecewise frequency extraction, Table 10. However, the offset does increase substantially to 29.50 MHz compared with the 5.50 MHz for a 250 MHz piecewise frequency extraction.

Table 12: Porphyry copper ore resonance metrics for piecewise and full band extraction

Piecewise Frequency Interval	Metric		Resonance Frequency Band (GHz)		Reference
	M 1	M 2	M 1	M 2	
100 MHz	0.064	0.037	2.6-2.7		*Figure 33* *Figure 34*
250 MHz	0.043	0.041	2.6-2.85		*Figure 49* *Figure 50*
Full Band Extraction (700 MHz)	0.043	0.051	2.6-2.7		*Figure 141* *Figure 142*

Each of the three piecewise frequency intervals extractions exhibits comparably sized metric values in the resonance frequency regime.

For Measurement 1 the 250 MHz piecewise frequency and full band extractions perform equally well in the resonance frequency band. The 100 MHz piecewise frequency extraction performs worst, with a larger reported metric.

However, for Measurement 2, the 100 MHz piecewise frequency extraction, the resonance metric is the smallest of the three extraction types. The full band extraction performs the worst in the resonance frequency interval due to the misalignment between the simulated and measured S_{ij} parameter (Figure 87).

For the piecewise 250 MHz and full band frequency extractions, the metric in the resonance frequency is large, compared with the rest of the metric in the remaining frequency bands. However, judging from the variation in metric, the dielectric loss factor and the dielectric constant between the individual frequency bands for the 250 MHz piecewise frequency extraction the full band extraction is preferred.

It is believed that the full band (resonance) metric will decrease with decreasing particle size and that the effect of successive crushed ore loadings (Measurement 1, 2, 3 … etc.) will be lessened.

It is important to note that qualitative user interpretation of the results is required to ascertain which extraction type is best for a specified combination of sample holder size and crushed ore particle size. A manual interpretation of the DBE Algorithm results is preferred over an automated process of frequency band selection. This will ensure that the results are more trustworthy and that a higher degree of extraction confidence is obtained for the extracted dielectric loss factor and dielectric constant.

For the remainder of the thesis *only full band extractions* are used to investigate the effect of particle size, ore mineralogy and repeated packing for crushed Porphyry Copper, Copper Carbonatite and Quartz Monzonite Porphyry Copper Ore.

6.13 Conclusions

Chapter 6 discussed the use of an Automatic Network Analyzer (ANA) to measure the dielectric properties of crushed ore in a waveguide system. The calibration standards to eliminate measurement error during the calibration of the HP-8510 ANA were discussed. Each standard compensates for possible errors in the equipment (e.g. systematic, random and drift). The calibration procedure uses known electrical standards to calibrate the ANA and include a sliding load, short, open, load and THRU connection standard.

The calibration procedure followed for all dielectric property measurements included in this thesis was discussed. The isolation, reflection and transmission procedures calibrate sequentially each measurement port of the ANA. A good calibration is imperative for reliable dielectric property measurement.

The reader was introduced to the DBE Algorithm, which uses a database of simulated dielectric properties to extract the effective bulk properties of a particulate load of crushed ore material. The metric, which is an average root mean squared variation parameter, used to quantify the goodness of fit between the S_{ij} parameter datasets was discussed. The metric uses the squared sum of the variation between the simulated and measured magnitude and phase angle component for each S_{ij} parameter, which is averaged over each frequency interval over which the dielectric property extraction is executed.

The cut-off frequency effect for both sample holders (WR284 and WR340) was observed in the 2.1-2.3 GHz frequency interval, although to a lesser extent for the WR340 sample holder. Subsequently, all full band extractions over the entire operational frequency interval will exclude the 2.1-2.3 GHz frequency interval in the extraction procedure as it influences the accuracy and reliability of the extracted dielectric constant and loss factor.

Polypropylene was used as reference material. The measured dielectric properties of polypropylene compared well to literature (Von Hippel, 1954). The complex permittivity of a solid 72.14x34.04x35 mm block of polypropylene was measured as $\varepsilon^*=2.54-0j$.

The dielectric properties of a solid 72.14x34.04x20 mm block of polyethyleneterathalyte used as sample holder windows were measured. The dielectric properties were extracted using the Baker-Jarvis Extraction Algorithm and found to be $\varepsilon^*=3.07-0.113j$.

An extensive comparison was made between the extracted dielectric properties for porphyry copper ore, over narrower piecewise 100 MHz and 250 MHz frequency intervals and a full band extraction. It was found that large metric values were obtained for larger particle size classes, indicating a poorer fit to the measured S_{ij} parameters. This was ascribed to wall effects.

With decreasing particle size, the reproducibility between individual measurements increased, as the wall effect diminished. With smaller particle size classes, the particulate load becomes more spatially homogeneous throughput the entire sample holder volume, resulting in an improved experimental fit to the measured S_{ij} parameters.

For extractions over piecewise 100 MHz and 250 MHz intervals, the extracted dielectric constant and loss factor varied significantly between the individual frequency intervals.

Both the narrower frequency interval extractions exhibited distinct insensitivities to the extracted dielectric properties across the 2.1-3 GHz frequency interval. Both extractions exhibited larger metrics in the resonance frequency interval, which indicated a poorer fit to the data. Both the 100 MHz and 250 MHz extractions tend to misalign the magnitude and phase angle components of the simulated S_{ij} parameters.

The full band extraction uses the entire frequency interval for use in the DBE Algorithm to extract a single dielectric constant and loss factor across the 2.1-3 GHz frequency interval. The magnitude and phase angle components of the simulated S_{ij} parameter are better aligned using full band extractions compared with the goodness of fit obtained over smaller 100 MHz and 250 MHz frequency intervals.

Full band extractions over the 2.3-3 GHz frequency interval were selected to be used to best determine the effect of particle size, ore mineralogy and sample holder size on the extracted dielectric constant and loss factor.

Chapter 7

Effect of Crushed Particle Size, Waveguide Sample Holder Size and Ore Mineralogy on the Extracted Dielectric Properties

7.1 Introduction

Chapter 7 will focus on the effects that particle size, ore mineralogy and sample holder size have on extracted dielectric properties. In Section 7.2 the effect that particle size has on the effective dielectric properties is investigated for Porphyry Copper (Section 7.2.1), Copper Carbonatite (Section 7.2.1) and Quartz Monzonite Porphyry Copper ore (Section 7.2.3). Section 7.3 investigates the effect of mineralogy and compares the extracted dielectric constant and loss factor for Porphyry Copper and Copper Carbonatite ore in the -5.6+4.75 mm, -4.75+3.35 mm and -3.35+2 mm particle size classes. The combined effect of repeated ore packing and sample holder size for representative samples of Porphyry Copper, Copper Carbonatite and Quartz Monzonite Porphyry Copper ore is investigated in Section 7.4. The chapter presents a conclusion of the main findings in Section 7.5.

7.2 Effect of Crushed Particle Size

The particle size of a crushed particulate ore load influences the extracted dielectric loss factor and dielectric constant. The amount of particulate matter that can physically fit into the waveguide sample holder is dependent on the particle size. Larger sized particles tend to have large void (air) spaces between the individual particles. Smaller sized particles tend to have

smaller void (air) space between the individual particles. It is expected that spatial homogeneity will affect the effective permittivity of the sample.

The ore packing density is dependent on the size of the sample cavity. It is therefore necessary to investigate the functional relationship not only between the particle size and the extracted dielectric properties, but also between the particle size and the size of the sample cavity and their combined effect. It is also essential to establish how the effective complex permittivity varies with particle size distribution within a sample cavity for a WR284 and WR340 waveguide system. This will aid to establish the limits of the particle size (for a limited size WR284 and WR340 waveguide sample cavity) for accurate extraction of the dielectric loss factor and dielectric constant.

For this purpose, the discussion is presented as follows to establish the various effects on the extracted dielectric loss factor and dielectric constant:

- Section 7.2.1 will investigate the effect of particle and sample cavity (WR284 and WR340) size for crushed Porphyry Copper ore.
- Section 7.2.2 will investigate the effect of particle and sample cavity (WR284 and WR340) size for crushed Copper Carbonatite ore.
- Section 7.2.3 will investigate the effect of particle and sample cavity (WR284 and WR340) size for crushed Quartz Monzonite Porphyry Copper ore.

The **extract.py** algorithm (Appendix E) reports the average extracted loss factor at 3 GHz for each of the individual frequency intervals. However, these values need to be corrected, for each of the frequency bands. A detailed discussion is presented in Appendix E. Hence, for the remainder of Chapter 7 the corrected dielectric loss factor is used.

However, the dielectric constant is reported at the midpoint for each of the frequency intervals and is therefore not corrected.

7.2.1 Effect of Crushed Particle Size: Porphyry Copper Ore

A full band frequency extraction (2.3-3 GHz) was used to establish the combined effect of particle and sample holder size on the extracted dielectric loss factor and dielectric constant. The results are summarised in Table 13.

The discussion of the results is confined to only Measurement 1 for the -26.5+2 mm particle size distribution for the WR 284 and WR 340 sample holders.

Table 13: Porphyry copper ore – extracted ε′ and ε″ (WR284 and WR340)

Particle Size (mm)	Sample Holder					
	WR 284			WR 340		
	ε'	ε''_{corr}	$\|\bullet\|$	ε'	ε''_{corr}	$\|\bullet\|$
-26.5+16	3.72	0.284	0.119	3.21	0.113	0.112
-16+11.2	2.79	0.113	0.051	2.84	0.079	0.038
-11.2+8	2.9	0.135	0.044	2.9	0.068	0.033
-8+6.7	2.88	0.147	0.050	2.87	0.057	0.033
-6.7+5.6	2.89	0.113	0.030	2.85	0.045	0.021
-5.6+4.75	2.87	0.083	0.025	2.86	0.045	0.020
-4.75+3.35	2.84	0.068	0.023	2.85	0.045	0.018
-3.35+2	2.84	0.068	0.023	2.73	0.045	0.020

The results in Table 13 are graphically presented in Figure 91 and Figure 93.

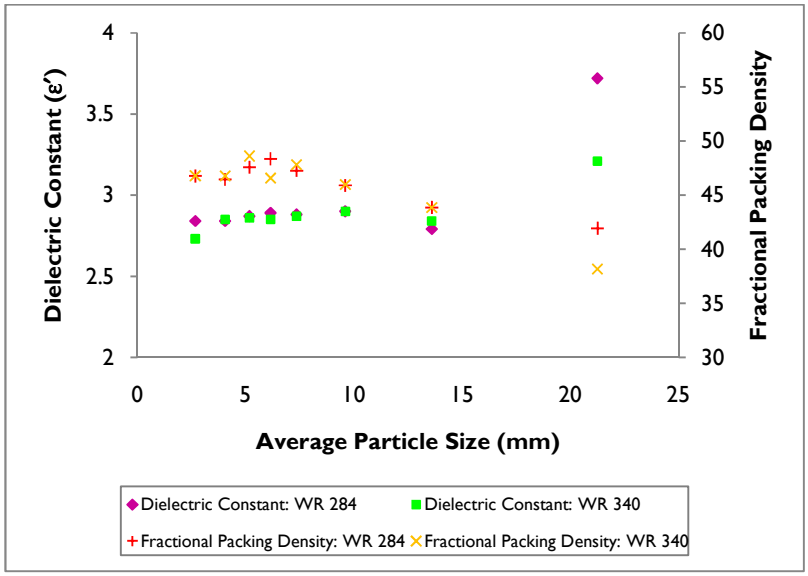

Figure 91: Porphyry copper ore - effect of d_p on extracted ε′ (Measurement 1)

From Figure 91 the extracted dielectric constant for the WR284 and WR340 sample holders is very similar for $\overline{d}_{P_{arithmetic}}$ < 15 mm. Comparing their individual fractional packing densities (Appendix D), it is seen that both sample holders have approximately the same fractional packing density across the whole particle size distribution except for the maximum particle size class (-26.5+16 mm). The extracted ε′ seem to exhibit small changes to the variation in the fractional packing density with increasing particle size.

However, for the -26.5+16 mm particle size class, a considerable difference is observed in the magnitude of the extracted ε′ value and the fractional packing density for both the WR284 and WR340 sample holders. The difference in the extracted dielectric constants also differs in magnitude from the rest of the values reported in the lower particle size classes. A much larger dielectric constant compared with the lower particle size class was determined for the -26.5+16 mm particle size class. To ascertain why this value differs so substantially from the rest, the

metric values for each particle size class was investigated. The results are graphically presented in Figure 92.

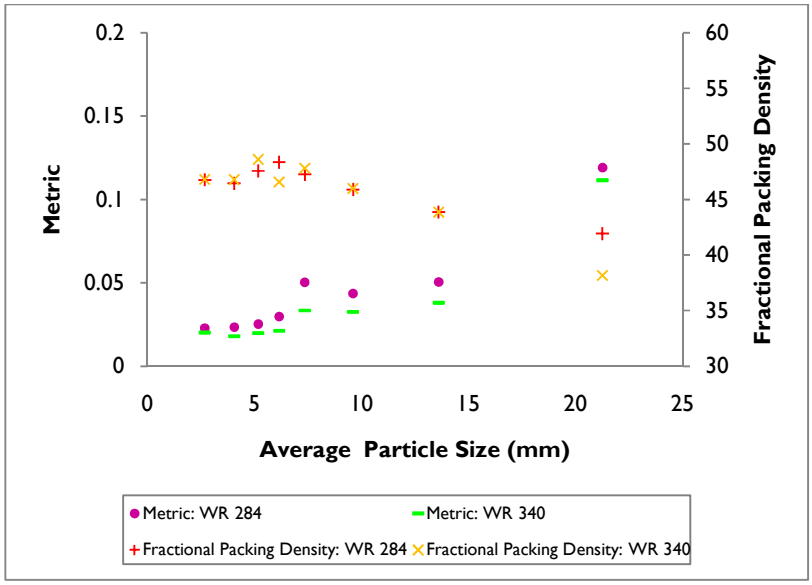

Figure 92: Porphyry copper ore - effect of d_p on extraction metric (Measurement 1)

From Figure 92 it is observed that the metric increases as the fractional packing density decreases with increasing particle size for both the sample holders, despite little difference between the extracted ε′ for the WR284 and WR340 sample holders. It is also noted that the extractions that were done with the WR340 sample resulted in smaller reported metrics indicating that the DBE Algorithm better fit the simulated and measured S_{ij} parameters for large waveguide sample holder size.

The large metric in the -26.5+16 mm particle size class compared with the rest of the reported values in the smaller particle size classes suggests that the extracted dielectric constant has been extracted with less confidence despite being similar in magnitude for the WR284 and WR340 sample holders.

The similar sized metrics however isolate the fractional packing density, which is influenced by wall effects due to the size of the sample holders and size of the crushed particles, as accountable for the variation in the extracted dielectric constant between the WR284 and WR340 sample holders.

The variation in magnitude in the reported dielectric constant for the -26.5+16 mm particle size class indicates that the larger particle size classes lends itself to doubtful DB extraction due to increased wall effects of the sample holder.

From Figure 91 and Figure 92 it is concluded that the extracted ε′ value is not influenced by the sample holder size for $\bar{d}_{P_{arithmetic}}$ < 15 mm or the waveguide sample holder size (WR284 and WR340).

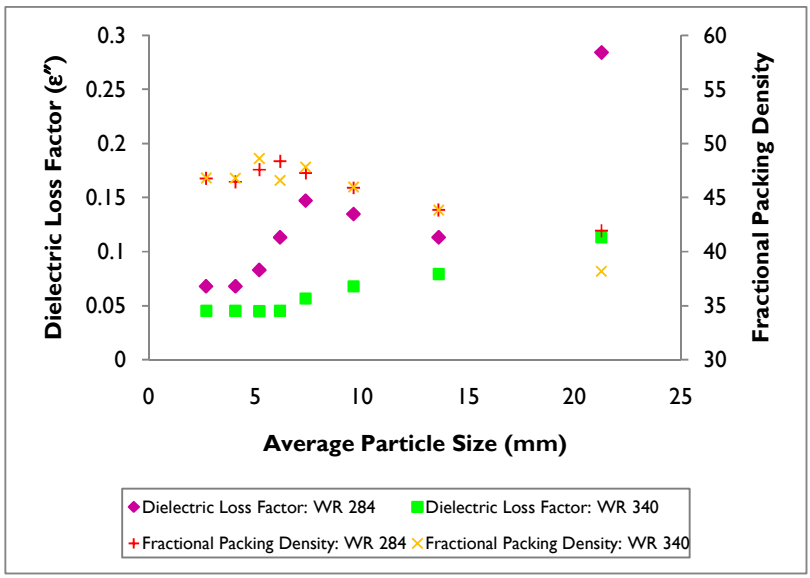

Figure 93: Porphyry copper ore - effect of d_p on ε″ (Measurement 1)

In Figure 93 a substantial variation in the extracted ε″ for the WR284 sample holder is observed amongst the different particle size classes. The same trend is seen for the WR340 sample holder, although not as severe as in the case for the WR284 sample holder.

In contrast to the dielectric constant, the variation between the WR284 and WR340 sample holders is independent of the fractional packing density. Despite similarity in the fractional packing density for the sample holders, the extracted dielectric loss factor for each particle size class differs substantially between the different sample holders.

The extracted ε'' seems to be affected the most by the size of the waveguide sample holder compared with the dielectric constant (Figure 91). This is presumed to be due to the apparent insensitivity of the DBE Algorithm to accurately determine ε'' from a measured set of S_{ij} parameters.

This observation is supported by the findings in Section 6.11 where the extracted ε'' value varies substantially for 100 MHz and 250 MHz piecewise frequency extractions whilst the extracted ε' value exhibited little variation between the different individual frequency bands.

7.2.2 Effect of Crushed Particle Size: Copper Carbonatite Ore

The full band extraction results for crushed Copper Carbonatite ore are summarised in Table 14.

Table 14: Copper carbonatite ore – extracted ε′ and ε″ (WR284 and WR340)

Particle Size (mm)	Sample Holder					
	WR 284			WR 340		
	ε'	ε''_{corr}	$\|\bullet\|$	ε'	ε''_{corr}	$\|\bullet\|$
-26.5+16	3.42	0.926	0.078			
-16+11.2	3.45	0.909	0.194			
-11.2+8	3.96	0.738	0.055			
-8+6.7	3.91	0.628	0.090			
-6.7+5.6	3.33	0.302	0.079			
-5.6+4.75	3.35	0.275	0.027	3.18	0.170	0.034
-4.75+3.35	3.14	0.239	0.023	3.15	0.113	0.023
-3.35+2	2.94	0.149	0.024	3.12	0.136	0.027

**No dielectric property measurement for Copper Carbonatite ore was conducted in the -26.5+5.6 mm particle size class (WR340) due to the unavailability of the ANA at the Department of Electrical Engineering, University of Stellenbosch. The ANA exhibited a measurement repeatability error due to the port 1/2 switching of the test set and a faulty mixer. The ANA was shipped to the USA to be repaired.*

With insufficient data for the WR340 sample in the -26.5+5.6 mm particle size distribution, the dielectric constant compares well between the sample holders in the -5.6+4.75 mm, -4.75+3.35 and -3.35+2 mm particle size classes.

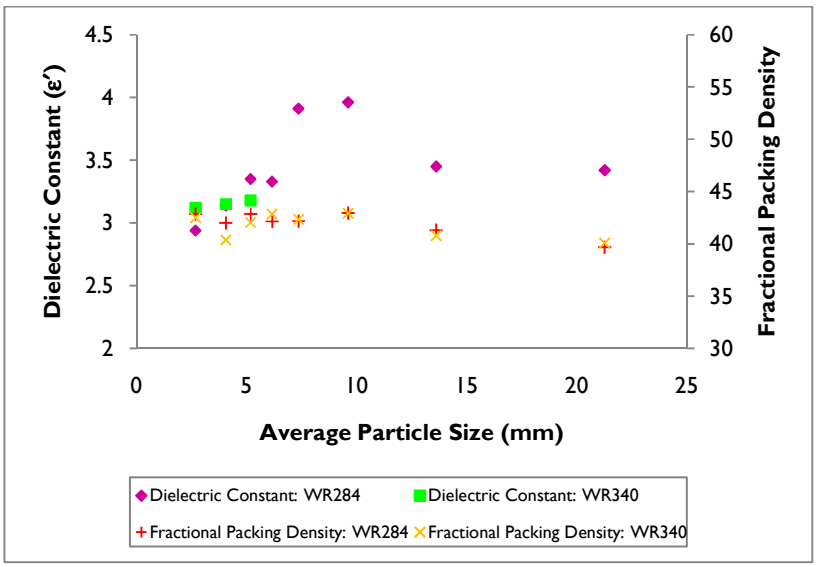

Figure 94: Copper carbonatite ore – effect of d_p on extracted ε′ (Measurement 1)

The extracted dielectric constant differs noticeably between the individual particle size classes compared with Porphyry Copper Ore (Figure 91). It is expected that for different ores, packed in the same sample holder, for corresponding particle size classes, approximately the same fractional packing density will be observed. When comparing Figure 91 and Figure 94, it is observed that this is not the case. In the smaller particle size classes, Porphyry Copper ore exhibited a larger average fractional packing density, compared with that of Copper Carbonatite. However, the packing density for the latter stays approximately unchanged with increasing particle size. For Porphyry Copper ore, the fractional packing density decreased sharply for $d_{p_{average}}$ >10 mm.

This anomaly may be ascribed to the morphology of the crushed particles for different ore types. The Copper Carbonatite is harder than the Porphyry Copper ore, with large grains of magnetite (Fe_3O_4), accounting for 43 wt% of the total ore composition. Subsequently the ore breaks differently when crushed, resulting in a difference in the physical shape of the individually formed particles for corresponding particles size classes.

The individual Copper Carbonatite ore particles across the particle size distribution were observed to be more elongated compared with the square shaped Porphyry Copper particles, which is believed to influence the fractional packing density (refer to Figure 103). For this thesis, the Copper Carbonatite ore was crushed using a standard laboratory jaw and cone crusher. The crushed material received from the University of Nottingham wwa initially been reduced in size using a hammer. This affects the breakage pattern of the ore, ultimately affecting the fractional packing density of the crushed ore.

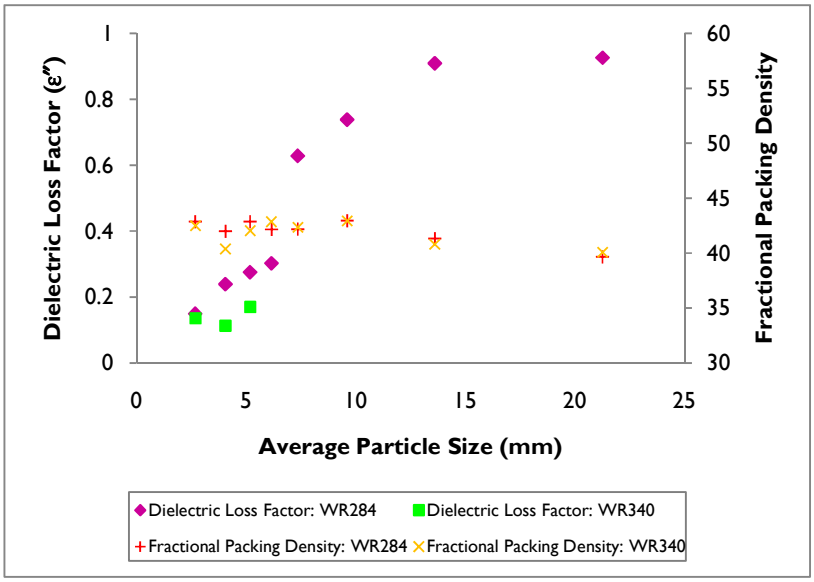

Figure 95: Copper carbonatite ore - effect of d_p on extracted ε″ (Measurement 1)

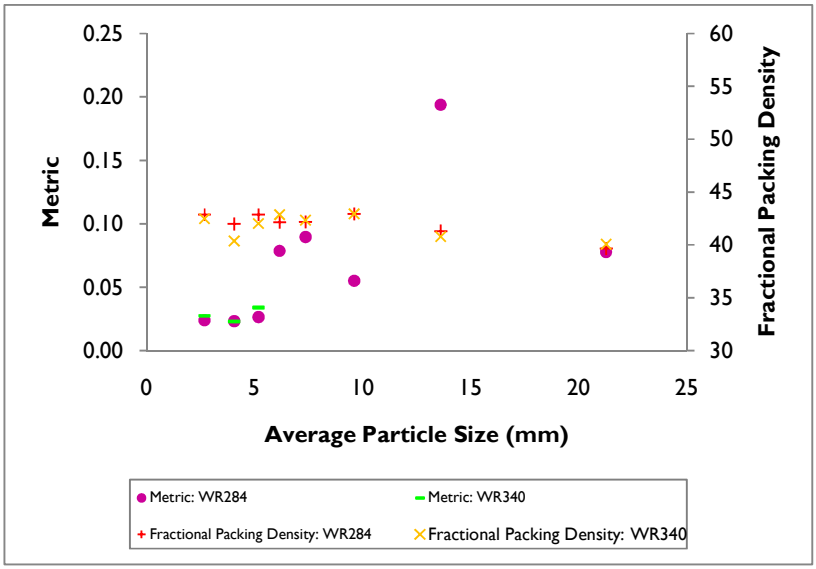

Figure 96: Copper carbonatite ore - effect of d_p on the extraction metric

The large ε″ value, 0.85, extracted for the -26.5+16 mm particle size class indicates that the wall-effect of the WR284 sample holder is a key factor that affects the extracted dielectric properties. The maximum metric, 0.1 is reported for the -16+11.2 mm particle size class. The metric is approximately 3 times the size of the metric in the -26.5+16 mm particle size class even though similar sized dielectric loss factors is extracted for both particle size classes.

7.2.3 Effect of Crushed Particle Size: Quartz Monzonite Porphyry Copper Ore

The full band extraction (2.3-3 GHz) results obtained for the dielectric property extraction for Quartz Monzonite Porphyry Copper ore are summarised in Table 15. ANA measurements were only conducted for the WR340 sample holder.

Table 15: Quartz monzonite porphyry copper ore - extracted ε′ and ε″ (WR340)

Particle Size (mm)	Sample Holder		
	WR 340		
	ε'	ε''_{corr}	$\|\bullet\|$
-19+16	2.78	0.0679	0.0197
-16+13	2.88	0.0906	0.0408
-13+9	2.73	0.0906	0.0349
-9+6	2.75	0.034	0.0156
-6+4	2.71	0.034	0.0135
-4+3	2.62	0.034	0.0156

The same order of magnitude ε′ and ε″ values for quartz monzonite porphyry copper ore were extracted compared with porphyry copper ore (Section 7.2.1). The extracted ε′ in Figure 97 stays approximately unchanged between the particle size classes despite a decrease in the fractional packing density with increasing particle size. The same observation was made for Porphyry Copper ore with the exception of the -26.5+16 mm particle size class. This suggests that for a larger sized sample holder, in this case WR340, the wall effects (expressed as fractional packing density) of the sample holder are mitigated, especially in the extraction of ε′.

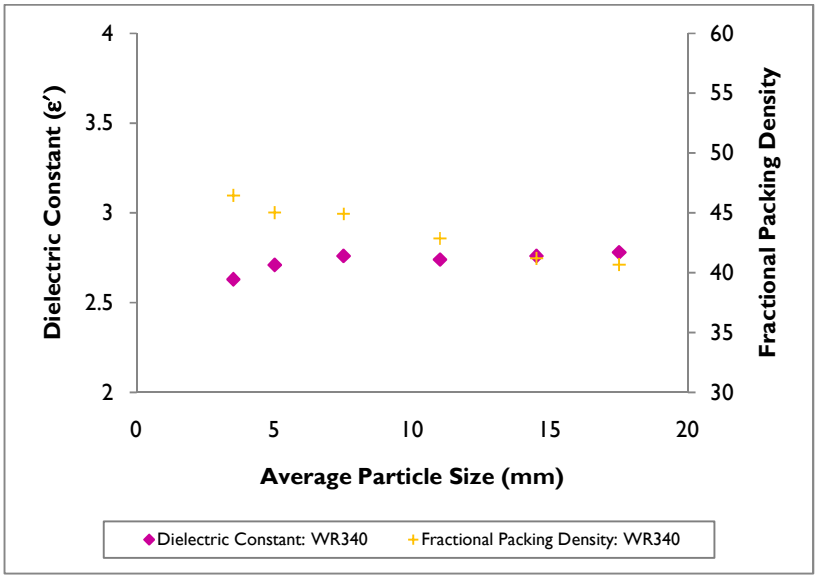

Figure 97: Quartz monzonite porphyry copper ore - effect of d_p on the extracted ε′ (Measurement 1)

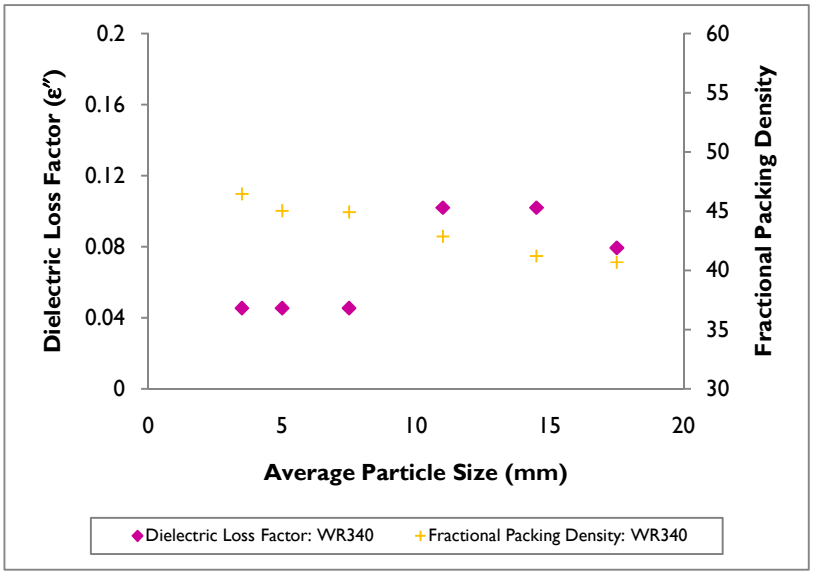

Figure 98: Quartz monzonite porphyry copper ore – effect of dp on the extracted ε″ (Measurement 1)

In contrast to the the extracted dielectric constant, the loss factor in Figure 98 exhibits a substantial increase in magnitude for the -19+16 mm, -16+13 mm and -13+9 mm particle size classes. From Figure 99 it is observed that the metrics in these particle size classes differ from thos of -9+6 mm, -6+4 mm and -4+3 mm particle size classes. For the -16+13 mm and -13+9 mm particle size classes the metric is the largest. Subsequently the extracted dielectric loss factor exhibits a maximum variation in these particle size classes reinforcing the belief that the dielectric loss factor is strongly influenced by the wall effects of the sample holder and hence the fractional packing density.

For the three smallest particle size classes, the dielectric loss factor stays constant, with similar reported metrics in each size class (Figure 99). The constant dielectric loss factor in these particle size classes, with similar associated metrics, means that the WR340 sample holder is the preferred (above the WR284) sample holder size for confident and reliable dielectric property extraction in the -9+3 mm particle size distribution.

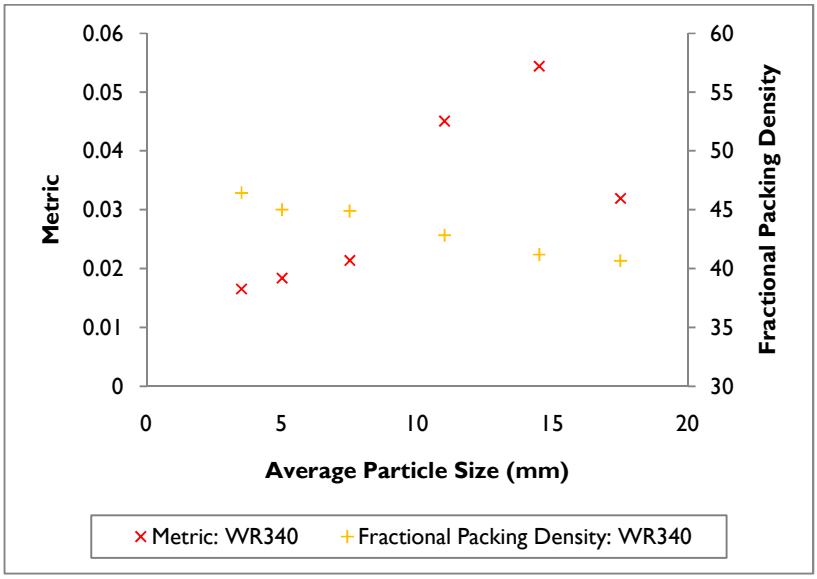

Figure 99: Quartz monzonite porphyry copper ore – effect of d_p on the extraction metric (Measurement 1)

With increasing particle size, the packing density decreases with an increase in the reported metric values. To account for the sample holder wall effects, the size of the sample holder must be chosen such that the dimensions are much larger than those of the particles.

7.3 Effect of Ore Mineralogy

The effect of mineralogy was investigated using Porphyry Copper and Copper Carbonatite ore. The extracted dielectric constants in the WR340 sample holder for the -5.6+4.75 mm, -4.75+3.35 mm and 3.35+2 mm particles size classes are presented in Table 16, as comparative data (extracted with the DBE Algorithm) were available only in these particle size classes.

Table 16: Porphyry copper and copper carbonatite ore - extracted ε′ and ε″ (-5.6+2 mm)

Particle Size (mm)	Porphyry Copper		Copper Carbonatite	
	ε'	ε''_{corr}	ε'	ε''_{corr}
-5.6+4.75	2.86	0.045	3.18	0.170
-4.75+3.35	2.85	0.045	3.15	0.113
-3.35+2	2.73	0.045	3.12	0.136

The extracted dielectric constants for the two ores are graphically compared in Figure 100.

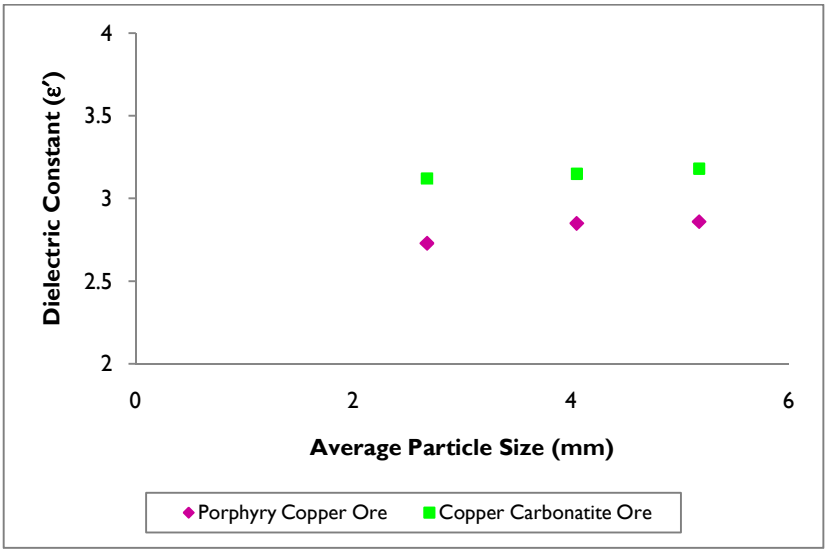

Figure 100: Porphyry copper and copper carbonatite ore - effect of mineralogy on ε′ (WR340)

The effect of mineralogy is noticeable in the extracted dielectric constant across the three particle size classes. For both ores, the extracted ε′ increases with increasing particle size. This is attributed to the wall effects of the sample holder and the ratio between the particle size and the size of the sample holder itself.

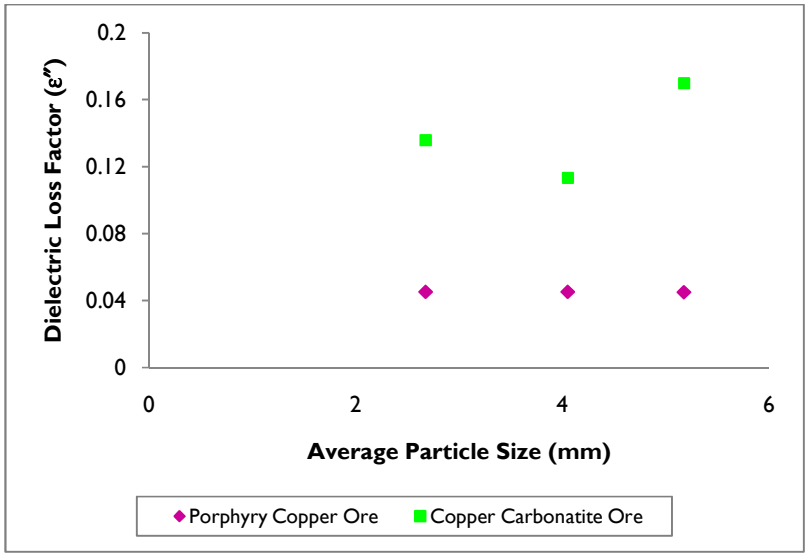

Figure 101: Porphyry copper and copper carbonatite ore - effect of mineralogy on ε″ (WR340)

The effect of mineralogy is also evident in the extracted dielectric loss factor (Figure 101). The Copper Carbonatite ore has a larger dielectric constant and loss factor compared with Porphyry Copper in corresponding particle size classes.

The major phase (43 wt%) in Copper carbonatite ore is magnetite (Fe_3O_4), known to be an excellent microwave absorber. The Fe_3O_4 mineral phase is coarsely textured with large grains. In Figure 103 the dark grey (almost black) particles are solid magnetite mineral grains.

Figure 102: Crushed porphyry copper ore (-6.8+5.6 mm)

Figure 103: Crushed copper carbonatite ore (-6.8+5.6 mm)

Porphyry copper contains 77 wt% transparent gangue mineral phase, predominantly made up of 34 wt% quartz (SiO_2). Pyrite (FeS_2), known to be a microwave absorber, accounts for 23 wt% of the total mineral phase make-up. This is less than the absorbent 43 wt% Fe_3O_4 mineral phase seen for Copper Carbonatite ore. Porphyry copper is not as a good microwave absorber as copper carbonatite ore. From Figure 103 it is observed that all mineral phases in the porphyry copper ore matrix are finely dispersed throughout each ore particle.

7.4 Effect of Sample Holder Size and Repeated Crushed Ore Packing

The combined effect of the sample holder size and repeated packing (Measurement 1 and 2) of the crushed ore load into the sample holder was investigated for crushed Porphyry Copper, Copper Carbonatite and Quartz Monzonite Porphyry Copper ore.

For each particle size class, both ANA measurements were conducted using the same ore sample. ANA measurement after re-packing of the same ore sample into the sample holder will establish the extent to which the randomized orientation of the individual particles influences the measured S_{ij} parameters and also the extracted dielectric constant and loss factor for a full band frequency extraction.

For different ANA measurements of the same particle size class, the DB extracted dielectric constant and loss factor should be (approximately) constant. However, repeatability in the extracted dielectric constant and dielectric loss factor is influenced by the crushed ore particle and sample holder size.

7.4.1 Porphyry Copper

The effect of successive crushed Porphyry Copper ore loadings in WR284 is illustrated in Figure 104. It is observed that the effect of repeated ore packing becomes significant with increasingly

larger particle size, noted by the variation in the extracted dielectric constant between Measurement 1 and 2 for $\bar{d}_p \geq 9.6$ mm (-11.2+8 mm particle size class).

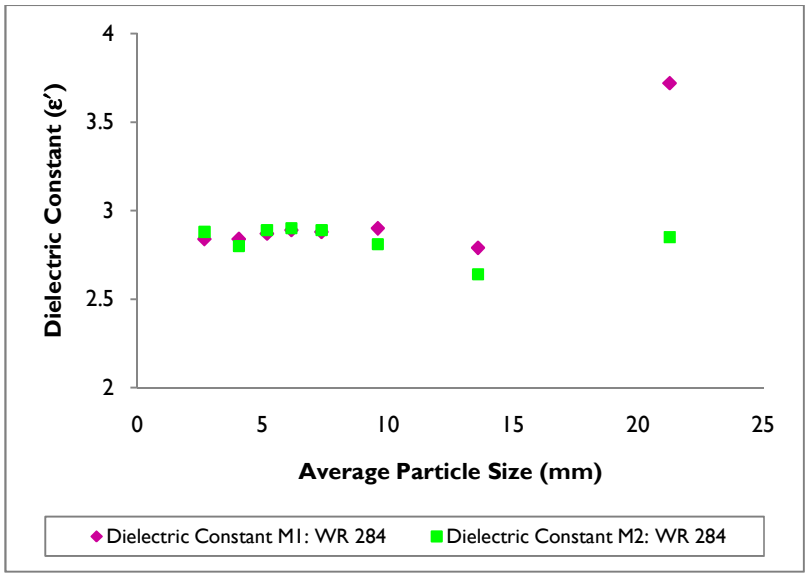

Figure 104: Porphyry copper ore - effect of repeated measurements on ε′ (WR284)

From Appendix F it is seen that the DBE Algorithm aligned the magnitude of the S_{ij} parameter for Measurements 1 and 2 for the -8+6.7 mm (Figure 134), -6.7+5.6 mm (Figure 135), -5.6+4.75 mm (Figure 136), -4.75+3.35 mm (Figure 137) and -3.35+2 mm (Figure 138) particle size classes.. Alignment of the resonances for successive ANA measurements results in similar extracted dielectric constants in the smaller particle size classes.

A larger degree of misalignment is observed for the -26.5+16 mm (Figure 131), -16+11.2 mm (Figure 132) and -11.2+8 mm (Figure 133) particle size classes. The dissimilarity in the magnitude of the S_{ij}-parameter across the 2.3-3 GHz frequency band gives rise to the variation in the extracted dielectric constant for the same particle size classes in Figure 104.

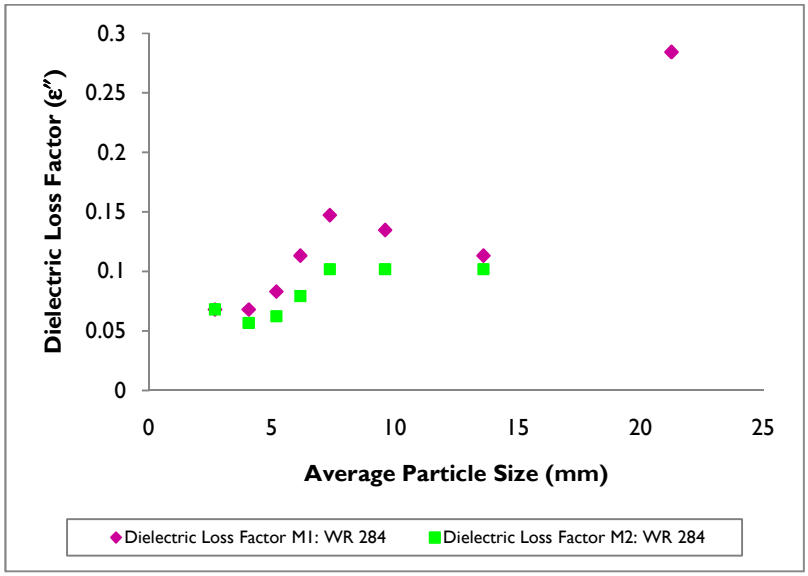

Figure 105: Porphyry copper ore – effect of repeated measurements on ε″ (WR284); ε″=0.985 in -26.5+16 mm

The ε″ values extracted with the database differ substantially between Measurements 1 and 2 as can be seen in Figure 105. As is the case for the dielectric constant, the difference between extracted values for the different measurements increases with increasing particle size. However, in the -16+11.2 mm and -11.2+8 mm particle size classes the difference in the extracted dielectric loss factor decreases compared with the smaller particle size classes. It is however, unclear why this occurs, but it should be remembered that the DBE Algorithm has been shown to introduce variation in the ε″ for successive individual dielectric property measurements.

For Measurement 2 the extracted dielectric loss factor in the -26.5+16 mm particle size class was omitted as it was excessively large compared with the rest of the loss factors. For the same particle size class, Measurement 1 reports a value of 0.23. Both values are inconsistent when compared with the remaining dielectric loss factors in the smaller particles size classes.

The difference in the S_{ij} parameter resonance minima, Appendix F , for each of the particle size classes is presented in Figure 106. The average $\triangle S_{ij}$ is taken as the mean of the minimum and maximum variation.

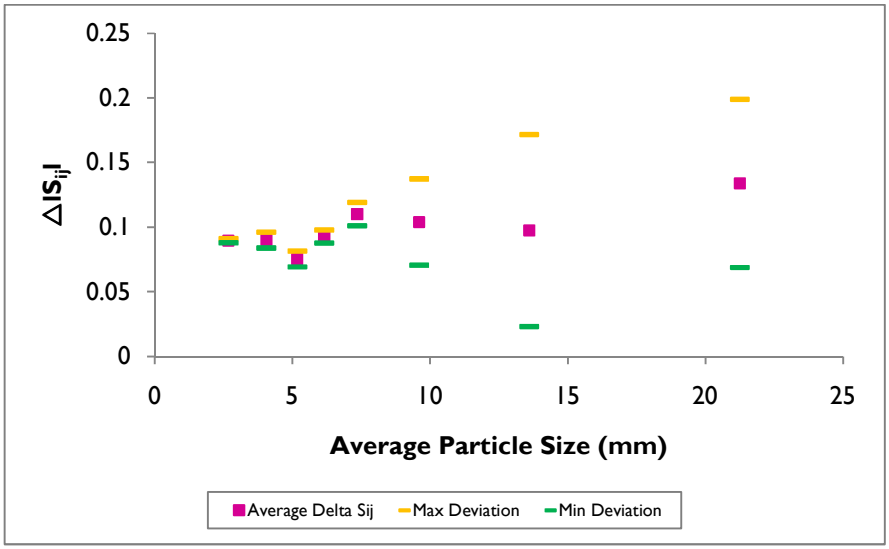

Figure 106: Porphyry copper ore - $\Delta|S_{ij}|$ for repeated measurements (WR284)

It is clear that the variation in the magnitude of the resonance S_{ij} parameter decreases with decreasing particle size (Figure 106). For the -26.5+16 mm, -16+11.2 mm and -11.2+8 mm particle size classes the substantial variation results in largely different extracted dielectric constants and loss factors (Figure 104, Figure 105).

For the -8+6.7 mm, -6.7+5.6 mm, -5.6+4.75 mm, -4.75+3.35 mm and -3.35+2 mm particle size classes the limited variation in the resonance S_{ij} parameter results in similar extracted dielectric constants. However, despite alignment of the resonance feature for different measurements, the DBE Algorithm fails to ensure repeatable extracted dielectric loss factors. However, the inability of the DBE Algorithm to produce repeatability in the extracted ε″ values is an inherent shortcoming of the extraction routine. This suggests that representing the particulate load as a homogeneous solid with effective dielectric properties does not produce exact property values. It is also possible that the metric function is relatively flat in the ε″ dimension.

It was concluded that, based on the alignment of resonance feature and the repeatability in the extracted dielectric constant, the upper particle size limit for reliable measurement and representation by an effective property is 8 mm.

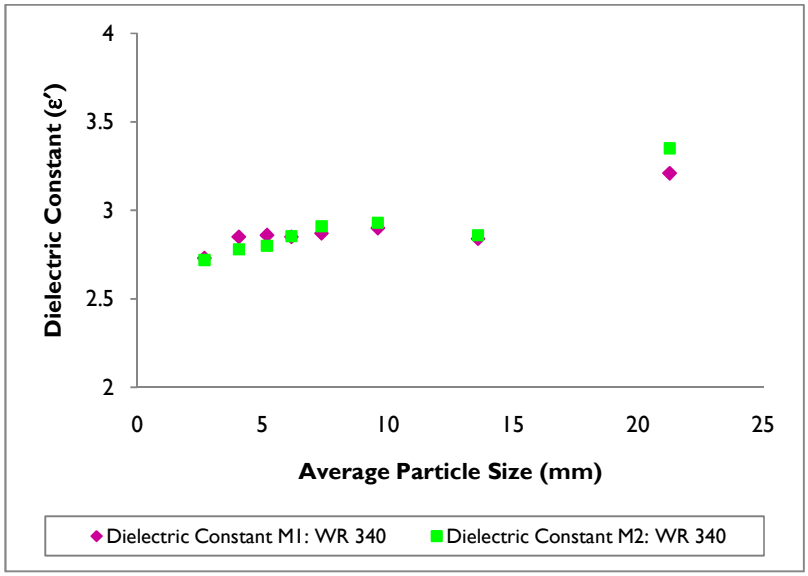

Figure 107: Porphyry copper ore - effect of repeated measurements on ε' (WR340)

The noticeable difference between the extracted dielectric constants for the WR284 sample holder, Figure 104, in the -16+11.2 mm and -11.2+8 mm particle size classes was reduced when using a WR340 sample holder (Figure 107).

For the -26.5+16 mm particle size class the difference in the extracted dielectric constant for Measurement 1 and 2 (WR340) was also significantly reduced, suggesting that for the larger sample holder, less variation in the extracted values is expected for larger particle sizes. The larger sample holder reduces the wall effects resulting in less variation in the extracted dielectric constant amongst the different particle size classes (Figure 107).

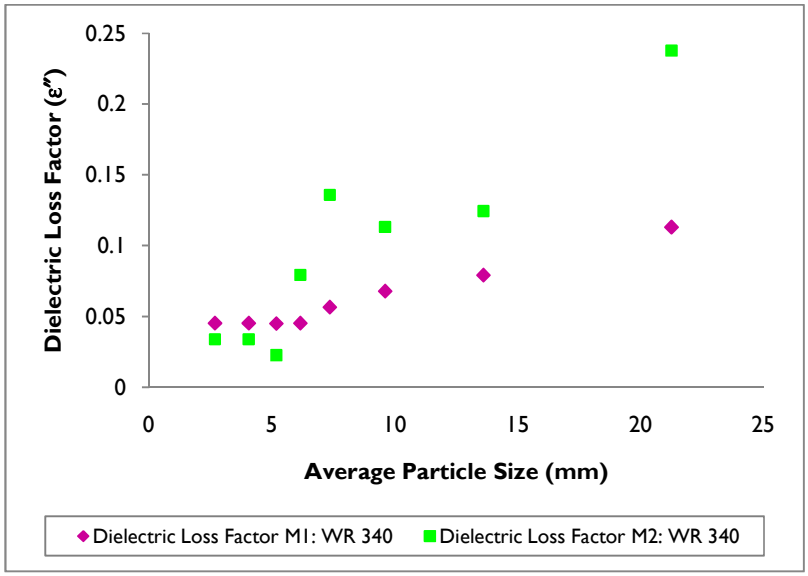

Figure 108: Porphyry copper ore - effect of repeated measurements on ε" (WR340)

From Figure 108 the reproducibility for the dielectric loss factor is seen to be poor for the WR 340 sample holder across the particle size distribution with the exception of the -4.74+3.35 mm and -3.35+2 mm particle size.

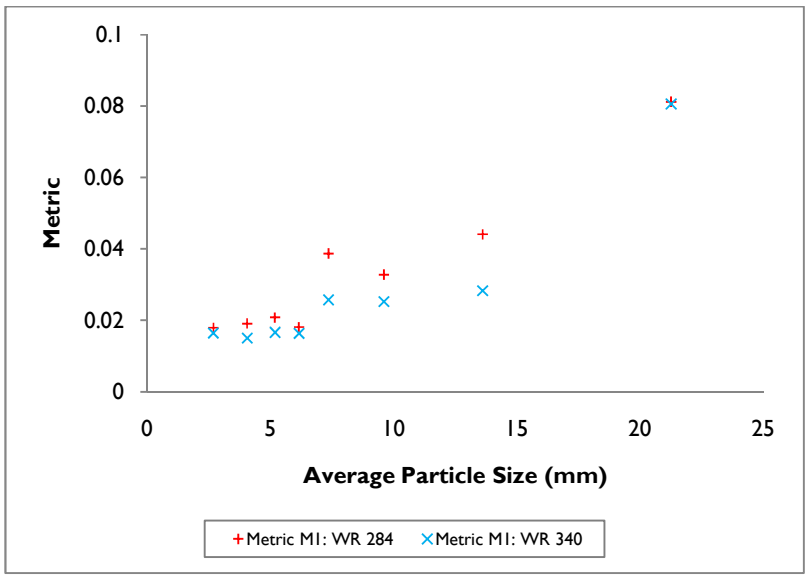

Figure 109: Porphyry copper ore - effect of waveguide sample holder size on metric

From Figure 109 the metrics indicate that the simulated scattering parameters are better fitted to the measured data for the WR340 sample holder than for the WR 284 sample holder. There is therefore a greater degree of confidence in the dielectric constant and loss factor extracted for the WR340 data. This is especially the case for the -16+11.2 mm, -11.2+8 mm and -8+6.7 mm particle size classes. The smaller metrics indicates a better experimental fit between the experimental and DB S_{ij} parameter.

Although the WR340 sample holder reduces the difference between the extracted dielectric properties for successive ANA measurements, it fails to reduce the extraction uncertainty associated with the -26.5+16 mm particle size class. This is observed in Figure 109 where the metrics for both sample holders are relatively large compared with those for other particle size classes. This is to the reduced spatial homogeneity on small length scales for the case of larger particles, and more importantly to the presence of wall effects due to the restricted size of the WR284 and WR340 sample holders relative to the particle size. Separation of these two effects was not possible with the data to hand.

7.4.2 Copper Carbonatite

For the WR284 sample holder, the extracted dielectric constant exhibits similarity for successive ANA measurements across the particle size distribution (Figure 110). However, for the -8+6.7 mm, -6.7+5.6 mm, -5.6+4.75, -4.75+3.35 and -3.35+2 mm particle size classes, the variation in the dielectric constant for successive measurements is smaller for the Porphyry Copper ore (Figure 104).For the -26.5+16 mm particle size class the extracted dielectric constant differs only slightly between successive measurements (Figure 110). This contrasts with the corresponding particle size class for crushed Porphyry Copper ore (Figure 104).

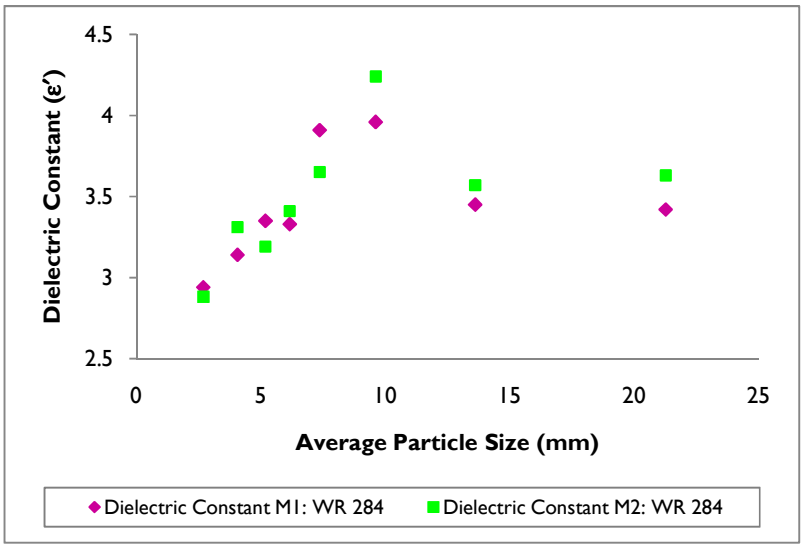

Figure 110: Copper carbonatite ore – effect of repeated measurements on ε′ (WR284)

These results confirm that particle and particle morphology, in combination with the size of the sample holder, affect the electromagnetic behaviour of the sample. For particles of nominally the same size class, repeated packing and measurement shows a greater effect for the carbonatite ore in the smaller size classes, suggesting that particle morphology affects the spatial homogeneity in this case more severely than for the porphyry ore. This is likely to be due in part to the inherent

breakage characteristics of the ore and also due to the method of breakage. The porphyry ore was jaw and cone crushed while the carbonatite was initially broken manually by hammer..

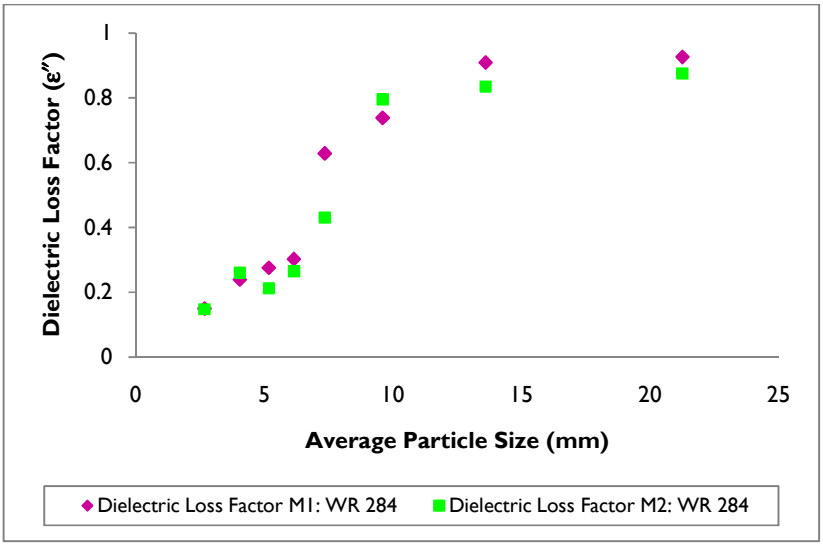

Figure 111: Copper carbonatite ore - effect of repeated measurements on ε″ (WR284)

Repeated measurements on different packings show reasonable agreement when the extracted property is ε″ (Figure 111). This contrasts somewhat with the result for the porphyry ore as can be seen by comparison with Figure 105. The extracted ε″ for Porphyry Copper ore showed poorer reproducibility, with the exception of the -4.75+3.35 mm an -3.35+2 mm particle size classes, between successive measurements. This tendency increased with increasing particle size. However, from Figure 111, it is clear that the extracted ε″ for copper carbonatite exhibits a greater degree of reproducibility for successive dielectric property extractions. It was also observed that the metric value increases with increasing particle size for both the WR284 and WR340 sample holders.

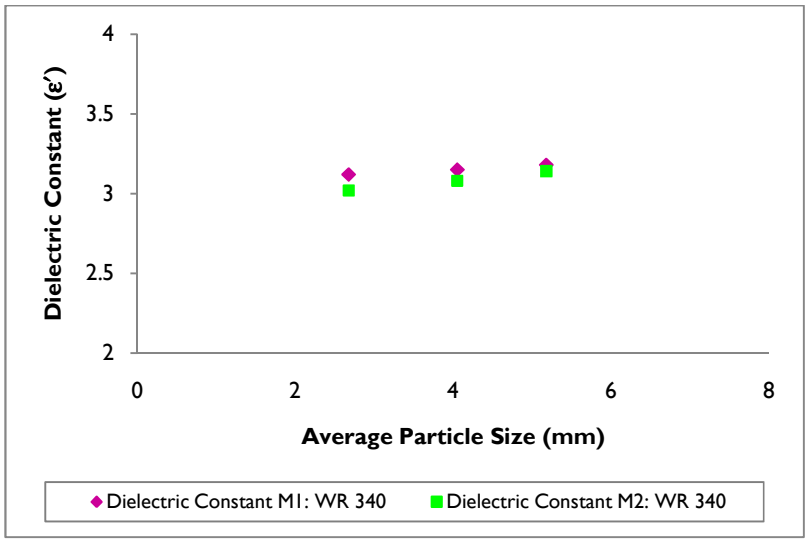

Figure 112: Copper carbonatite - effect of repeated measurements on ε′ (WR340)

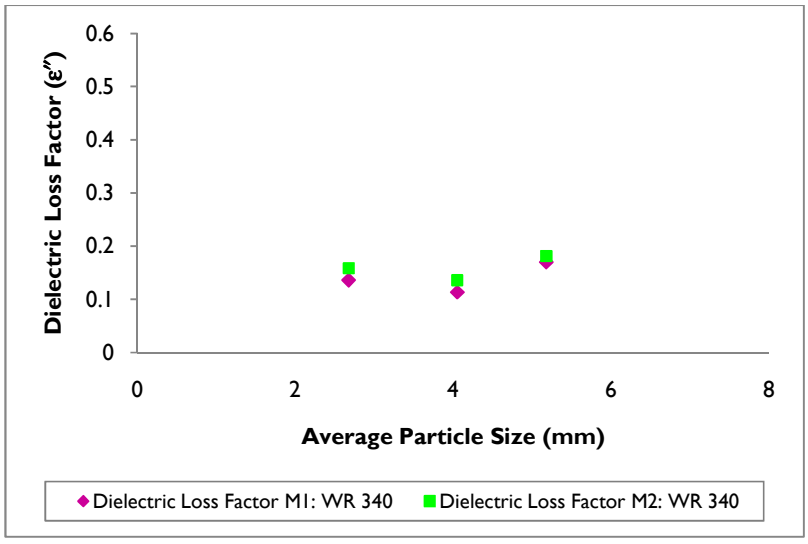

Figure 113: Copper carbonatite - effect of repeated measurements on ε″ (WR340)

For the WR340 sample holder, only the -5.6+4.75 mm, -4.75+3.35 mm and -3.35+2 mm particle size classes were used for dielectric property extraction. From Figure 112 and Figure 113 it is seen that the larger sample holder size increases the reproducibility between measurements considerably when compared with the corresponding particle size classes measured in the WR284 sample holder (Figure 110 and Figure 111).

7.4.3 Quartz Monzonite Porphyry Copper

For Quartz Monzonite Porphyry Copper ore, the effect of repeated ore packing was investigated only for the WR340 sample holder. The particle size distribution of interest is -19+3 mm. The extracted dielectric constant for Quartz Monzonite Porphyry Copper ore is presented in Figure 114.

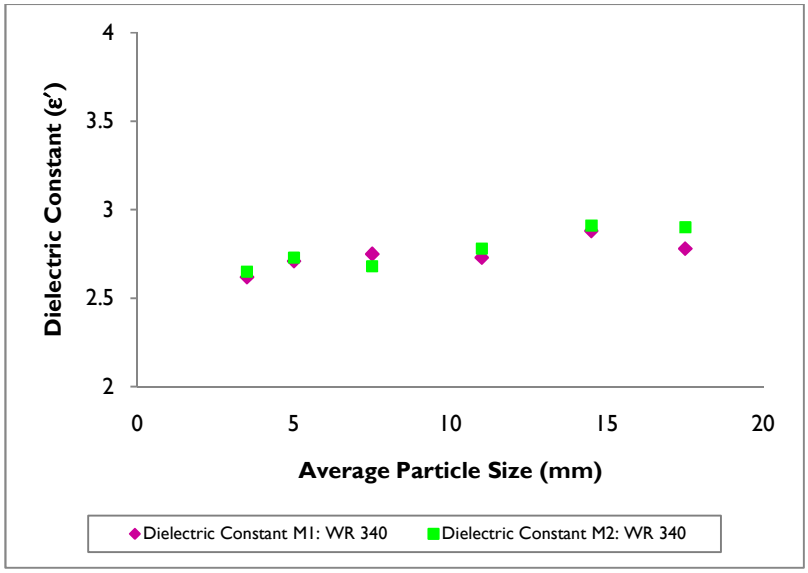

Figure 114: Quartz monzonite porphyry copper ore - effect of repeated measurements on ε′ (WR340)

No significant difference between the dielectric constant for Measurement 1 and 2 was observed across the particle size distribution except for the the -19+16 mm particle size class. As in the case for Porphyry Copper ore, the difference in the extracted dielectric constant is attributed to the wall effects of the sample holder in combination with the particle size. Extraction repeatability in the dielectric constant was achieved for the -16+3 mm particle size distribution. The variation in the ε′ for Measurements 1 and 2 in the -19+16 mm particle size class is substantiated by the variation in the metrics due to the poorer fit between the simulated and measured S_{ij} parameters (Figure 116).

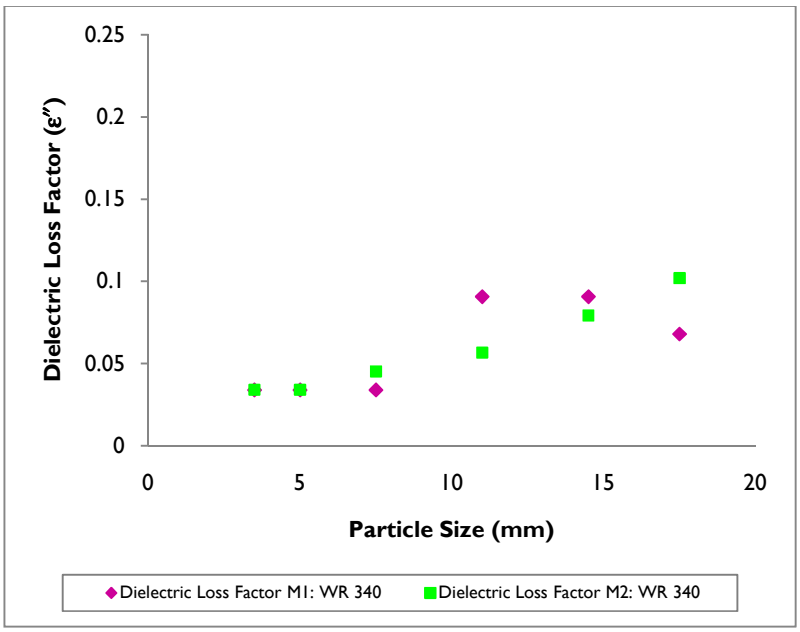

Figure 115: Quartz monzonite porphyry copper - effect of repeated measurements on ε" (WR340)

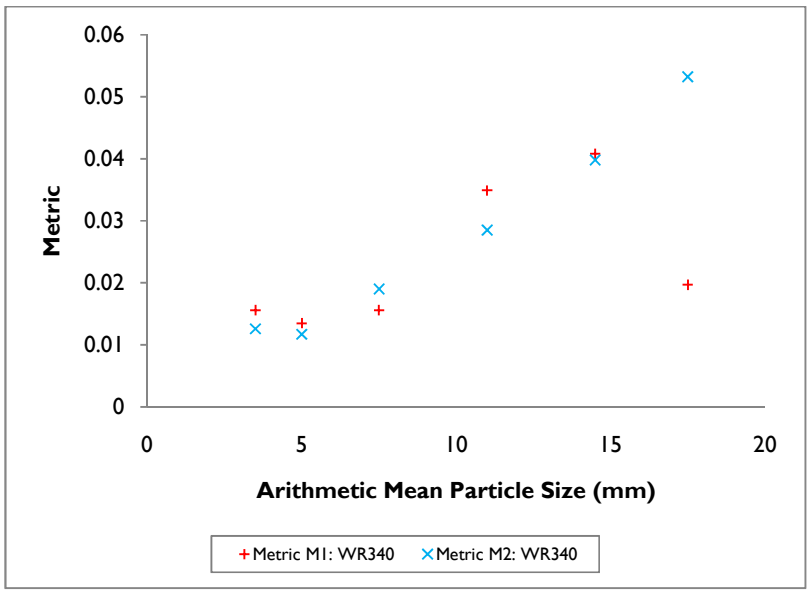

Figure 116: Quartz monzonite porphyry copper - effect of repeated measurements on metric (WR340)

The extracted dielectric loss factor differs for Measurement 1 and 2 for corresponding particle size classes. The same tendency is observed for Porphyry Copper and Copper Carbonatite ore in both WR284 and WR340 sample holders. As is the case of the Copper Carbonatite and Porphyry Copper, ore the dielectric loss factor of the Quartz Monzonite Porphyry Copper ore is strongly affected by the particle size. Extraction repeatability in the dielectric loss factor is poor and large variation between individual measurements is observed.

From Figure 116 it is observed that the metric increases for both Measurement 1 and 2 with increasing particle size, suggesting that as the particle size increases, the fitting of the S_{ij} parameters by the DBE algorithm becomes poorer. It is suggested that for this ore, as with all the ores, at least two spatial effects are responsible for the results observed. Spatial homogeneity decreases on a small length scale as particle size increases. It can be imagined that beyond a certain particle size this spatial inhomogeneity will make the fitting of effective dielectric properties modelling for a solid, homogeneous load, inappropriate. Second, as particle size increases within sample holders of fixed size, wall effects will become increasingly significant. Currently the results in this thesis do not allow these two effects to be separated.

7.5 Conclusions

Chapter 7 investigated the effect of particle size, sample holder size, ore mineralogy and repetitive packing on the extracted dielectric constant and loss factor.

For Porphyry Copper Ore, the dielectric constant exhibited a large degree of similarity for dielectric property extractions in the WR284 and WR340 sample holders across the particle size distribution, except for the -26.5+16 mm particle size class. For this particle size class the wall effect of the sample holders wa observed in the decrease in the fractional packing density. The extracted dielectric constant tends to stay approximately unchanged with increasing particle size except at this largest size

The dielectric loss factor exhibited variation between the particle size classes for ANA measurements conducted in the WR284 and WR340 sample holders. The variation tends to increase with increasing particle size. The same trend was observed for the Copper Carbonatite and Quartz Monzonite Porphyry Copper ores.

The effect of ore mineralogy was evident in the extracted properties for Copper Carbonatite and Porphyry Copper Ore. The carbonatite ore consists mainly of magnetite (Fe_3O_4), known to be an excellent microwave absorber compared with porphyry copper ore which contains 34 wt% quartz (SiO_2) transparent gangue mineral phase. It is concluded that Porphyry Copper is not as good a microwave absorber as copper carbonatite ore; hence a smaller ε' and ε'' value were reported.

For all three ores of interest, the WR340 sample holder reduces the difference in the extracted dielectric constant and loss factor values due to the decrease in the wall effects of the sample holder.

Chapter 8

Conclusion and Recommendations

8.1 Conclusion

In this thesis, the dielectric property measurement of crushed ore and its extraction from measured S_{ij} parameter data with a Database Extraction Algorithm is presented. The particle size class were used, categorised by a -distribution, Three ores, namely porphyry copper, copper carbonatite and quartz monzonite porphyry copper were investigated and properties were extracted for size classes in the range -26.5+2 mm.

A flanged waveguide measurement system was used for measurements utilising sample holders in the WR284 and WR340 standard size. The sample holders were fitted with PET dielectric windows to retain the material under test. Measurement of the scattering parameters from which dielectric properties were to be extracted was carried out with the aid of an HP 8510 Automatic Network Analyzer connected to the sample holders via two coaxial cables. Scattering parameter measurements were conducted in the 2.1-3 GHz frequency interval. Each ore size class was measured twice.

The waveguide sample holder and measurement system were simulated in QuickWave3D®. In the simulations a solid homogeneous block was used to represent the crushed particulate load By changing the complex permittivity of the load, a database of scattering parameters over the 2.1-3 GHz frequency range was generated for each dielectric constant and loss factor pairs.

The DBE Algorithm fitted the simulated S_{ij} parameters, expressed as a magnitude and phase angle, to the measured values over piecewise 100 MHz, 250 MHz or 700 MHz (full band extraction) frequency intervals. The goodness of fit was indicated by a metric representing a weighted root mean squared variation between the magnitude and phase angle components of

the measured and simulated S_{ij} parameter. In each of the frequency intervals, the extracted dielectric constant and loss factor were obtained based on the obtained minimum metric. The DB extracted dielectric properties for polypropylene confirmed the accuracy to which the physical dielectric property measurement and extraction was conducted. The extracted dielectric constant and loss factor of 2.54 (literature: 2.54) and 0 (literature: 7.01×10^{-4}) respectively, correspond to literature (Von Hippel, 1954).

Full band extractions, executed over a 700 MHz frequency interval, include a high degree of featured frequency space. The featured space provides for sufficient data used in the DBE Algorithm to extract the complex permittivity of the crushed ore load with smaller metrics than for piecewise extraction using smaller frequency intervals. For full band extractions, the DBE Algorithm better aligns the resonance feature between the simulated and measured S_{22} parameters. Alignment of the resonance in the 2.6-2.8 GHz frequency interval is critical for confident dielectric property extraction. Extractions over narrower 100 MHz and 250 MHz frequency intervals tend to exhibit larger variation in the extracted dielectric properties amongst the individual frequency intervals. Smaller piecewise extractions tended to exclude and misplace the resonance feature, resulting in large metrics in the resonance frequency interval and hence high levels of extraction uncertainty.

It was found that ore mineralogy has a profound effect on the extracted dielectric constant and loss factor. For Copper Carbonatite the dielectric constant was higher than for Porphyry Copper due to the larger fraction microwave transparent gangue mineral in the latter that reduces the dielectric constant value.

It was found for particle size classes that are of the same order of magnitude as the dimensions of the sample holder, the wall effects of the sample holder become increasingly significant. With increasing wall effects, the DB metric becomes larger indicating a larger degree of uncertainty (confidence) in the extracted values. The larger WR340 sample holder lessens the wall effects of the sample holder compared with the WR284 sample holder.

For smaller particle size classes, the extracted dielectric constant for repeated measurements and repacked samples exhibited a large degree of reproducibility in both sample holder sizes. However, for a WR340 sample holder the reproducibility increased amongst successive measurements for larger particle size classes when compared with the WR284 waveguide sample holder. It is also believed the spatial homogeneity, which is a function of particle size, affects the degree to which the properties of the ore could be represented by a single effective complex permittivity.

For both the WR284 and WR340 waveguide sample holders the -16+11.2 mm particle size class was found to be the upper limit of the -26.5+2 mm particle size distribution for reliable extraction of an effective dielectric constant and loss factor. The -26.5+16 mm particle size class is of the same order of magnitude as the waveguide geometrical dimensions. Hence, the wall effects of the sample holder dominates the extracted dielectric properties resulting in less reliable extracted dielectric property values.

8.2 Recommendations

The thesis only looked at individual particle size classes and the extracted dielectric properties thereof. However, typical pre-treatment of run of mine ore will not only be limited to a specific particle size distribution. Conveyor feeds to the microwave applicator unit would typically consist of a wide particle size distribution. It is recommended that for future studies, the individual particle size classes be combined as it would more realistically represent typical industrial conditions. The DBE Algorithm will extract one value for the dielectric constant and dielectric loss factor for an entire particle size distribution.

The thesis concentrated on three copper mineral ores. It is recommended that other mineral ores be investigated such as iron and nickel bearing ores.

The largest sample holder used in this thesis was the WR340 standard waveguide size operating in the S-band frequency regime. For future studies, it is recommended to use larger sample holders (e.g. WR430, WR650 and WR770) with lower operational frequencies to better represent industrial processes. The larger waveguide size, will allow for larger particle sizes to be investigated.

It is recommended that future studies need to investigate the effect of particle morphology (shape) on the extracted dielectric properties of the particulate load. It is further recommended that by using larger waveguide, the effect of spatial homogeneity, as distinct from wall effects, is investigated.

References

1. Ali A., Bradshaw S.M. Understanding the Effects of Mineralogy, Ore Texture and Microwave Power Delivery on Microwave Treatment of Ores. Cape Town: University of Stellenbosch, 2010.
2. Baker-Jarvis B. Transmission/Reflection and Short-Circuit Line Permittivity Measurements. Boulder: US Department of Commerce, 1990.
3. Bradshaw S., Louw L., van der Merwe C. Reader H., Kingman S., Celuch M., Kijewska W. "Techno-Economic Considerations in the Commercial Microwave Processing of Mineral Ores." Journal of Microwave Power & Electromagnetic Energy VOL. 40 NO.4, 2007: 228-240.
4. Cloete J.H. “High Precision Measurement of Complex Permittivity and Permeability at Microwave Frequencies.” IEEE Symposium on Antennas and Propagation and Microwave Theory and Techniques VOL. AP/MTTS-90 Proceedings. Somerset West, 1990. pp.365-372.
5. Contelles-Cervera M., Canos A.J., Peneranda-Foix F.L., de Los Reyes E. “Measuremnet of Dielectric and Magnetic Properties of Ferrite Slabs in the Microwave Region.” 10th International Conference on Microwave and RF Heating. Modena: Microwave Appication Group, 2005. 20-23.
6. Fitzgibbon K.E., Veasey T.J. “Thermally assisted liberation - a review.” Mineral Engineering 3 (1/2) (1990): 181-185.

7. Fouche C. Measurement of Dielectric Properties of Materials. University of Stellenbosch, 2004.

8. HP Product Note 8510-3. “Measuring the Dielectric Constant of Solids with the HP 8510 Network Analyzer.” 1985.

9. HP Product Note 8510-5A. “Network Analysis, Specifying Calibration Standards for the HP 8510 Network Analyzer.” 1985.

10. Jones D.A., Kingman S.W., Whittles D.N., Lowndes I.S. “The Influence of microwave energy delivery method on strength reduction in ore samples.” Chemical Engineering and Processing (2006)

11. Kingman S.W., Jackson A., Cumbane A., Bradshaw S.M., Rowson N.A., Greenwood R. “Recent developments in microwave-assisted comminution.” International Journal of Mineral Processing 74 (1-4) (2003): 71-83.

12. Kraus, Fleisch and. Electromagnetics with Applications 5th Edition. McGraw-Hill, 1999.

13. Louw W.J. Microwave Heating of Multiphase Materials: Modelling and Measurement. Stellenbosch: University of Stellenbosch, 2005.

14. Meredith R.J. Engineers' Handbook of Industrial Microwave Heating. London: Institution of Electrical Engineers, 1998.

15. Metaxas A.C., Meredith R.J. Industrial Microwave Heating. London: Peregrine, 1983.

16. Nelson S.O. “Agricultural Applications of Dielectric Measurements.” IEEE Transactions on Dielectrics and Electrical Insulation 13. 2006. 688-702.

17. Nelson S.O. Dielectric Measuring Techniques and Applications. ASAE Paper No. 983067. St. Joseph: ASAE, 1998.

18. Nelson S.O. "Dielectric Properties of Agricultural Products and some Applications." Research in Agricultural Engineering 54 (2008 (2)): 104-112.

19. Nelson S.O. "Estimating the permittivity of solids from measurements on granular and pulverised materials." Materials Research Society Symposium Proceedings. Reno, Nevada: Microwave Processing of Materials, 1988.

20. Nelson S.O., Bartley P.G.,. "Measuring frequency and temperature dependent permittivities of food amterials." IEEE transactions on instrumentation and measurement 51(4). 2002. 589-592.

21. Nicholson A.M., Ross G.F. "Measurement of the Intrinsic Properties of Materials by Time Domein Techniques." IEEE Transactions on Instrumentation and Measurement, VOL. IM-19. 1970. pp.377-382.

22. Nkohla, M.A. Characterization of Ferrochrome Smelter Slag and its Implications in Metal Accounting. Cape Town, South Africa: Cape Peninsula University of Technology, 2006.

23. Nyfos E., Vainikainen P. Industrial Microwave Sensors, Chapter 2. Boston: Artech House, Norwood, 1989.

24. Osepchuk J.M. "A History of Microwave Heating Applications." IEEE Transactions on Microwave Theory and Techniques, VOL. MTT-32, No.9 (1984): 1200-1223.

25. Pauli M., Kayster, T., Wiesbeck W. “Waveguide Measurement Setup for Material Parameter Determination of Soils and Liquids.” 10th International Conference on Microwave and RF Heating. Modena: Microwave Application Group, 2005. 37-40.

26. Pitard, F.F. Pierre Gy's Sampling Theory and Sampling Practice: Heterogeneity, Sampling Correctness and Statistical Process Control 2nd ed. Boca Raton, New York: CRC Press, 1993.

27. Pozar D.M. Microwave Engineering 2nd Edition. John Wiley & Sons, Inc., 1998.

28. Reader H. Personal correspondance. Stellenbosch, 2009.

29. Requena-Perez, M.E., Dominquez-Tortajada, E., Diaz-Morcillo, A. and Monzo-Cabrera, J. "Measurement of Multilayer Structures Inside Waveguides by Means of Inverse Calculation." 10 th International Conference on Microwave and High Frequency Heating. Modena, Italy, 2005. 8-11.

30. Rhodes M. Introduction to Particle Technology, Chinchester: John Wiley & Sons Ltd, 1998, p.320.

31. Sahyoun C. Rowson N.A., Kingman, S.W., Groves L., Dorfling, J.C. and Bradshaw, S.M. “The Influence of Microwave Pre-Treatment on Copper Flotation Plant Performance.” SAIMM 105(1) (2005): 7-14.

32. Stuchly S., Matuszewski M. “A Combined Total Reflection Transmission Method in Application to Dielectric Spectroscopy.” IEEE Transactions on Instrumentation and Measurement, VOL. IM-27. 1978. pp.285-288.

33. Talbot P., Konn A.M., Brousseau C. “Electromagnetic Characterisation of Fine-Scale Particulate Composite Materials.”

34. Tromans D. "Mineral comminution: Energy efficiency considerations." Minerals Engineering, 2008: 613-620

35. Venkatesh M.S., Raghavan G.S.V. “An Overview of Dielectric Properties Measuring Techniques.” Canadian Biosystems Engineering VOL 47 (2005): 15-30.

36. Von Hippel A. Dielectric Materials and Applications. New York: John Wiley, 1954.

37. Weil C.M. “The Electromagnetic Properties of Materials Program at NIST.” Materials Research Society Research Symposium Proceedings VOL.269 . San Francisco: Materials Research Society, 1992. pp.517-526.

38. Weir W.B. “Automatic Measurement of Complex Constant and Permeability at Microwave Frequancies.” Proceedings of the IEEE, VOL. 62, No. 1. 1974. 33-36.

39. Wills, B.A. Mineral Processing Technology. Burlington: Butterworth-Heinemann, 1997.

Appendix A

Vibratory Sieve Test

Appendix A presents the results of the vibratory sieve test that was performed (Section 4.3) for each of the ores of interest. A sieve test result form and screen analysis graph for each ore is presented followed by a brief discussion on the findings. The following needs mentioning:

- Dry sieving was the method of choice.
- The duration of the sieve test were chosen to be 15 minutes.
- Each test sieve is of circular shape with an internal diameter of 200 mm.
- The sieving medium of choice was a woven metal cloth with square aperture openings.

A1 Copper Carbonatite Ore

The completed sieve test results is summarised in Table 17:

Table 17: Completed Sieve Test Result – Copper Carbonatite Ore (-26.5+2 mm)

Particle Size			Sieve Fractions		Nominal aperture size	Cumulative undersize
mm			g	%	mm	%
	d >	26.5	0	0	26.5	100.0
26.5	≥ d >	16	278.3	10.9	16	89.1
16	≥ d >	11.2	255.3	10.0	11.2	79.2
11.2	≥ d >	8	292.8	11.4	8	67.8
8	≥ d >	6.7	326.5	12.7	6.7	55.0
6.7	≥ d >	5.6	244.6	9.5	5.6	45.5
5.6	≥ d >	4.75	173.9	6.8	4.75	38.7
4.75	≥ d >	3.35	263.8	10.3	3.35	28.4
3.35	≥ d >	2	218.7	8.5	2	19.9
	d >	2	509.7	19.9	*Final undersize*	
Total			2563.6	100		

The sieve test results are graphically represented by the cumulative undersize graph on a logarithmic scale in Figure 117.

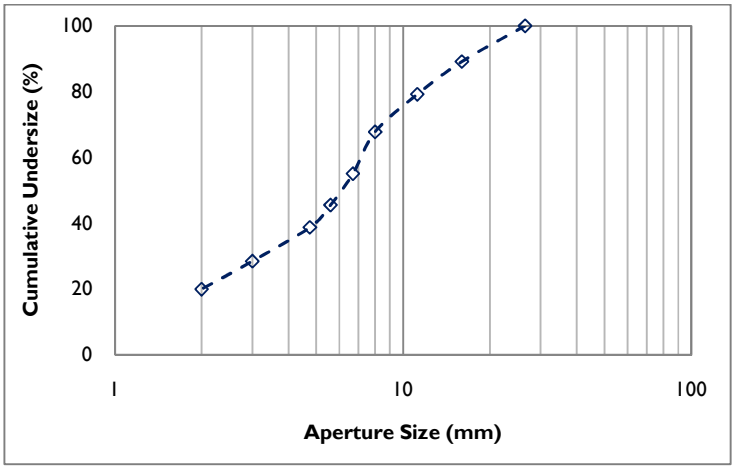

Figure 117: Cumulative undersize as a function of nominal aperture size

Crushing of the Copper Carbonatite Ore produced a typical S-shaped cumulative undersize graph with d_{50}=6.12 mm.

A2 Porphyry Copper Ore

The completed sieve test results is summarised in Table 18:

Table 18: Completed Sieve Test Result - Porphyry Copper Ore (-26.5+16 mm)

Particle Size			Sieve Fractions		Nominal aperture size	Cumulative undersize
mm			g	%	mm	%
	d >	26.5	0	0	26.5	100.0
26.5	≥ d >	16	257.6	8.3	16	91.7
16	≥ d >	11.2	279.6	9.0	11.2	82.7
11.2	≥ d >	8	282.4	9.1	8	73.5
8	≥ d >	6.7	186.5	6.0	6.7	67.5
6.7	≥ d >	5.6	208.4	6.7	5.6	60.8
5.6	≥ d >	4.75	301.1	9.7	4.75	51.1
4.75	≥ d >	3.35	606.4	19.6	3	31.5
3.35	≥ d >	2	486.2	15.7	2	15.8
	d >	2	488.2	15.8	*Final undersize*	
Total			3096.4	100		

No formal sieve test was conducted to obtain the the -31.5+26.5 mm (211.5 g), -12.5+9.5 mm (531.5 g) and -4.75+0 mm (1480.1 g) particle size fractions. These size fractions was received from the University of Nottingham and hence not created at the University of Stellenbosch, South Africa, as part of the sample preparation phase of this thesis.

The sieve results are graphically represented by the cumulative undersize graph on a logarithmic scale in Figure 118.

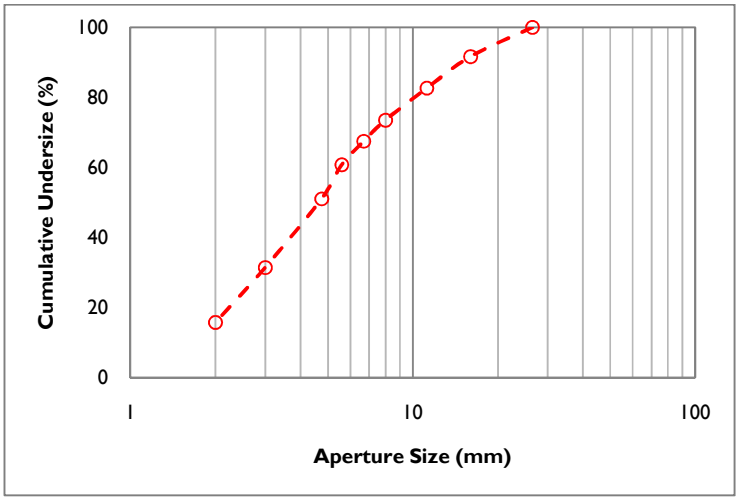

Figure 118: Cumulative undersize as a function of nominal aperture size

Crushing of the Porphyry Copper Ore produced a typical S-shaped cumulative undersize graph with d_{50}=4.66 mm. Large amounts of smaller sized particle was generated during the primary crushing phase of the ore compared with the crushing of the Copper Carbonatite Ore. This is attributed to a smaller specified jaw crusher aperture size during crushing.

A3 Quartz Monzonite Porphyry Copper Ore

The Quartz Monzonite Porphyry Copper Ore samples were received from the University of Nottingham, bagged into particle size fractions of -19+16 mm, -16+13 mm, -13+9 mm, -9+6 mm, -6+4 mm and -4+3 mm samples. The vibratory sieve test results is included as part of this thesis, however the mass of the sieved sample for $d_p < 3$ mm and $d_p > 19$ mm is not known.

Table 19: Completed Sieve Test Result - Porphyry Copper Ore (-26.5+16 mm)

Particle Size			Sieve Fractions		Nominal aperture size	Cumulative undersize
mm			g	%	mm	%
	d >	19	0	0	19	100.0
19	≥ d >	16	250.1	16.2	16	83.8
16	≥ d >	13	261	16.9	13	66.9
13	≥ d >	9	259.3	16.8	9	50.0
9	≥ d >	6	261.8	17.0	6	33.1
6	≥ d >	4	298.9	19.4	4	13.7
4	≥ d >	3	210.9	13.7	3	0.0
	d >	3	0	0.0	*Final undersize*	
Total			1542	100		

The sieve results are graphically represented by the cumulative undersize graph on a logarithmic scale in Figure 119.

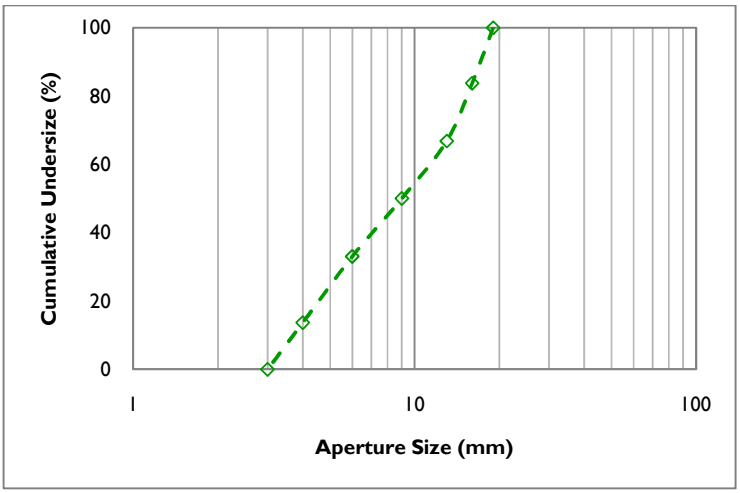

Figure 119: Cumulative undersize as a function of nominal aperture size

Crushing of the Quartz Monzonite Porphyry Copper Ore produced a cumulative undersize graph with d_{50}=9 mm.

Appendix B

Experimental Ore Density Results

Appendix B presents the determination procedure of the ore density. A water displacement procedure is used to determine the respective ore densities.

A known mass of ore is added to known volume of water. The increase in volume of the combined particle/water mixture is equal to the volume of the crushed ore particles. To obtain a well-averaged ore density, three (n=3) individual tests are performed of which the mean crushed ore mass is determined by Equation 14 :

Equation 14: Mean mass of ore for n-tests

$$\bar{m}_n = \frac{\sum_{i=1}^{n} m_i}{n}$$

Likewise, the mean displaced water volume across the three individual tests (i=3) is determined by Equation 15:

Equation 15: Mean water volume displaced

$$\bar{V}_n = \frac{\sum_{i=1}^{n} V_i}{n}$$

Hence, the mean ore density is calculated by Equation 16:

Equation 16: Ore Density

$$\rho_{ore} = \frac{\bar{m}_n}{\bar{V}_n}$$

After each experiment the wetted ore was dried for 1h at 80°C to limit the effect of water entrainment, within the porous structure of the ore, during future experimental tests to be

conducted and to ensure that ore losses is kept to a minimum. The experimental densities is presented below:

Ore Name	Experimental Density
	kg/m³
Porphyry Copper Ore	2428
Copper Carbonatite Ore	2891
Quartz Monzonite Porphyry Copper Ore	2447

For all three the copper ores the -11.2+8 mm particles size class was used to determine the density of the ore.

After wetting the samples were placed in an dry oven at 80°C for 1 day to ensure that micro pores of the ore structure is dried completely due to the dependence of dielectric properties on moisture content (Nelson, 2008).

B1 Copper Carbonatite Ore

	Mass Loading	Displaced Water Volume	Density
No	(g)	(ml)	(g/ml)
1	192.6	65	2963
2	274.8	95	2893
3	310.0	110	2818

Average Mass Loading: 259.1 g
Average Displace Water Volume: 90 ml
Average Density: 2891g/ml

B2 Porphyry Copper Ore

	Mass Loading	Displaced Water Volume	Density
No	(g)	(ml)	(g/ml)
1	67.2	28	2400
2	92.3	37	2495
3	124.2	52	2388

Average Mass Loading: 94.6 g

Average Displace Water Volume: 39 ml

Average Density: 2428 g/ml

B3 Quartz Monzonite Porphyry Copper Ore

	Mass Loading	Displaced Water Volume	Density
No	(g)	(ml)	(g/ml)
1	43.1	17	2535
2	62.7	26	2412
3	86.2	36	2394

Average Mass Loading: 86.2 g

Average Displace Water Volume: 36 ml

Average Density: 2394 g/ml

Appendix C

Representative Sampling Methods

Appendix C presents additional information about the various representative sampling procedures used in industry and the academia to obtain smaller representative samples of the bulk ore material which will statistically still exhibit the intrinsic characteristics of the bulk mass. The following procedures will be briefly discussed briefly, based on work done by, Nkohla, 2006.

- Splitting procedures
- Shovelling procedures
- Apparatus Sampling Procedures
- Quartering Procedures

C1 Splitting Procedures

Sectorial Splitting

Crushed material is fed via a funnel onto a vibratory channel. The vibration causes the material to move along the axis of the channel. The material falls under gravitation to a number of equally spaced rotating collection beakers. Effectively the feed material is divided into smaller representative amounts equal to the number of beakers.

Sectorial splitters are excellent mass reduction tools and performs best when operated at a constant ore feed rate, angular velocity en vibratory rate.

Riffle Splitting

Riffle splitters, Figure 120, are usually a metal V-shaped structure with a series of chutes to either side of the splitter. Material is introduced to the feed side of the splitter and the outlet is discharged into two collection bins effectively dividing the original amount of material into two halves. The process can be repeated until the required amount of material is collected in the collection bin.

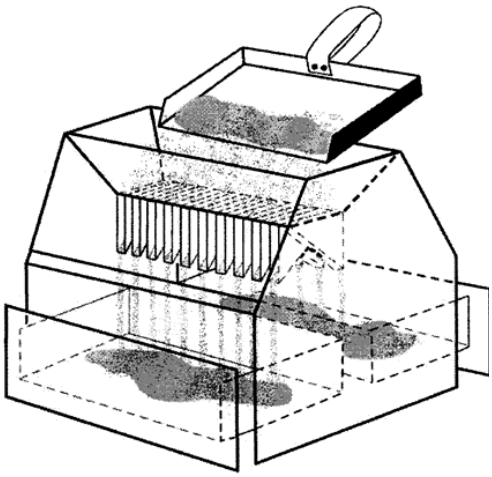

Figure 120: Riffle splitter (Nkohla, 2006)

The effectiveness of riffle splitters is strongly dependent on the skill of the operator as the feed material needs to be fed to the splitter in such a fashion that all the chutes receives the same amount of material. The latter can be difficult to achieve depending on the particle size of the material being fed to the splitter.

Two distinct advantages need mentioning:

- Riffle splitters are excellent mass reduction tools. If operated correctly riffle splitters will split a crushed load of material into two equally sized sub-samples with any one passing.
- Very little to no material is lost during the riffle splitting procedure. This is especially advantageous when only a limited amount of material is available.

C2 Shovelling Procedures

Alternate Shovelling

Alternate shovelling involves the splitting of a mass of particles into two piles. This is done by randomly taking a series of scoops from the original sample mass and grouping even and uneven scoop numbers. Both the piles should contain the same amount of scoops with each scoop being the same size. It is suggested that the minimum amount of scoops in each pile should be at least nine. A major drawback of this method is that the mass reduction of the original sample mass is rather slow and that a large grouping and segregation error is maintained when taking scoops from the original sample mass. Segregation and grouping errors have a severe impact on the accurateness of the sampling process.

Fractional Shovelling

Fractional shovelling involves the reduction of the original sample mass into predetermined amount of piles (called sub-sample piles starting at N=1, 2, 3…). This is done by taking an N-amount of scoops from the original sample mass and creating each sub-sample in that same order, starting at sub-sample 1 and ending at sub-sample N. Material is added to each sub-sample by taking a scoop from the bulk material in the same order as the sub-samples were generated.

As with alternate shovelling a major drawback of this method is that, the mass reduction of the bulk material is rather slow and a large segregation error is dominant.

Degenerate Fractional Shovelling

Degenerate fractional shovelling is very much the same as fractional shovelling, the only difference being that only one sub-sample is generated and hence only one out of so many scoops forms part of the representative sub-sample pile with the rest being discarded. With this method only about 10% of the bulk material forms part of the representative sample mass. Due to the availability of only one sub-sample, (un)intended bias error can be introduced.

C3 Apparatus Sampling Procedures

Table Splitter

A table splitter consists out of a flat, inclined, surface on which triangular blocks are fitted. These blocks splits the feed material into a smaller samples as the material is passes down the surface incline, whilst retaining the rest of the material on the table surface. This method is not generally recommended due to the large operator bias and the bulky nature of the apparatus.

V-blending

V-blending devices are used to homogenise crushed ore samples by means of the rotation of the sample container and the subsequent discharge of its contents. However this sampling method lacks accurate representativeness due to the segregation of the ore material whilst the sample is discharged, possibility of further segregation of the ore material as it is discharged from the V-blender and the large influence that sampling has prior to V-blending.

Despite the theoretical importance of V-blending, as one of the multitude of different representative sampling techniques, its use is restricted.

Vibratory Spatula

The use of a vibratory spatula should be avoided as the vibratory action of the device increases the segregation of the sample particles due to the difference in sample mass, particle size and shape. The same analogy is evident when using a vibratory sieve shaker to produce a particle size distribution.

Grab Sampling

Grab sampling involves taking a random mass of material from the top of the original sample mass with the aid of a metal scoop. Most often these scoops are designed incorrectly (trough-shape vs. square-shape) which result in an unrepresentative sample being taken.

Despite this obvious drawback grab sampling also does not provide each particle the same statistical probability of being sampled. This is especially problematic in a sample of heterogeneous particles where the individual particles differ from each other in terms of their physical characteristics. The result is bias and hence not representative of the original particle mass and hence grab sampling should be avoided.

Incremental Sampling

Incremental sampling is a process where a representative sample is generated by the reunion of a number of increments taken from a sample. Increments are taken with the aid of a scoop as in the case with grab sampling. This method lends itself to representative sampling, however representative sampling can be very tedious when large amounts of material needs to be processed. Each sub-sample will consist of at least 30 equally spaced increments taken randomly across the pile of particles (Pitard, 1993).

C4 Quartering Procedures

Coning and Quartering

Coning and quartering is a process where an amount of particles is mixed and discarded into a cone-shaped structure. The cone is then flattened and divided into four quarters (N=1, 2, 3 and 4). Two alternate quarters are combined to form a the representative sample, whilst the remaining two quarters are discarded.

Coning and quartering suffers from three distinct disadvantages:

1. Particle correlations in each of the four quadrants are preserved. When the alternate quarters are combined, this effect becomes even more prominent.

2. The grouping and segregation of particles is persistent throughout the quartering process which lends itself to biased results.

3. The mass reduction process is slow and therefore an considerable amount of time is required to process large amounts of crushed ore.

Rolling and Quartering

Rolling and quartering is a variation of the coning and quartering procedure, the only difference being that mixing of the particles occur. This causes the particles that tend to group together to break apart, allowing for a greater degree of probability that all particles have the same chance of being sampled. The original sample is firstly placed in a conical pile on a piece of paper. The pile is then flattened after which the material is mixed by rolling it back and forth using the outer edges of the sheet of paper as a mixing device. The material is then assembled in the middle of the sheet, by lifting the corners, and again flattened. The rest of the splitting procedure is the same as for the coning and quartering procedure. The procedure becomes extremely tedious when large quantities of material needs to be processed due to the addition of a mixing step.

Appendix D

Fractional Packing Density

Appendix D presents the fractional packing density for each of the ore of interest in the WR284 (72.14 *x* 34.04 *x* 35 mm) and WR340 (86.36 *x* 43.18 *x* 35 mm) sample holders as a function of particle size. The fractional packing density serves as indication as to how much of the particulate load can fit in sample holder cavity per particle size class which varies roughly between 36% and 48%. The fractional packing density results for the Porphyry Copper, Copper Carbonatite and Quartz Monzonite Porphyry Copper ore is presented as follows:

D1: Fractional packing density: WR284 sample holder (sample cavity thickness: 35 mm)
Particle size distribution: -26.5+2 mm

D2: Fractional packing density: WR340 sample holder (sample cavity thickness: 35 mm)
Particle size distribution: -26.5+2 mm

D3: Fractional packing density: WR284 sample holder (sample cavity thickness: 20 mm)
Particle size classes: -31.5+26.5 mm, -12.5+9.5 mm and -4.75+0 mm

D4: Fractional packing density: WR284 sample holder (sample cavity thickness: 25 mm)
Particle size classes: -31.5+26.5 mm, -12.5+9.5 mm and -4.75+0 mm

D5: Fractional packing density: WR284 sample holder (sample cavity thickness: 35 mm)
Particle size classes: -31.5+26.5 mm, -12.5+9.5 mm and -4.75+0 mm

D6: Fractional packing density: WR340 sample holder (sample cavity thickness: 35 mm)
Particle size classes: -31.5+26.5 mm, -12.5+9.5 mm and -4.75+0 mm

D1 WR284

Copper Carbonatite Ore

Particle Size Class (mm)	Mass Loading (g)			Average Mass Loading (g)	Average Particle Volume (ml)	Average Packing Fraction (%)	Maximum Packing Fraction (%)	Minimum Packing Fraction (%)
	No.1	No.2	No.3					
-26.5+16	103	98.3	94.3	98.53	34.08	39.66	41.45	37.95
-16+11.2	101.6	105.9	100.5	102.67	35.51	41.32	42.62	40.45
-11.2+8	111	104.5	104.6	106.70	36.91	42.94	44.67	42.06
-8+6.7	104.8	103.4	106.2	104.80	36.25	42.18	42.74	41.61
-6.7+5.6	104.2	105.3	104.7	104.73	36.23	42.15	42.38	41.94
-5.6+4.75	107.4	104.8	107.3	106.50	36.84	42.86	43.22	42.18
-4.75+3.35	104.6	103.8	104.6	104.33	36.09	41.99	42.10	41.77
-3.35+2	104.6	108.8	106.1	106.50	36.84	42.86	43.79	42.10

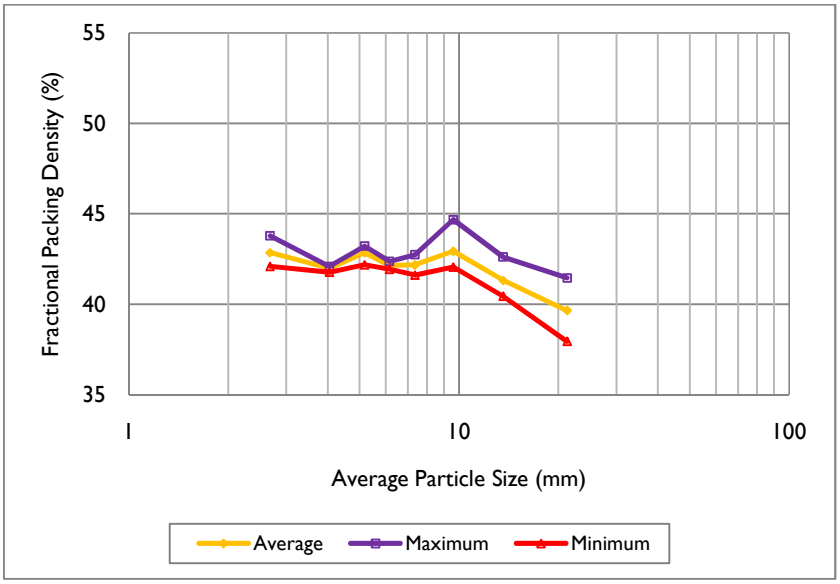

Figure 121: Copper carbonatite - fractional packing density (WR284)

Porphyry Copper Ore

Particle Size Class (mm)	Mass Loading (g)			Average Mass Loading (g)	Average Particle Volume (ml)	Average Packing Fraction (%)	Maximum Packing Fraction (%)	Minimum Packing Fraction (%)
	No.1	No.2	No.3					
-26.5+16	88.1	84.6	89.8	87.5	36.04	41.93	43.03	40.54
-16+11.2	91.5	93.1	90	91.5	37.70	43.86	44.61	43.13
-11.2+8	96.9	93.7	96.7	95.8	39.44	45.89	46.43	44.90
-8+6.7	97.9	98.6	99.4	98.6	40.62	47.27	47.63	46.91
-6.7+5.6	101.2	101.5	100	100.9	41.56	48.35	48.64	47.92
-5.6+4.75	97.2	99.8	100.9	99.3	40.90	47.58	48.35	46.58
-4.75+3.35	96.2	96.4	98.2	96.9	39.92	46.45	47.06	46.10
-3.35+2	98.9	97.1	96.8	97.6	40.20	46.77	47.39	46.39

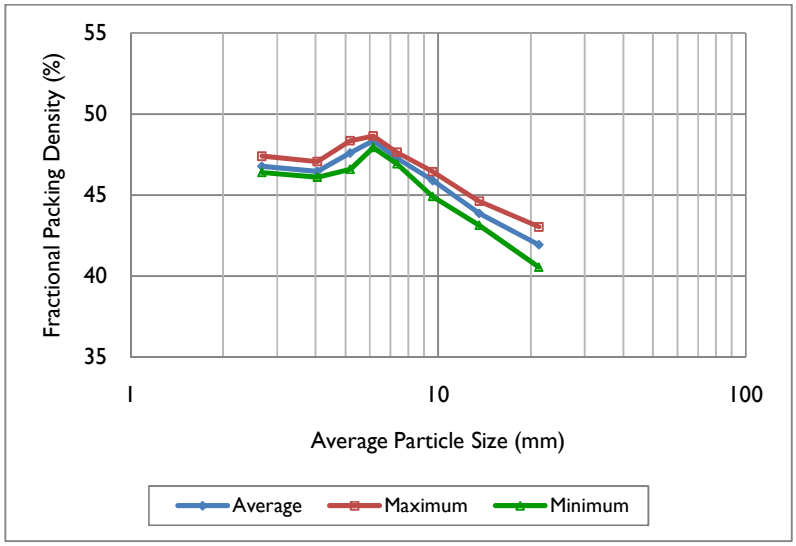

Figure 122: Porphyry copper - fractional packing density (WR284)

Quartz Monzonite Porphyry Copper Ore

Particle Size Class (mm)	Mass Loading (g)			Average Mass Loading (g)	Average Particle Volume (ml)	Average Packing Fraction (%)	Maximum Packing Fraction (%)	Minimum Packing Fraction (%)
	No.1	No.2	No.3					
-19+16	80.9	76.9	75.5	77.77	31.78	36.98	38.47	35.90
-16+13	85.0	90.3	85.4	86.90	35.51	41.32	42.94	40.42
-13+9	90.3	87.7	87.1	88.37	36.11	42.02	43.94	41.41
-9+6	97.2	96.3	93.4	95.63	39.08	45.47	46.22	44.41
-6+4	97.2	95.7	95.7	96.20	39.31	45.74	46.22	45.50
-4+3	96.2	98.8	100.7	98.57	40.28	46.87	47.8 8	45.74

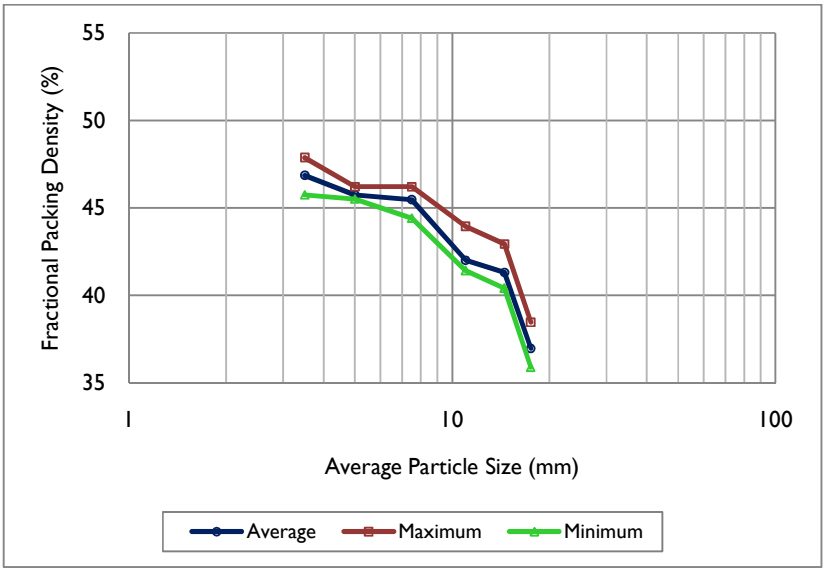

Figure 123: Quartz monzonite porphyry copper - fractional packing density (WR284)

D2 WR340

Copper Carbonatite Ore

Particle Size Class (mm)	Mass Loading (g)			Average Mass Loading (g)	Average Particle Volume (ml)	Average Packing Fraction (%)	Maximum Packing Fraction (%)	Minimum Packing Fraction (%)
	No.1	No.2	No.3					
-26.5+16	144.5	156.7	152.4	151.20	52.30	40.07	41.53	38.30
-16+11.2	150.9	156.4	154.5	153.93	53.25	40.80	41.45	39.99
-11.2+8	160.3	159.4	166.4	162.03	56.05	42.94	44.10	42.25
-8+6.7	161.6	157.5	160.2	159.77	55.26	42.34	42.83	41.74
-6.7+5.6	161.6	161.5	162.1	161.73	55.94	42.86	42.96	42.80
-5.6+4.75	159.8	158.9	157.2	158.63	54.87	42.04	42.35	41.66
-4.75+3.35	152.0	153.5	151.5	152.33	52.69	40.37	40.68	40.15
-3.35+2	158.0	162.9	160.0	160.30	55.45	42.48	43.17	41.87

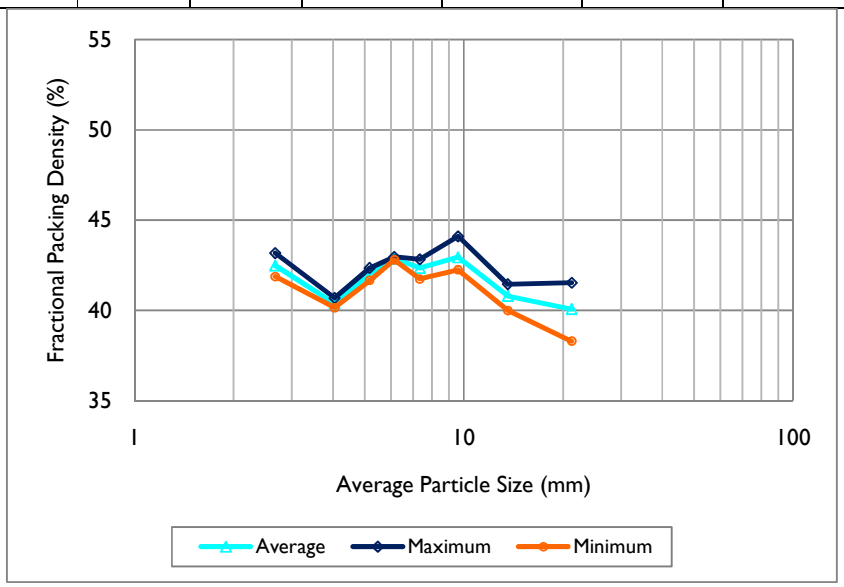

Figure 124: Copper carbonatite - fractional packing density (W340)

Porphyry Copper Ore

Particle Size Class (mm)	Mass Loading (g)			Average Mass Loading (g)	Average Particle Volume (ml)	Average Packing Fraction (%)	Maximum Packing Fraction (%)	Minimum Packing Fraction (%)
	No.1	No.2	No.3					
-26.5+16	119.7	121.9	121.2	120.93	49.81	38.16	38.47	37.77
-16+11.2	140.6	134.7	141.6	138.97	57.24	43.85	44.68	42.51
-11.2+8	144.4	144.8	147.9	145.70	60.01	45.98	46.67	45.57
-8+6.7	152.4	150.3	151.8	151.50	62.40	47.81	48.09	47.43
-6.7+5.6	145.5	149.7	147.6	147.60	60.79	46.58	47.24	45.91
-5.6+4.75	153.1	156.4	152.6	154.03	63.44	48.61	49.35	48.16
-4.75+3.35	149.1	150.6	145.1	148.27	61.07	46.79	47.52	45.79
-3.35+2	148.5	148.1	148.3	148.30	61.08	46.80	46.86	46.74

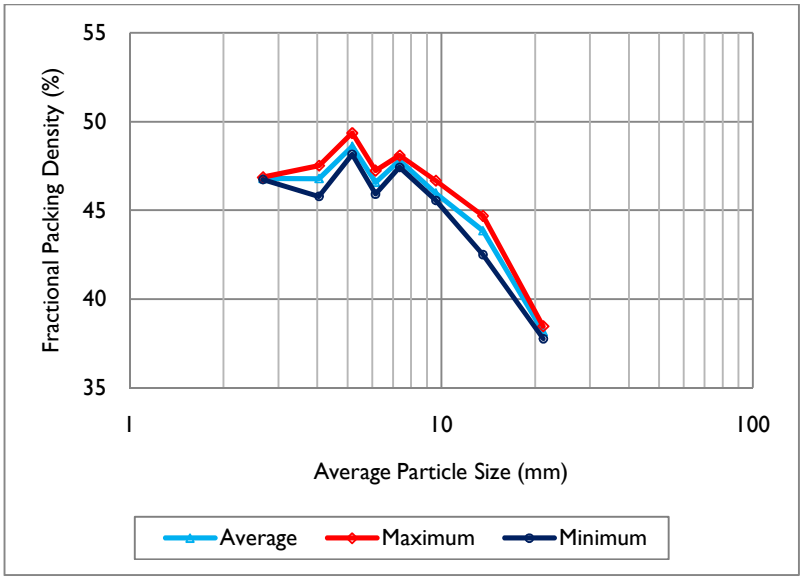

Figure 125: Porphyry copper - fractional packing density (WR340)

Quartz Monzonite Porphyry Copper Ore

Particle Size Class (mm)	Mass Loading (g)			Average Mass Loading (g)	Average Particle Volume (ml)	Average Packing Fraction (%)	Maximum Packing Fraction (%)	Minimum Packing Fraction (%)
	No.1	No.2	No.3					
-19+16	129.4	130.3	130.1	129.93	53.10	40.68	40.80	40.52
-16+13	132.1	130.2	132.4	131.57	53.77	41.20	41.46	40.77
-13+9	135.3	137.1	138.2	136.87	55.93	42.85	43.27	42.36
-9+6	144.5	142.5	143.3	143.43	58.62	44.91	45.24	44.62
-6+4	142.7	142.6	146.0	143.77	58.75	45.02	45.71	44.65
-4+3	147.5	151.4	146.1	148.33	60.62	46.45	47.41	45.75

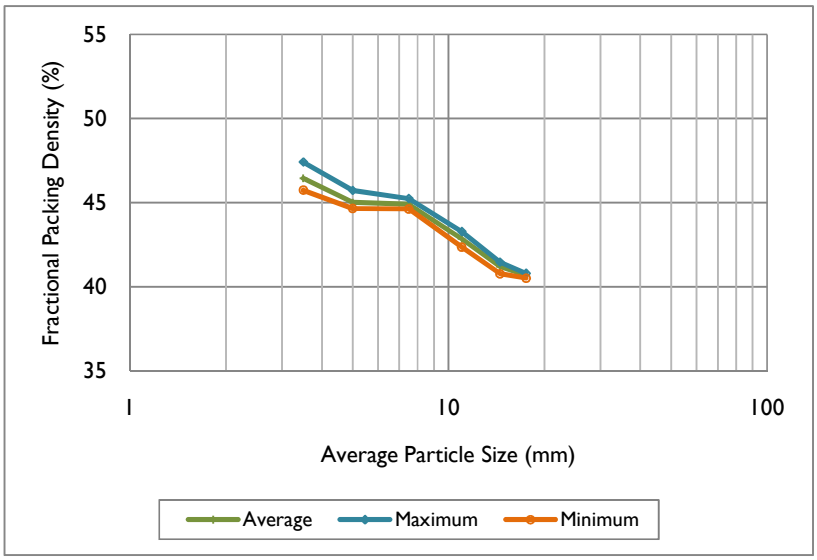

Figure 126: Quartz monzonite porphyry copper – fractional packing density (WR340)

D3 WR284 (Sample cavity thickness: 20 mm)

Particle Size Class (mm)	Mass Loading (g)			Average Mass Loading (g)	Average Particle Volume (ml)	Average Packing Fraction (%)	Maximum Packing Fraction (%)	Minimum Packing Fraction (%)
	No.1	No.2	No.3					
-31.5+26.5	38.9	61.6	44.4	48.30	16.43	33.45	42.66	26.94
-12.5+9.5	77.6	67.7	75.5	73.60	25.03	50.97	53.74	46.89
-4.75+0	89.4	89.6	88.6	89.20	30.34	61.78	62.05	61.36

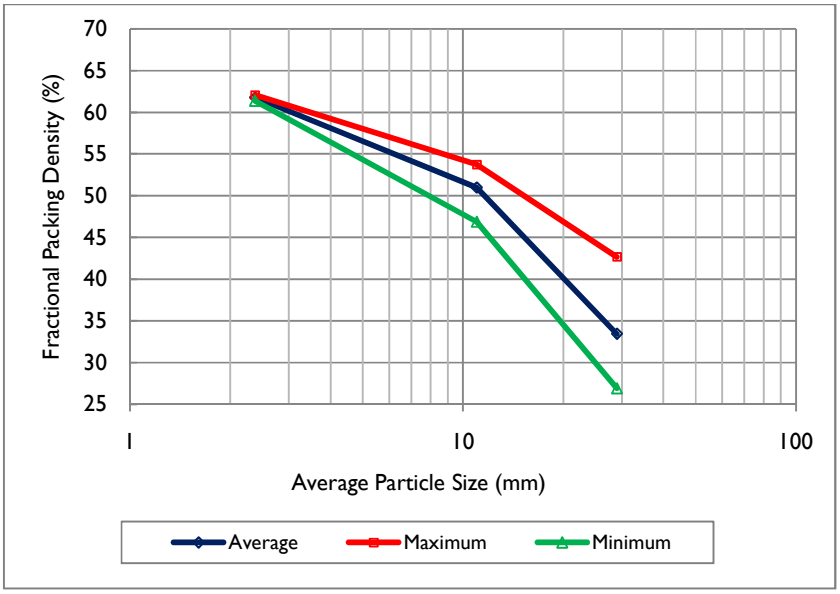

Figure 127: Porphyry copper - fractional packing density (WR284)

D4 WR284 (Sample cavity thickness: 25 mm)

Particle Size Class (mm)	Mass Loading (g)			Average Mass Loading (g)	Average Particle Volume (ml)	Average Packing Fraction (%)	Maximum Packing Fraction (%)	Minimum Packing Fraction (%)
	No.1	No.2	No.3					
-31.5+26.5	73.6	69.3	74.2	72.37	24.61	40.09	41.11	38.40
-12.5+9.5	93.9	95.5	95.4	94.93	32.29	52.60	52.91	52.03
-4.75+0	109.9	110.9	111.4	110.73	37.66	61.35	61.72	60.89

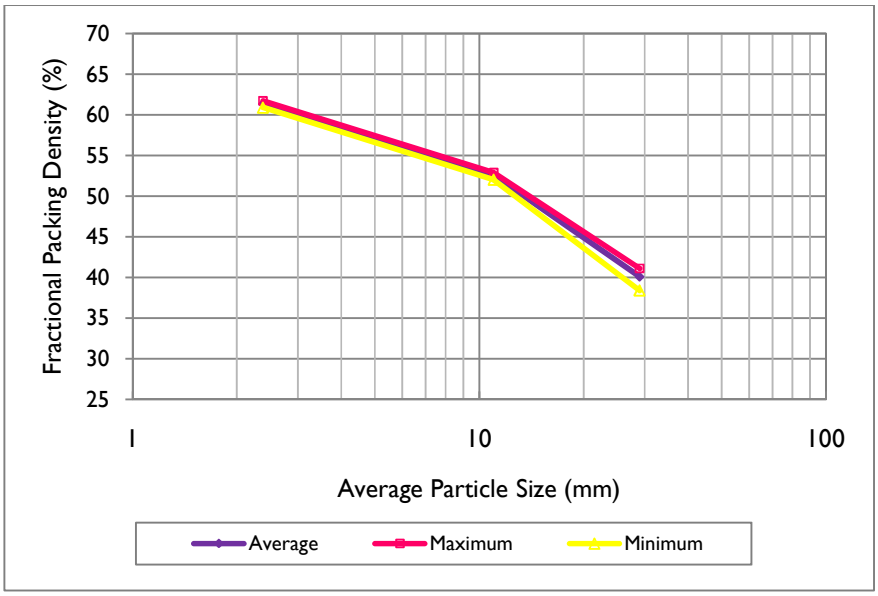

Figure 128: Porphyry copper - fractional packing density (WR284)

D5 WR284 (Sample cavity thickness: 35 mm)

Particle Size Class (mm)	Mass Loading (g)			Average Mass Loading (g)	Average Particle Volume (ml)	Average Packing Fraction (%)	Maximum Packing Fraction (%)	Minimum Packing Fraction (%)
	No.1	No.2	No.3					
-31.5+26.5	102.8	107.9	108.1	106.27	36.15	42.05	42.78	40.68
-12.5+9.5	119.9	123.3	121.5	121.57	41.35	48.11	48.80	47.45
-4.75+0	147.6	149.7	146.8	148.03	50.35	58.58	59.24	58.10

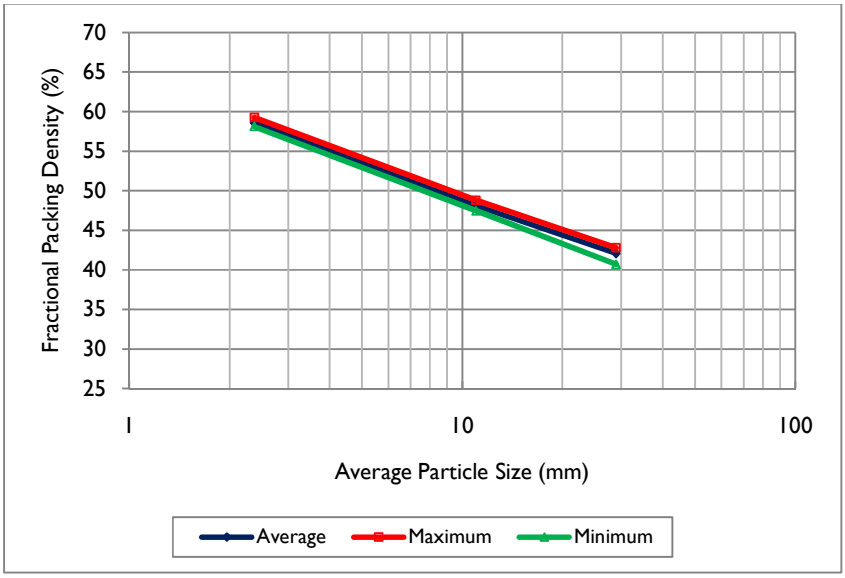

Figure 129: Porphyry copper - fractional packing density (WR284)

D6 WR340 (Sample cavity thickness: 35 mm)

Particle Size Class (mm)	Mass Loading (g)			Average Mass Loading (g)	Average Particle Volume (ml)	Average Packing Fraction (%)	Maximum Packing Fraction (%)	Minimum Packing Fraction (%)
	No.1	No.2	No.3					
-31.5+26.5	140.1	135.5	139.4	138.33	47.05	36.05	36.51	35.31
-12.5+9.5	179.9	181	185.7	182.2	61.97	47.48	48.40	46.88
-4.75+0	216.5	216.6	218.5	217.2	73.88	56.60	56.94	56.42

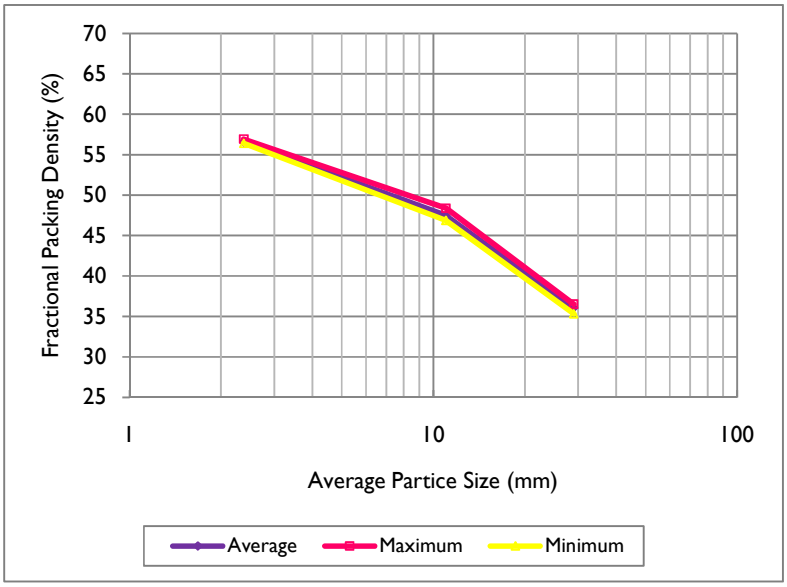

Figure 130: Porphyry copper - fractional packing density (WR340)

Appendix E

Extract.py DBE Algorithm Programme

Appendix E presents the **extract.py** program used by the DBE Algorithm to extract the dielectric properties of the crushed ore samples.

```
import measurements as me
import propextract.algorithm as alg

import propextract.results as res
import matplotlib.pyplot as plt
import database
import propextract.measurement as mes

m = me.measurements_20100311()

meas = m[2]

alg.DB()
algo = alg.DB()

db = meas.sampleholder().db(database.base_dir, 'DBWR284_air_rem') # Vir WR340 is databaas naam 'DBWR340_air_rem'
db.save_for_prop('S_parameters_DBE Algorithm_Esc2 -3.35+2 35mm m1_Full Band Extraction_2.3-3 GHz.csv', 2.84, 0.07)
db.limit(1) # - as net wil toets

algo.set_database(db)
algo.set_freq_range(2.3e9, 3e9) # bv. werk met data van 2.3-3GHz
#algo.set_band(250e6)
#algo.set_whole_band()
#algo.FromPort1()
algo.FromPort2()
#algo.useBothPorts()
algo.solve(meas)

print algo.metric()

algo.save('esc2 -3.35+2 35mm m1.s2p, 20100325, WR284, port 2, full band extraction, 2.3-3GHz.csv')
#algo.save('Air WR284 35mm, whole band, MHz intervals, both ports.csv')

rplot = res.MaterialPropertyPlotter()
rplot.linear_plot1(algo)

mplot = res.MeasurementPlotter()
mplot.log_plot1(meas)

dbplot = res.DBPlotter(db)
dbplot.log_plot1(2.84,0.07)

# rplot.linear_plot2(bj)

plt.show()

# rplot = res.MaterialPropertyPlotter()
# rplot.linear_plot1(DBextract)
# rplot.linear_plot2(DBextract)

#rplot = res.MaterialPropertyPlotter()
#rplot.linear_plot1(nwr)

# mplot = res.MeasurementPlotter()
# mplot.log_plot1(m[1])
# mplot.linear_plot2(m[1])
```

After completion of the dielectric property extraction the **extract.py** program generates the result in the form:

```
≫ Frequency Section: 2.1 – 3 GHz          … (1)
≫ Min – Max Metric: 0.051648 – 0.478100   … (2)
≫ [3.42-0.197j]                           … (3)
≫ [0.051648]                              … (4)
```

The extraction was done for crushed -6.7+5.6 mm Copper Carbonatite ore, with a full band extraction, 2.1 GHz – 3 GHz.

- Line (1) describes the frequency band that was used during the dielectric property extraction with the selected f_{start} and f_{end} frequencies. The frequency band could be either a full band extraction, or a segmented extraction in different frequency intervals (e.g. 100 MHz, 250 MHz etc.) If frequency intervals are chosen, lines (1) until (4) would be generated for every frequency interval (e.g. 2.1 GHz – 2.2 GHz, 2.2 GHz – 2.3 GHz etc.)
- Line (2) describes the range of $\|\bullet\|$ values in a specific frequency interval calculated using Equation 11.
- Line (3) provides the extracted dielectric properties of the material under test in the form $\varepsilon^* = \varepsilon' + \varepsilon'' j$. Per definition ε'' is negative (-). The ε'-value stays constant for a chosen frequency interval created in the `results.csv` file and is the same at any frequency point, f_{point}, in the specific frequency band. The reported value is the true value for the specific frequency interval. However, the reported (uncorrected) ε''-value is given at 3 GHz. The uncorrected dielectric loss factor is denoted as ε''_{uncorr}. To correct for the frequency shift from 3 GHz to the f_{point}, Equation 17 are used:

Equation 17: Frequency correction at 3 GHz

$$\varepsilon''_{corr,point} = \frac{3}{f_{point}} \times \varepsilon''_{uncorr,point}$$

In Equation 17, f_{point} can be replaced with the average frequency, f_{ave}, which denotes the arithmetic average of the specific frequency band used calculated using Equation 18. In such cases $\varepsilon''_{corr,point}$ is replaced by the band averaged dielectric loss factor, $\varepsilon''_{corr,interval}$, applicable to each of the frequency intervals between $f_{start,interval}$ and $f_{end,interval}$.

Equation 18: Average Frequency Interval

$$f_{ave} = \left(\frac{f_{start,inter} + f_{end,interval}}{2} \right) GHz$$

In (4) the $\|\bullet\|_{\min}$-value for the frequency interval is reported for which the fit between the simulated and measured S_{ij} is best. The $\|\bullet\|_{\min}$-value is somewhere in the frequency interval with ε' and $\varepsilon''_{corr,interval}$ at this point.

Appendix F

Comparison of Measured $|S_{ij}|$ Parameters for Repeated Dielectric Property Measurement

Appendix F represents the magnitude of the measured S_{ij}-parameter for two successive dielectric property measurements (denoted as measurement 1 and measurement 2) for a particulate load of crushed porphyry copper ore in the -26.5+16 mm, -16+11.2 mm, -11.2+8 mm, -8+6.7 mm, -6.7+5.6 mm, -5.6+5.75 mm, -4.75+3.35 mm and -3.35+2 mm particle size classes.

Porphyry Copper Ore

WR284

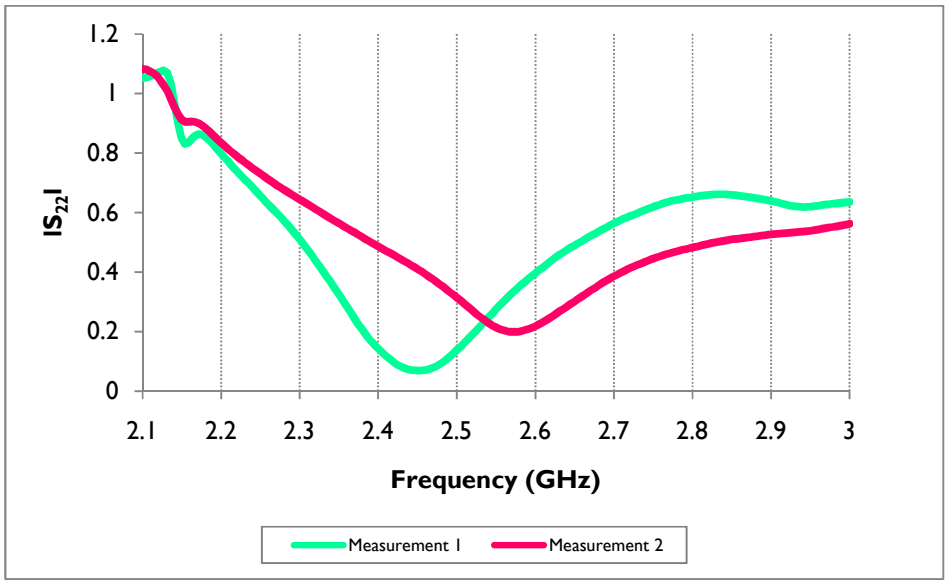

Figure 131: $|S_{22}|$ comparison between measurement 1 and 2 (-26.5+16 mm)

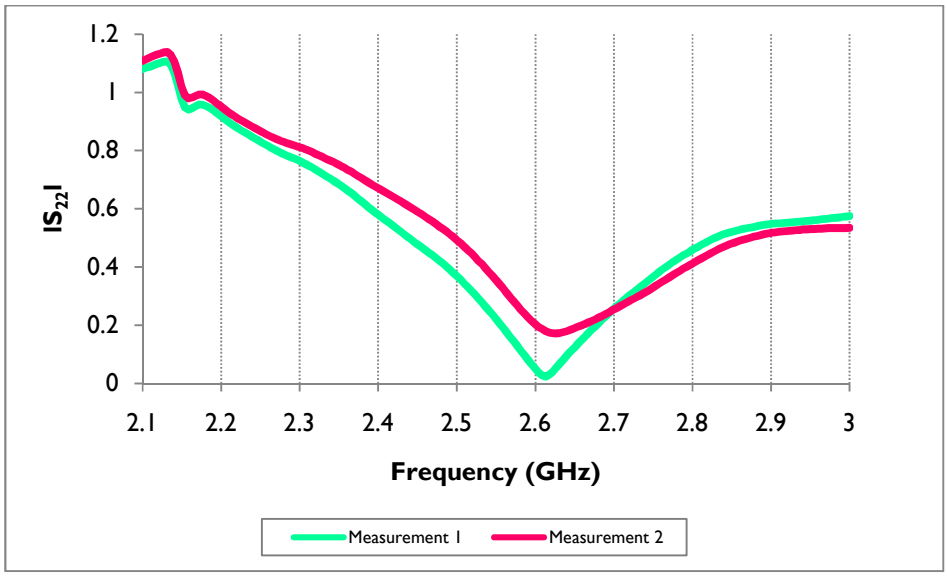

Figure 132: $|S_{22}|$ comparison between measurement 1 and 2 (-16+11.2 mm)

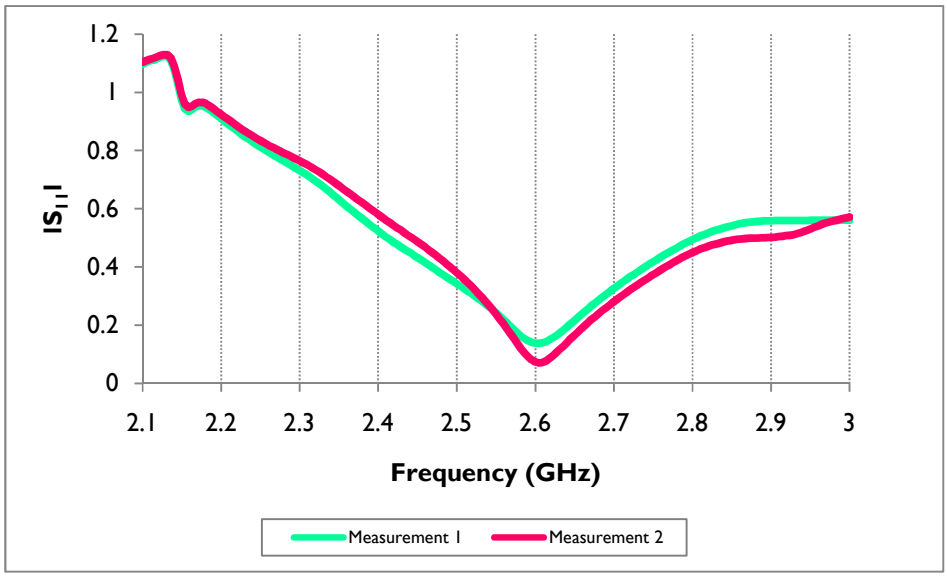

Figure 133: $|S_{11}|$ comparison between measurement 1 and 2 (-11.2+8 mm)

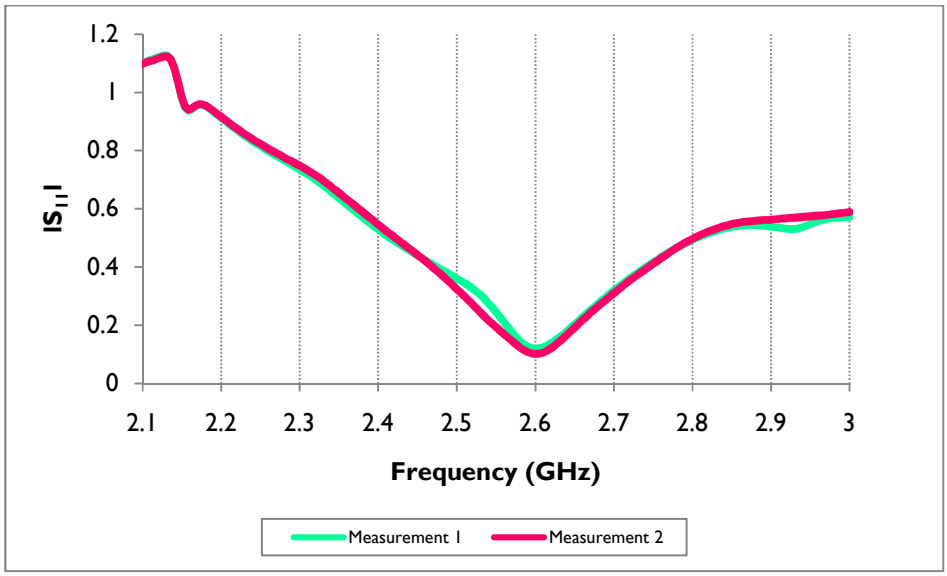

Figure 134: $|S_{11}|$ comparison between measurement 1 and 2 (-8+6.7 mm)

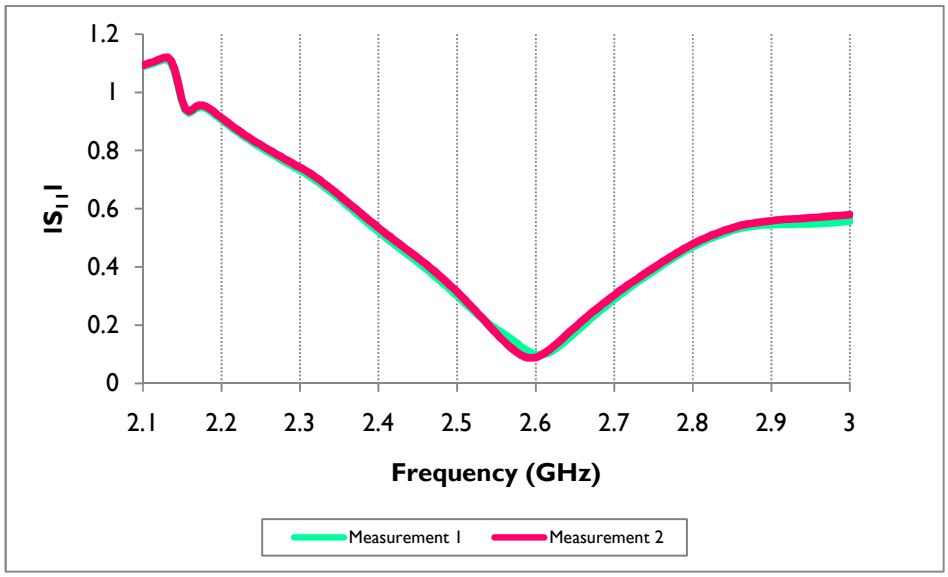

Figure 135: $|S_{11}|$ comparison between measurement 1 and 2 (-6.7+5.6 mm)

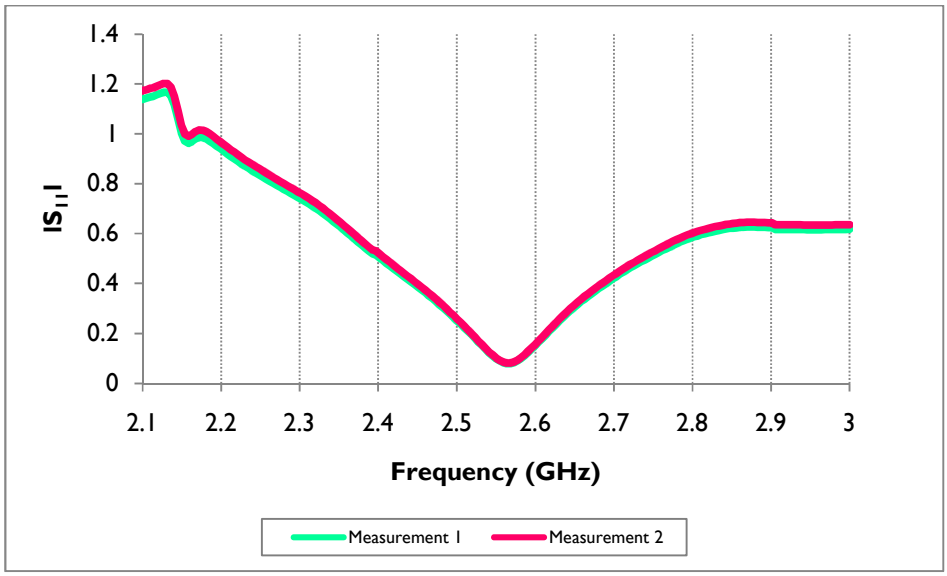

Figure 136: $|S_{11}|$ comparison between measurement 1 and 2 (-5.6+4.75 mm)

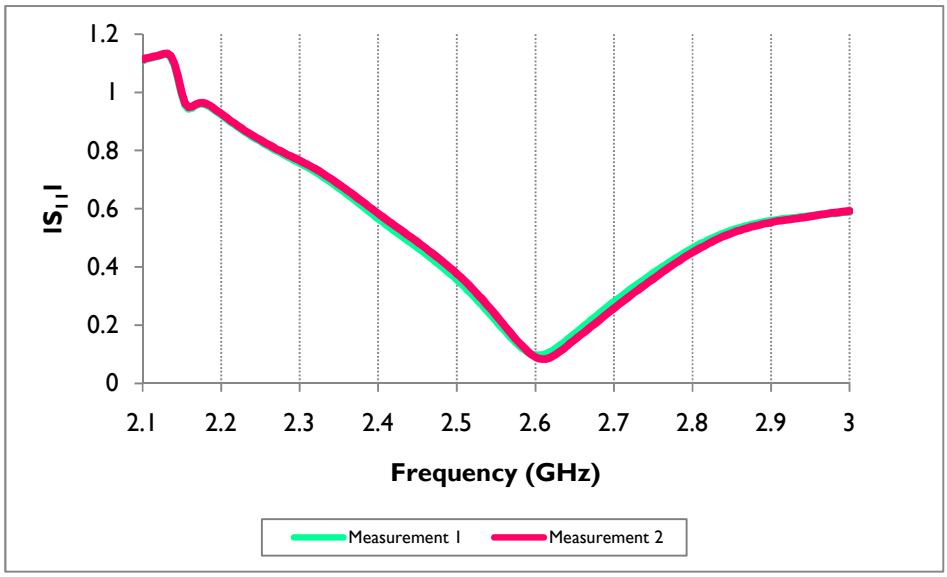

Figure 137: $|S_{11}|$ comparison between measurement 1 and 2 (-4.75+3.35 mm)

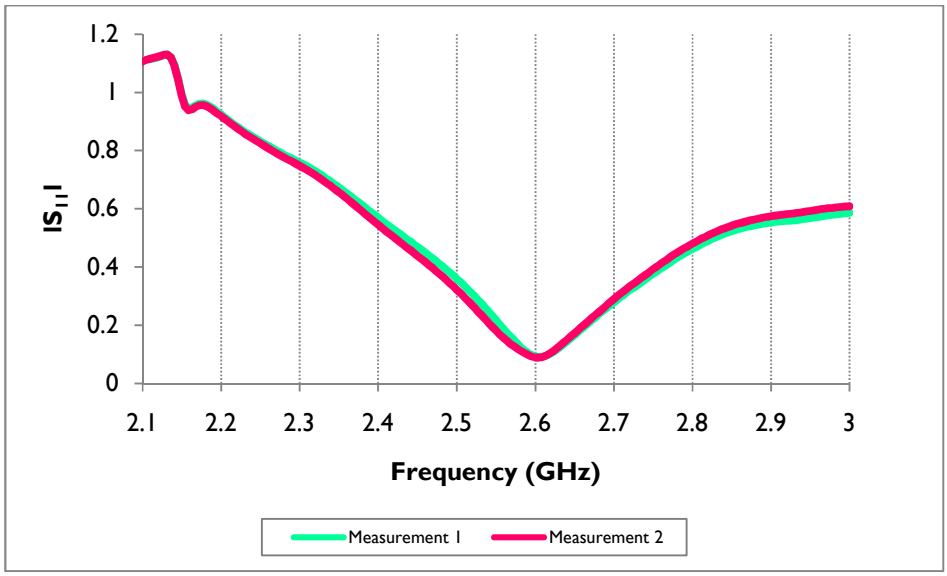

Figure 138: $|S_{11}|$ comparison between measurement 1 and 2 (-3.35+2 mm)

Appendix G

ANA Port Selection

Appendix G presents the ANA port selection (Section 6.10) for each of the dielectric property measurements based on the minimum metric obtained for the extraction of the dielectric properties of air (ε*=1-0j).

WR284

The selected ANA ports for dielectric property extractions in the WR284 sample holder are provided below:

Particle Size (mm)	Measurement 1		Measurement 2	
	Porphyry Copper Ore	Copper Carbonatite	Porphyry Copper Ore	Copper Carbonatite
-26.5+16	Port 2	Port 2	Port 2	Port 2
-16+11.2	Port 2	Port 2	Port 2	Port 2
-11.2+8	Port 1	Port 2	Port 1	Port 2
-8+6.7	Port 1	Port 2	Port 1	Port 2
-6.7+5.6	Port 1	Port 2	Port 1	Port 2
-5.6+4.75	Port 1	Port 2	Port 1	Port 2
-4.75+3.35	Port 1	Port 2	Port 1	Port 2
-3.35+2	Port 1	Port 2	Port 1	Port 2

WR340

The selected ANA ports for dielectric property extractions in the WR340 sample holder are provided below:

Particle Size (mm)	Measurement 1		Measurement 2	
	Porphyry Copper Ore	Copper Carbonatite	Porphyry Copper Ore	Copper Carbonatite
-26.5+16	Port 2		Port 2	
-16+11.2	Port 2		Port 2	
-11.2+8	Port 2		Port 2	
-8+6.7	Port 2		Port 2	
-6.7+5.6	Port 2		Port 2	
-5.6+4.75	Port 2	Port 2	Port 2	Port 2
-4.75+3.35	Port 2	Port 2	Port 2	Port 2
-3.35+2	Port 2	Port 2	Port 2	Port 2

Particle Size (mm)	Measurement 1	Measurement 2
	Quartz Monzonite Porphyry Copper Ore	
-19+16	Port 2	Port 2
-16+13	Port 2	Port 2
-13+9	Port 2	Port 2
-9+6	Port 2	Port 2
-6+4	Port 2	Port 2
-4+3	Port 2	Port 2

Appendix H

Extracted Dielectric Properties

Appendix H presents the dielectric results obtained from the dielectric property extraction using the DBE Algorithm for each of three ores of interest. The results is categorised according to the frequency intervals chosen in the `extract.py` program of the DBE Algorithm. For each of the ores both measurements (1 and 2) is presented

Sample Holder	Crushed Ore		
	Porphyry Copper Ore	**Copper Carbonatite**	**Quartz Monzonite Porphyry Copper Ore**
WR284	Figure 139- Figure 154	Figure 155- Figure 170	
WR340	Figure 171- Figure 186	Figure 187- Figure 192	Figure 193- Figure 204

H1 WR284

Porphyry Copper Ore

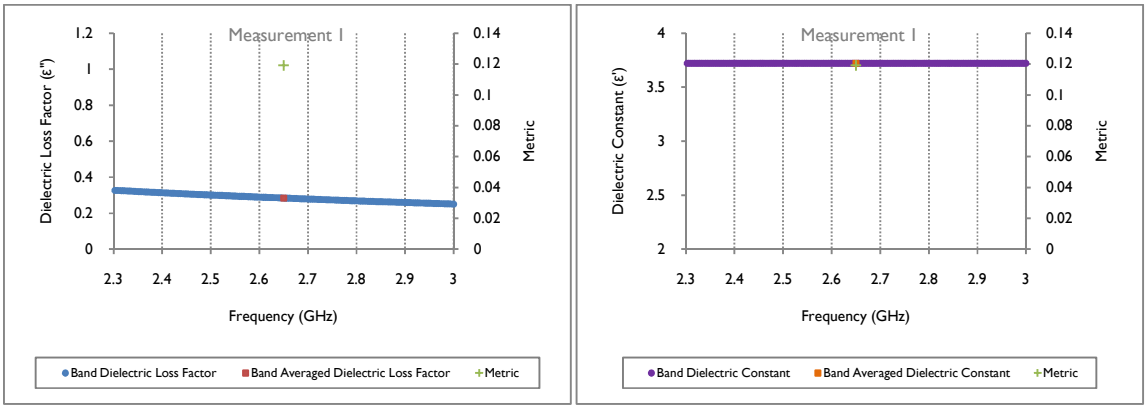

Figure 139: DB extracted ε′ and ε″ (Measurement 1, -26.5+16 mm)

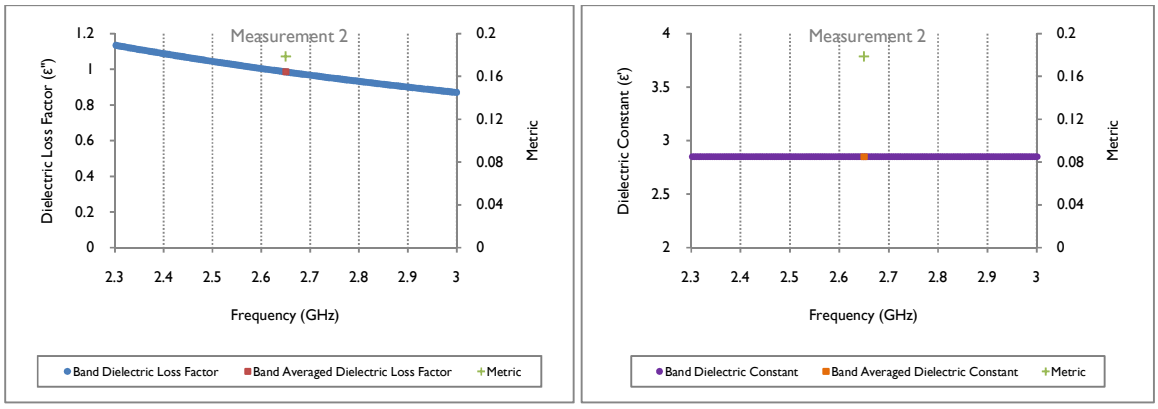

Figure 140: DB extracted ε′ and ε″ (Measurement 2, -26.5+16 mm)

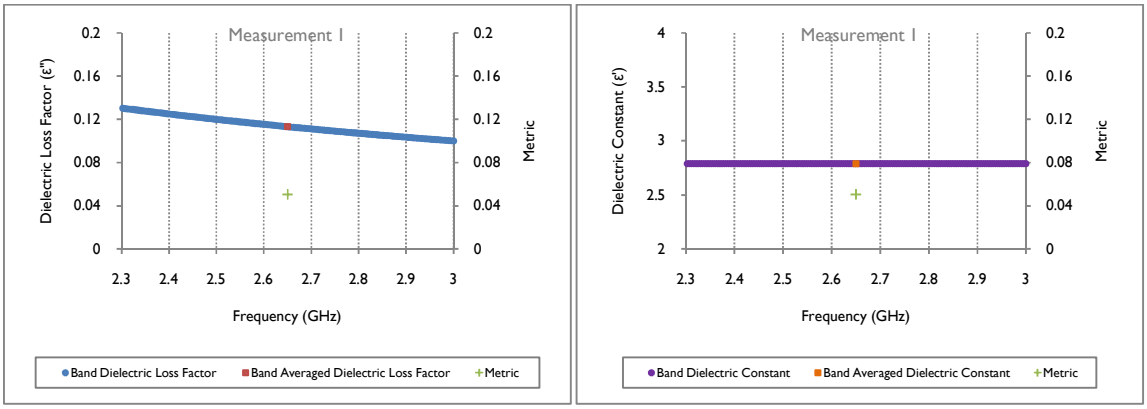

Figure 141: DB extracted ε′ and ε″ (Measurement 1, -16+11.2 mm)

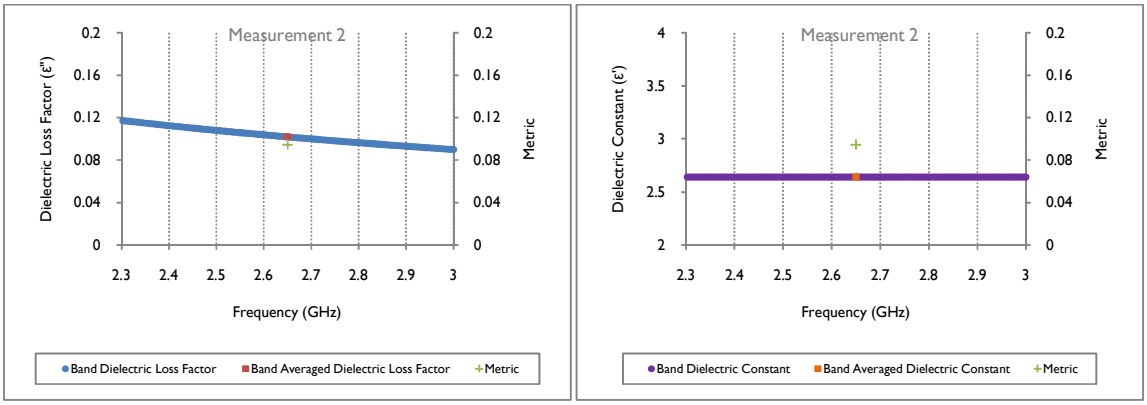

Figure 142: DB extracted ε′ and ε″ (Measurement 2, -16+11.2 mm)

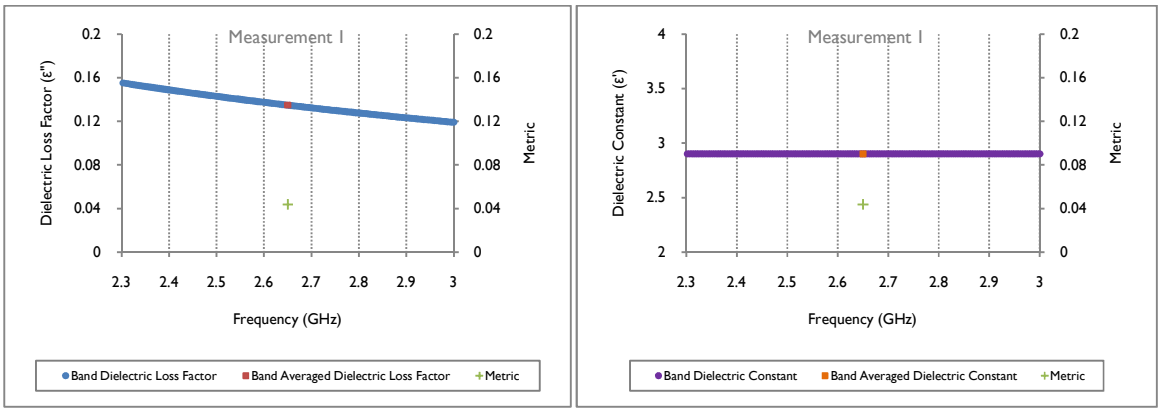

Figure 143: DB extracted ε′ and ε″ (Measurement 1, -11.2+8 mm)

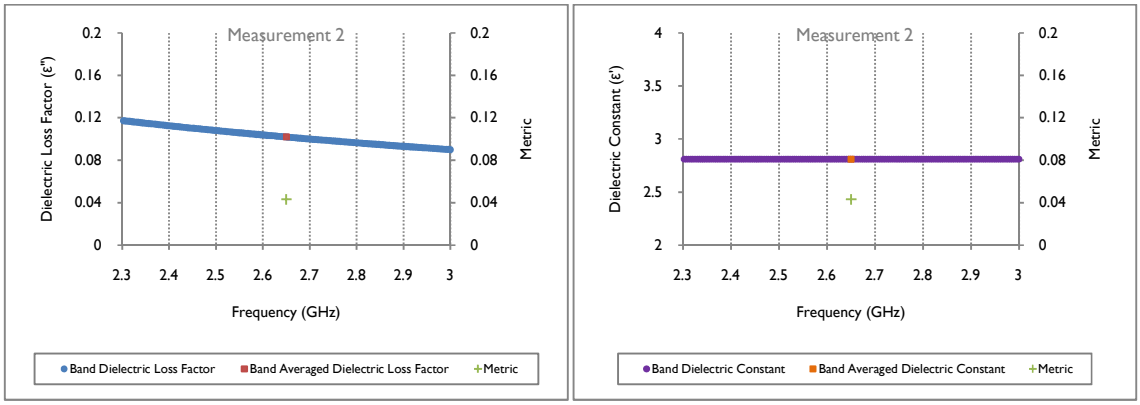

Figure 144: DB extracted ε′ and ε″ (Measurement 2, -11.2+8 mm)

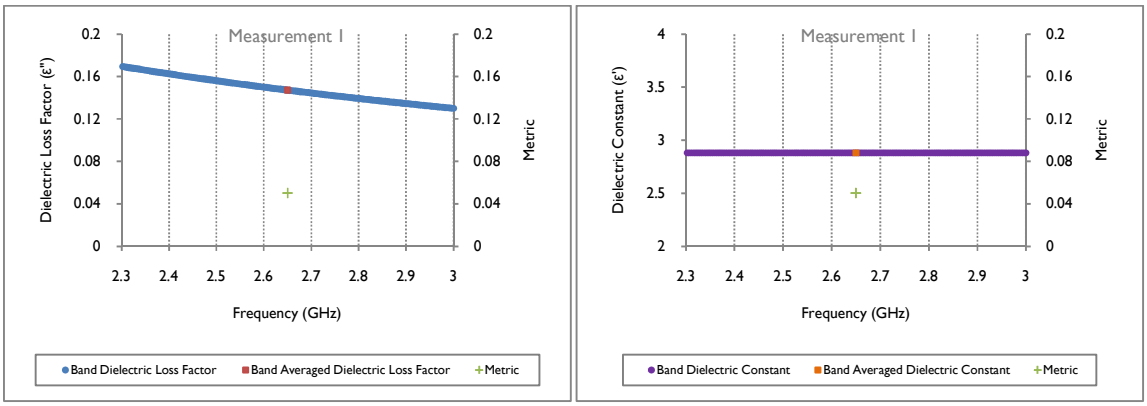

Figure 145: DB extracted ε′ and ε″ (Measurement 1, -8+6.7 mm)

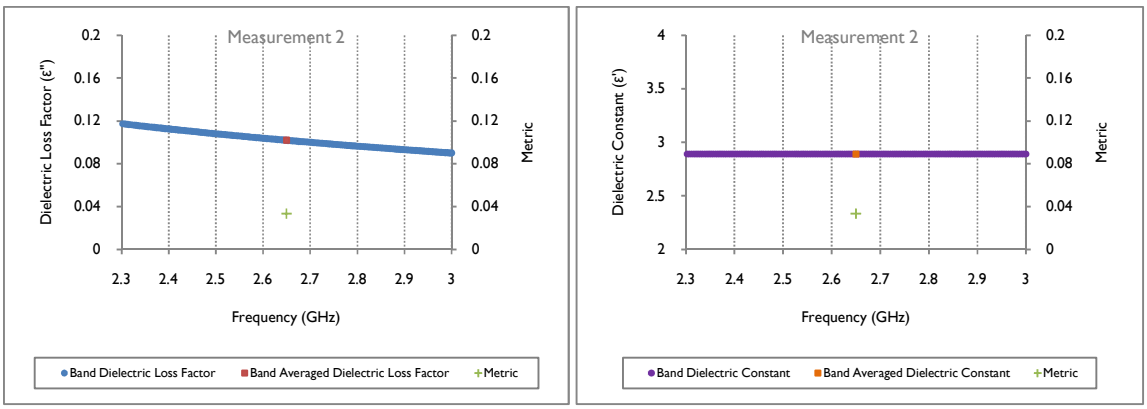

Figure 146: DB extracted ε′ and ε″ (Measurement 2, -8+6.7 mm)

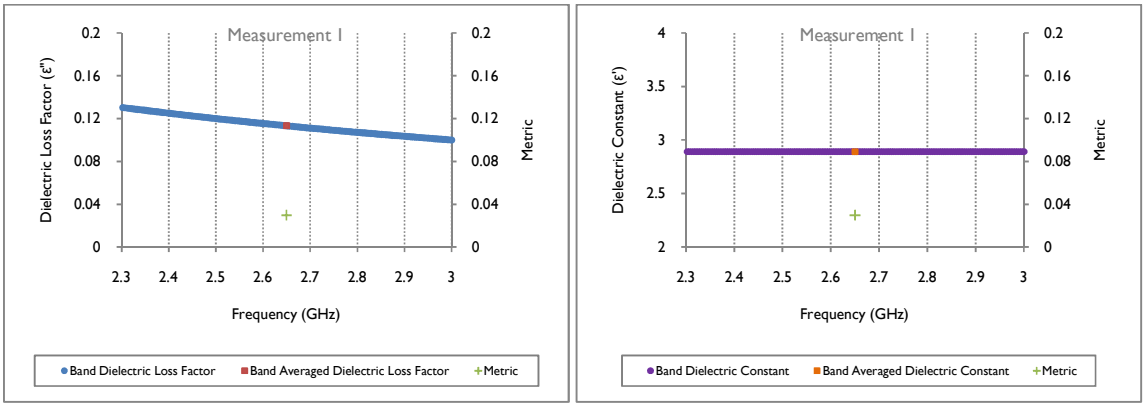

Figure 147: DB extracted ε′ and ε″ (Measurement 1, -6.7+5.6 mm)

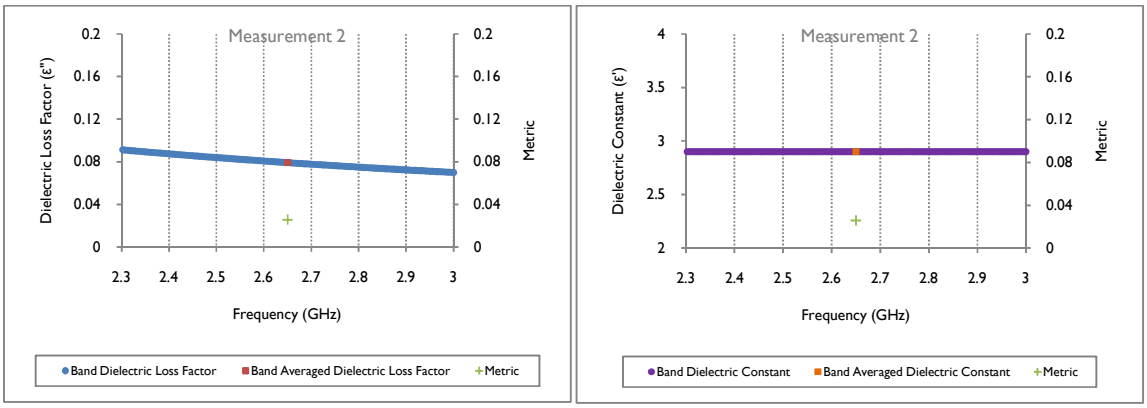

Figure 148: DB extracted ε′ and ε″ (Measurement 2, -6.7+5.6 mm)

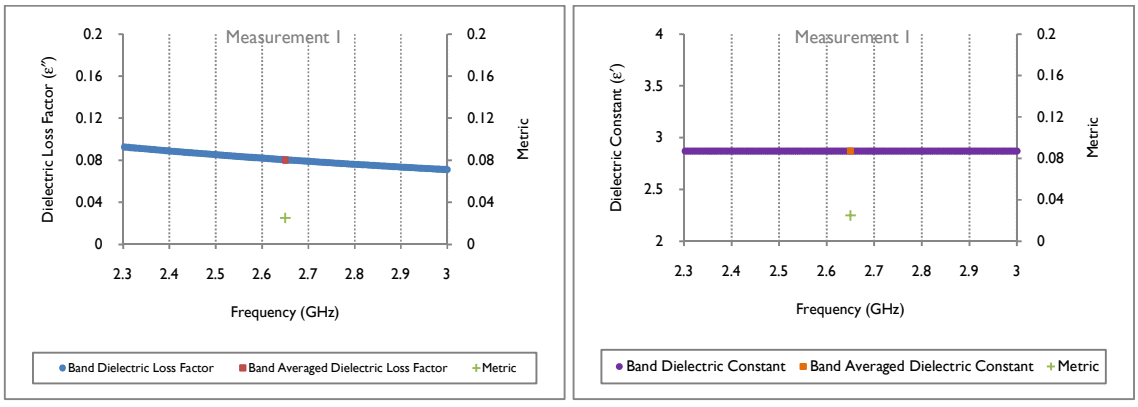

Figure 149: DB extracted ε′ and ε″ (Measurement 1, -5.6+4.75 mm)

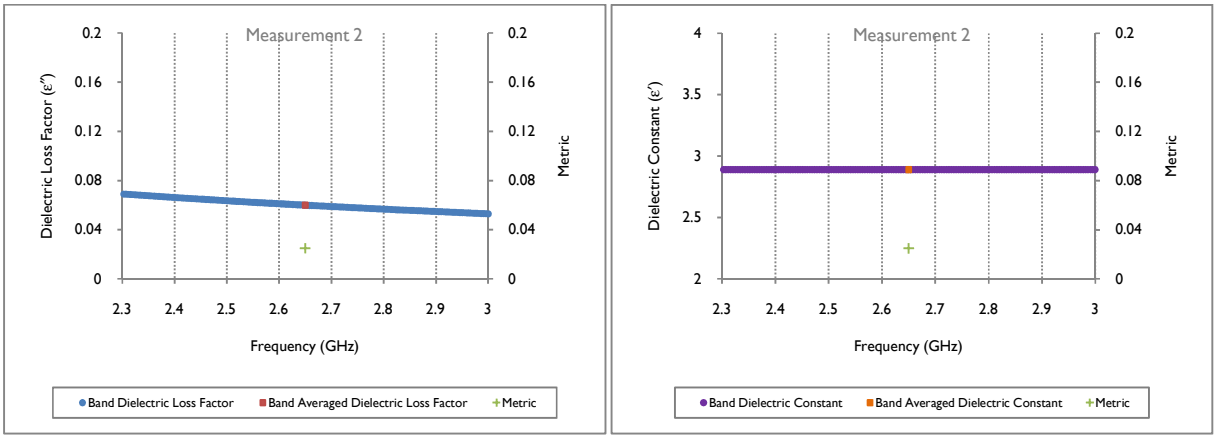

Figure 150: DB extracted ε′ and ε″ (Measurement 2, -5.6+4.75 mm)

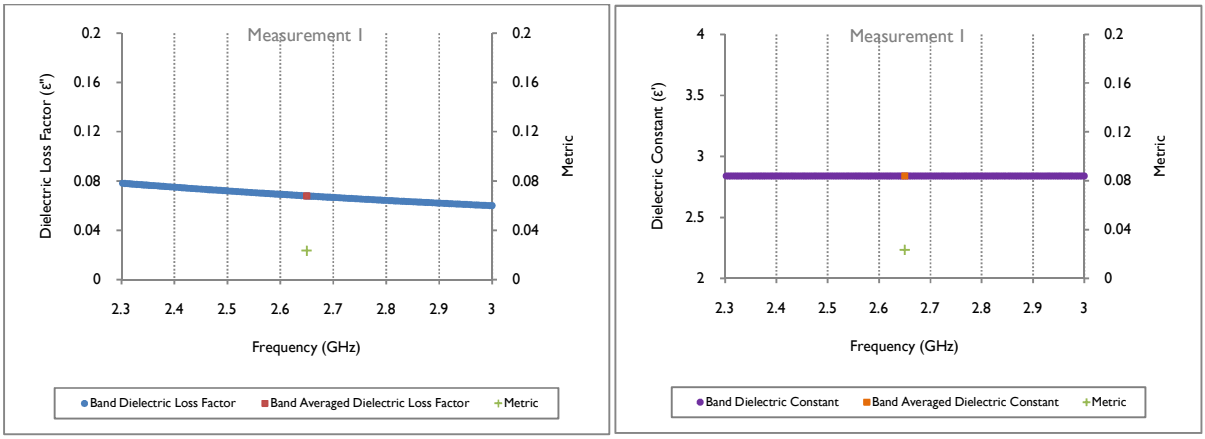

Figure 151: DB extracted ε′ and ε″ (Measurement 1, -4.75+3.35 mm)

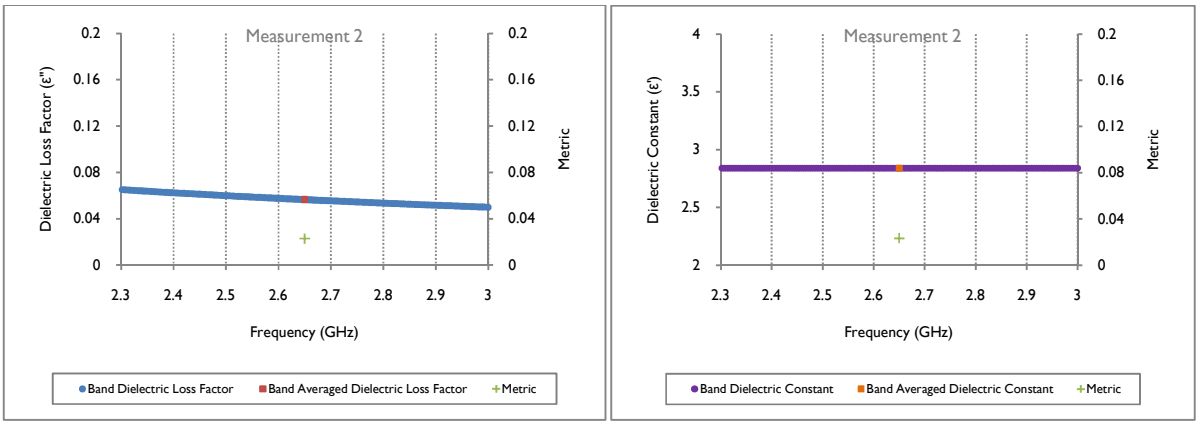

Figure 152: DB extracted ε′ and ε″ (Measurement 2, -4.75+3.35 mm)

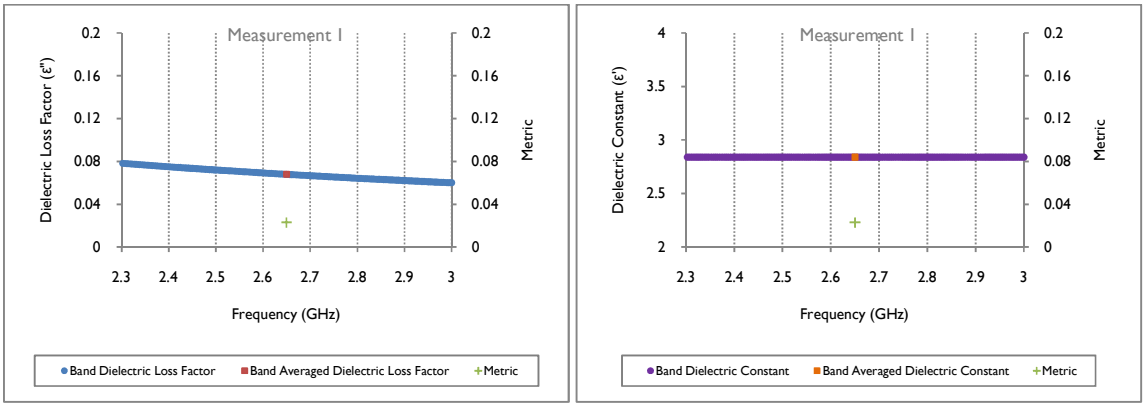

Figure 153: DB extracted ε′ and ε″ (Measurement 1, -3.35+2 mm)

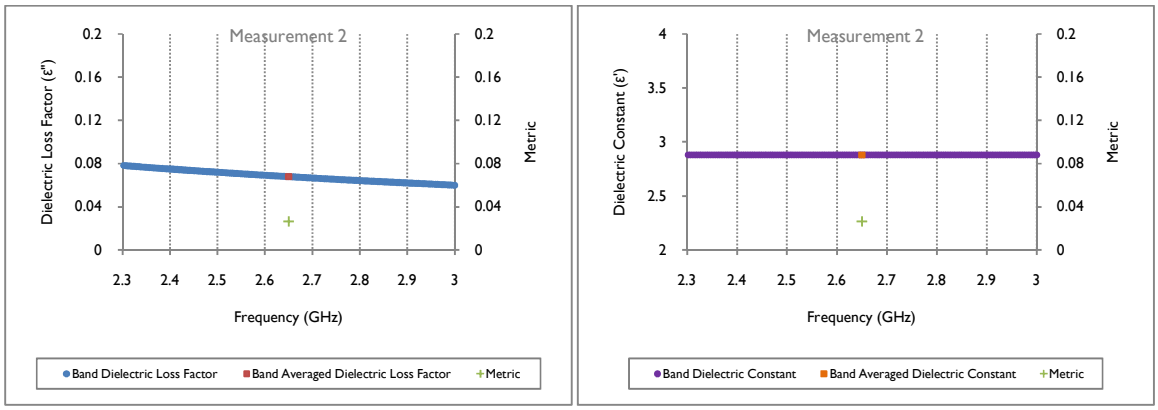

Figure 154: DB extracted ε′ and ε″ (Measurement 2, -3.35+2 mm)

Copper Carbonatite Ore

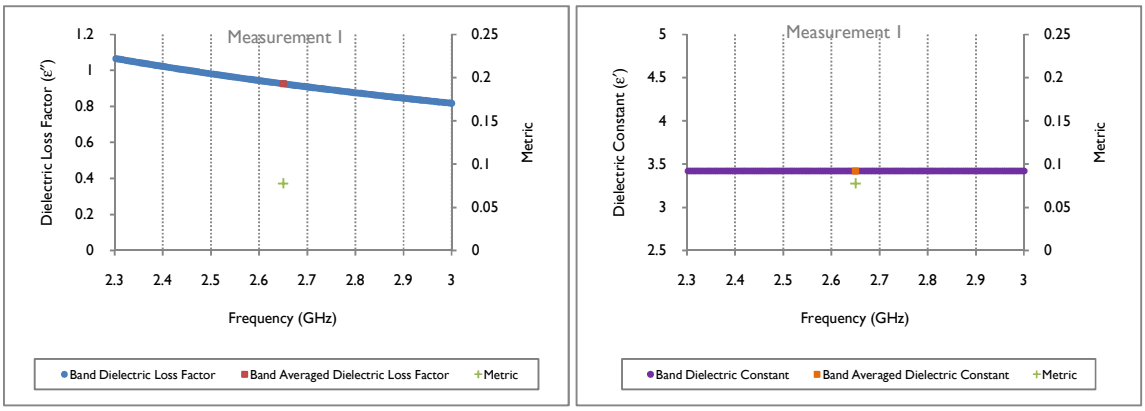

Figure 155: DB extracted ε′ and ε″ (Measurement 1, -26.5+16 mm)

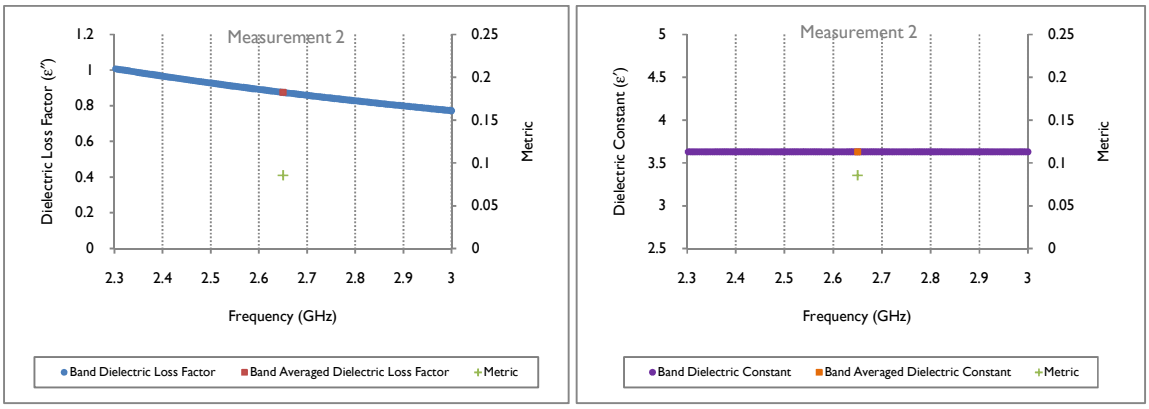

Figure 156: DB extracted ε′ and ε″ (Measurement 2, -26.5+16 mm)

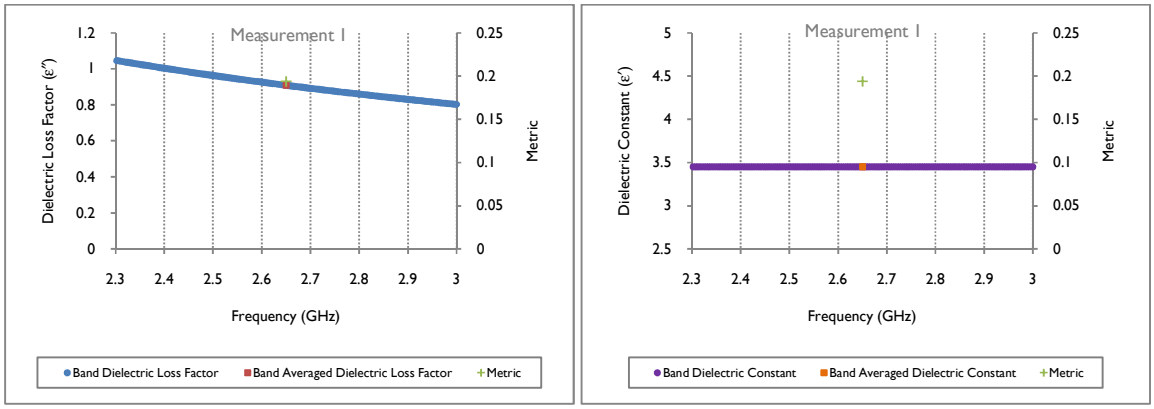

Figure 157: Extracted Dielectric Constant and Loss Factor (Measurement 1, -16+11.2 mm)

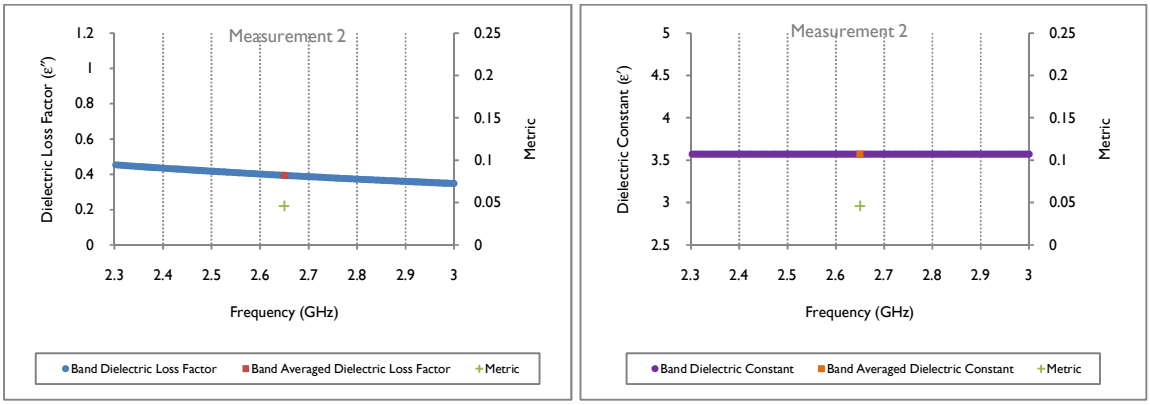

Figure 158: DB extracted ε′ and ε″ (Measurement 2, -16+11.2 mm)

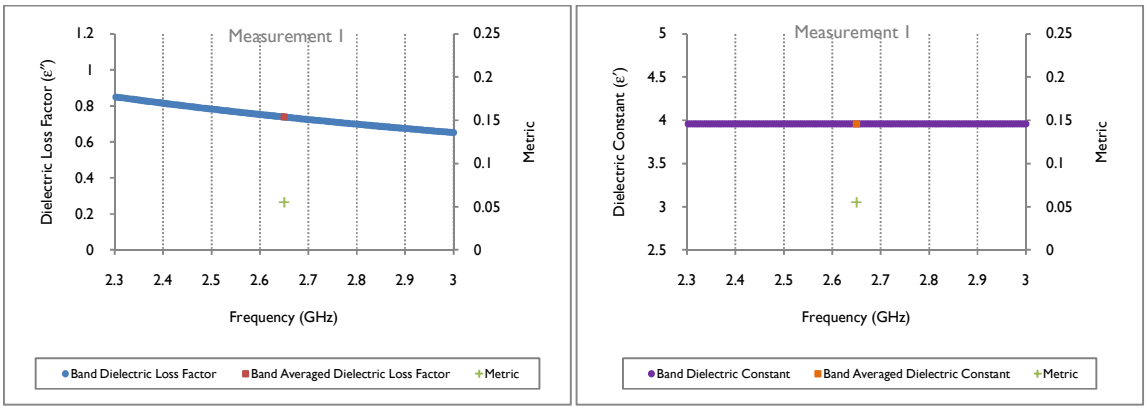

Figure 159: DB extracted ε′ and ε″ (Measurement 1, -11.2+8 mm)

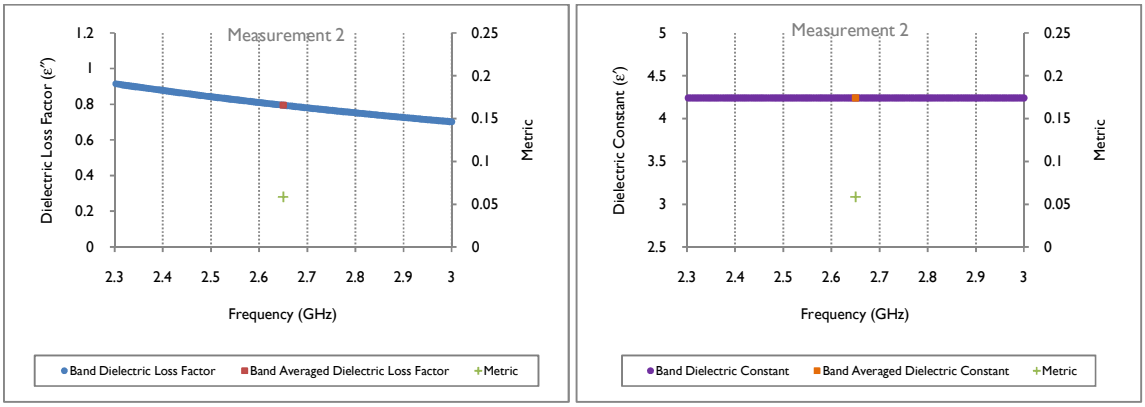

Figure 160: DB extracted ε′ and ε″ (Measurement 2, -11.2+8 mm)

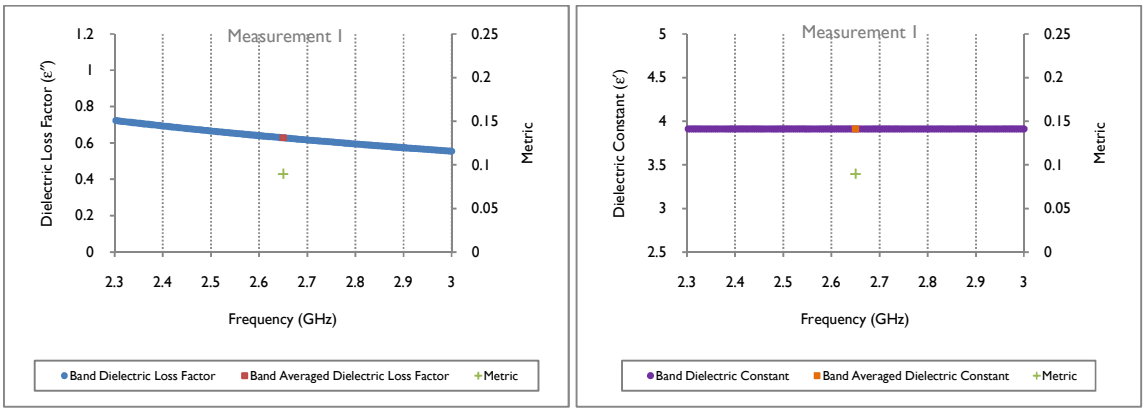

Figure 161: DB extracted ε′ and ε″ (Measurement 1, -8+6.7 mm)

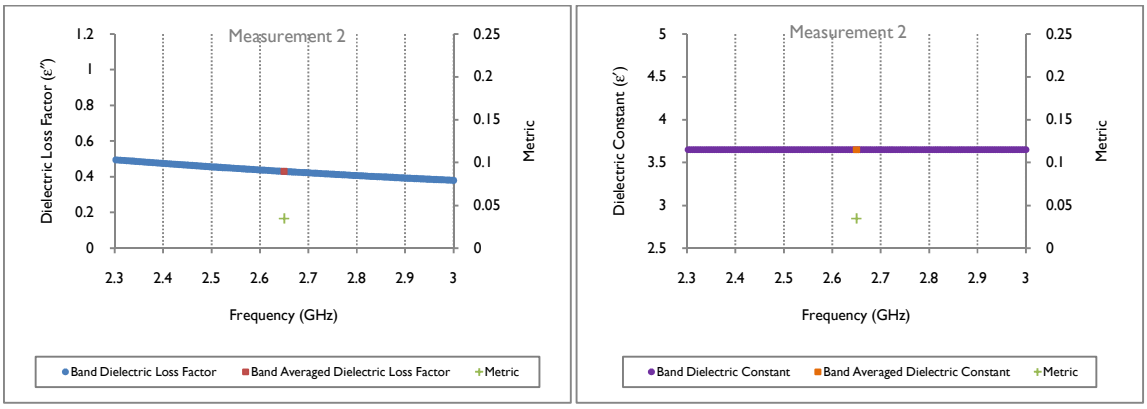

Figure 162: DB extracted ε′ and ε″ (Measurement 2, -8+6.7 mm)

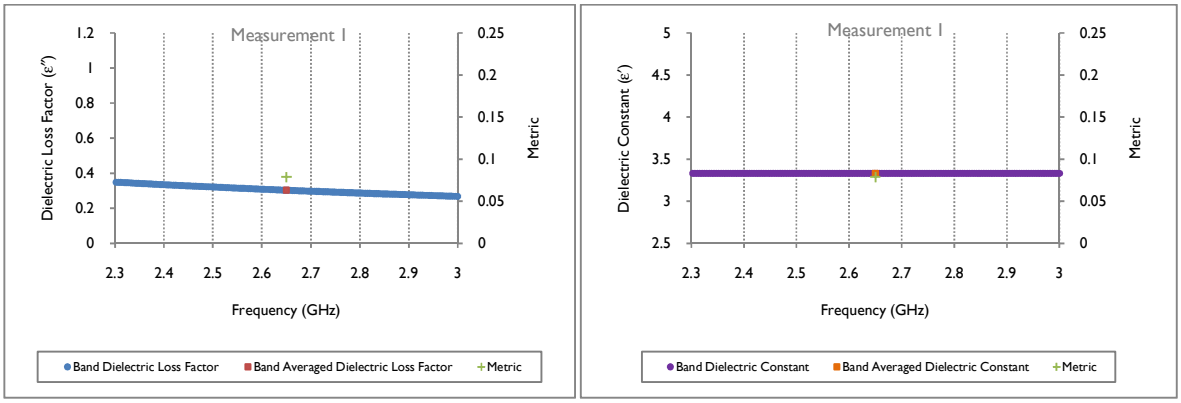

Figure 163: DB extracted ε′ and ε″ (Measurement 1, -6.7+5.6 mm)

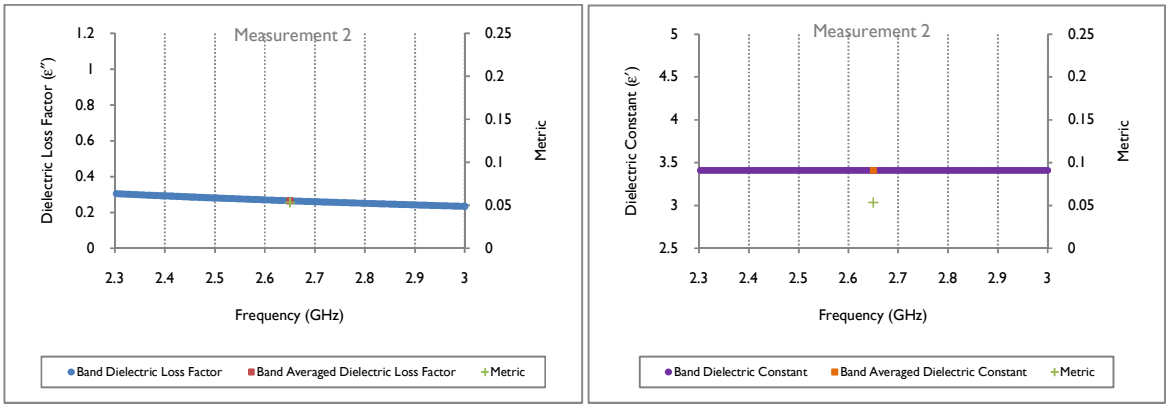

Figure 164: DB extracted ε′ and ε″ (Measurement 2, -6.7+5.6 mm)

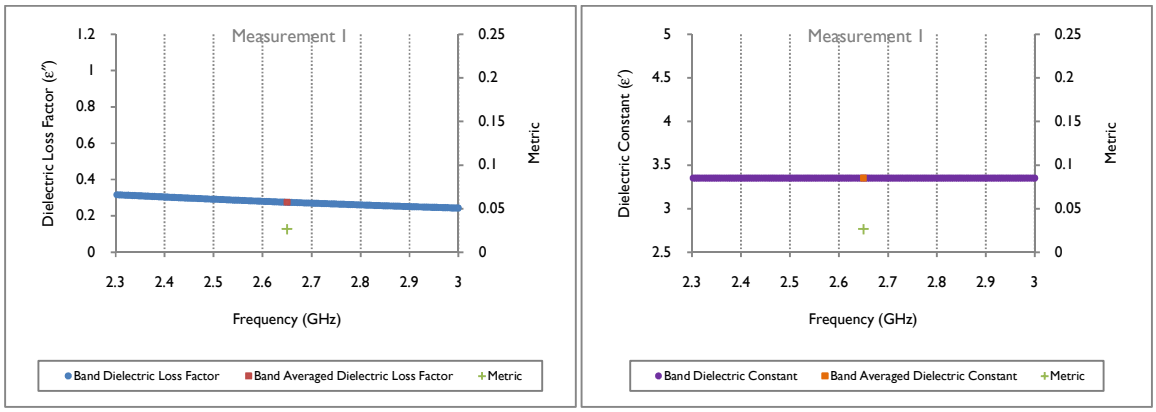

Figure 165: DB extracted ε′ and ε″ (Measurement 1, -5.6+4.75 mm)

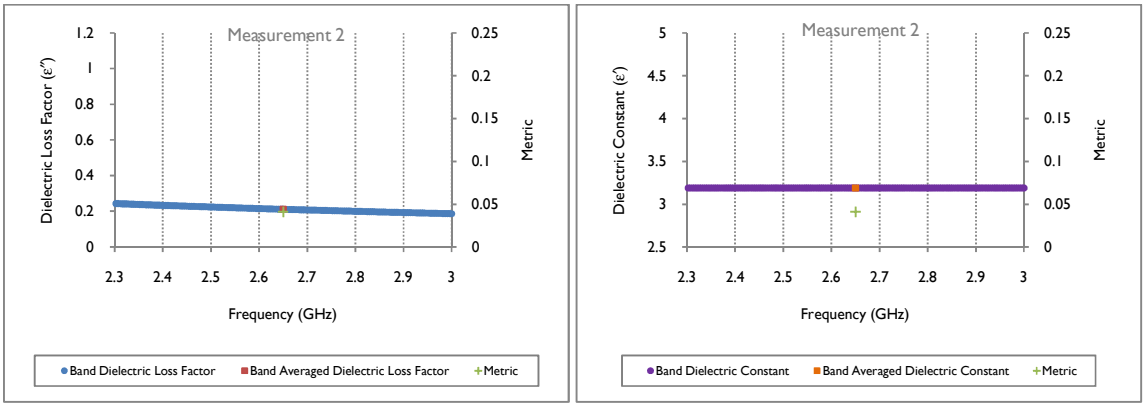

Figure 166: DB extracted ε′ and ε″ (Measurement 2, -5.6+4.75 mm)

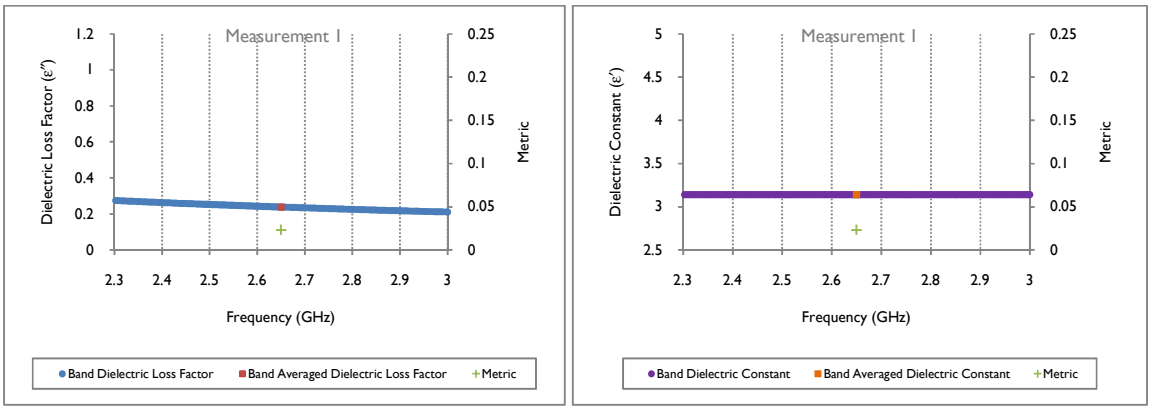

Figure 167: DB extracted ε′ and ε″ (Measurement 1, -4.75+3.35 mm)

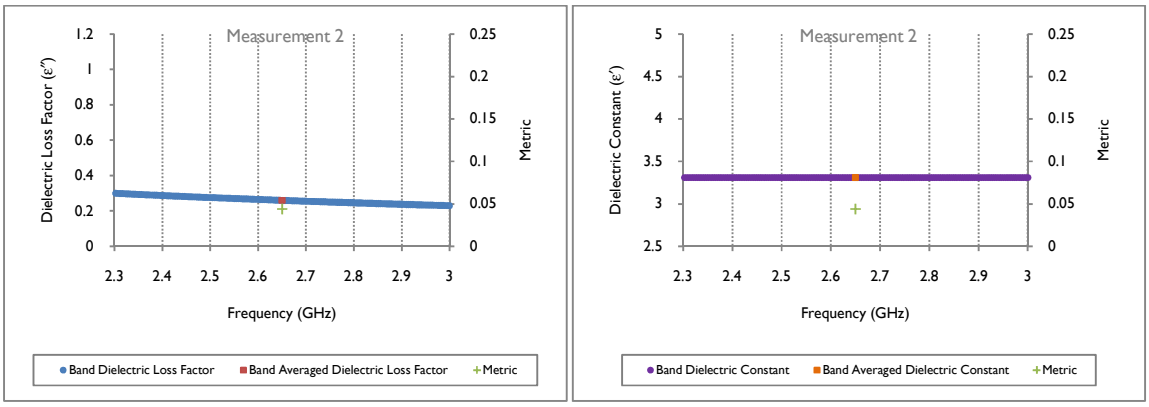

Figure 168: DB extracted ε′ and ε″ (Measurement 2, -4.75+3.35 mm)

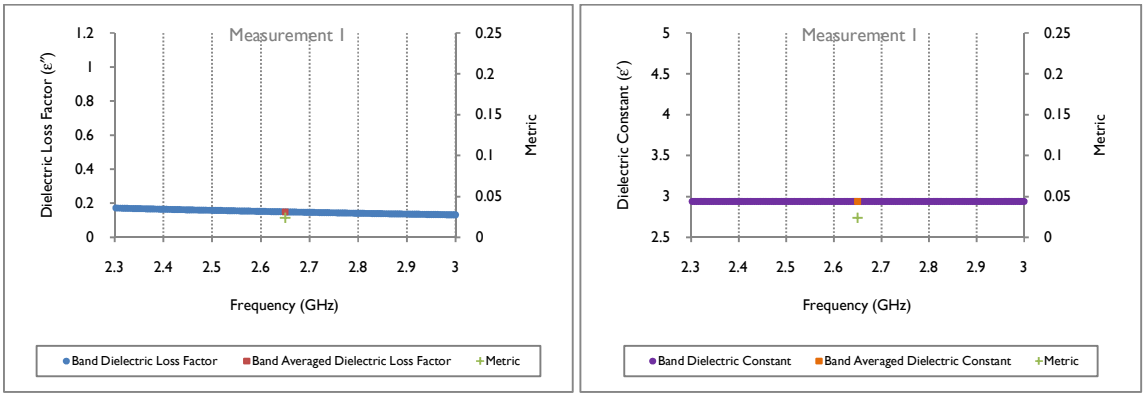

Figure 169: DB extracted ε′ and ε″ (Measurement 1, -3.35+2 mm)

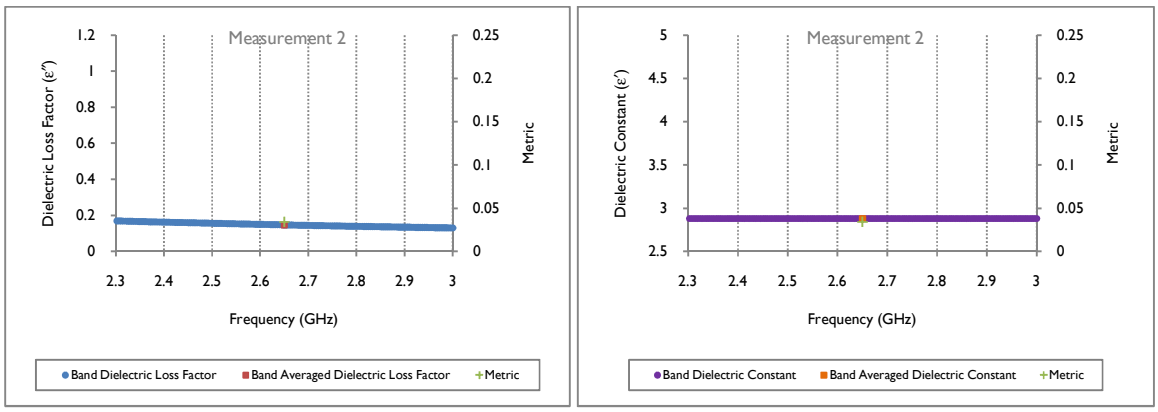

Figure 170: DB extracted ε′ and ε″ (Measurement 2, -3.35+2 mm)

H2 WR340

Porphyry Copper Ore

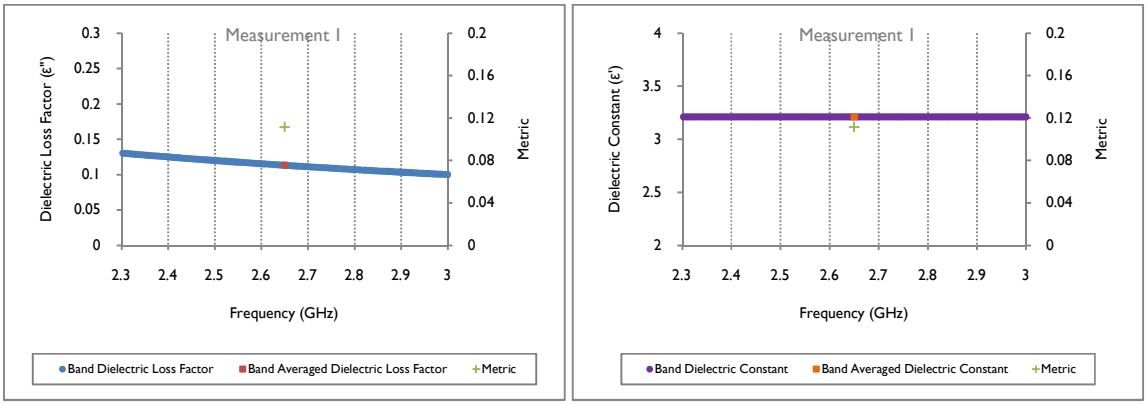

Figure 171: DB extracted ε′ and ε″ (Measurement 1, -26.5+16 mm)

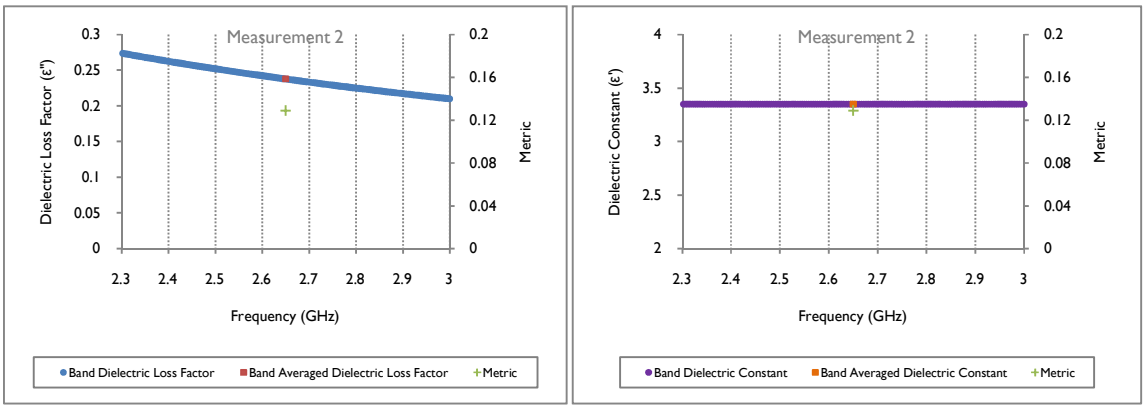

Figure 172: DB extracted ε′ and ε″ (Measurement 2, -26.5+16 mm)

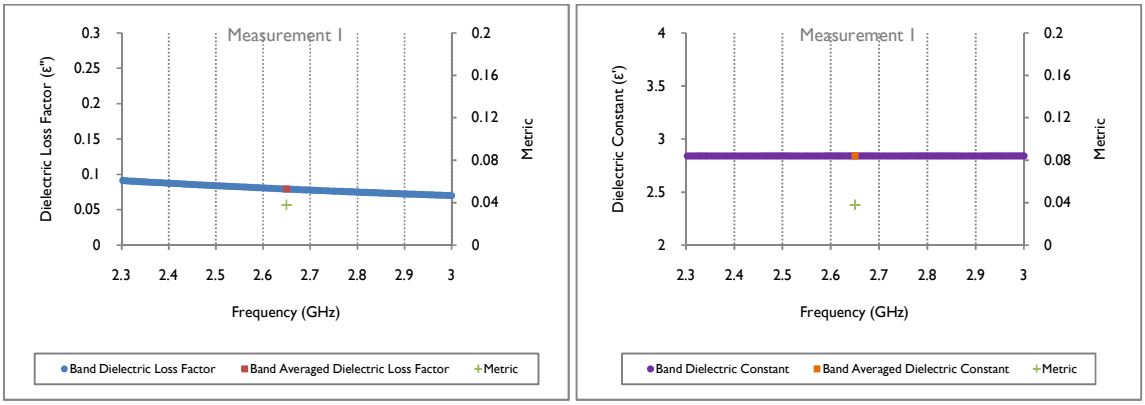

Figure 173: DB extracted ε′ and ε″ (Measurement 1, -16+11.2 mm)

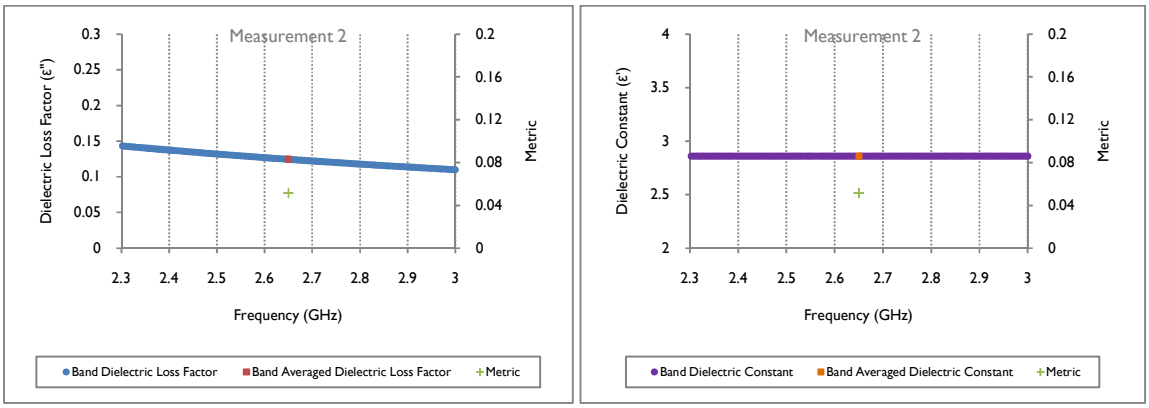

Figure 174: DB extracted ε′ and ε″ (Measurement 2, -16+11.2 mm)

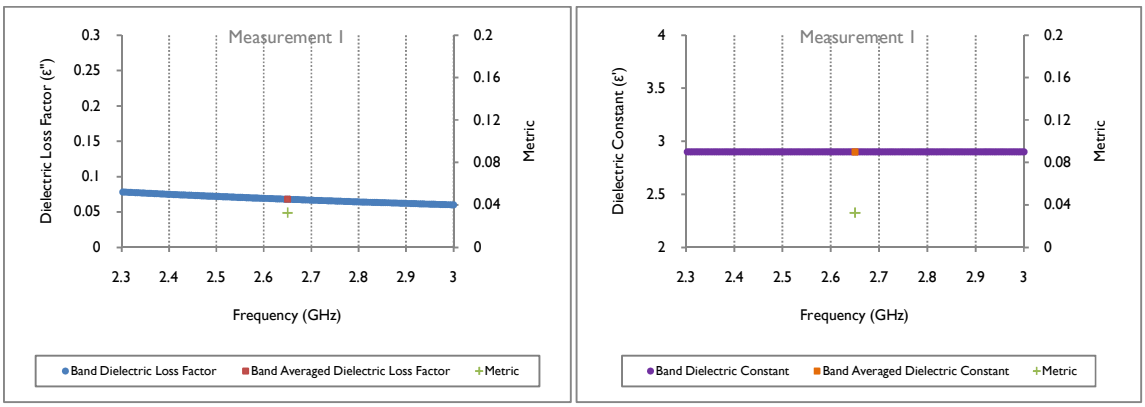

Figure 175: DB extracted ε′ and ε″ (Measurement 1, -11.2+8 mm)

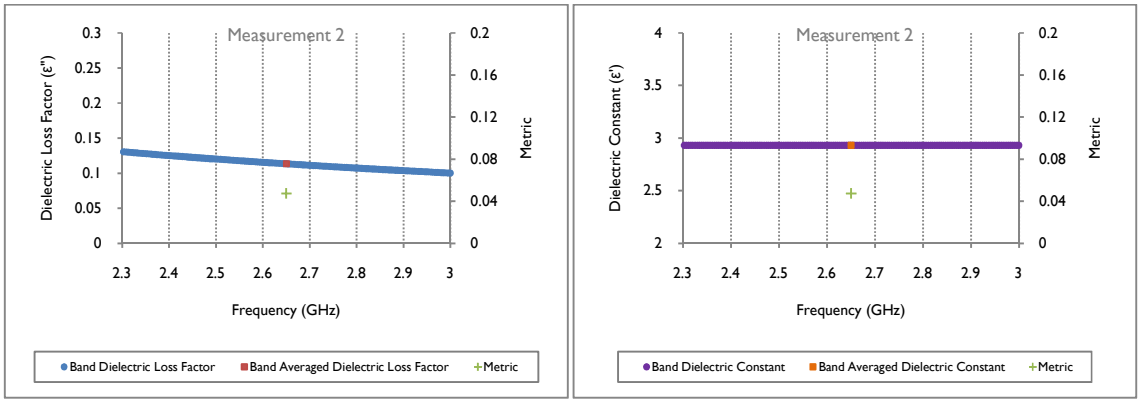

Figure 176: DB extracted ε′ and ε″ (Measurement 2, -11.2+8 mm)

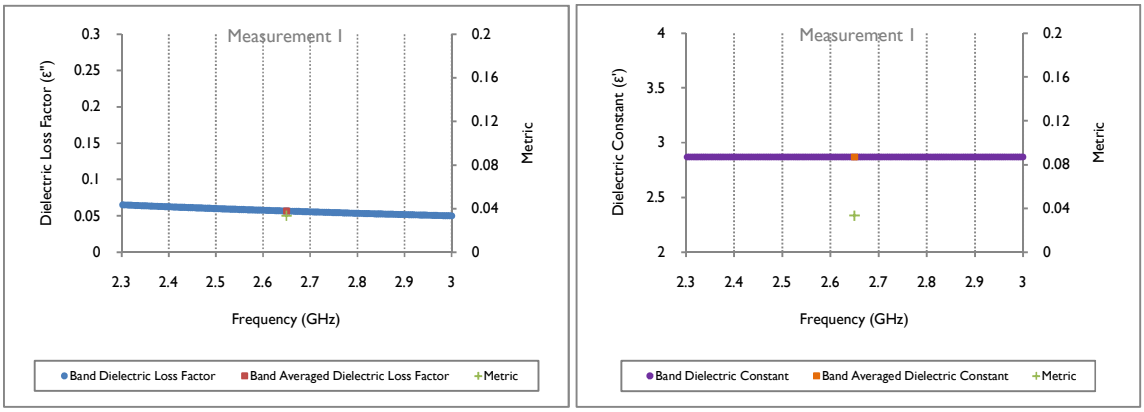

Figure 177: DB extracted ε′ and ε″ (Measurement 1, -8+6.7 mm)

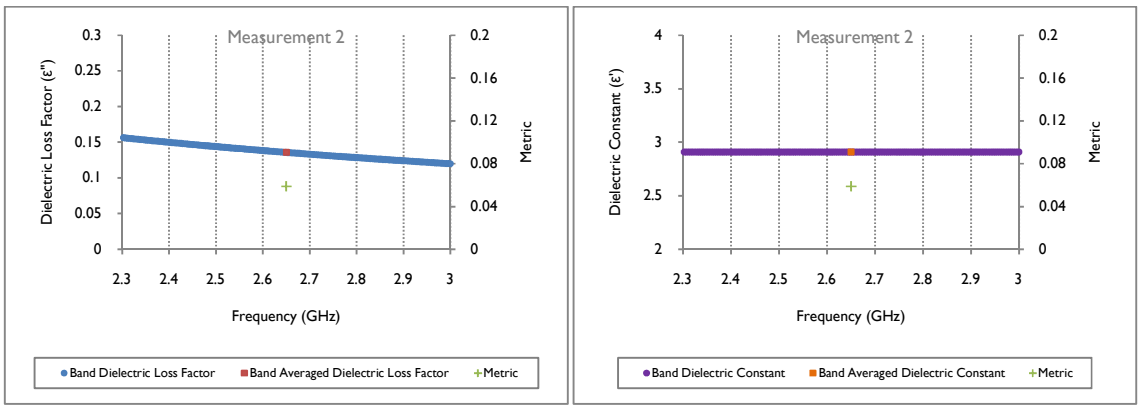

Figure 178: DB extracted ε′ and ε″ (Measurement 2, -8+6.7 mm)

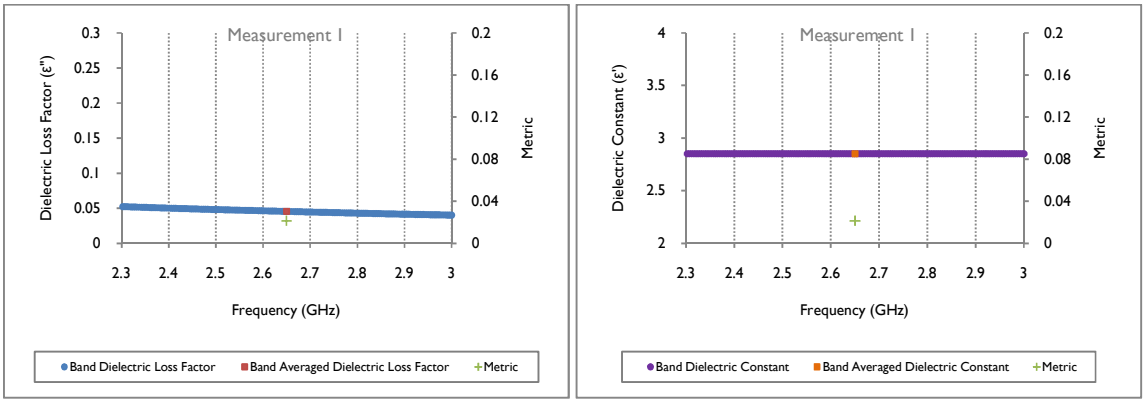

Figure 179: DB extracted ε′ and ε″ (Measurement 1, -6.7+5.6 mm)

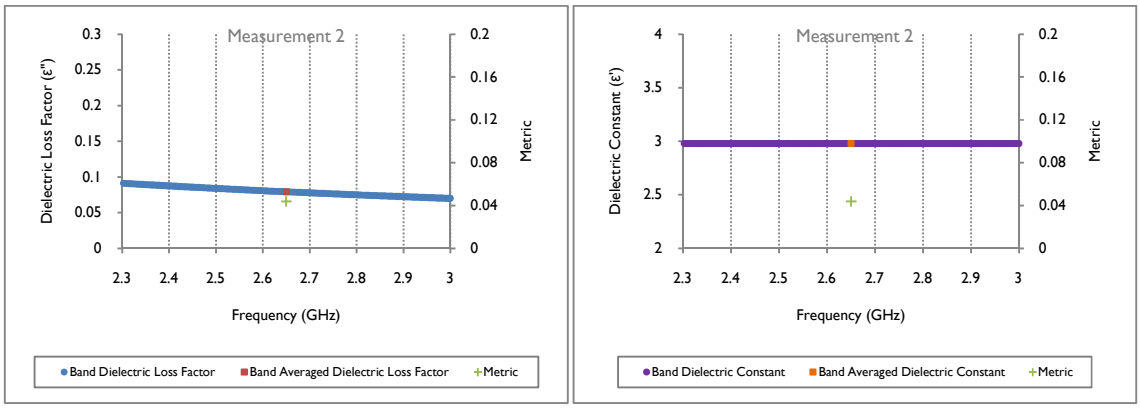

Figure 180: DB extracted ε′ and ε″ (Measurement 2, -6.7+5.6 mm)

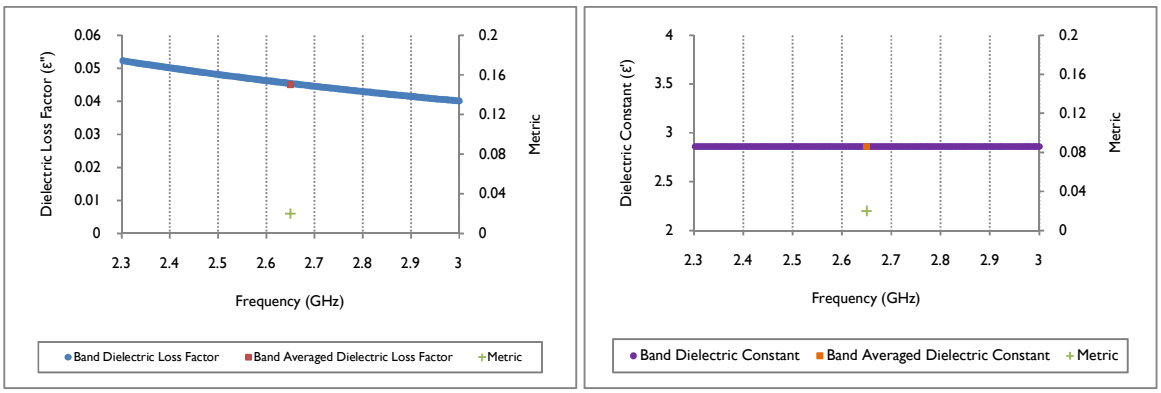

Figure 181: DB extracted ε′ and ε″ (Measurement 1, -5.6+4.75 mm)

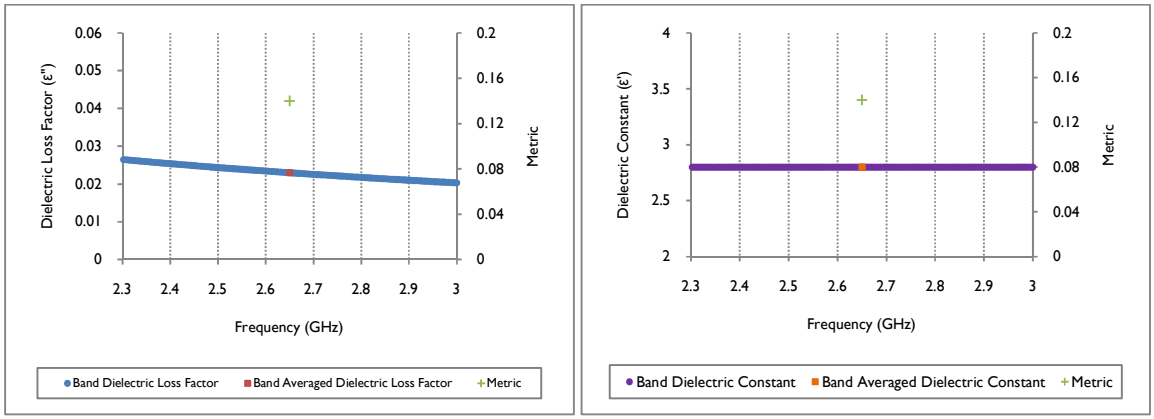

Figure 182: DB extracted ε′ and ε″ (Measurement 2, -5.6+4.75 mm)

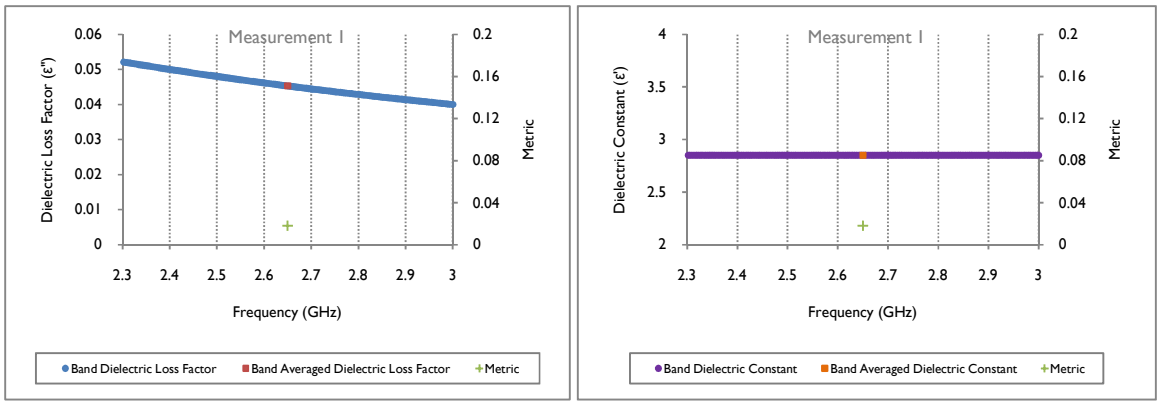

Figure 183: DB extracted ε′ and ε″ (Measurement 1, -4.75+3.35 mm)

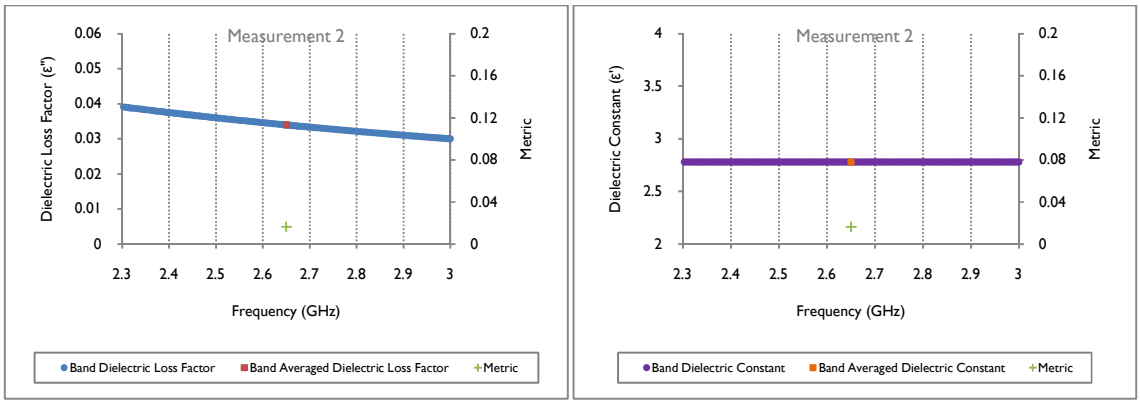

Figure 184: DB extracted ε′ and ε″ (Measurement 2, -4.75+3.35 mm)

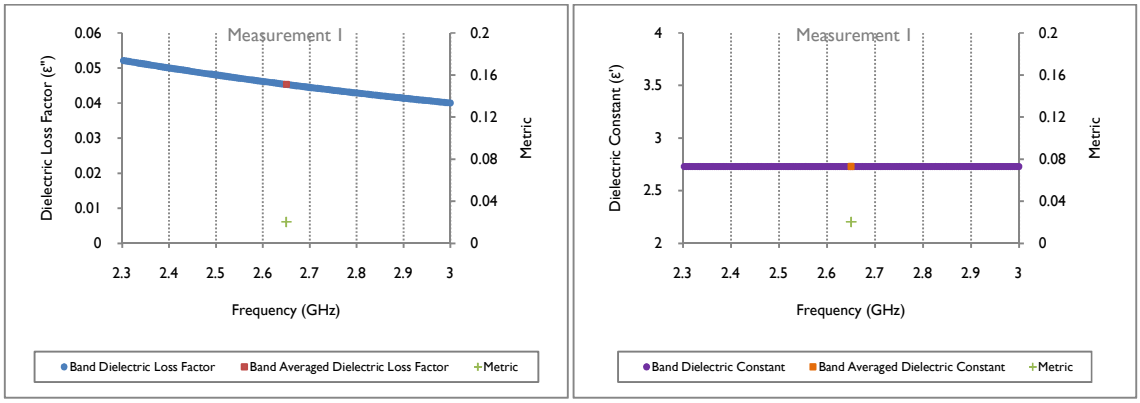

Figure 185: DB extracted ε′ and ε″ (Measurement 1, -3.35+2 mm)

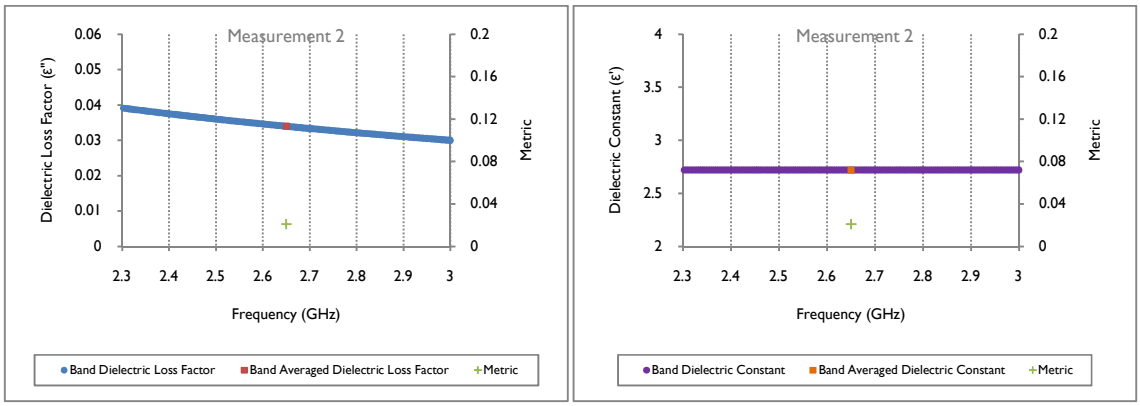

Figure 186: DB extracted ε′ and ε″ (Measurement 2, -3.35+2 mm)

Copper Carbonatite Ore

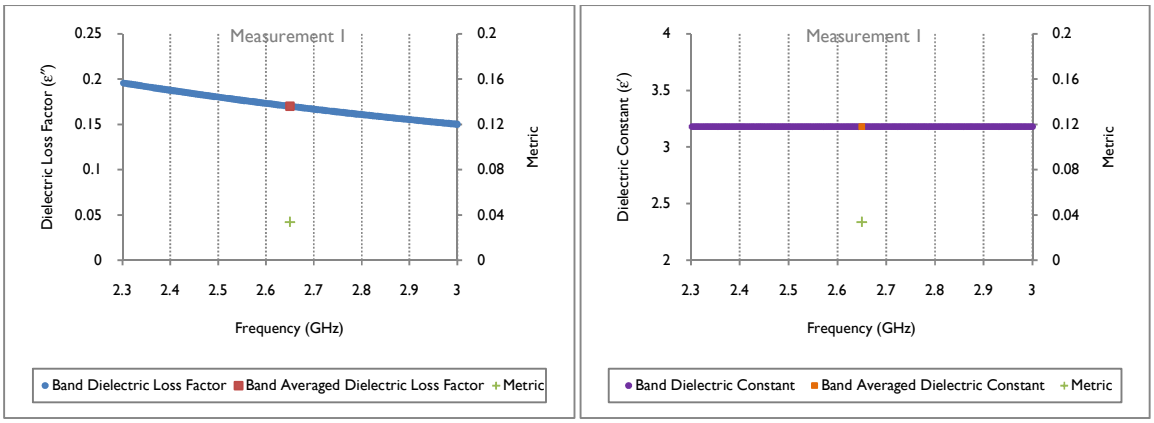

Figure 187: DB extracted ε′ and ε″ (Measurement 1, -5.6+4.75 mm)

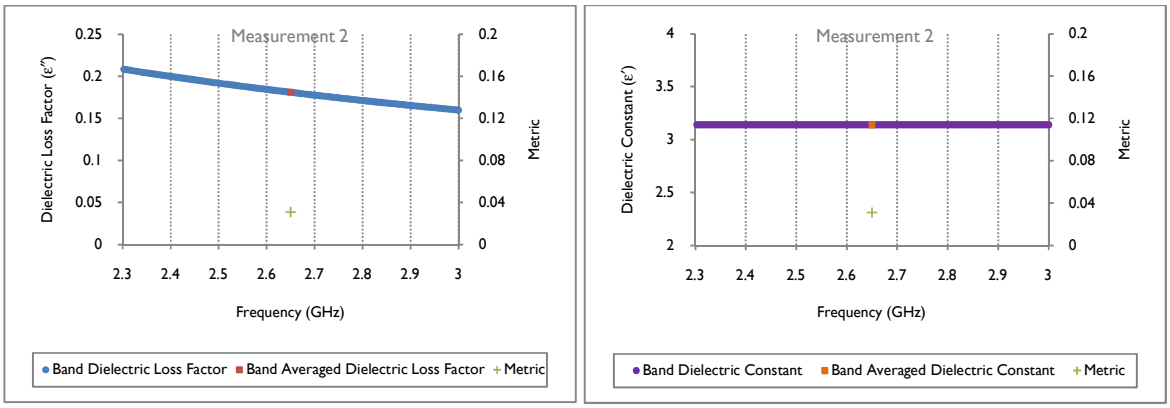

Figure 188: DB extracted ε′ and ε″ (Measurement 2, -5.6+4.75 mm)

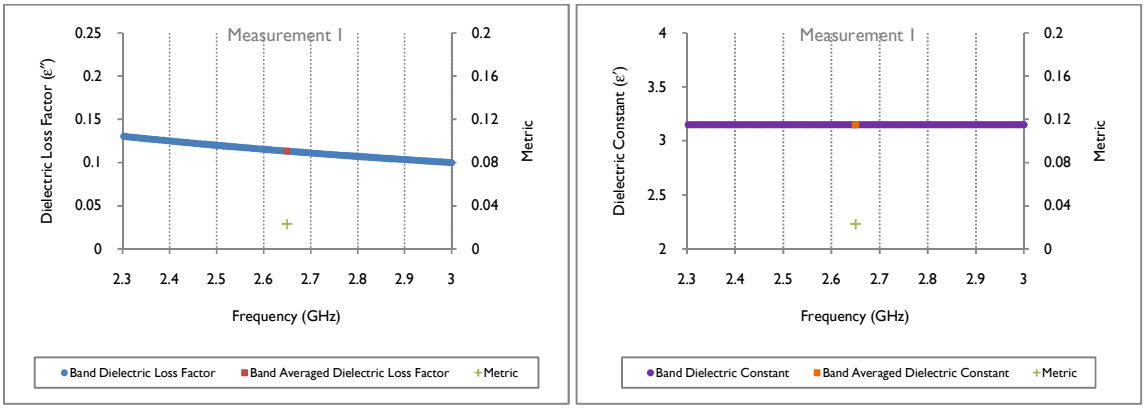

Figure 189: DB extracted ε′ and ε″ (Measurement 1, -4.75+3.35 mm)

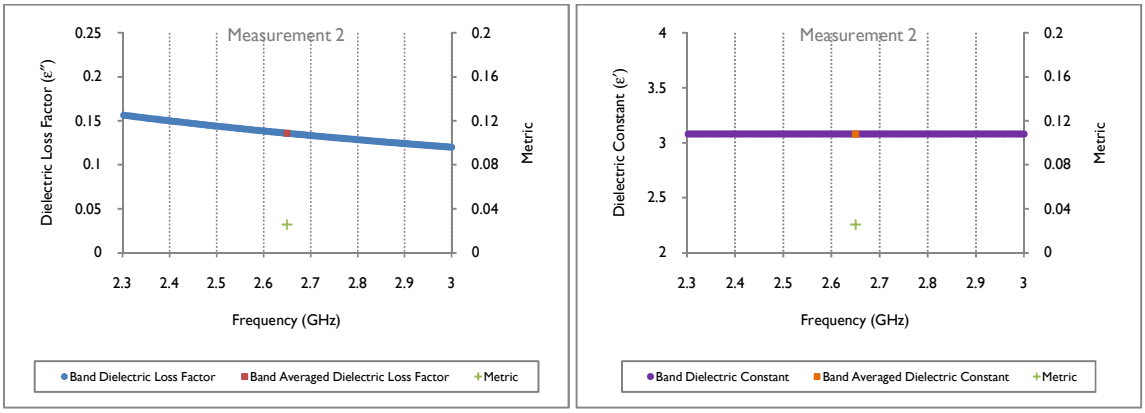

Figure 190: DB extracted ε′ and ε″ (Measurement 2, -4.75+3.35 mm)

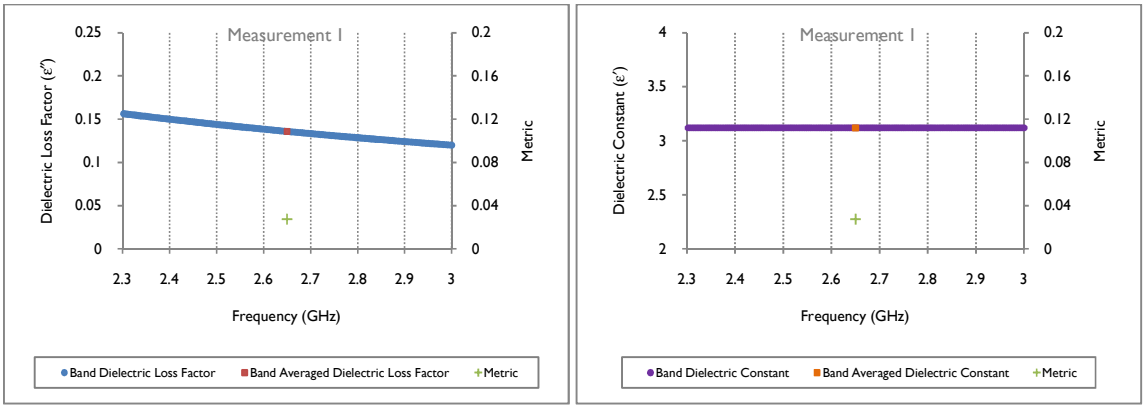

Figure 191: DB extracted ε′ and ε″ (Measurement 1, -3.35+2 mm)

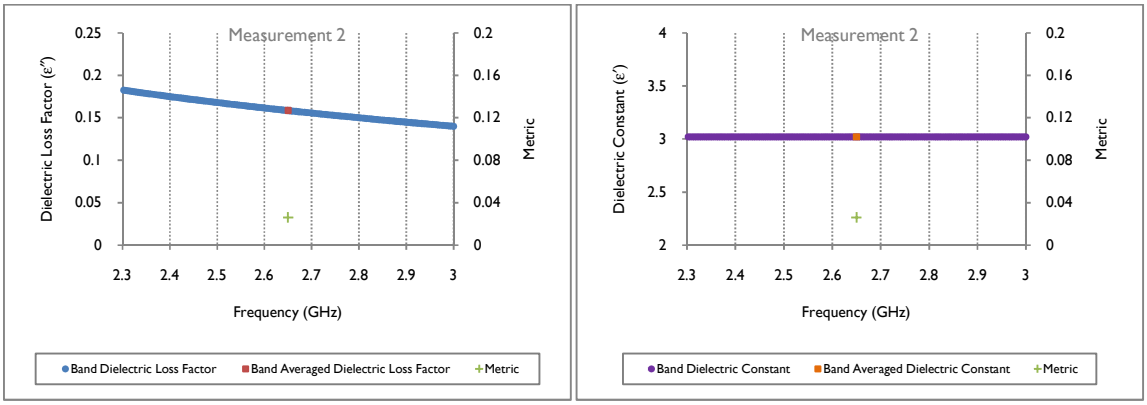

Figure 192: DB extracted ε′ and ε″ (Measurement 2, -3.35+2 mm)

Quartz Monzonite Porphyry Copper Ore

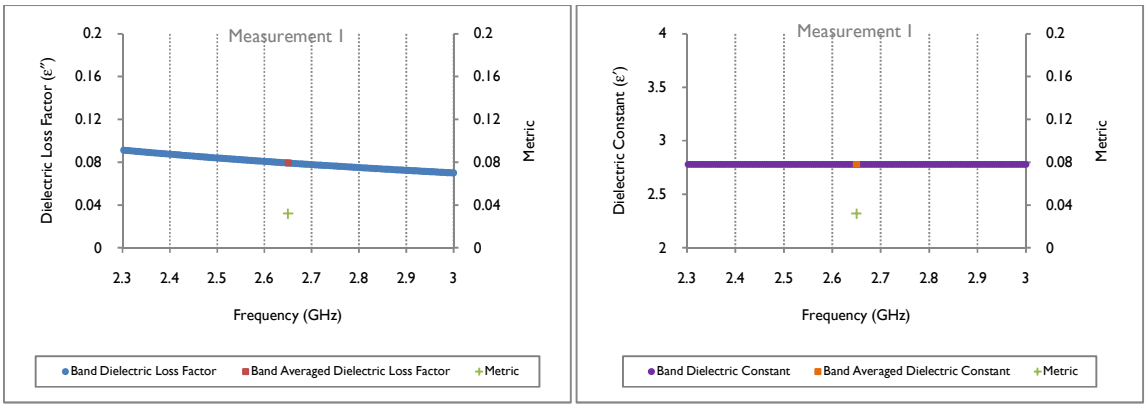

Figure 193: DB extracted ε′ and ε″ (Measurement 1, -19+16 mm)

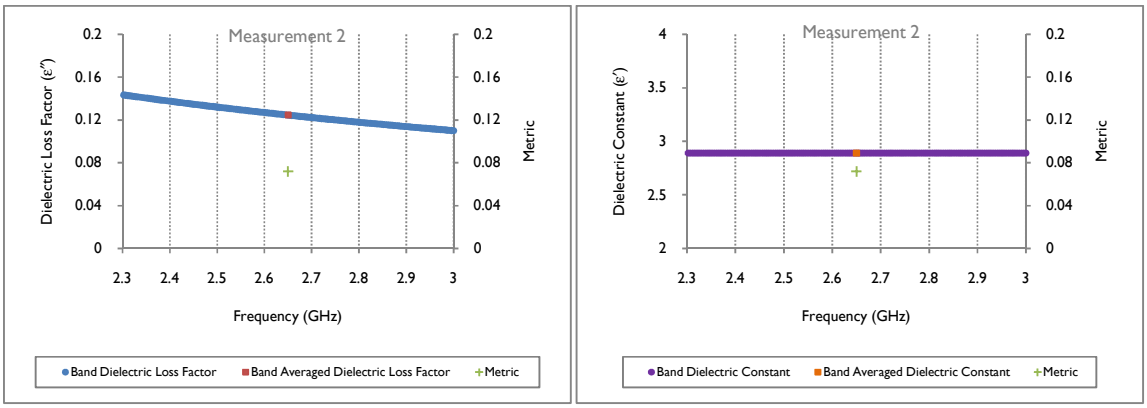

Figure 194: DB extracted ε′ and ε″ (Measurement 2, -19+16 mm)

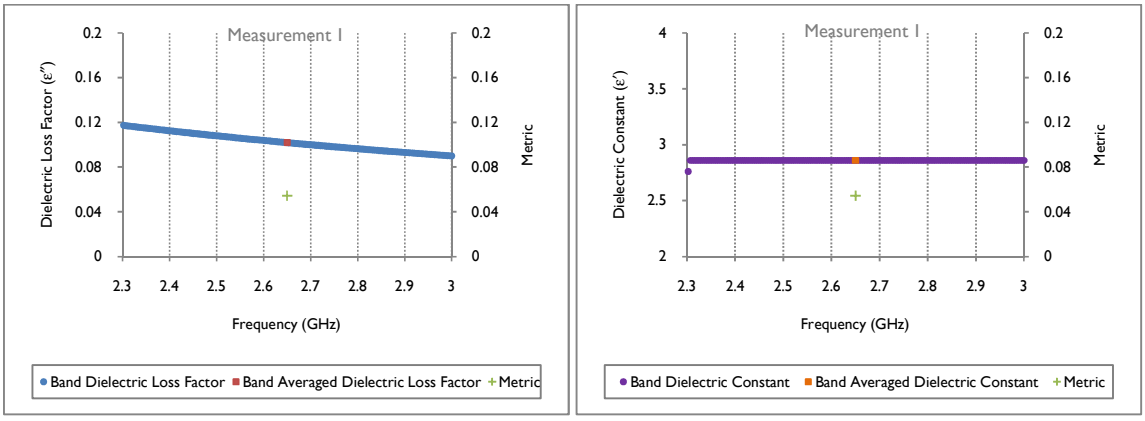

Figure 195: DB extracted ε′ and ε″ (Measurement 1, -16+13 mm)

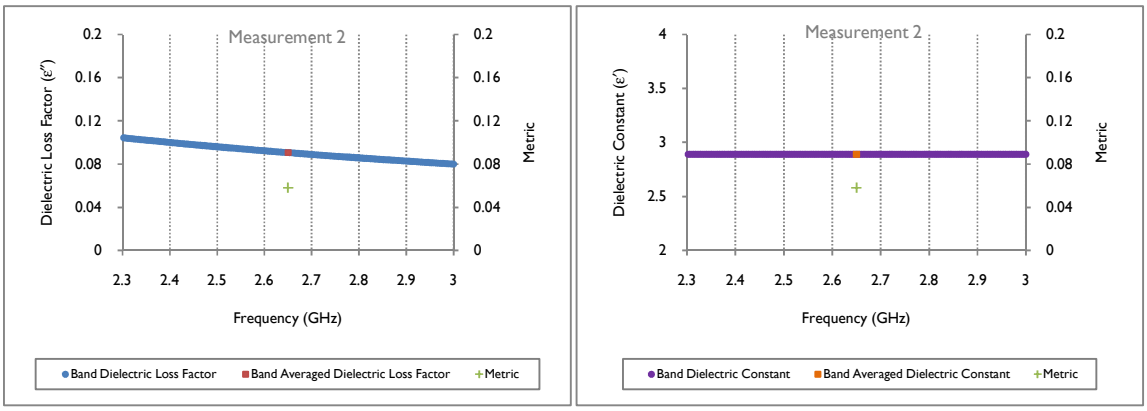

Figure 196: DB extracted ε′ and ε″ (Measurement 2, -16+13 mm)

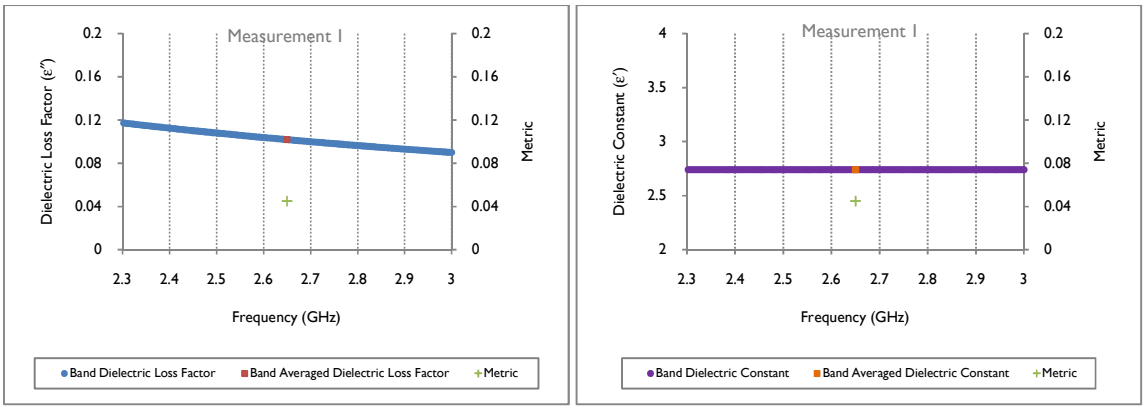

Figure 197: DB extracted ε′ and ε″ (Measurement 1, -13+9 mm)

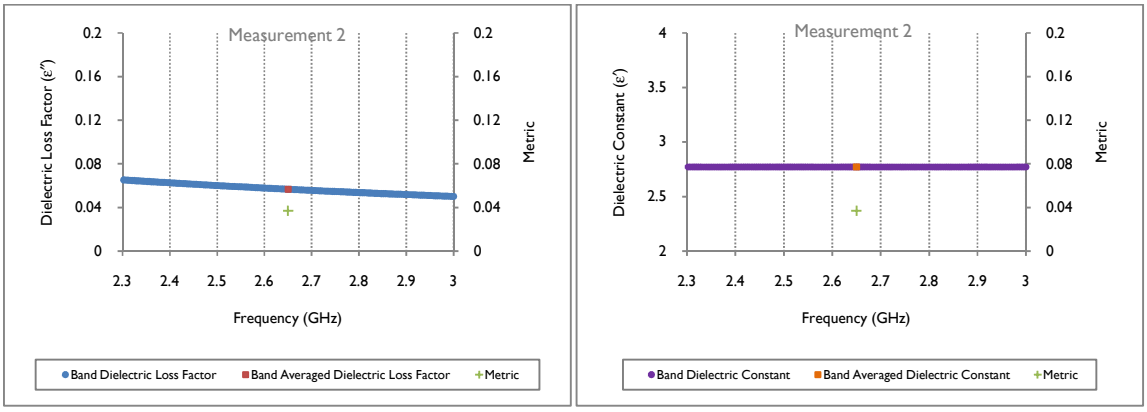

Figure 198: DB extracted ε′ and ε″ (Measurement 2, -13+9 mm)

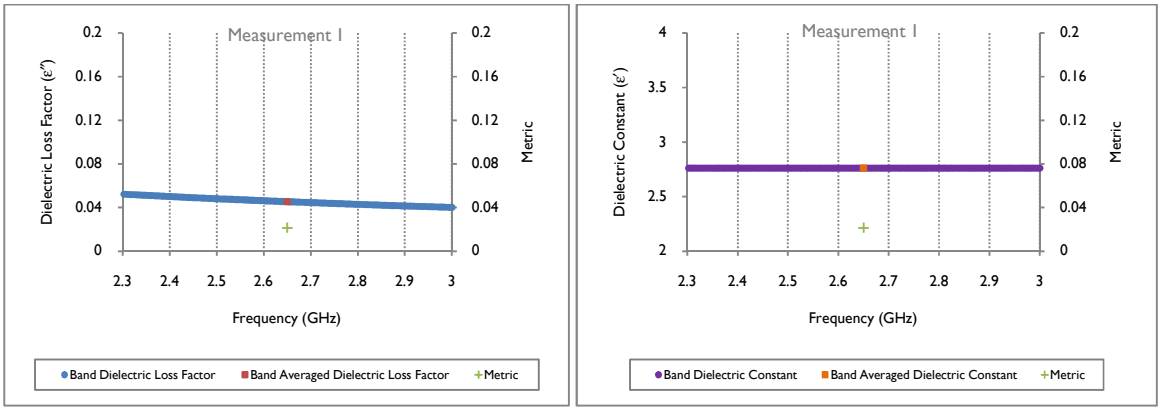

Figure 199: DB extracted ε′ and ε″ (Measurement 1, -9+6 mm)

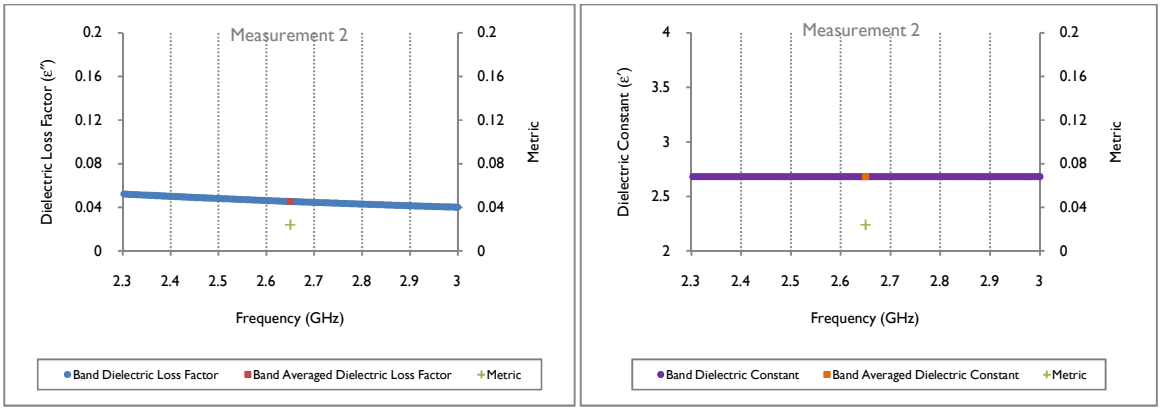

Figure 200: DB extracted ε′ and ε″ (Measurement 2, -9+6 mm)

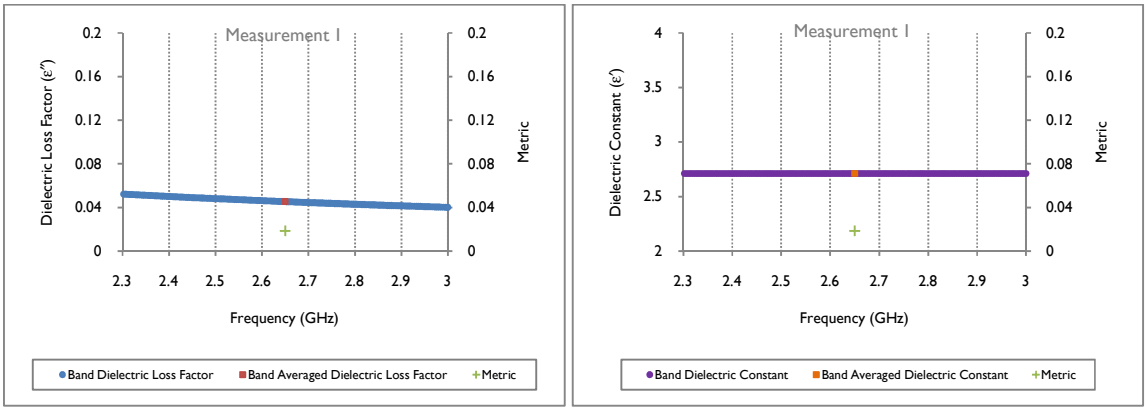

Figure 201: DB extracted ε′ and ε″ (Measurement 1, -6+4 mm)

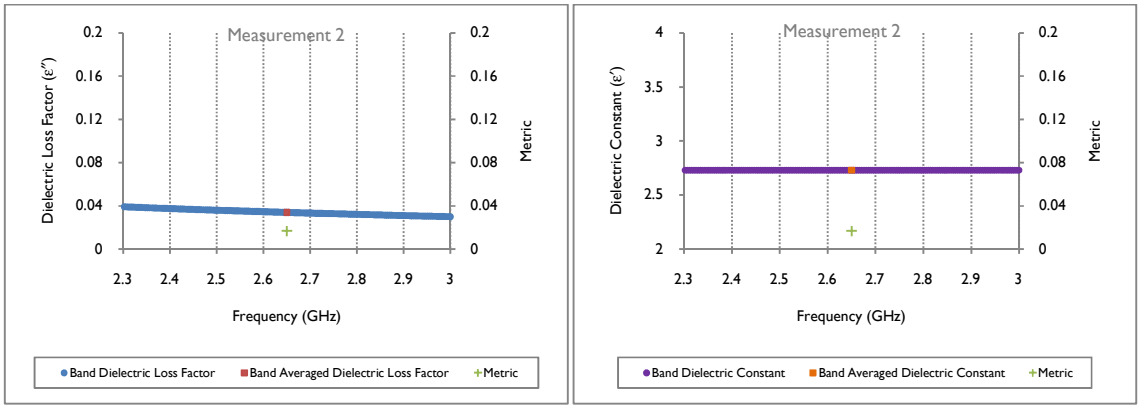

Figure 202: DB extracted ε′ and ε″ (Measurement 2, -6+4 mm)

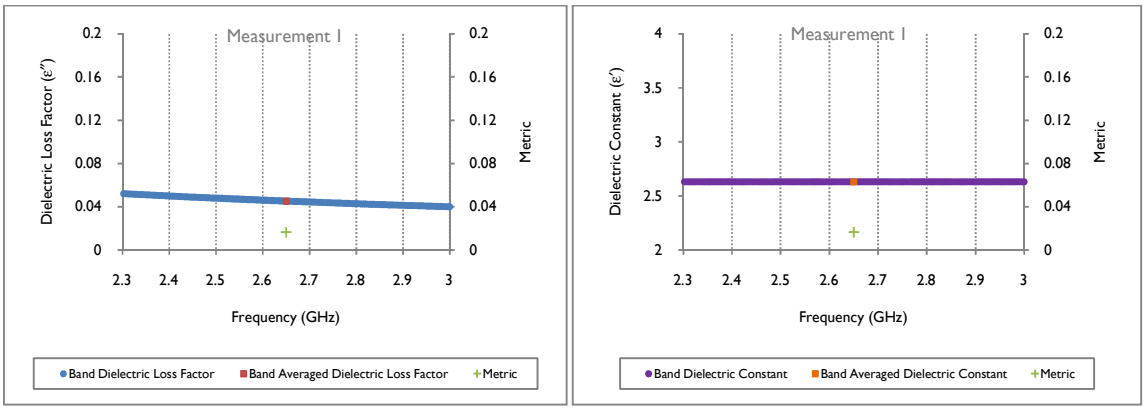

Figure 203: DB extracted ε′ and ε″ (Measurement 1, -4+3 mm)

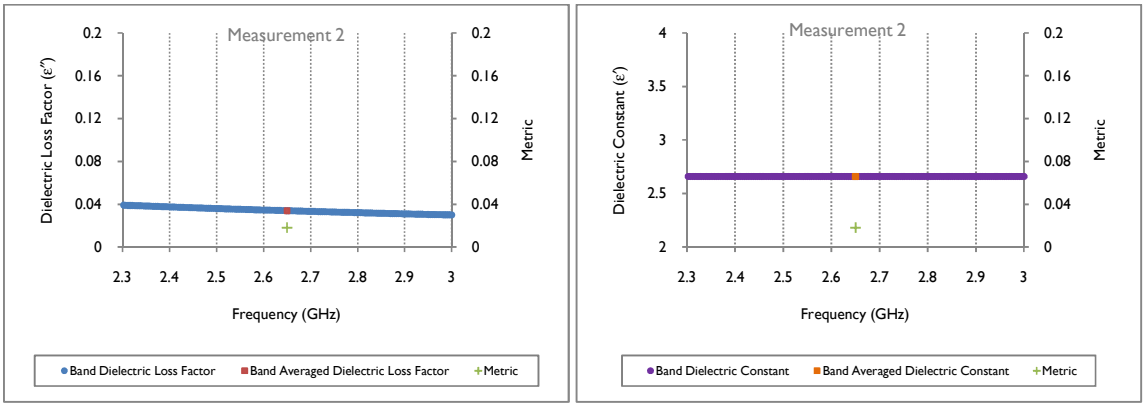

Figure 204: DB extracted ε′ and ε″ (Measurement 2, -4+3 mm)

Appendix I

Waveguide Sample Holder Design and Construction

Appendix I gives the design drawings of the waveguide sample holders that were constructed for use in the thesis.

Both the WR284 and WR340 sample holders were machined from solid blocks of mild steel. Mild steel was selected as the material of construction due to its high degree of machinability.

Each of the sample holders was fitted with guide pins to ensure that the removable lid fitted squarely onto the trough -shaped base structure.

The dielectric PET windows were inserted into the trough, forming the particulate cavities.

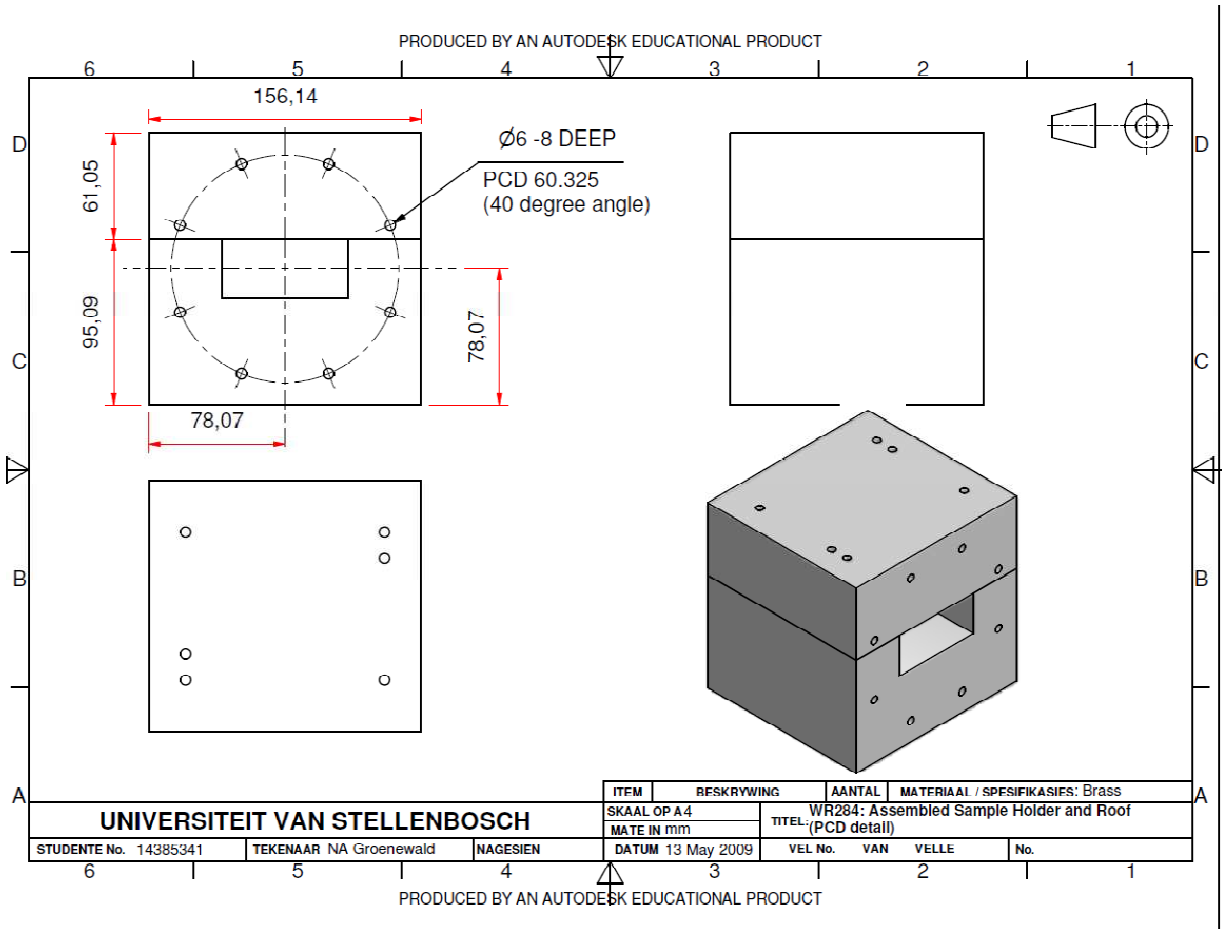
PRODUCED BY AN AUTODESK EDUCATIONAL PRODUCT
156,14
Ø6 -8 DEEP
PCD 60.325
(40 degree angle)
61,05
95,09
78,07
78,07
ITEM
BESKRYWING
AANTAL
MATERIAAL / SPESIFIKASIES: Brass
UNIVERSITEIT VAN STELLENBOSCH
SKAAL OP A4
MATE IN mm
TITEL: WR284: Assembled Sample Holder and Roof (PCD detail)
STUDENTE No. 14385341
TEKENAAR NA Groenewald
NAGESIEN
DATUM 13 May 2009
VEL No.
VAN
VELLE
No.
PRODUCED BY AN AUTODESK EDUCATIONAL PRODUCT

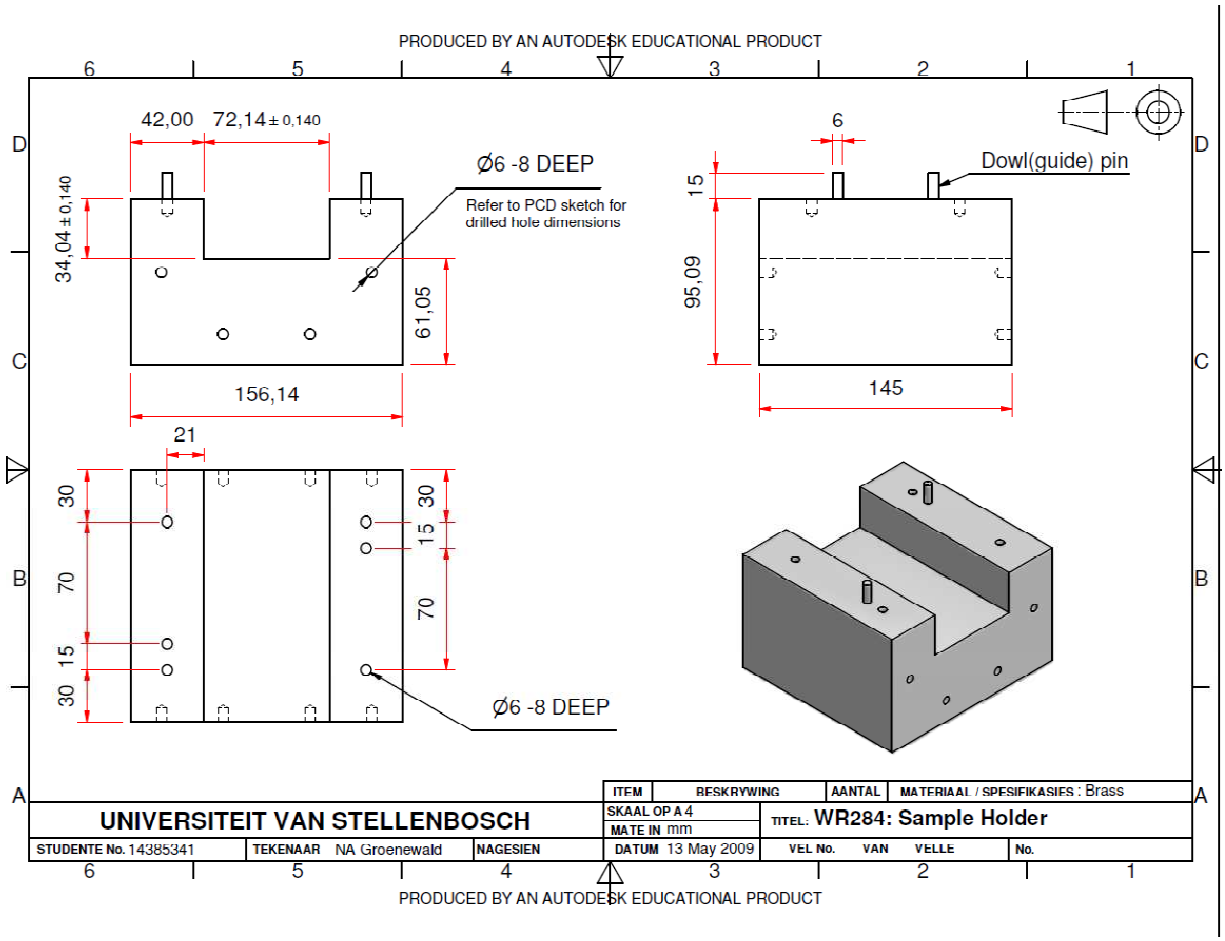
PRODUCED BY AN AUTODESK EDUCATIONAL PRODUCT
42,00
72,14 ± 0,140
34,04 ± 0,140
Ø6 -8 DEEP
Refer to PCD sketch for drilled hole dimensions
61,05
156,14
21
30
70
15
30
30
15
70
Ø6 -8 DEEP
6
Dowl(guide) pin
15
95,09
145
ITEM
BESKRYWING
AANTAL
MATERIAAL / SPESIFIKASIES : Brass
UNIVERSITEIT VAN STELLENBOSCH
SKAAL OP A 4
MATE IN mm
TITEL: WR284: Sample Holder
STUDENTE No. 14385341
TEKENAAR NA Groenewald
NAGESIEN
DATUM 13 May 2009
VEL No.
VAN
VELLE
No.
PRODUCED BY AN AUTODESK EDUCATIONAL PRODUCT

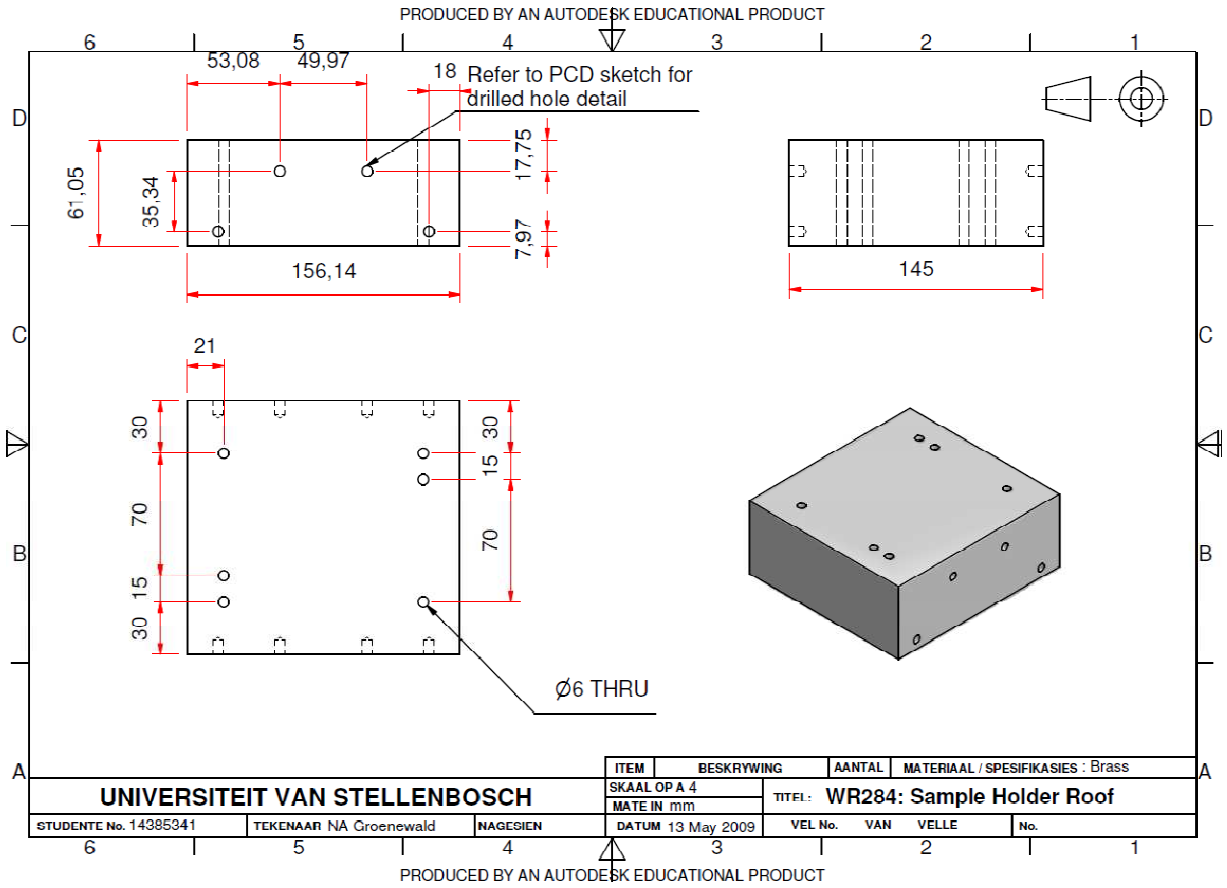
PRODUCED BY AN AUTODESK EDUCATIONAL PRODUCT
53,08
49,97
18
Refer to PCD sketch for drilled hole detail
61,05
35,34
17,75
7,97
156,14
145
21
30
70
15
30
30
15
70
Ø6 THRU
ITEM
BESKRYWING
AANTAL
MATERIAAL / SPESIFIKASIES : Brass
UNIVERSITEIT VAN STELLENBOSCH
SKAAL OP A 4
MATE IN mm
TITEL : WR284: Sample Holder Roof
STUDENTE No. 14385341
TEKENAAR NA Groenewald
NAGESIEN
DATUM 13 May 2009
VEL No. VAN VELLE
No.
PRODUCED BY AN AUTODESK EDUCATIONAL PRODUCT

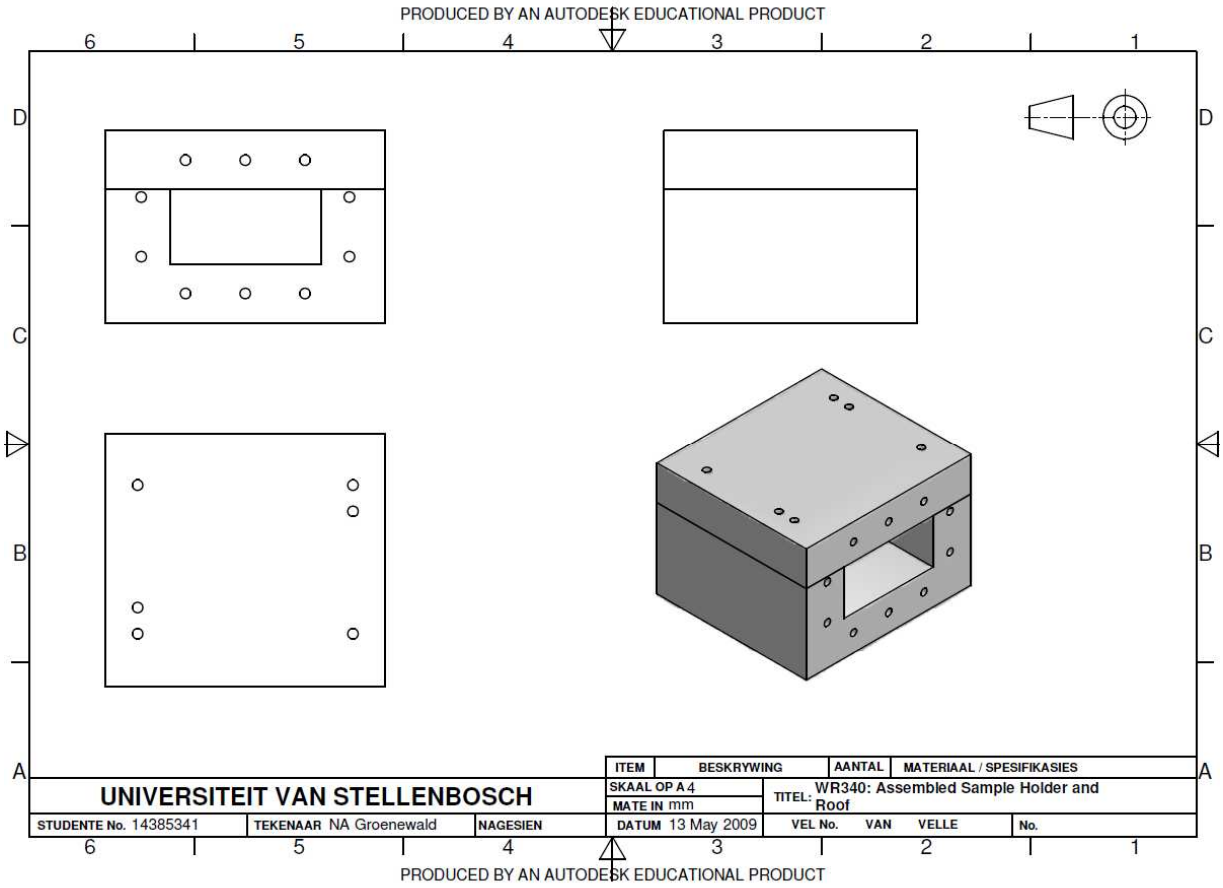
PRODUCED BY AN AUTODESK EDUCATIONAL PRODUCT
6
5
4
3
2
1
D
C
B
A
ITEM
BESKRYWING
AANTAL
MATERIAAL / SPESIFIKASIES
UNIVERSITEIT VAN STELLENBOSCH
SKAAL OP A4
MATE IN mm
TITEL: WR340: Assembled Sample Holder and Roof
STUDENTE No. 14385341
TEKENAAR NA Groenewald
NAGESIEN
DATUM 13 May 2009
VEL No.
VAN
VELLE
No.
PRODUCED BY AN AUTODESK EDUCATIONAL PRODUCT

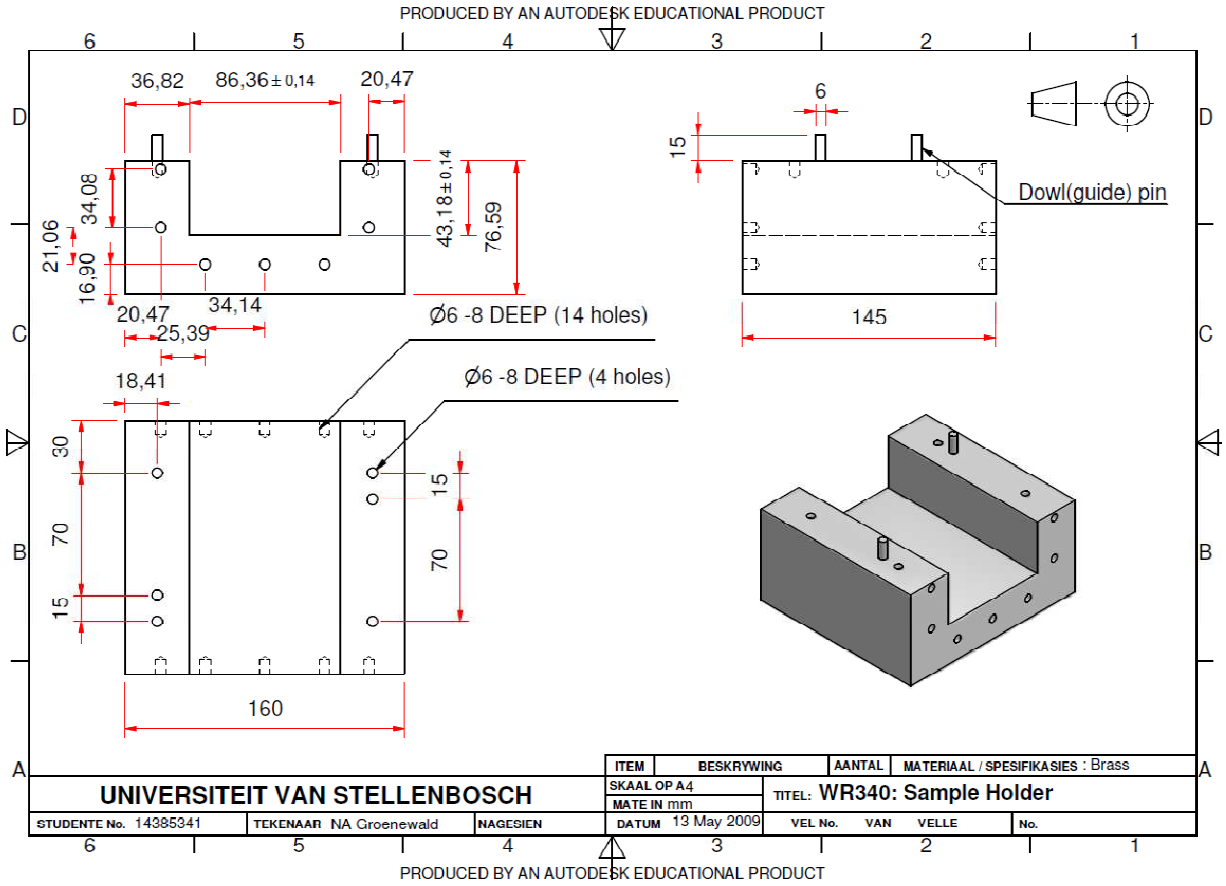
PRODUCED BY AN AUTODESK EDUCATIONAL PRODUCT
36,82
86,36 ± 0,14
20,47
34,08
21,06
16,90
43,18 ± 0,14
76,59
20,47
34,14
25,39
Ø6 -8 DEEP (14 holes)
Ø6 -8 DEEP (4 holes)
18,41
30
70
15
15
70
160
6
15
Dowl(guide) pin
145
ITEM
BESKRYWING
AANTAL
MATERIAAL / SPESIFIKASIES : Brass
UNIVERSITEIT VAN STELLENBOSCH
SKAAL OP A4
MATE IN mm
TITEL: WR340: Sample Holder
STUDENTE No. 14385341
TEKENAAR NA Groenewald
NAGESIEN
DATUM 13 May 2009
VEL No.
VAN
VELLE
No.
PRODUCED BY AN AUTODESK EDUCATIONAL PRODUCT

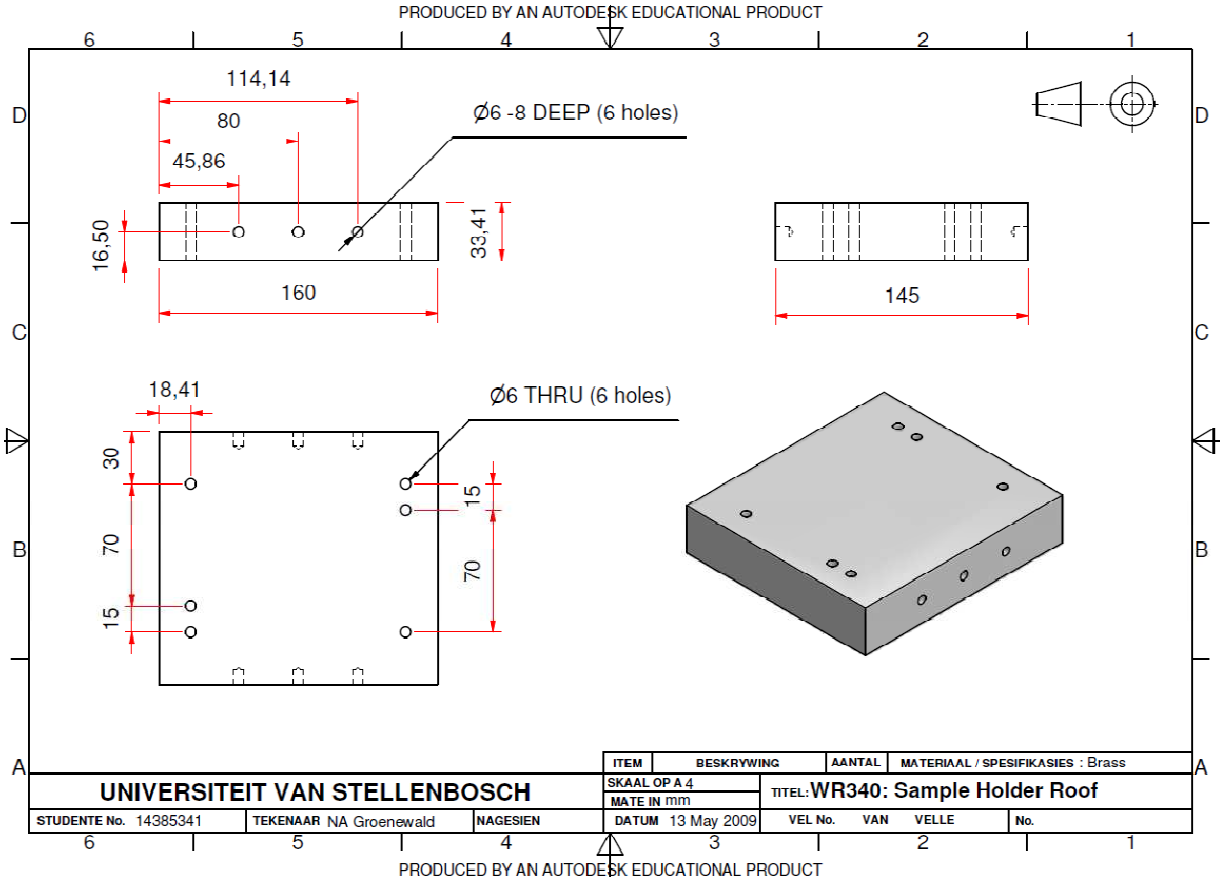
PRODUCED BY AN AUTODESK EDUCATIONAL PRODUCT
114,14
80
45,86
Ø6 -8 DEEP (6 holes)
16,50
33,41
160
145
18,41
Ø6 THRU (6 holes)
30
70
15
15
70
ITEM
BESKRYWING
AANTAL
MATERIAAL / SPESIFIKASIES : Brass
UNIVERSITEIT VAN STELLENBOSCH
SKAAL OP A 4
MATE IN mm
TITEL: WR340: Sample Holder Roof
STUDENTE No. 14385341
TEKENAAR NA Groenewald
NAGESIEN
DATUM 13 May 2009
VEL No.
VAN
VELLE
No.
PRODUCED BY AN AUTODESK EDUCATIONAL PRODUCT